



Project from the European Union's
Horizon 2020 Marie Skłodowska-Curie Action
under grant agreement N° 721484



Ph.D. in Chemical Sciences
University of Naples Federico II
XXXIII Cycle

Characterisation of the lipopolysaccharide and peptidoglycan and their structural determinants when bound to major proteins involved in its transport across the periplasm

Ph.D. Candidate
María del Pilar García del Vello Moreno
Pilar Garcia-Vello

Tutor
Prof. Cristina De Castro

2017-2021

© 2021 – Pilar Garcia-Vello

All rights reserved

Table of Contents

Abbreviations

Monosaccharide abbreviations and symbols

Amino acid abbreviations and symbols

Lipid and other abbreviations and symbols

Abstract

List of Figures

List of Tables

Chapter 1. Introduction

Chapter 2. Results and discussion

Chapter 3: General conclusion

Chapter 4: Material and methods

Acknowledgements

References

Extended Table of Contents

Abbreviations	I
Monosaccharide abbreviations and symbols	IV
Amino acid abbreviations and symbols	V
Lipid and other abbreviations and symbols	V
Abstract	VI
List of Figures	XI
List of Tables	XVII
Chapter 1 Introduction	1
1.1. Cell surface of Gram-negative and Gram-positive bacteria.....	1
1.2. The Gram-negative bacteria cell envelope.....	3
1.3. Lipopolysaccharide	7
1.3.1. Structure of LPS.....	7
1.3.2. Host immune response to LPS	12
1.3.3. LPS building machineries	16
1.4. Peptidoglycan.....	26
1.4.1. Structure of PG	26
1.4.2. Host immune response to PG.....	30
1.4.3. PG biosynthesis and transport.....	33
1.4.4. PG hydrolysis.....	36
1.5. Biogenesis of the cell envelope: elongasome and divisome	40
1.6. Antibiotic resistance	44
1.6.1. Need for urgent action and new antibiotics	44
1.6.2. Antibiotics: targets and resistance	46
1.7. Commensal bacteria	50
1.7.1. Commensal microbiota: an overview	50
1.7.2. Gut microbiota	51
1.7.3. LPS and PG of gut microbiota	54
1.7.4. <i>Akkermansia muciniphila</i>	56
1.7.5. <i>Fusobacterium nucleatum</i>	60
1.8. Aims of the thesis.....	63
Chapter 2 Results and discussion	65
Part 1. LPS and PG from commensal bacteria	67
2.1. The lipooligosaccharide of <i>Akkermansia muciniphila</i> Muc ^T	69
2.1.1. Production and purification of the LOS of <i>A. muciniphila</i>	69
2.1.2. Compositional analysis of the Nonasaccharide and the Tetradecasaccharide	72
2.1.3. NMR analysis of the Nonasaccharide of <i>A. muciniphila</i>	73
2.1.4. NMR analysis of the Tetradecasaccharide of <i>A. muciniphila</i>	79
2.1.5. Structural characterisation of the Lipid A of <i>A. muciniphila</i>	85
2.1.6. Inner core determination of the LOS of <i>A. muciniphila</i>	89
2.1.7. Immunological properties of the LOS of <i>A. muciniphila</i>	91
2.1.8. Discussion	92

2.2. The peptidoglycan composition of <i>Akkermansia muciniphila</i> Muc ^T	96
2.2.1. Purification and analysis of the peptidoglycan of <i>A. muciniphila</i>	96
2.2.2. Discussion	98
2.3. The lipopolysaccharide of <i>Fusobacterium nucleatum</i> ATCC 51191.....	101
2.3.1. Production and purification of the LPS of <i>F. nucleatum</i>	101
2.3.2. Structural characterisation of the O-polysaccharide of <i>F. nucleatum</i> 102	
2.3.3. Structural characterisation of the lipid A of <i>F. nucleatum</i>	111
2.3.4. Immunological properties of the LPS of <i>F. nucleatum</i>	114
2.3.5. Discussion	115
2.4. The role of the LPS of <i>F. nucleatum</i> in colorectal cancer development..	117
2.4.1. Outer membrane vesicles compositional analysis	117
2.4.2. Immunological properties of <i>F. nucleatum</i> derived LPS and OMVs	123
2.4.3. Discussion	124
2.5. The peptidoglycan composition of <i>F. nucleatum</i> ATCC 51191	127
2.5.1. Purification and analysis of the peptidoglycan of <i>F. nucleatum</i>	127
2.5.2. Discussion	130
Part 2. Study of trans-envelope machineries.....	133
2.6. Effects BAM complex mutations on LPS production.....	135
2.6.1. Isolation and purification of the LOS of <i>E. coli</i> mutants	136
2.6.2. Monosaccharide compositional analysis of the LOS.....	136
2.6.3. ¹ H NMR profiling of the core of LOS of <i>E. coli</i> mutants	138
2.6.4. Lipid profiling by GC-MS of the LOS of <i>E. coli</i> mutants	139
2.6.5. MALDI analysis of the lipid A of <i>E. coli</i> mutants.....	141
2.6.6. Discussion	144
2.7. New NMR tool for the study LPS-protein interaction	145
2.7.1. LOS production and purification	146
2.7.2. Fully de-acylated LOS production and purification	146
2.7.3. Fully de-acylated lipid A production and purification.....	147
2.7.4 Active nuclei insertion into the fully-deacylated lipid A.....	149
2.7.5. Discussion	152
2.8. LptA interaction with PG hydrolysis machineries	154
2.8.1. LptA as amidase activator.....	154
2.8.2. Interaction LptA and amidase regulators	156
2.8.3. Discussion	157
Chapter 3 General conclusion.....	159
Chapter 4 Material and methods.....	165
4.1. Strains, plasmids, primers, bacterial and growth conditions.....	167
4.1.1. BAM mutants.....	167
4.1.2. LptA and LptAm mutant	168
4.1.3. <i>Akkermansia muciniphila</i> Muc ^T	169
4.1.4. <i>Fusobacterium nucleatum</i>	169
4.1.5. <i>Escherichia coli</i> K12.....	169
4.2. LPS, LOS and OMV isolation procedures	169
4.2.1. PCP extraction	170
4.2.2. Hot water-phenol extraction and enzymatic digestion.....	170

4.2.3. SDS-PAGE	171
4.2.4. Outer membrane vesicles isolation	171
4.2.5. De-acylated LPS isolation.....	172
4.2.6. Isolation of the lipid A	173
4.2.7. De-acylated lipid A isolation	173
4.3. LPS composition and structure determination	173
4.3.1. GC-MS.....	174
4.3.2. NMR	176
4.3.3. MALDI-TOF MS and MS/MS	177
4.3.4. ESI FT-ICR MS	178
4.4. LPS amidation treatment.....	179
4.5. Peptidoglycan isolation	179
4.6. Peptidoglycan mucopeptides compositional analysis.....	180
4.7. LptA and LptAm production and purification.....	182
4.8. LptA, LptAm and PG assays	182
4.8.1. Amidase activity test.....	182
4.8.2. Ni ²⁺ -NTA beads <i>in-vitro</i> pull-down assay	183
4.9. Immunological assays	183
4.9.1. HEK-Blue cells	183
4.9.2. Recombinant Siglec-Fc proteins	184
4.9.3. Human primary immune cells.....	185
4.11. Image flow cytometry	186
Acknowledgements.....	187
References	189

Abbreviations

Ab	Antibody
ACP	Acyl Carrier Protein
ATP	Adenosine triphosphate
AMG	Acetylated Methyl Glycosides
Ami	Amidase
BSA	Bovine Serum Albumin
CD	Cluster of differentiation
CID	Collision-Induced Dissociation
CLR	C-type Lectin-like Receptor
CM	Cytoplasmic Membrane
CNRS	Centre National de la Recherche Scientifique
COSY	Correlation Spectroscopy
CSDB	Carbohydrate Structure Database
CTV	Cell Trace Violet
DC	Dendritic cell
DCC	Dicyclohexylcarbodiimide
DMEM	Dulbecco's Modified Eagle Medium
DMF	Dimethylformamide
DODN-LOS	Fully de-acylated lipooligosaccharide
DPBS	Dulbecco's Phosphate-buffered Saline
ECDC	European Centre for Disease Prevention and Control
EDC	N-ethyl-N'-(3-(dimethylamino)propyl)carbodiimide
EDTA	Ethylenediaminetetraacetic acid
ESI	Electrospray ionisation
ESI FT-ICR MS	Electrospray Ionisation Fourier Transform Ion Cyclotron Resonance Mass Spectrometry
GC-MS	Gas Chromatography – Mass Spectrometry
GMEM	Glasgow Modified Essential Medium
GlcN I	Reducing glucosamine of the lipid A
GlcN II	Non-reducing glucosamine of the lipid A
HMBC	Heteronuclear Multiple Bond Correlation
HSQC	Heteronuclear Single Quantum Coherence
HSQC-TOCSY	Heteronuclear Single Quantum Coherence - Total Correlation Spectroscopy
IL	Interleukin
IPTG	β -D-1-thiogalactopyranoside
LBP	LPS-Binding Protein
LC-MS	Liquid Chromatography - Mass Spectrometry
LOS	Lipooligosaccharide
Lpp	Braun's lipoprotein
LPS	Lipopolysaccharide
Lpt	Lipopolysaccharide transport protein

LT	Lytic Transglycosylase
moM ϕ	Monocyte derived macrophage
MALDI	Matrix-Assisted Laser Desorption/Ionisation
MAMP	Microbial-associated molecular pattern
MBL	Mannose Binding Lectin
MCE	Mammalian Cell Entry
MINCLE	Macrophage-inducible C-type lectin
Mla	Maintenance of lipid asymmetry complex
moDC	Monocyte-derived dendritic cell
MOI	Multiplicity of infection
Mpp	Murein peptide permease
NF- κ B	Nuclear Factor kappa B
NHS	N-hydroxysuccinimide
NMR	Nuclear Magnetic Resonance
NOD	Nucleotide Oligomerisation Domain protein
NOESY	Nuclear Overhauser Enhancement Spectroscopy
NONA	Nonasaccharide
OD	Optical Density
OM	Outer Membrane
OMP	Outer Membrane Protein
OMV	Outer Membrane Vesicle
ON	Overnight
Opp	Oligopeptide permease
OPS	O-polysaccharide
P	Phosphate
PBMC	Peripheral Blood Mononuclear Cells
PBP	Penicillin-binding protein
PBS	Phosphate-buffered saline
PCP	Phenol/chloroform/light petroleum
PE	Fluorescence labelled antibody
PEtN	2-amino-ethyl phosphate
PFA	Paraformaldehyde
PG	Peptidoglycan
PGRPs	Peptidoglycan Recognition Proteins
PMA	Phorbol 12-Myristate 13-Acetate
PMAA	Partially Methylated Acetylated Alditols
PRR	Pattern Recognition Receptor
R	Substituent
Rcs	Regulator of capsule synthesis
RegIII	Regenerating gene family protein III C-type lectins
ROESY	Rotating frame Overhauser Effect Spectroscopy
RT	Room temperature
SEAP	Secreted Embryonic Alkaline Phosphatase
SDS	Sodium Dodecyl Sulfate

SDS-PAGE	Sodium Dodecyl Sulfate-PolyAcrylamide Gel Electrophoresis
Sec-pathway	General Secretion route of unfolded proteins of CM
Siglecs	Sialic acid-binding immunoglobulin-like lectins
SNFG	Symbol Nomenclature for Glycans
Spp	Subspecies
SSCN	Synthesis and Structure of Carbohydrates in Naples
T1-6SS	OM type 1-6 protein secretion systems
Tat-pathway	Twin-arginine translocation pathway
TETRAD	Tetradecasaccharide
TNF α	Tumour Necrosis Factor alpha
TLR	Toll-Like Receptor
TOCSY	Total Correlation Spectroscopy
TRP	Transient Receptor Potential
UDP	Uridine diphosphate
UMP	Uridine monophosphate
UC	Ultra-centrifuge
Und-PP	Undecaprenyl diphosphate
Und-P	Undecaprenyl phosphate
UPLC	Ultra-Performance Liquid Chromatography
WHO	World Health Organisation

Monosaccharide abbreviations and symbols

	anhMurNAc	β -1,6-anhydro-N-acetylmuramic acid
	Ara4N	4-amino-4-deoxy-L-arabinose
	Fuc	L-fucose
	FucNAc4N	4-deoxy-N-acetyl-D-fucosamine
	Gal	D-galactose
	GalN	D-galactosamine
	GalNAc	D-acetylgalactosamine
	Glc	D-glucose
	GlcN	D-glucosamine
	GlcNAc	D-N-acetylglucosamine
	GlcN3N	2,3-diamino-2,3-dideoxy-D-Glc
	D-GlcNAc3NA	2-acetamido-3-amino-2,3-dideoxy-D-glucuronic acid
	Hep	L-glycero-D-manno-heptosepyranonose
	Kdo	3-deoxy-D-manno-oct-2-ulosonic acid
	Ko	D-glycero-D-talo-oct-2-ulosonic acid
	Man	D-mannose
	MurNAc	N-Acetylmuramic acid
	Neu5Ac	N-Acetylneuraminic acid
	QuiNAc	N-Acetyl-D-quinovosamine
	Rib	Ribose

This Ph.D. thesis used the Symbol Nomenclature for Glycans (SNFG) (Varki *et al.*, 2015).

Amino acid abbreviations and symbols

	m-A ₂ pm	meso-diaminopimelic acid
	D-Ala	D-alanine
	L-Ala	L-alanine
	Arg	Arginine
	D-iGlu	D-isoglutamate
	Gly	Glycine
	Lnt	Lanthionine
	Lys	Lysine
	D-Ser	D-serine

Lipid and other abbreviations and symbols

	Und	Undecaprenyl	
	C12:0	Dodecanoic acid	Lauric acid
	C13:0	Tridecanoic acid	
	C14:0	Tetradecanoic acid	Myristic acid
	C14:0 (3-OH)	3-hydroxy tetradecanoic acid	
	C15:0	Pentadecanoic acid	
	C15:0 (3-OH)	3-hydroxy pentadecanoic acid	
	C16:0	Hexadecanoic acid	Palmitic acid
	C16:0 (3-OH)	3-hydroxy hexadecanoic acid	
	C16:1	Hexadecenoic acid	
	C17:0	Heptadecanoic acid	Margaric acid
	C18:0	Octadecanoic acid	Stearic acid
	C18:1 ⁹	(9Z)-Octadec-9-enoic acid	Oleic acid
	P	Phosphate	

Saturated fatty acids are named as C_x:0, being x the number of carbons present in the chain; C-2 hydroxylated fatty acids are named as C_x:0 (2-OH); C-3 hydroxylated fatty acids are named as C_x:0 (3-OH); Unsaturated fatty acids C_x:y^{z1,z2,...}, being y the number of double bonds and z1 (z2 etc) the position of the double bonds. *i*-: iso, *a*-: anteiso

Abstract

Gram-negative bacteria possess an outer membrane (OM), a lipidic bilayer that surrounds a thin peptidoglycan (PG) layer and the cytoplasmic membrane (CM). The OM is an asymmetric bilayer whose outer leaflet is mainly composed by lipopolysaccharides (LPSs). LPS and PG have a direct role in antibacterial resistance and in the communication bacteria-host.

There are many open questions on how the bacterial surface of pathogens and commensals interacts with the host in order to escape immune recognition and produce harmful or beneficial effects as well as regarding the details on how the bacterial envelope is built.

Therefore, the main focus of this Ph.D. thesis is to contribute to the characterisation of the LPS and PG to increase the knowledge on the interaction of pathogen and commensal Gram-negative bacteria with the host and to deepen the understanding of their structural determinants when bound to major proteins involved in its transport across the periplasm. With that aim the composition, structure and immune activities of the LPS and PG of *Akkermansia muciniphila* and *Fusobacterium nucleatum* is disclosed and the trans-envelope machineries of the model bacterium *Escherichia coli* studied.

A. muciniphila is one of the few bacteria that successfully inhabits the mucus layer of humans and other mammals' intestines. Not only its presence is associated with a healthy intestine, but also it seems to improve insulin sensitivity, increase the mucosal barrier function, regulate glycemia levels, and reduce fat accumulation, insulinemia, cholesterol, body weight gain and inflammation in the intestine and body.

The lipooligosaccharide (LOS or rough LPS) of *A. muciniphila* Muc^T is very complex: it includes more than the two canonical units of Kdo, is rich in fucose

units and most of the fatty of the lipid A are branched at the penultimate carbon. The LOS seems to be a mild activator of TLR4, while it is a relevant activator of TLR2 which may play a role in the development of the beneficial effects of the bacterium.

The PG of *A. muciniphila* Muc^T contains muropeptides with de-*N*-acetylated glucosamine, being the first time, such structure is described in a Gram-negative bacterium. Moreover, this modification of the PG has been linked to the avoidance of recognition by NOD-1 immune receptors and therefore bacterial clearance.

F. nucleatum is an oral commensal that plays a crucial role in the formation of biofilms, being also involved in extra-oral disorders such as intrauterine infections and colorectal cancer, in which the subspecies *animalis* is the most commonly isolated.

The LPS of *F. nucleatum* spp. *animalis* ATCC 51191 has a trisaccharide repeating unit rich in amino- and aminuronic-monosaccharides, and a lipid A similar to that of *Burkholderia cenocepacia*. In addition, *F. nucleatum* ssp. *polymorphum* ATCC 10953, *F. nucleatum* ssp. *animalis* ATCC 51191 and *F. nucleatum* ssp. *nucleatum* ATCC 25586 full cells, outer membrane vesicles (OVMs), and LPSs stimulate monocyte-derived dendritic cells leading to an increased production of TNF α , IL-8 and IL-6, while in monocyte-derived macrophages the stimulation leads to the production of IL-10, IL-6 and IL-8 and to low levels of TNF α . These effects are measured in the three strains and seem to be mediated by Siglec-7, a sialic acid receptor, even though the O-antigen of only two of the strains tested (ATCC 10953 and 25586) expose this monosaccharide or the sialic acid-like molecule fusaminic acid.

The PG of *F. nucleatum* spp. *animalis* ATCC 51191 presents an alteration of the most common stem peptide by substitution of the L-meso-diaminopimelic acid by

the sulfur-containing diamino acid lanthionine or another amino acid. This may be crucial to avoid the recognition by NOD-1 immune receptors potentiating colorectal cancer development.

The trans-envelope machineries were studied on *E. coli*, because of its importance as antibiotic-resistant "priority pathogen" of WHO and due to the fair amount of existing literature.

The T5SS that transports, folds and insets β -barrel proteins in the OM is comprised of Skp, SurA, DegP and the BAM complex (that consists of four lipoproteins BamB, BamC, BamD, BamE and one OMP named BamA). In order to determine the extent of their influence on the composition and structure of LPS, the *E. coli* mutants $\Delta surA$, Δskp , $\Delta degP$, $\Delta bamB$, $\Delta bamC$, and $\Delta bamE$ were produced and the structure of their LPS determined. The results suggested that the alterations on the BAM machinery do not significantly alter the composition nor the structure of the LPS, providing an insight on the mechanism by which the alteration of the BAM machinery may alter the integrity of the OM.

The LPS transportation machinery (Lpt) deploys seven LPS transport proteins named Lpt A-G that extracts the LPS from the external leaflet of the CM, transports it across the periplasm and the PG, flips it across the OM and locates the LPS in its external face. All Lpt proteins are essential, which makes them candidates as targets for new antibiotics. There are many open questions on the working of this machinery, for instance the details of the interaction sites of the hydrophobic pocket and how the periplasmic bridge is formed.

During this Ph.D., the development of a semi-synthetic lipid A with active nuclei instead of acyl chains was attempted in order to study the details of the interaction between LPS-Lpt proteins by NMR. The introduction of a paramagnetic group on the fully de-acylated lipid A failed, but the introduction of fluoropropanoyl chloride seemed to be partially successful. However, the product presents a high

level of contamination that prevented the reliable determination of the product as well as the interaction studies.

In addition, it is disclosed that LptA does not act as an amidase regulator for AmiA, AmiB nor AmiC nor as a ligand for the amidase activators YgeR or NlpD. Leaving unanswered the question on how the hole on the PG is open for the Lpt bridge.

In conclusion, the architecture of bacterial envelope is crucial for the interaction with the host and the knowledge of the structure of its components is a fundamental prerequisite to proceed with functional studies, and to dissect the role of each component.

In this frame, the knowledge of the molecular determinants of the bacteria of the microbiota is preliminary. Through the characterisation of LPS and PG, this Ph.D. thesis demonstrates that they have unexpected structures and activities. Likewise, their transport across the periplasm, dissected on model organisms, still presents many gaps to be filled. Thus, our understanding of the cell envelope and of its metabolism is still to an early stage, but it is mature enough to devise alive bacteria and/or synthetic analogues of their surface structures for clinical applications.

Part of this Ph.D. thesis was adapted from the following articles co-written by the author of the present thesis:

Garcia-Vello P, Speciale I, Chiodo F, Molinaro A, De Castro C. Carbohydrate-based adjuvants. *Drug Discov Today Technol.* 2020. In press. doi: 10.1016/j.ddtec.2020.09.005

Garcia-Vello P, Di Lorenzo F, Lamprinaki D, Notaro A, Speciale I, Molinaro A, Juge N, De Castro C. Structure of the O-antigen and the lipid A from the lipopolysaccharide of *Fusobacterium nucleatum* ATCC 51191. *ChemBiochem.* 2020. doi: 10.1002/cbic.202000751.

Lamprinaki D, Hellmich C, Garcia-Vello P, Bowles KM, De Castro C, Crocker P, Juge N. Siglec-7 contributes to the immunomodulation induced by *F. nucleatum* ssp. in colorectal cancer. Pending submission.

Garcia-Vello P, Di Lorenzo F, Zamyatina A, Molinaro A, De Castro C. Lipopolysaccharide lipid A: promising molecule for new immunity-based therapies and antibiotics. Pending Submission.

Garcia-Vello P, Speciale I, Di Lorenzo F, Molinaro A, De Castro C. Dissecting lipopolysaccharide composition by GC-MS and MALDI spectrometry. *Methods Mol Biol.* Springer Nature. 2021. Under revision.

Garcia-Vello P, Di Lorenzo F, Nicolardi S, Tytgat H, Plovier H, Speciale I, Notaro A, Garozzo D, Laguri C, Molinaro A, Silipo A, De Vos W, De Castro C. The lipooligosaccharide structure and immunological activities of *Akkermansia muciniphila* Muc^T. In preparation.

List of Figures

Figure 1.1. Gram-positive and Gram-negative cell envelope. Gram-positive bacteria possess a cytoplasmic membrane (CM) that is protected by a thick layer of peptidoglycan (PG). The PG is characterised by the presence of teichoic acids and lipoteichoic acids. Gram-negative bacteria are distinguished for their extra hydrophobic membrane layer, the outer membrane (OM) that covers a thin PG layer and the CM. The space between the CM and the OM is known as periplasm.	2
Figure 1.2. From left to right: LPS transport machinery Lpt and Phospholipid transport machineries with MCE proteins (Mla, YebST, PqiABC and LetB) and Tol-Pal system for the retrograde transport of phospholipids and PbgA cardiolipin transporter.	4
Figure 1.3. From left to right: regulator of capsule synthesis (Rcs), β -barrel membrane protein assembly (BAM) and Lol lipoprotein transport complex.	6
Figure 1.4. Lipopolysaccharide schematic representation. LPS are complex glycoconjugates structurally divided in the lipid A, the core oligosaccharide and O-polysaccharide (or O-antigen).	7
Figure 1.5. Lipid A of <i>E. coli</i> with the backbone [P \rightarrow 4- β -D-GlcpN-(1 \rightarrow 6)- α -D-GlcpN-1 \rightarrow P], hexa-acylated (4+2 pattern). GlcNI: reducing α -D-glucosamine; GlcN II non-reducing β -D-glucosamine.	9
Figure 1.6. Structure of the lipid A and part of the inner core of <i>E. coli</i> . The differences in conformation alter the inclination of the glucosamine disaccharide with respect to the membrane surface or tilt angle. The larger tilt angle, the more endotoxic the lipid A is. <i>E. coli</i> 's lipid A is very endotoxic, as it is <i>bis</i> -phosphorylated and asymmetrically hexa-acylated, producing a tilt angle bigger than 50°. Modified from Seydel <i>et al.</i> , 2000.	14
Figure 1.7. Lipid A and O-polysaccharide biosynthesis by the Raetz and Wzx/Wzy pathways.	20
Figure 1.8. Msba and Lpt transport systems. ABC protein MsbA flips the rough LPS or LOS from the inner to the outer leaflet of the CM. Then the membrane protein WaaL forms a β -glycoside bond between the OPS and the outer core. The final LPS is then extricated from the CM by the ABC transport system LptB ₂ FG and the protein membrane LptC. Subsequently, LptA carries it across the periplasm and, finally, the β -barrel protein LptD with the OM lipoprotein LptE place the LPS in the external face of the OM. The LPS are pushed by a continuous stream of LPSs from the CM to the OM and the energy is provided by cytoplasmic ATP hydrolysis. Modified from Bishop 2019.	22
Figure 1.9. Interaction LptC and LPS in solution. a. [¹ H, ¹⁵ N]-correlation spectrum and b. [¹ H, ¹³ C]-correlation spectrum of labelled LptC in presence (red) and absence (black) of 0.8 mg/mL of LPS. c. LptC upon LPS binding on a ribbon representation. d. Surface representation of the LptC-LPS model. The two LptC molecules are coloured differently to visualize the localisation of the intermolecular interface and cavity where the LPS binds (Laguri <i>et al.</i> , 2017).	25
Figure 1.10. Structure of PG of <i>E. coli</i> . PG is composed by linear chains of a repeating β -D-N-acetylglucosamine (GlcNAc) 1,4-linked to β -D-N-acetylmuramic acid (MurNAc) disaccharide. The PG strand ends with 1,6-anhydro-N-acetylmuramic acid (anhMurNAc). In nascent PG and PG precursors, MurNAc has a peptide chain attached usually formed by: L-alanine (L-Ala) – D-isoglutamate (D-iGlu) - meso-diaminopimelic acid (m-A ₂ pm) – D-alanine (D-Ala) - D-alanine. There can be an amide bond (cross-link) between the	

amino group of m-A₂pm and the carbonyl of D-Ala 4 of another peptide. Modified from Desmarais *et al.*, 2013. 27

Figure 1.11. Variation in the structure of the PG on the carbohydrate backbone or the stem peptide. Glycan strands modifications confer PG resistance to lysozyme and other components of the innate immune system. Stem peptide modifications facilitate immune system evasion and confer resistance to some antibiotics..... 29

Figure 1.12. Synthesis of peptidoglycan. In the cytoplasm: The nucleotide precursor UDP-GlcNAc is synthesised from fructose-6-phosphate by the Glm enzymes. MurA, MurB, MurC, MurD, MurE and MurF synthesize UDP-N-acetylmuramyl-pentapeptide. MraY transfers the UDP-MurNAc-pentapeptide from UDP-Mpp to und-P, generating the lipid I. Afterwards, MurG transfers a GlcNAc from UDP-GlcNAc to Lipid I to produce the lipid II. MurJ flips lipid II from the inner to the outer leaflet of the CM. **In the periplasm:** transglycosylases transfer MurNAc of the nascent lipid-linked PG to the GlcNAc of a lipid II. Transpeptidases cross-link peptides protruding from different glycan strands to form a net-like structure. DD-transpeptidases form 3→4 bond and LD-transpeptidases form 3→3 bond. Modified from Typas *et al.*, 2012. 34

Figure 1.13. PG hydrolases action site. N-acetylglucosaminidases hydrolyse the terminal non-reducing GlcNAc. The N-acetylmuramidases hydrolyse the β,1,4-bonds between MurNAc and GlcNAc. The lytic transglycosylases are N-acetyl muramidases that LTs recognise the bond between MurNAc and GlcNAc and catalyse the intramolecular cyclisation of MurNAc into anhMurNAc. The N-acetylmuramyl-L-Ala amidases or simply amidases cleave the amide bond between MurNAc and the L-Ala residue of the stem peptide. The endopeptidases hydrolyse the peptide cross-link in a non-terminal part of the peptide and can be DD, DL or LD. The carboxypeptidases can cleave the bond between terminal amino acids of the stem peptide and can be DD, DL or LD..... 37

Figure 1.14. Elongasome and divisome of *E. coli*. PG sacculus is elongates and divides controlled by the bacterial cytoskeleton and associate proteins of the elongasome and the divisome. In addition, elongasome and divisome are somehow involved in the elongation and division of the OM and the CM (Hugonnet *et al.*, 2016). 40

Figure 1.15. Antibiotics and their targets in the bacteria. 46

Figure 1.16. Main phyla and variability of bacterial microbiota in the different body sites and factors that alter microbiota populations. 51

Figure 1.17. Schematic view of the small intestine and the colon (Johansson and Hansson 2016)..... 53

Figure 1.18. Phylogenetic profiling of *Akkermansia muciniphila*. The numbers on the node indicate the percentage of statistical support for different nodes using neighbour-joining / maximum likelihood algorithms of Gupta, Bhandari, and Naushad 2012. 57

Figure 1.19. Phylogenetic profile of *Fusobacterium nucleatum*. Modified from Brennan and Garrett 2019..... 61

Figure 2.1.1. SDS-PAGE with silver staining 9 μL sample. **A.** *E. coli* LPS; Hot phenol/water extraction; **B.** Precipitate after enzymatic digestion of aqueous phase; **C.** Precipitate UC after enzymatic digestion of aqueous phase; **D.** Supernatant UC after enzymatic digestion of aqueous phase; **E.** Precipitate centrifuge after enzymatic digestion phenol phase; **F.** Precipitate UC after enzymatic digestion phenol phase; **G.** Supernatant UC after enzymatic digestion phenol phase. 69

Figure 2.1.2. Mild acid hydrolysis was performed on the full LOS of *A. muciniphila* Muc^T (16 mg) in order to separate the polysaccharidic chain from the lipid A. In the supernatant, mix of different polysaccharides was obtained and separated by HPLC (High Performance Liquid Chromatography system Agilent 1100 Phenomenex C18 Reversed Phase in

isocratic conditions; flow =0.8 mL/min and monitoring the eluate with a refractive index detector (206 nm). The HPLC resulted in a chromatogram with four differentiated peaks named from A to D. ¹H NMR experiments are presented in figure 2.1.3..... 70

Figure 2.1.3. ¹H NMR spectra recorded for the fractions obtained by purification by HPLC of the polysaccharidic mix resulting from the acid hydrolysis of the crude LOS of *A. muciniphila* Muc^T (600 MHz). A and C contained two different polysaccharides respectively, B a mix of the polysaccharides from fractions A and C. Finally, D, presented an impure mix. The polysaccharides A and C were a nonasaccharide (NONA) and a tetradecasaccharide (TETRA) respectively..... 71

Figure 2.1.4. Negative-ion MALDI-TOF mass spectrum of the a. nonasaccharide and the b. tetradecasaccharide of *A. muciniphila* Muc^T..... 71

Figure 2.1.5. Partially methylated alditol acetated method results of a. nonasaccharide and b. tetradecasaccharide fractions obtained by purification by HPLC of the polysaccharidic mix resulting from the acid hydrolysis of the crude LOS of *A. muciniphila* Muc^T..... 72

Figure 2.1.6. Expansion of HSQC spectrum recorded for NONA from *A. muciniphila* Muc^T (600 MHz, 32 °C). Grey densities correspond to “CH₂” carbons. The structure is reported in figure 2.1.11 and labels refer to table 2.1.1. 73

Figure 2.1.7. Expansion of TOCSY (black) and COSY (cyan/red) spectra of the NONA from *A. muciniphila* Muc^T (600 MHz, 32 °C). Labels refer to table 2.1.1. 76

Figure 2.1.8. Expansion of HMBC (black) and HSQC-TOCSY (red) spectra of the NONA from *A. muciniphila* Muc^T (600 MHz, 32 °C). Labels refer to table 2.1.1..... 76

Figure 2.1.9. Expansion of HMBC (black) and HSQC (blue) spectra of the NONA from *A. muciniphila* Muc^T (600 MHz, 32 °C). Labels refer to table 2.1.1. 78

Figure 2.1.10. Expansion of TROESY (black) and COSY (cyan/red) spectra of the NONA from *A. muciniphila* Muc^T (600 MHz, 32 °C). Labels refer to table 2.1.1..... 78

Figure 2.1.11. Structure of the NONA from *A. muciniphila* Muc^T using Symbol Nomenclature for Glycans (SNFG). Labels refer to table 2.1.1. 79

Figure 2.1.12. HSQC spectrum expansion of the TETRAD from *A. muciniphila* Muc^T (950 MHz, 27 °C) the structure is reported in figure 2.1.16. Labels refer to table 2.1.2.80

Figure 2.1.13. Expansion of TOCSY (black) and COSY (cyan/red) spectra of the TETRAD from *A. muciniphila* Muc^T (950 MHz, 27 °C). Labels refer to table 2.1.2..... 82

Figure 2.1.14. Expansion of HMBC (black), HSQC-TOCSY (blue) and HSQC (cyan) spectra of the TETRAD from *A. muciniphila* Muc^T (950 MHz, 27 °C). Labels refer to table 2.1.2. 83

Figure 2.1.15. Expansion of ROESY (black) and COSY (cyan/red) spectra of the TETRAD from *A. muciniphila* Muc^T (950 MHz, 27 °C). Labels refer to table 2.1.2..... 83

Figure 2.1.16. Structure of the TETRAD from *A. muciniphila* Muc^T using SNFG. Labels refer to table 2.1.2. 84

Figure 2.1.17. GC-MS profile of *A. muciniphila* Muc^T LOS lipid compositional analysis C16:0, C16:1 and C18:0 are impurities or cell derived fatty acids. 85

Figure 2.1.18. Negative ion MALDI mass spectrum of the lipid A from *A. muciniphila* Muc^T. Differences of 28 amu are reported in the spectrum. The families of lipid A species differing in the acylation degree were also indicated as “Hexa-acylated”, “Penta-acylated”, “Tetra-acylated” and “Tri-acylated”. P: phosphate group. The relevant ion peaks are described in the text and in table 2.1.3. 86

Figure 2.1.19. Negative ion MS/MS spectrum of *m/z* 1922.6 of the lipid from *A. muciniphila* Muc^T. This is a representative ion peak of the cluster ascribed to *bis-*

phosphorylated hexa-acylated lipid A species. The main fragments' assignment is indicated in the spectrum. The proposed structure is reported in the inset.	87
Figure 2.1.20. Reflectron negative ion spectrum of the NH ₄ OH-treated lipid A disclosing the location of the secondary acyl chains.	88
Figure 2.1.21. Proposed structure for the main <i>bis</i> -phosphorylated lipid A species of <i>A. muciniphila</i> Muc ^T . The absolute configuration of the primary acyl chains and the anomeric configuration of the two GlcN residues are based on literature data.	88
Figure 2.1.22. Positive mode ESI FT-ICR MS of de-acylated <i>A. muciniphila</i> MucT polysaccharide. The intact polysaccharide was not detected. Instead, the signals from intense protonated in-source fragment ions characterised the mass spectrum.	89
Figure 2.1.23. Preliminary results on the structure LOS of <i>A. muciniphila</i> MucT. The substitution pattern of the central Kdo remains to be disclosed.	91
Figure 2.1.24. Analysis of the immune activity of LOS, saccharide and lipid A of <i>A. muciniphila</i> Muc ^T on HEK-Blue hTLR4 and hTLR2 cells. NF-κB and AP-1 induced the production of SEAP, which was quantified spectrophotometrically. Bars represent the median values from 3 independent replicates.	92
Figure 2.2.1. A. Separation of muropeptides <i>A. muciniphila</i> Muc ^T . Muropeptides were released from PG by cellosyl, reduced using sodium borohydride, and separated by C ₁₈ reversed-phase HPLC. The interpretation of the labelled peaks is in table 2.2.1. B. MS spectrum of peak 3 corresponding to the de- <i>N</i> -acetylated Tetra-muropeptide.	97
Figure 2.3.1. On the left: electrophoresis analysis: A. <i>E. coli</i> O111:B4 LPS (8 μg). B. <i>F. nucleatum</i> ATCC 51191 LPS (8 μg) C. BlueEye protein standard. (12% SDS-PAGE and visualised by silver staining). On the right: GC-MS profile of <i>F. nucleatum</i> ATCC 51191 LPS: D. acetylated methyl glycosides, E. lipid compositional analysis. <i>i</i> : impurities; C16:1 and C18:0 are impurities or cell derived fatty acids.	101
Figure 2.3.2. ¹ H NMR spectrum (600 MHz) of the OPS of <i>F. nucleatum</i> ATCC 51191. The analysis was carried out at (a) neutral pH (550 μL D ₂ O, 25°C); (b) acid pH (550 μL D ₂ O + 4 μL of DCl conc, 37°C), and (c) alkaline pH (550 μL D ₂ O + 4 μL of NaOD 4 M, 25°C).	103
Figure 2.3.3. ¹ H, ¹³ C HSQC spectrum of the OPS of <i>F. nucleatum</i> ATCC 51191 (600 MHz, 25 °C, 550 μL of D ₂ O, neutral pH). P ₁ and P ₃ are not relevant signals related to minor species.	104
Figure 2.3.4. ¹ H TOCSY (red) and ¹ H NOESY (black) spectra of the OPS of <i>F. nucleatum</i> ATCC 51191 (600 MHz, 25 °C, 550 μL of D ₂ O, neutral pH).	107
Figure 2.3.5. On the left and middle part ¹ H TOCSY (red) and ¹ H NOESY (black) spectra, on the right ¹ H, ¹³ C HSQC at acid pH of the OPS of <i>F. nucleatum</i> ATCC 51191 (600 MHz, 37 °C, 550 μL D ₂ O + 4 μL of DCl conc). P ₁ and P ₃ are not relevant signals related to minor species.	109
Figure 2.3.6. Structure of the OPS isolated from <i>F. nucleatum</i> ATCC 51191. 4)-β-D-GlcpNAcA-(1-4)-β-D-GlcpNAc3NA1aA-(1-3)-α-D-FucpNAc4NR-(1-. R= Acetyl (60%). When R = Ac, residues are labelled A , B and C , when R = H residues are labelled A' , B' and C'	109
Figure 2.3.7. Negative-ion MALDI-TOF (reflectron mode) mass spectrum of the lipid A of <i>F. nucleatum</i> ATCC 51191. Differences of 28 amu are reported in the spectrum. The families of lipid A species differing in the acylation degree were also indicated as “Hexa-acylated”, “Penta-acylated” and “Tetra-acylated”. P: phosphate group.	111
Figure 2.3.8. Negative-ion MALDI MS/MS spectrum of precursor ion at <i>m/z</i> 1801.1 of the lipid A of <i>F. nucleatum</i> ATCC 51191. This is a representative ion peak of the cluster	

ascribed to hexa-acylated and *bis*-phosphorylated lipid A species. The main fragments are indicated in the spectrum. The proposed structure is reported in the inset. The loss of C₁₂H₂₄O (184 mass units) and C₁₄H₂₈O (212 mass units) indicated was due to a rearrangement on primary acyl chains when their 3-OH group is free, thus contributing to the establishment of the secondary acyl substitution. 112

Figure 2.3.9. Proposed structure for the main *bis*-phosphorylated hexa-acylated lipid A species of *F. nucleatum* ATCC 51191. The absolute configuration of the primary acyl chains and the anomeric configuration of the two GlcN residues are based on literature data. 113

Figure 2.3.10. Immunostimulation of monocyte-derived dendritic cells (moDCs) and monocyte-derived macrophages (moMφs) when exposed to the LPS of *F. nucleatum* ATCC 51191. Bars represent the median values from 3 replicates. 114

Figure 2.4.1. Response factor calculated for C14:0 versus C16:0 (in mol) (on the left) and C18:0 versus C16:0 (on the right). 118

Figure 2.4.2. Acetylated *O*-methyl glycosides results of the OMVs of *F. nucleatum* 10953, *F. nucleatum* 25586 and *F. nucleatum* 51191. QuiNAc: N-Acetyl-quinovosamine, Neu5Ac: N-Acetylneuraminic acid, Fuc2NAc4NAc: 2,4-diamino-fucose, GlcNAc3NAlaA: 2,3-diamino-3N-alanine-glucuronic acid, *i*: unknown. 120

Figure 2.4.3. Total fatty acid composition analysis by methanolysis of the OMVs of *Fusobacterium nucleatum* 10953, *F. nucleatum* 25586 and *F. nucleatum* 51191. 121

Figure 2.4.4. *F. nucleatum*-derived OMVs mediated moDC and moMφ cytokine induction. Bars represent the median values from 3 independent replicates. 124

Figure 2.4.5. *F. nucleatum* LPS mediated moDC and moMφ cytokine induction. Bars represent the median values from 3 independent replicates. 124

Figure 2.5.1. Separation of mucopeptides of *E. coli* D456 and *F. nucleatum* ATCC 511191 (first preparation). Mucopeptides were released from PG by cellosyl, reduced with sodium borohydride and separated by C₁₈ reversed-phase HPLC. 128

Figure 2.5.2. Separation of mucopeptides *F. nucleatum* ATCC 511191 (second preparation). Mucopeptides were released from PG by cellosyl, reduced using sodium borohydride, and separated by C₁₈ reversed-phase HPLC. The interpretation of the labelled peaks is in table 2.5.1. 128

Figure 2.6.1. Wild form LOS along with the structure of the glycan part. Dotted lines mean a not stoichiometric substitution. 135

Figure 2.6.2. SDS-PAGE profiles of *E. coli* mutants, as specify in the picture. Each sample is about 8 μg, 12% SDS-PAGE and visualised by silver staining. 136

Figure 2.6.3. Monosaccharide of *E. coli* K12 WT. Rhamnose (Rha), mannose (Man), galactose (Gal), glucose (Glc), glucosamine (GlcN), L-*glycero*-D-*manno*-Heptose (Hep), 3-deoxy-D-*manno*-octulosonic acid (Kdo), impurities (*i*). 137

Figure 2.6.4. Monosaccharide composition of *E. coli* WT and mutants. Areas are normalised with respect to that of Glc and are not corrected with a response factor. 137

Figure 2.6.5. Monosaccharide percentual area of *E. coli* WT and of its mutants. 138

Figure 2.6.6. ¹H NMR profile of the oligosaccharides derived from mild acid hydrolysis of the LOS (600 MHz, 25 °C, 550 μL D₂O). 139

Figure 2.6.7. Chromatogram of the fatty acid compositional analysis. The colour code corresponds to: **Green**: fatty acids that belong to the lipid A; **Blue**: fatty acids that probably belong to the lipid A; and, **Red**: fatty acids from phospholipids. 140

Figure 2.6.8. Fatty acids composition of *E. coli* WT and of its mutants. Areas were normalised with respect to that of C14:0 and not corrected with a response factor. 141

Figure 2.6.9. Fatty acids percentual area of <i>E. coli</i> WT and of its mutants.	141
Figure 2.6.10. MALDI spectra in negative mode measured for the different lipid As. In the short notation reported for the WT, the presence of two GlcN units is omitted.	143
Figure 2.7.1. LOS derived molecules to be used as substrate for the introduction of active nuclei. A. LOS from <i>E. coli</i> K12. B. Fully de-acylated LOS from <i>E. coli</i> K12. C. Fully de-acylated lipid A from <i>E. coli</i> K12.	145
Figure 2.7.2. A. Acetylated methyl glycosides (AMG) of the crude LOS of <i>E. coli</i> K12. B. Fatty acid analysis of the crude LOS of <i>E. coli</i> K12. <i>i.</i> : impurities.	146
Figure 2.7.3. ¹ H NMR of the DODN-LOS of <i>E. coli</i> K12 after purification by chromatography (600 MHz, 25 °C).....	147
Figure 2.7.4. ¹ H NMR and ¹ H, ¹³ C HSQC spectra of the DODN-lipid A of <i>E. coli</i> K12 (600 MHz, 25 °C, 550 μL D ₂ O).....	148
Figure 2.7.5. MALDI-TOF-TOF and MS/MS in negative polarity of the DODN-lipid A obtained from <i>E. coli</i> K12.	149
Figure 2.7.6 a. ¹⁹ F-NMR of the N,N'-difluoropropanoyl-DODN-lipid A (700 MHz, 27 °C, 550 μL D ₂ O). b. ¹ H NMR and ¹ H, ¹ H COSY dqf of N,N'-difluoropropanoyl-DODN-lipid A (positive red, negative green) (600 MHz, 27 °C, 550 μL D ₂ O). c. ¹ H NMR and ¹ H, ¹³ C HSQC of the N,N'-difluoropropanoyl-DODN-lipid A extension of the dicyclohexylisourea (850 MHz, 27 °C, 550 μL D ₂ O). d. ¹ H NMR and ¹ H, ¹³ C HSQC of the DODN-Lipid A of <i>E. coli</i> K12 (black) N,N'-difluoropropanoyl-DODN-lipid A (red) (850 MHz, 27 °C, 550 μL D ₂ O).....	150
Figure 2.7.7. ¹ H NMR and ¹ H, ¹³ C HSQC of the DODN-lipid A (black) and the N,N'-doxyl stearate-DODN-lipid A after ascorbate treatment (red) (850 MHz, 27 °C).....	151
Figure 2.8.1. HPLC chromatogram of the activity test of the amidases AmiA, AmiB and AmiC with amidase regulators or LptAHis or LptAmHis. Muropeptides: a. Tetra, b. Tetratetra. c and d are amidase products.	155
Figure 2.8.2. Electrophoresis of the <i>in-vitro</i> pull-down assay. (12% acrylamide, 5 μl marker, 10 μl sample, preheated 10 min 100 °C, 120 V, Coomassie staining). A. LptAHis with YgeR or NlpD and LptAmHis with YgeR or NlpD. The no visualisation of YgeR nor NlpD in fraction E evidences that no interaction occurs. B. Control: LptAHis, LptAmHis, YgeR and NlpD separately. LptAHis and LptAmHis bind the Ni ²⁺ -NTA beads thanks to the His-tag but not YgeR nor NlpD. M: Protein marker PageRuler™; A: Applied fraction; E: eluate.	156
Figure 3.1. Summary findings on the LOS and PG of <i>A. muciniphila</i> Muc ^T	161
Figure 3.2. Summary findings on the LPS and PG of <i>F. nucleatum</i> ATCC 51191.	163
Figure 3.3. Study of the trans-envelope machineries. From left to right: Mutations in BAM do not alter LOS composition; LptA do not act as amidase regulator nor interact with the tested amidase regulators; and the first attempts for the development of a semi-synthetic lipid A with active nuclei were performed.	164
Figure 4.1. Schematic view of the techniques used for the LPS structural characterisation.	174
Figure 4.2. Reaction mechanism of the amidation of the DODN-lipid A using the DCC and 3-fluoropropanoyl chloride in pyridine, argon and DMF.....	179

List of Tables

Table 1.1. Specificity of the receptors involved in LPS recognition: toll-like receptor 4 (TLR4), toll-like receptor 2 (TLR2), C-type lectins receptor (CLR), the transient receptor potential (TRP) channel, some caspases, the complement and antibodies.	12
Table 1.2. Specificity of the receptors involved in PG recognition: nucleotide oligomerisation domain proteins (NOD-1 and NOD-2), peptidoglycan recognition proteins (PGRP1, PGRP2, PGRP3, PGRP4) and the C-type lectins regenerating gene family protein III (RegIII) and mannose binding lectin (MBL).....	31
Table 1.3. Antibiotics that target OM building machineries.	49
Table 1.4. Isolation sites of <i>A. muciniphila</i> in the digestive track. Modified from Geerlings et al 2018.....	58
Table 2.1.1. Proton (¹ H) (plain text) and carbon (¹³ C) (<i>italic</i>) NMR chemical shifts of the NONA polysaccharide from <i>A. muciniphila</i> Muc ^T (600 MHz, 32 °C, D ₂ O).....	75
Table 2.1.2. Proton (¹ H) (plain text) and carbon (¹³ C) (<i>italic</i>) NMR chemical shifts of the TETRAD polysaccharide from <i>A. muciniphila</i> Muc ^T (950 MHz, 27 °C, D ₂ O).....	81
Table 2.1.3. The main MALDI-TOF MS ion peaks <i>A. muciniphila</i> Muc ^T lipid A. Report of the predicted mass and the proposed interpretation of the substituting fatty acids and phosphates on the lipid A backbone. <i>See</i> figure 2.1.18 for full spectrum.....	86
Table 2.2.1. Reduced muropeptides detected in <i>A. muciniphila</i> Muc ^T . Peak numbers refer to the labels of figure 2.2.1.....	97
Table 2.2.2. Summary of the results of the alignment search between <i>Akkermansia muciniphila</i> Muc ^T (taxid: 349741) and PG modifying enzymes of different microorganism.....	99
Table 2.3.1. Proton (¹ H) and carbon (¹³ C) (<i>italic</i>) NMR chemical shifts of the OPS of <i>F. nucleatum</i> ATCC 51191 (600 MHz, 25 °C, 550 μL of D ₂ O, neutral pH). The chemical shifts of the methyl protons belonging to the N-acetyl groups resonated at about ¹ H 2.1-1.8 ppm.....	105
Table 2.3.2. Proton (¹ H) and carbon (¹³ C) (<i>italic</i>) NMR chemical shifts of the OPS of <i>F. nucleatum</i> ATCC 51191(600 MHz, 37 °C, 550 μL D ₂ O + 4 μL of DCl conc).	110
Table 2.3.3. The main MALDI-TOF MS ion peaks <i>F. nucleatum</i> ATCC 51191 lipid A. Report of the predicted mass and the proposed interpretation of the substituting fatty acids and phosphates on the <i>F. nucleatum</i> ATCC 51191 lipid A backbone. <i>See</i> figure III.3.6 for full spectrum.....	113
Table 2.4.1. Fatty acids methylesters of OMVs.	122
Table 2.5.1. Reduced muropeptides detected in <i>F. nucleatum</i> ATCC 51191. Peak numbers refer to the labels of figure 2.5.2.	129
Table 2.7.1. Proton (¹ H) (plain text) and carbon (¹³ C) (<i>italic</i>) NMR chemical shifts of the DODN-lipid A of <i>E. coli</i> K12 (600 MHz, 25 °C, 550 μL D ₂ O).	148

Chapter 1

Introduction

1.1. Cell surface of Gram-negative and Gram-positive bacteria

The cell envelope is a dynamic and complex structure that protects bacteria from the surrounding environment. The bacterial surface is critical to determine the interactions with the environment (Persat *et al.*, 2015). Many microbial-associated molecular patterns (MAMPs) are located in the bacterial surface such as lipopolysaccharide (LPS), peptidoglycan (PG), lipoteichoic acids and lipoproteins. The MAMPs are distinct, evolutionarily conserved and essential chemical signatures of pathogens that can be detected by host pattern recognition receptors (PRRs) and trigger an innate immunity response (Mogensen 2009).

Bacteria can be classified into two main groups depending on the chemical composition of their cell envelopes: Gram-positive and Gram-negative. The name allude to the capacity of retain or not the crystal violet when stained (Coico 2005).

Gram-positive bacteria possess a cytoplasmic membrane (CM) that is surrounded by a thick layer of PG (30 - 100 nm). Within the PG layer, there are teichoic acids and lipoteichoic acids. Teichoic acids are polyalcohols composed by ribitol, glycerol and phosphates that are covalently bound to the PG. Conversely, when teichoic acids are covalently bound to the lipids of the CM, they are called lipoteichoic acids (Rajagopal and Walker 2017) (Fig.1.1).

Gram-negative bacteria are distinguished for their extra membrane, the outer membrane (OM) that surrounds a thin PG layer (2 - 8 nm) and the CM or inner membrane (Konovalova, Kahne, and Silhavy 2017; Simpson *et al.*, 2015) (Fig.1.1). The space between the CM and the OM is known as periplasm. The periplasmic width is approximately 21 nm in *Escherichia coli* (Matias *et al.*, 2003). The periplasm is a gel-like compartment that provides stability to the cell envelope (Hobot *et al.*, 1984). Numerous important functions are contained within the periplasm such as PG synthesis, cell division, envelope stress responses, export machineries to the OM, etc (Miller and Salama 2018).

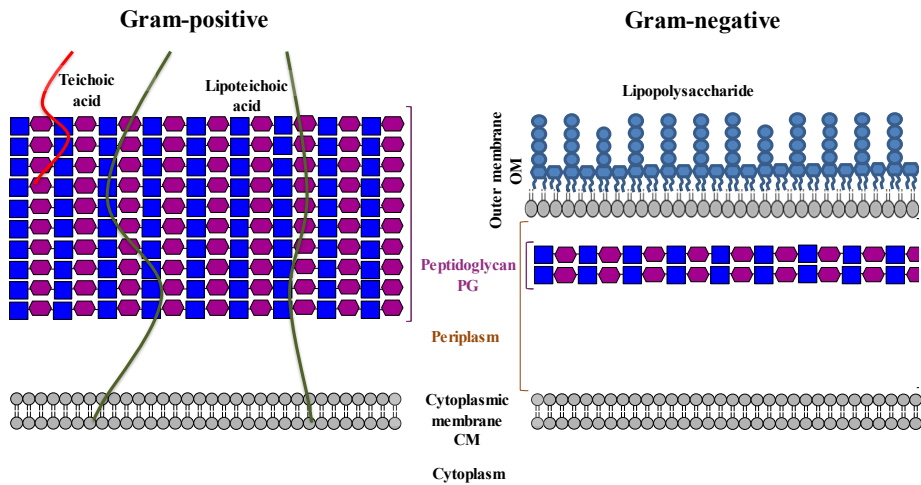


Figure 1.1. Gram-positive and Gram-negative cell envelope. Gram-positive bacteria possess a cytoplasmic membrane (CM) that is protected by a thick layer of peptidoglycan (PG). The PG is characterised by the presence of teichoic acids and lipoteichoic acids. Gram-negative bacteria are distinguished for their extra hydrophobic membrane layer, the outer membrane (OM) that covers a thin PG layer and the CM. The space between the CM and the OM is known as periplasm.

However, not all bacteria fit into the Gram-negative or Gram-positive classification. Some families such as *Mycobacteriaceae* have a unique cell envelope structure and are classified as acid fast (Kenneth and Ray 2004).

1.2. The Gram-negative bacteria cell envelope

The CM and OM have different composition and permeability properties. The CM is a symmetric lipid bilayer composed mainly by phospholipids and it is very permeable to small hydrophobic molecules. In *E. coli* the principal phospholipids of the CM are phosphatidyl ethanolamine and phosphatidyl glycerol, and in lesser amounts phosphatidyl serine and cardiolipin. In addition, the und-P, the ubiquitous lipid carrier of bacterial cell wall precursors, is synthesised in the CM by undecaprenyl pyrophosphate synthase and undecaprenyl pyrophosphate phosphatase (Silhavy, Kahne, and Walker 2010). The OM is an asymmetric bilayer whose outer leaflet is mainly composed by LPSs and the inner leaflet by phospholipids. The OM is permeable to small hydrophilic compounds and acts as a selective barrier that allows interaction with the environment and material exchange. The different permeability properties of the CM and the OM protect the cell from numerous harmful compounds and makes antibiotics development against Gram-negative bacteria especially difficult (Konovalova, Kahne, and Silhavy 2017; Simpson *et al.*, 2015).

Gram-negative bacteria can selectively uptake nutrients and secrete compounds to the media like toxins. These actions are mediated by the OM proteins (OMPs), that are not only involved in the uptake and secretion of compounds, but also, in the building and maintenance of the OM itself. OMPs are mainly β -barrel proteins and lipoproteins. β -barrel proteins straddle the OM while lipoproteins are located in its inner leaflet (Silhavy, Kahne, and Walker 2010). None of the constituents of the OM is synthesised *in situ*.

The LPS is synthesised on the inner leaflet of the CM and transported to the OM by the lipopolysaccharide transport proteins named Lpt A-G (Fig.1.2) (*see* 1.3.3.2 LPS transport system to the OM) (Bishop 2019; Okuda *et al.*, 2016). Phospholipids are synthesised in the CM. Although it is known that there is an equilibrium of their amount between CM and OM (Jones and Osborn 1977), the

transport system of phospholipids is not fully understood yet as many systems seem to be implicated, like the members of the mammalian cell entry (MCE) protein family (MlaD, YebT, PqiB and LetB). MlaD is part of the maintenance of lipid asymmetry complex (Mla) which imports phospholipids extracted from the OM (Fig.1.2) (Ekiert *et al.*, 2017). YebT, PqiB and LetB form continuous central hydrophobic tunnels of hexameric rings stacked together to transport phospholipids from the CM to the OM and may be bidirectional. YebT and PqiB are part of bigger transport systems the YebST complex and PqiABC complex respectively (Fig.1.2) (Isom *et al.*, 2020; Liu *et al.*, 2020; Ekiert *et al.*, 2017).

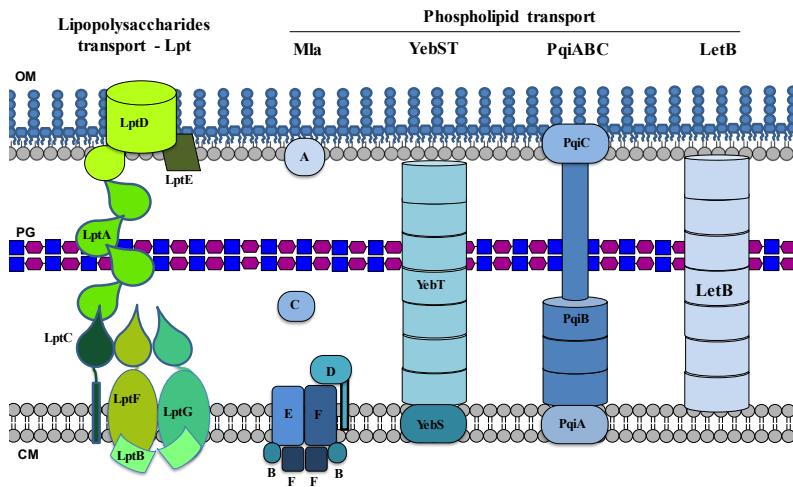


Figure 1.2. From left to right: LPS transport machinery Lpt and Phospholipid transport machineries with MCE proteins (Mla, YebST, PqiABC and LetB) and Tol-Pal system for the retrograde transport of phospholipids and PbgA cardiolipin transporter.

Tol-Pal complex seems to be required in *E. coli* for the retrograde transport of phospholipids (Shrivastava, Jiang, and Chng 2017). The Tol-Pal system is composed by TolQ, TolR, TolA (TolQRA), TolB and Pal. TolQ, TolR and TolA are located in the CM. TolB, is in the periplasm and Pal is a PG-binding OM lipoprotein (Fig.1.2) (Egan 2018). Also PbgA is involved as cardiolipin transporter from the CM to the OM (Fig.1.2) (Dong *et al.*, 2016). Another system implicated is the Lpt OM phospholipase PldA that degrades surface phospholipids

and acts as a sensor of phospholipid accumulation in the outer leaflet of the OM. This triggers a cascade to increase LPS production to maintain OM asymmetry (Fig.1.2) (May and Silhavy 2018).

All proteins are synthesised by the ribosomes that are located in the cytoplasm. Therefore, transport machineries are necessary to place CM, periplasmic and OM proteins in their final locations (Dalbey and Kuhn 2012). Proteins are transported across the CM by two major pathways: the general Secretion route (Sec-pathway) to transport unfolded proteins and insert membrane proteins into the CM, and, the Twin-arginine translocation pathway (Tat-pathway) for folded proteins (Natale *et al.*, 2008). Transported across the OM occurs by type 1-6 protein secretion systems (T1SS, T2SS, T3SS T4SS, T5SS, T6SS) (Green and Mecsas 2016).

β -barrel proteins, like LptD or OmpA, are transported by a combination of Sec and T5SS systems (Okuda *et al.*, 2016). The T5SS that transports β -barrel proteins is comprised of Skp, SurA, DegP and the BAM complex (Leo *et al.*, 2012). First, the Sec translocon moves the β -barrel proteins across the CM by interacting with their N-terminal leader sequence. Subsequently, chaperones Skp and SurA transport them across the periplasm to the BAM (β -barrel assembly machinery) complex, which folds and inserts them in the OM. The BAM complex consists of four lipoproteins BamB, BamC, BamD, BamE and one OMP named BamA (Fig.1.3) (Noinaj *et al.*, 2017). DegP can also act as a chaperone, it switches between a chaperone and a protease function in a temperature dependent manner (Sklar *et al.*, 2007). Lipoproteins, like LptE or Braun's lipoprotein, are transported by a combination of Sec and Lol systems (Okuda *et al.*, 2016). Braun's lipoprotein (Lpp) is anchored in the OM at its N-terminus and the PG at its C-terminus, stabilizing the cell envelope (Boags *et al.*, 2019). The Lol system is composed by the periplasmic chaperone LolA, the OM receptor LolB and the ATP-binding cassette LolCDE (Fig.1.3). First, the LolCDE translocate the

lipoproteins in the CM. Subsequently, LolA transports them to LolB which localised the lipoproteins in the OM (Tokuda and Matsuyama 2004).

The OM integrity is regulated by different response systems. In *E. coli* and other Enterobacteria, the σ^E -dependent envelope stress response prevents misfolded OMPs accumulation (Lima *et al.*, 2013). In normal conditions, RseA binds to σ^E in the CM, avoiding its association with RNA polymerase. In the presence of misfolded OMPs, RseA is degraded and σ^E drives to the transcription of proteases (that degrade misfolded OMPs) and chaperones and assembly factors (that repair the OM). σ^E also blocks the transcription of many OMPs (Nicoloff *et al.*, 2017).

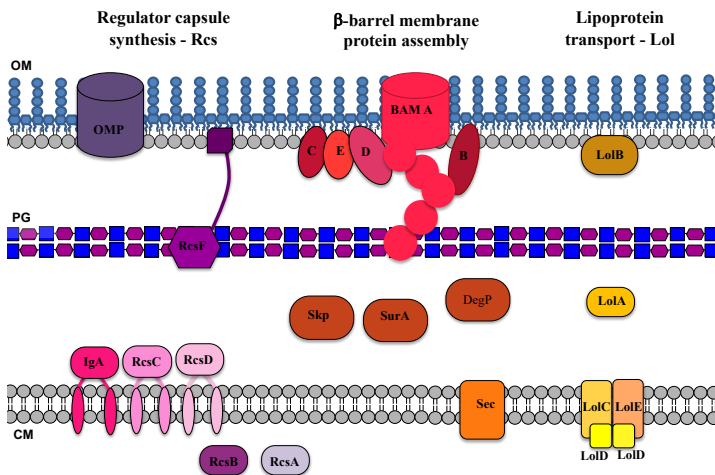


Figure 1.3. From left to right: regulator of capsule synthesis (Rcs), β-barrel membrane protein assembly (BAM) and Lol lipoprotein transport complex.

Also, in Enterobacteria, the regulator of capsule synthesis (Rcs) system monitors the integrity of the OM (Fig.1.3). RcsF is a sensor that detects defects on OM. Under normal conditions, RcsF interacts with BamA which funnels RcsF into OMPs such β-barrel OmpA to keep it inactivated (Rodríguez-Alonso *et al.*, 2020). If BamA is altered RcsF remains free to interact to IgaA (Cho *et al.*, 2014). Then IgaA starts the cascade RcsC, D and B by a multi-step phosphorelay (Hussein *et al.*, 2018). RcsB alone or with RcsA activates capsule synthesis, limits cell motility and activates transcription of other genes (Wall *et al.*, 2018).

1.3. Lipopolysaccharide

The lipopolysaccharide (LPS) is the main component of the external leaflet of the OM (*E. coli* cell possesses 2×10^6 LPS molecules) (Whitfield and Trent 2014). It gives stability to the OM and protection from the environment. As well, LPSs are virulence factors that contribute to bacterial induced pathologies and gut microbiota beneficial effects.

1.3.1. Structure of LPS

LPS are complex structures composed by carbohydrates and lipids. Furthermore, they are structurally divided in three moieties: the lipid A, the core oligosaccharide and O-polysaccharide (OPS or O-antigen) (Fig.1.4).

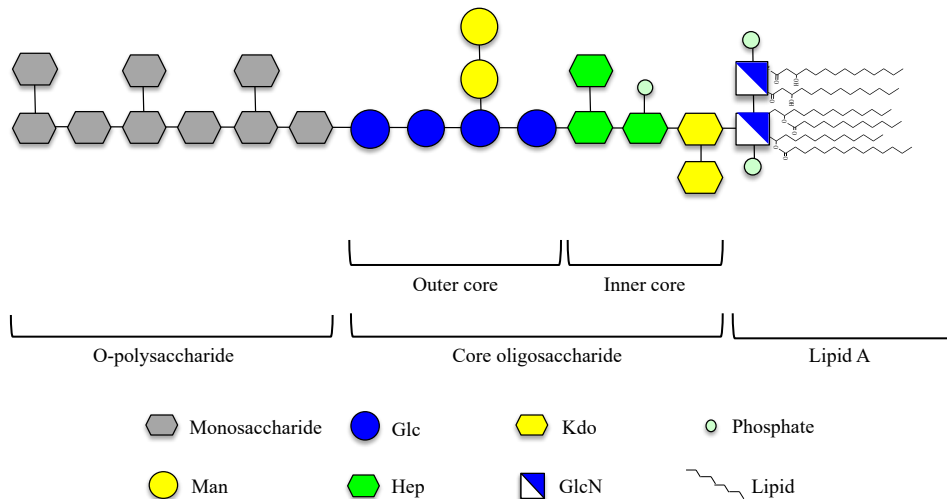


Figure 1.4. Lipopolysaccharide schematic representation. LPS are complex glycoconjugates structurally divided in the lipid A, the core oligosaccharide and O-polysaccharide (or O-antigen).

1.3.1.1. Lipid A

The lipid A is the hydrophobic anchor to the OM of the LPS whose architecture is very preserved amongst species. Generally, the lipid A is composed by a β -(1 \rightarrow 6)-linked glucosamine disaccharide with different levels of phosphorylation and acylation with saturated and unsaturated fatty acid chains (Molinaro *et al.*, 2015). Phosphorylation usually occurs at position O-1 of the reducing GlcN (GlcN I) and position O-4' of the non-reducing GlcN (GlcN II). Therefore, the general lipid A backbone is [P \rightarrow 4- β -D-GlcpN-(1 \rightarrow 6)- α -D-GlcpN-1 \rightarrow P] (Fig.1.5) (Raetz 1990). The compositional modifications of the lipid A include the replacement of the GlcN disaccharide of the lipid A by 2,3-diamino-2,3-dideoxy-D-Glc (GlcN3N) disaccharide (Plötz *et al.*, 2000).

The phosphate groups can be absent or further substituted. For example, phosphate groups can be replaced by mannose (Schwudke *et al.*, 2003) or D-galacturonic acid (Plötz *et al.*, 2000) to neutralize the negative charges of the lipid A which reduces LPS affinity for cationic peptides. Phosphates can also be further decorated with 4-amino-4-deoxy-L-arabinose (Ara4N) (Zhou *et al.*, 2001), 2-amino-ethyl phosphate (PEtN) (Zhou *et al.*, 2001) or by further phosphate groups generating a pyrophosphoryl moiety (Lamarche *et al.*, 2008). Some of these substituents such as Ara4N and PEtN neutralize the negative charges of the lipid A phosphate groups. Likewise, phosphates neutralisation alters lipid A immune recognition (Kong *et al.*, 2012).

The number, length, type, distribution and symmetry of acyl chains depends on the single lipid A species and have great consequences on the OM fluidity as it changes the hydrophobicity and van der Waals interactions (Anandan and Vrielink 2020). The removal, addition or branching of one acyl chain favours the evasion from the host immune system (Kawasaki, Ernst, and Miller 2004). In addition, the acyl chains of the lipid A can be hydroxylated. For example, in *Acinetobacter baumannii* the 2-hydroxylation of the lauric acid (C12:0 2-OH)

protects the cell from polymyxin B, colistin, human β -defensin 3 and antimicrobial peptides. It is also important for immune evasion as it mitigates inflammation (Bartholomew *et al.*, 2019).

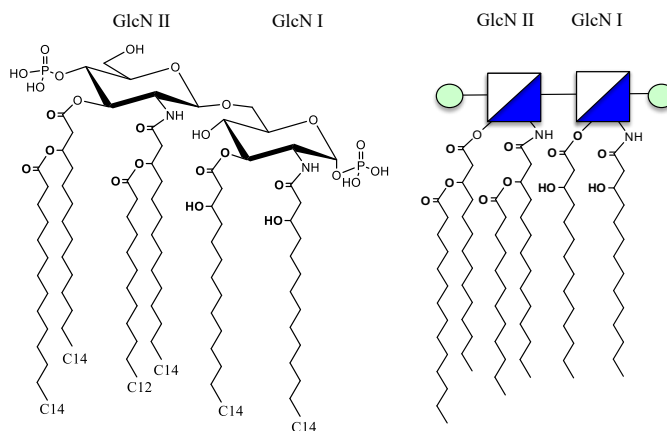


Figure 1.5. Lipid A of *E. coli* with the backbone [P \rightarrow 4- β -D-GlcpN-(1 \rightarrow 6)- α -D-GlcpN-1 \rightarrow P], hexa-acylated (4+2 pattern). GlcNI: reducing α -D-glucosamine; GlcN II non-reducing β -D-glucosamine.

1.3.1.2. Core oligosaccharide

The core oligosaccharide is a hydrophilic part that usually contains between 6 and 10 monosaccharides and can be further substituted with other residues in stoichiometric or non-stoichiometric fashion (Silipo and Molinaro 2010). It is divided into the inner and the outer core.

The inner core is usually composed by various *L-glycero-D-manno*-heptopyranones (Hep) and two or more 3-deoxy-*D-manno*-oct-2-ulosonic acids (Kdo) that link the core to the lipid A (Fig.1.6). Some species contain *D-glycero-D-manno*-heptose as well (Zych and Sidorczyk 1989) or *D-glycero-D-talo*-oct-2-ulosonic acid (Ko) instead of Kdo (Kawahara *et al.*, 1987). It can also be decorated, especially on the Hep which can contain phosphate, pyrophosphate, PEtN, Ara4N, uronic acids or amino acids such as glycine that neutralize the negative charge of the lipid A (Holst and Molinaro 2010; Holst 2002). The outer

core has higher structural variability among species, being mainly composed by hexoses and hexosamines often branched (Erridge *et al.*, 2002).

Hep and Kdo are present in almost all cores and are exclusive components of LPS. They have a very distinctive structure and produce a very characteristic fragmentation pattern when studied by Mass Spectrometry (Lam *et al.*, 2014; Gronow *et al.*, 2010). This can be used as an indication of the presence of LPS in a sample.

1.3.1.3. O-polysaccharide

The O-polysaccharide (OPS) or O-antigen constitutes the outermost part of the LPS and helps the bacterium to resist antimicrobials (Nikaido 1976), cleavage by the immune system (Najdenski *et al.*, 2003) and environmental stress (Yan *et al.*, 2012). It is also important for biofilm formation (Yan *et al.*, 2012), colonisation (Edwards *et al.*, 2000) and adaptation to the environment (Tao *et al.*, 1992).

The LPS that contains OPS is known as “smooth LPS”, but not all Gram-negative bacteria possess OPS, some LPS consist exclusively of the core oligosaccharide and lipid A. When the OPS is missing, the LPS is called lipooligosaccharide (LOS) or R (rough)-form LPS because of the appearance of the colony grown on a solid medium. A minimal LOS (lipid A and Kdo) is required for *E. coli*'s viability, in laboratory conditions (Raetz and Whitfield 2002).

The OPS is composed by 1 - 40 repeating units each made of up to nine different monosaccharides, so the final size of the OPS can be up to one hundred sugars. The OPS structures thus differ in terms of monosaccharides composition and connection mode, and are used to classify as serotypes, bacteria of the same species, where the differences sometimes are related to just small variations of the biosynthetic pathway (Whitfield *et al.*, 2020; De Castro *et al.*, 2010). Some unique monosaccharides have been described in OPS like abequose, colitose,

paratose or tyvelose among many others (Silipo *et al.*, 2014; Lerouge and Vanderleyden 2002; Gamian *et al.*, 2000; Tuffal *et al.*, 1998). The most common arrangement of sugar residues is the cyclic form, however, residues in the open form have been described as well (Vinogradov and Sidorczyk 2001). In addition, non-carbohydrate substituents are often present such as phosphate, amino acids, sulphate, methyl, acetyl, or formamide groups (Komandrova *et al.*, 2010; Muldoon *et al.*, 2001; Gamian *et al.*, 2000; Adinolfi *et al.*, 1996). Each small difference in composition has great consequences on the chemical properties of the sugar chain. Therefore, the detailed characterisation of the number of carbon atoms, aldose or ketose nature; stereochemistry; absolute configuration (D or L); anomeric centre (α or β); cyclic or open form; neutral, acidic and basic nature; number of hydroxyl groups replaced with a hydrogen atom (deoxy, dideoxy, etc.) or by other groups (amino functions, acid groups, etc.); decorations of the hydroxyl or other groups (acetylated, phosphate linked, amino acid linked, etc.), the specific attachment site, the linear or branched nature of the polysaccharide and the number of repeating units is fundamental in the study of its properties.

1.3.2. Host immune response to LPS

LPSs are surface components that play a crucial role in the host-pathogen relation, as well as in symbiont interactions. LPS is a MAMP that can be recognised and bound by various receptors: toll-like receptor 4 (TLR4), TLR2, the transient receptor potential (TRP) channel, some caspases, C-type lectins receptor (CLR) and the complement, as well as generate antibodies production. Immune recognition causes inflammation, fever and the activation of the adaptive immunity depending on the LPS structure (Park and Lee 2013; Raetz and Whitfield 2002). LPSs is located in the bacterial surface or secreted in the medium in the so-called outer membrane vesicles (OMVs) (Li *et al.*, 2020) and may be freely liberated into the medium, as well as their fragments.

Table 1.1. Specificity of the receptors involved in LPS recognition: toll-like receptor 4 (TLR4), toll-like receptor 2 (TLR2), C-type lectins receptor (CLR), the transient receptor potential (TRP) channel, some caspases, the complement and antibodies.

Receptor	Ligand
TLR4	Lipid A
TLR2	To be disclosed
TRP channel	Lipid A
Caspases	Lipid A
CLR	Polysaccharides
Complement	Polysaccharides
Antibodies	O-polysaccharide specificity

TLR4 is a pattern recognition receptor (PRR) of the mammal innate immune system. In humans, TLR4 are expressed in the surface of peripheral blood lymphocytes, myeloid subsets, monocytes, macrophages, granulocytes, dendritic cells, adipocytes, microglia, astrocytes, dermal micro-vessel endothelium, umbilical vein endothelium, brain endothelial cell line, small intestine, colon,

ileum, kidney, liver, lung, pancreas and placenta among others (Vaure and Liu 2014). LPS recognition activates macrophages and the production of pro-inflammatory cytokines. A LPS molecule is first recognised and recruited by the LPS-binding protein (LBP) which presents it to the CD14 receptor, and then carries it to the TLR4/MD-2 complex which dimerizes. The dimerisation of the TLR4 drives a cytoplasmic cascade that leads to the transcription of the nuclear factor- κ B, mitogen-activated protein kinase, pro-inflammatory cytokines and induction of interferon regulatory factor 3 and interferon-1 (Mazgaen and Gurung 2020; Vaure and Liu 2014). However, it is interesting to note that in physiological conditions low levels of LPS are removed from the blood to limit inflammatory responses (Mazgaen and Gurung 2020). TLR4 recognizes the LPS through the lipid A in a structure-dependent manner, determined by the phosphorylation and acylation patterns. It was demonstrated that the phosphate is essential for the homo-dimerisation of the TLR4/MD-2 complexes (Molinaro *et al.*, 2015). As well, inclination of the glucosamine disaccharide with respect to the membrane surface or tilt angle is a key factor for immune recognition. The larger the tilt angle, the more endotoxic the lipid A is. The differences in conformation alter the tilt angle and therefore the immune recognition. The *bis*-phosphorylated hexa-acylated lipid A specie with a 4 + 2 distribution of the acyl chains (*E. coli* like) (Fig.1.6) is, indeed, highly immunostimulatory, as its tilt angle is higher than 50°. Its recognition and the following downstream cascade can lead to sepsis. Some lipid A are agonists of TLR4/MD-2 complex and some are partially agonists or antagonists (Seydel *et al.*, 2000). This feature has been used for the development lipid A derivatives that can induce moderate immune responses as vaccine adjuvants like the monophosphoryl lipid A (Garcia-Vello *et al.*, 2020) or that limit the inflammatory effect of LPS during sepsis such as Eritoran (Opal *et al.*, 2013).

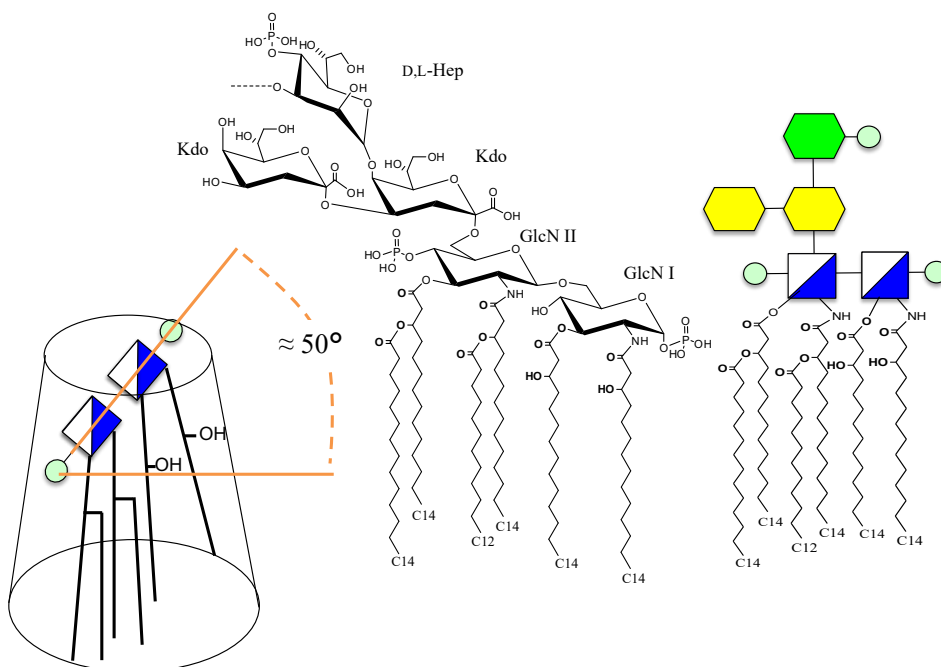


Figure 1.6. Structure of the lipid A and part of the inner core of *E. coli*. The differences in conformation alter the inclination of the glucosamine disaccharide with respect to the membrane surface or tilt angle. The larger tilt angle, the more endotoxic the lipid A is. *E. coli*'s lipid A is very endotoxic, as it is bis-phosphorylated and asymmetrically hexa-acylated, producing a tilt angle bigger than 50°. Modified from Seydel *et al.*, 2000.

Kdo and Hep residues also physically bind TLR4. Their presence in the LPS increases the affinity for the receptor and the inflammatory responses, although they are not essential for the recognition (Cochet and Peri 2017). Monosaccharides decorating the lipid A, such as Ara4N, can also be involved in the interaction (Di Lorenzo *et al.*, 2015).

It has recently been demonstrated that some atypical LPS can also activate TLR2, with a synergic effect with the TLR4 for the production of nuclear factor- κ B. The activation of TLR2 seem to be fundamental for the colonisation of the gut microbiota (Di Lorenzo *et al.*, 2020; Chavarría-Velázquez *et al.*, 2018).

Less studied, the TRP channels and caspases also recognize the lipid A. TRP channels are present in sensory neurons and epithelial cells and they recognize

the lipid A of extracellular LPS. LPS recognition produces calcium influx that leads to neuron activation and the release of signalling peptides that generate pain during inflammation or nitric oxide production in the airways to easy bacteria elimination (Mazgaen and Gurung 2020; Meseguer *et al.*, 2014). Human caspases 4 and 5 are the only known receptors to recognize lipid A in the cytoplasm. However, the mechanisms of LPS internalisation in monocytes remain unclear (Viganò *et al.*, 2015).

Lipid A recognition by the innate immune system can be prevented by the OPS. Not only by physically covering the lipid A, but also, by the molecular mimicry with which OPS resemble host antigens (Moran *et al.*, 1996). However, a particular OPS can stimulate the production of specific antibodies or the complement of the adaptative immune system (serovar-specificity) (Raetz and Whitfield 2002; Erridge *et al.*, 2002). When complement recognition happens in the tips of the OPS, and the polysaccharide chain is very long, lysis of the bacteria is not possible. The modifications on the OPS increase the potential virulence of the bacteria as it helps avoiding the immune system (Liang-Takasaki *et al.*, 1982). However, the capacity of some OPS to stimulate specific and memory immunity is used for vaccines production (Stefanetti *et al.*, 2019).

C-type lectin-like receptor (CLR) is a group of PRRs of the innate immune system. CLR can recognize many microbial polysaccharides, mainly by their mannose, fucose and glucose. This way, CLR internalizes the microbial polysaccharides and present them to the T-cells (van Kooyk and Rabinovich 2008). There are numerous CLR, some of which recognize LPS, like the macrophage-inducible C-type lectin (MINCLE). MINCLE strongly binds LPS inducing cytokines production; as well, it is implicated in the downregulation of the TLR4 and recognizes changes in the microbiota (Patin *et al.*, 2017; Matsumoto *et al.*, 1999). Also, the C-type lectin DC-SIGN on human dendritic cells (DC) recognize the polysaccharidic part of LPS producing DC maturation,

cytokines and T-cell polarisation (Van Vliet *et al.*, 2009). The C-type lectin SIGNR1 on macrophages stimulates cytokine production and TLR4 oligomerisation (Nagaoka *et al.*, 2005). In addition, Galactose-Type Lectin can recognize the outer core of *E. coli* (Maalej *et al.*, 2019) and of *Neisseria gonorrhoea* (Van Vliet *et al.*, 2009). Finally, sialic acid-binding immunoglobulin-like lectins (Siglecs) are a large family of lectins found on innate immune cells and tumour-infiltrating T cells, which inhibit immune activation after sensing sialic acid-containing glycans (Crocker, Paulson, and Varki 2007). Several pathogens have evolved molecular mimicry by displaying sialylated structures on their surface like *Campylobacter jejuni* strains can interact with Siglec-7 and Siglec-1 *via* their LOS (Heikema *et al.*, 2010) and to Siglec-10 *via* a sialic acid-like molecule, pseudaminic acid, of flagella (Stephenson *et al.*, 2014).

1.3.3. LPS building machineries

LPS are present in the outer leaflet of the OM, however they are synthesised in the cytoplasm and need to be transported through the cytoplasmic membrane, the periplasm and PG layer and, finally, flipped and assembled in the external leaflet of the OM. *E. coli* exports approximately 70,000 LPS molecules per minute to the OM (Whitfield and Trent 2014).

The transport system has been studied in *E. coli*, *Klebsiella*, *Pseudomonas*, *Salmonella*, *Neisseria* and *Haemophilus*, presenting some differences. The following section focuses on what is known about *E. coli* due to the fair amount of existing literature and because it was the bacterium used for the experiments disclosed in the results section on the interaction with the Lpt proteins and the PG. However, the mechanism by which many of these enzymes operate is not clear yet and it is not known how representative this may be of all Gram-negative bacteria.

1.3.3.1. LPS biosynthesis

The LPS biosynthesis starts by the formation of the inner core and the lipid A in the inner leaflet of the CM in a process known as the Raetz pathway. First, the enzyme LpxA acylates the hydroxyl at position 4 of the Uridine diphosphate N-acetylglucosamine (UDP-GlcNAc) with a 3-hydroxy tetradecanoic acid ((S)-3-hydroxymyristic acid or C14:0 3-OH), generating UDP-3-O-(3-OH-acyl)-GlcNAc. The acyl carrier protein (ACP) acts as substrate donor. Consecutively, LpxC removes the acetyl to free the amino function of the glucosamine for the LpxD to introduce another C14:0 3-OH acyl chain. Afterwards, LpxH cleaves the pyrophosphate bond present at the O-1 of UDP-2,3-diacylglucosamine to generate 2,3-diacylglucosamine-1-phosphate (lipid X) and Uridine monophosphate (UMP). Then, the LpxB conjugates the 6-OH of the lipid X with the anomeric carbon of a UDP-2,3-diacylglucosamine to yield β -(1-6)-tetraacyl-disaccharide-1-phosphate and UDP. At that point, the kinase LpxK phosphorylates the position 4' to yield the molecule known as Lipid IV_A and a protein encoded by WaaA transfers two Kdo units. To finish the synthetic pathway of lipid A, LpxL and LpxM add the last acyl chains, these enzymes require the substrate to contain Kdo to work. This last step is not highly preserved, making possible the modifications of the acylation pattern of the lipid (Fig.1.7). Thereafter, the enzymes WaaC and WaaF heptosyltransferases add the heptoses to finish the inner core. Subsequently, the core region can be modified by the enzymes WaaP (kinase), WaaY (phosphorylase), WaaQ (adds branch to the heptose) and WaaZ (adds third Kdo residue). Finally, WaaG and other glycosyltransferases finish the outer core (Greenfield and Whitfield 2012; Gronow *et al.*, 2010; Raetz *et al.*, 2007; Ray *et al.*, 1984; Takayama *et al.*, 1983) (Fig.1.7).

This rough LPS or LOS composed by lipid A and core oligosaccharide is then flipped from the inner leaflet to the outer leaflet of the CM. Transporter ABC

protein MsbA accommodates the acyl chains in its hydrophobic moiety and generates hydrophilic interactions with the GlcN units of the LOS. Translocation occurs by a flip-flop mechanism with ATP hydrolysis (Mi *et al.*, 2017) (Fig.1.7).

Simultaneously, the different monosaccharides of the OPS are synthesised inside the cell from glucose and fructose. The synthesis of the OPS in most cases requires a lipid acceptor on which the polysaccharide is built by the action of glycosyl transferases. The diversity in OPS among bacteria require the existence of multiple glycosyl transferases (Freeze *et al.*, 2015; Leipold *et al.*, 2007). Afterwards, the lipid carrier linked to the polysaccharide is flipped from the inner leaflet to the outer leaflet of the CM. The three pathways of this tumble are: the Wzx/Wzy dependent pathway, the ABC-transporter dependent pathway and the Synthase dependent pathway. The Wzx/Wzy and the ABC-transporter dependent pathways have been described in *E. coli* groups 1 and 2 respectively (Raetz and Whitfield 2002).

The Wzx/Wzy pathway is the most prevalent and it is characteristic of OPS repeating units with ramifications and monosaccharide heterogeneity. The lipid acceptor is undecaprenyl phosphate (Und-P or C55-P), a C55-isoprenoid alcohol derivative involved in the peptidoglycan and polysaccharide capsule's synthesis as glycan and lipid membrane carrier. The Und-P accepts a hexose-1-P from UDP-hexose to yield an undecaprenyl diphosphate (Und-PP)-linked intermediate; this reaction is catalysed by the different glycosyltransferases. When one repeating unit of the OPS is finished, the UndPP-linked-saccharide repeating unit is transported across the CM by the flippase Wzx and polymerised in the periplasm by the enzyme polymerase Wzy. The Wzy transfers each repeating unit from its UndPP to the reducing end of another UndPP- growing OPS creating glycosidic bonds. This step is repeated for each repeating unit present in the OPS, recycling the und-PP. Finally, the Wzz processing protein stops the elongation of the OPS by an unknown mechanism (Islam and Lam 2014)

(Fig.1.7). Once the LOS and the final OPS are anchored in the external leaflet of the CM, they have to be linked to the lipid A. WaaL shows great specificity for the LOS (lipid A + core), but no for the UndPP-OPS. The details of this reaction are still to be disclosed (Hong *et al.*, 2018; Ruan *et al.*, 2018) (Fig.1.7).

Diversely, in the ABC-transporter dependent pathway or adenosine triphosphate-(ATP-) binding cassette, the full OPS is created on the lipid acceptor before its transport across the CM. The lipid acceptor depends on the polysaccharide synthesised. An OPS unit of eight to ten sugar units is embedded between the carbohydrate-binding domain and the nucleotide-binding domain. It is a pathway confined to linear OPS structures (Bi and Zimmer 2020).

Finally, in the synthase-dependent pathway, the secretion of the OPS can happen with or without different lipid acceptors. Both synthesis and transport are catalysed by a membrane glycosyl transferase (Whitney and Howell 2013).

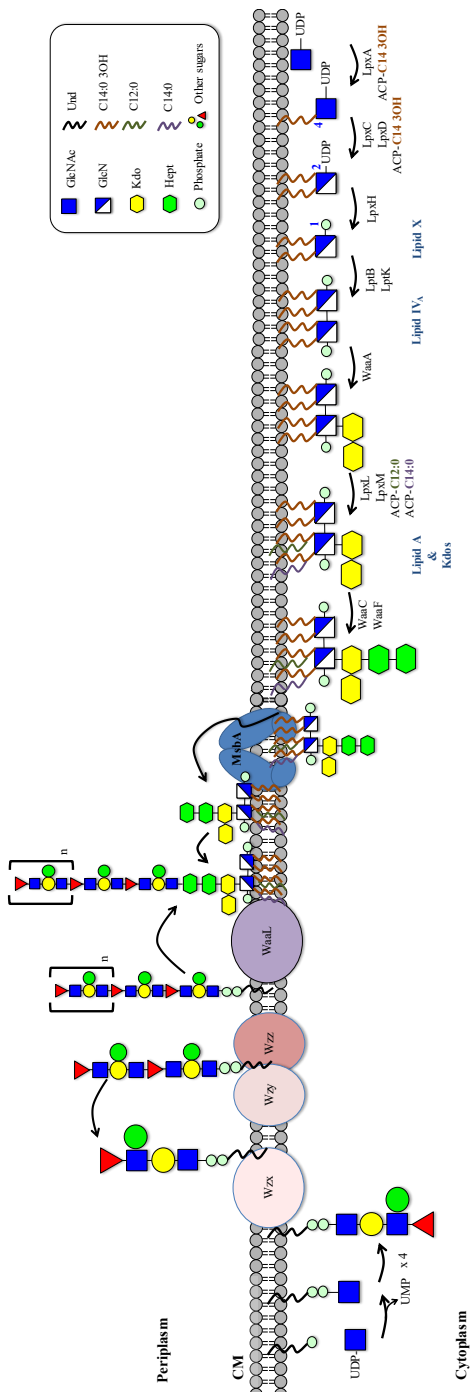


Figure 1.7. Lipid A and O-polysaccharide biosynthesis by the Ractz and Wzx/Wzy pathways.

1.3.3.2. LPS transport system to the OM

LPS transportation machinery deploys seven lipopolysaccharide transport proteins named Lpt A-G. This complex extracts the LPS from the external leaflet of the CM, transports it across the periplasm and the PG layer, flips it across the OM and locates the LPS in its external face (Fig.1.8). All Lpt proteins are essential, which makes them good targets for new antibiotics candidates. The LPS acyl chains interact with the Lpt proteins hydrophobic pocket (Bishop 2019; Hicks and Jia 2018; Dong *et al.*, 2017; Chng *et al.*, 2010).

Lpt proteins physically interact with each other and form a continuous β -jellyroll across the hydrophilic periplasm between LptA and the periplasmic domains of LptC, LptF and LptG, and LptD, (Luo *et al.*, 2017; Botos *et al.*, 2016; Tran *et al.*, 2010) (Fig.1.10). Lpt proteins work similarly to a PEZ candy dispenser. The LPSs in the Lpt machinery are pushed by a continuous stream of LPS from the CM to the OM. The energy for this transport against concentration gradient is provided by cytoplasmic ATP hydrolysis (Bishop 2019; Hicks and Jia 2018; Okuda *et al.*, 2016). LptA and LptD are under control of the σ^E regulon, which is activated under stress. Furthermore, defects in LPS transport are detected because LPS displaces RseA from RseB, freeing RseA to be cleaved which initiates the σ^E stress response.(Polissi and Sperandeo 2014; Lima *et al.*, 2013). LPS transport is limited by an imbalance between lipids in the CM and OM, the ATPase activity in the CM is somehow inhibited past a threshold concentration of LPSs in the OM (Xie *et al.*, 2018).

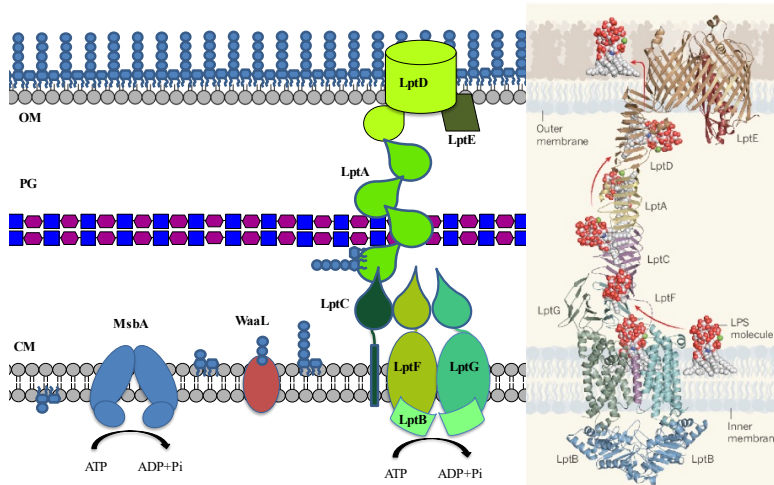


Figure 1.8. Msba and Lpt transport systems. ABC protein MsbA flips the rough LPS or LOS from the inner to the outer leaflet of the CM. Then the membrane protein WaaL forms a β -glycoside bond between the OPS and the outer core. The final LPS is then extricated from the CM by the ABC transporter LptB₂FG and the protein membrane LptC. Subsequently, LptA carries it across the periplasm and, finally, the β -barrel protein LptD with the OM lipoprotein LptE place the LPS in the external face of the OM. The LPS are pushed by a continuous stream of LPSs from the CM to the OM and the energy is provided by cytoplasmic ATP hydrolysis. Modified from Bishop 2019.

LptB₂FG is an ABC transporter located in the CM. LptB is an ATPase dimer and it is the most conserved unit of the system. The LptB dimer constitutes the nucleotide-binding domains of the complex, binding and hydrolysing ATP. The ATP hydrolysis provides the energy for the LPS transport (Sherman *et al.*, 2014). The trans-membrane helices of LptF and LptG translocate the LPS. These transmembrane domains rotate towards each other when LptB dimerizes thanks to the hydrolysis of ATP. The rotation of the transmembrane domains forms a cavity with the same shape and properties than the LPS. The entrance of the LPS to the cavity is ATP-independent (Li *et al.*, 2019; Owens *et al.*, 2019; Tang *et al.*, 2019; Dong *et al.*, 2017). Afterwards, ATP binding produces the closure of the LptB dimer and the collapse of the LptFG cavity moving LPS to the Lpt periplasmic bridge (Lundstedt *et al.*, 2020). In addition, LptF has a gate that can be opened or closed ensuring unidirectional movement from LptC to LptA (Owens *et al.*, 2019).

The assembly of LptC, A and D is known as the periplasmic bridge, it is composed by one LptC, one LptD and a multimer of LptA. The bridge sequesters the lipid A to allow the LPS diffusion through the aqueous compartment. However, it is not known how the bridge is built (Laguri *et al.*, 2017; Schultz and Klug 2017).

LptC is a trans-membrane protein of the CM with one N-terminal trans-membrane helix and a β -jellyroll domain. Both terminal regions of the β -jellyroll domain interact with LptB₂FG and LptA giving stability to the transport system. The catalytic domain of LptC is oriented toward the periplasm and consists of a twisted boat structure with two β -sheets facing each other (Tran *et al.*, 2010). During LPS transportation, LptG breaks its contact with LptC to facilitate the displacement of the trans-membrane domain of the sub-unit. The positive residues of the trans-membrane helix of LptC create a positively charged pocket that strongly binds the LPS and moves it towards the periplasm facilitating the LPS movement. LptC can inhibit the transport by LptC inserting its transmembrane helix between the two transmembrane domains of LptFG (Li *et al.*, 2019).

LptA is a periplasmic protein formed by 16 consecutive antiparallel β -strands, folded to resemble a slightly twisted β -jellyroll (Suits *et al.*, 2008). LptA tends to form polymers in a head-to-tail fashion in solution. The length of the multimer of LptA in the Lpt transport system remains unknown, it might vary, allowing the system to adapt to changes in the periplasmic width. However, it has been probed that the Lpt transport can successfully occur with only one subunit of LptA, although the affinity for LPSs decreases. The protein seems to “open” to bind the LPS as the N-terminal strand unfolds slipping the LPS into the binding pocket (Laguri *et al.*, 2017; Schultz *et al.*, 2017). LptA binds LptDE with higher affinity than LptC. This indicates that during Lpt assembly, LptA may join LptD/E in the OM and then polymerise until reaching LptC in the CM (Chng *et al.*, 2010). It

remains to be disclosed how LptA is built across the PG layer, there should be a “hole” in the PG. PG hydrolases are necessary to insert macromolecular structures into or across the PG (Priyadarshini *et al.*, 2007) and may be involved in Lpt transport machinery building. Lpt transport system and PG machineries may somehow regulate each other.

LptD is a β -barrel protein with a β -jellyroll periplasmic N-terminal domain. LptE is a lipoprotein located between the extracellular loops of LptD, partially blocking LptD extracellular opening. LptD has a lateral gate whereby first the lipid A and then the polysaccharide moieties are translocated to the OM (Dong *et al.*, 2017; Botos *et al.*, 2016; Malojčić *et al.*, 2014). For the correct functionality, LptD needs its disulphide bonds to be formed which depends on proper assembly of LptD with LptE. These disulfide bonds limit the size of the lateral gate on the periplasmic side and therefore it limits LPSs insertion in the inner leaflet of the OM (Freinkman *et al.*, 012). LptD and LptE are assembled by the BAM and Lol complexes respectively (Okuda *et al.*, 2016).

1.3.3.3. Study of the interaction LPS-proteins

The knowledge of the specific binding sites of LPSs with Lpt proteins or host receptors is important to develop antibiotics that attack Lpt machineries or medicines that target host receptors to produce vaccines, prevent sepsis or reproduce the beneficial effects of gut microbiota bacteria. The study of the interaction proteins-LPS is difficult due to the complexity of both structures. Structural biology approaches as nuclear magnetic resonance (NMR) can be techniques of choice to study these interactions (Gimeno *et al.*, 2020; Maalej *et al.*, 2019; Laguri *et al.*, 2018; 2017; Park and Lee 2013) (Fig.1.9).

For the NMR interaction studies, glycans can be labelled with isotopes or tags of fluorine or paramagnetic groups (Gimeno *et al.*, 2020). Although NMR interaction studies of lectins and the outer core of LPS have been performed

without any labelling (Maalej *et al.*, 2019). Labelling with the isotopes ^2H , ^{13}C , ^{15}N , ^{18}O or ^{34}S , prevents the apparition of overlaps and signal broadening (Laguri *et al.*, 2017). Fluorine is a NMR sensitive nucleus, whose chemical shift strongly depends on the environment (Dalvit and Vulpetti 2019). A paramagnetic group instead causes the fast relaxation of the nuclei in the neighbourhoods (Tesch and Nevzorov 2014); therefore, the signals of atoms in close contact with the LPS are expected to disappear in the spectrum giving an indication of which amino acids are involved in the interaction. To the best of my knowledge, the LPS labelling with tags of fluorine and/or paramagnetic groups has never been performed.

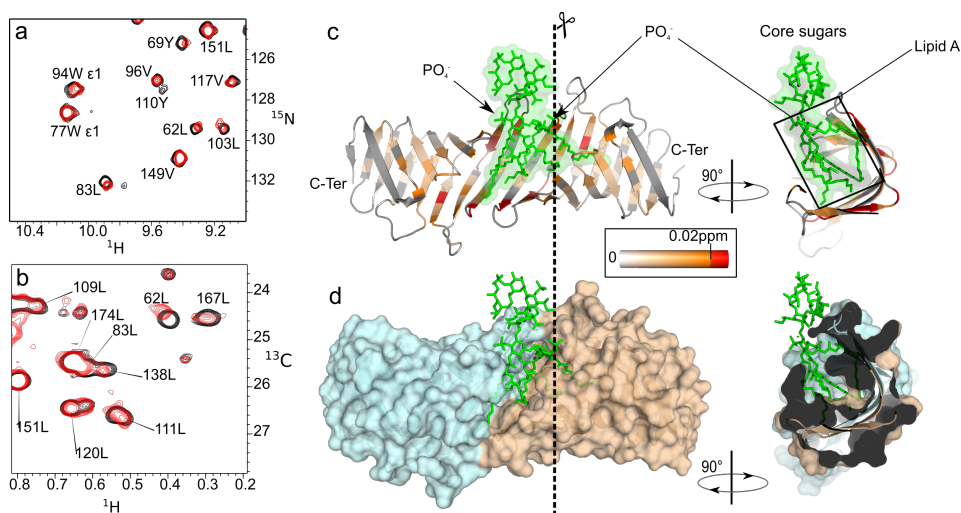


Figure 1.9. Interaction LptC and LPS in solution. **a.** [^1H , ^{15}N]-correlation spectrum and **b.** [^1H , ^{13}C]-correlation spectrum of labelled LptC in presence (red) and absence (black) of 0.8 mg/mL of LPS. **c.** LptC upon LPS binding on a ribbon representation. **d.** Surface representation of the LptC-LPS model. The two LptC molecules are coloured differently to visualize the localisation of the intermolecular interface and cavity where the LPS binds (Laguri *et al.*, 2017).

1.4. Peptidoglycan

The peptidoglycan (PG) or murein sacculus forms a continuous layer around the CM in almost all bacteria. It protects the cell from bursting due to the turgor of several atmospheres and maintains the species-specific shape of the bacterial cell. The PG itself and its biosynthetic pathway are essential and targeted by some of the most important classes of antibacterial compounds (like the β -lactams and glycopeptides) and enzymes (for example, lysozyme). PG is an excellent target for antibiotic treatment of infections in humans because the eukaryotic cells lack PG and some of its monomeric amino acids. PG-specific antibiotics are therefore expected to have no side-effects (Liu and Breukink 2016).

1.4.1. Structure of PG

PG is composed by linear chains of a repeating disaccharide of β -D-N-acetylglucosamine (GlcNAc) 1,4-linked to β -D-N-acetylmuramic acid (MurNAc) (Fig.1.10) (Schleifer and Kandler 1972). MurNAc is a *gluco*-configured hexose with an acetamido group at position 2 and D-lactoyl moiety at position 3 that has only been described in PG and its precursors. *E. coli* and other well-studied bacteria have β -1,6-anhydro-N-acetylmuramic acid (anhMurNAc) instead of the reducing MurNAc at the glycan chain end (Mengin-Lecreulx *et al.*, 1996; Höltje *et al.*, 1975) (Fig.1.10). The relative abundance of anhMurNAc correlates inversely with the average glycan strand length (Glauner 1988). The glycan strand length does not correlate with the thickness of the PG layer (Vollmer *et al.*, 2008). In *E. coli* the glycan strands range from 1-80 disaccharide units and their average length is 35 to 40 disaccharide units (Glauner and Höltje 1990). Other Gram-negative bacteria have longer (*Proteus morgani*) or shorter (*Helicobacter pylori*) average glycan chain lengths.

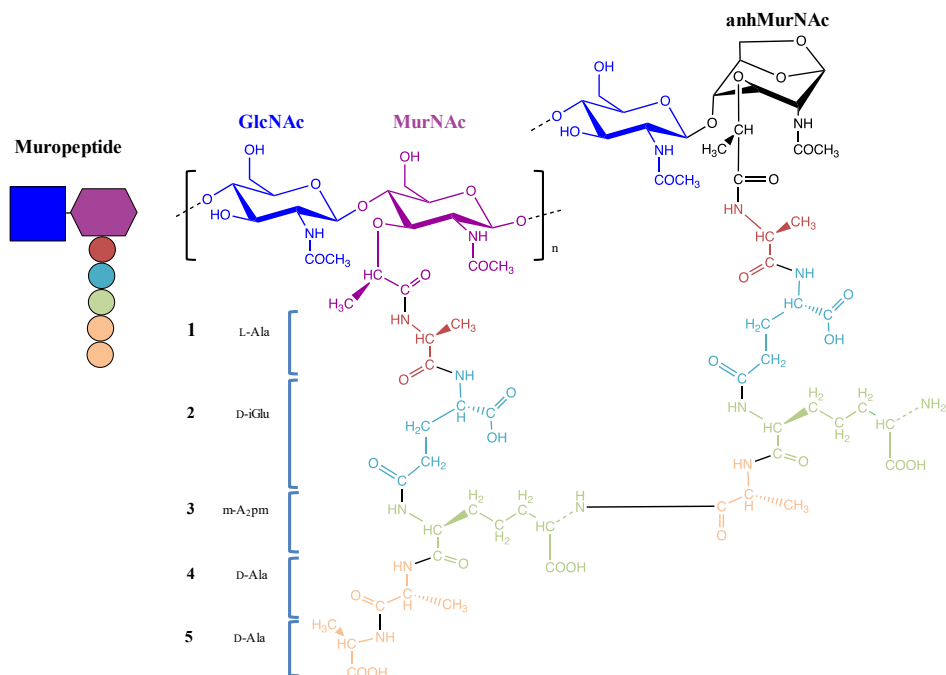


Figure 1.10. Structure of PG of *E. coli*. PG is composed by linear chains of a repeating β -D-N-acetylglucosamine (GlcNAc) 1,4-linked to β -D-N-acetylmuramic acid (MurNAc) disaccharide. The PG strand ends with 1,6-anhydro-N-acetylmuramic acid (anhMurNAc). In nascent PG and PG precursors, MurNAc has a peptide chain attached usually formed by: L-alanine (L-Ala) – D-isoglutamate (D-iGlu) - meso-diaminopimelic acid (m-A₂pm) – D-alanine (D-Ala) - D-alanine. There can be an amide bond (cross-link) between the amino group of m-A₂pm and the carbonyl of D-Ala 4 of another peptide. Modified from Desmarais *et al.*, 2013.

Similarly, some Gram-positive bacteria like *Bacillus subtilis* have very long glycan strands (up to 5,000 disaccharide units (Hayhurst *et al.*, 2008), whereas others like *Staphylococcus aureus* has particularly short glycan chains (average ~12 disaccharide units (Boneca *et al.*, 2000). Many bacteria like *Neisseria gonorrhoeae* modify their glycan strands which confers PG resistance to lysozyme and other components of the innate immune system (Sukhithasri *et al.*, 2013; Rosenthal *et al.*, 1980). De-N-acetylation of GlcNAc and/or MurNAc or O-acetylation of the O-6 of the MurNAc impairs the action of lysozymes secreted by the host immune system (Vollmer and Seligman 2010; Bera *et al.*, 2005). MurNAc can be glycolated on the amino function to become N-glycolylmuramic acid (MurNGc) (Také *et al.*, 2016) or can be modified to have an intramolecular

amide bond between the carboxyl group of the lactone at 3 and the NH₂ at 2 to generate a muramic acid δ -lactam structure (Atrih *et al.*, 1996; Popham *et al.*, 1996). In Gram-positive bacteria, the MurNAc can be covalently linked at position 6 with chains of teichoic acid or teichuronic acid (Dramsı *et al.*, 2008).

In the final PG precursor and the nascent PG, MurNAc has a pentapeptide attached to the D-lactoyl moiety. In *E. coli* and almost all Gram-negative bacteria, the peptide sequence is: L-alanine (L-Ala) – D-isoglutamate (D-iGlu) – L-meso-diaminopimelic acid (m-A₂pm) – D-alanine (D-Ala) – D-alanine (Fig.1.10) (Schleifer and Kandler 1972). The presence of D-amino acids make PG resistant to common peptidases which recognise L→L bonds (Cava *et al.*, 2011). The third amino acid, m-A₂pm, is present also in some Gram-positive bacteria PG (Bacillus, Mycobacteria, Clostridia, Lactobacillus, Corynebacteria, Propionobacteria and Actinomycetes) (Schleifer and Kandler 1972). Many other Gram-positive bacteria, such as *Staphylococcus* or *Streptococcus*, have L-Lys at position 3 that can carry a ‘branch’ made of 1-7 L-amino acids or glycine (Vollmer *et al.*, 2008; Ferain *et al.*, 1996; Schleifer and Kandler 1972). The mature PG contains most commonly tetrapeptides (L-Ala–D-iGlu–m-A₂pm/L-Lys –D-Ala), tripeptides (L-Ala–D-iGlu–m-A₂pm/L-Lys) and dipeptides (L-Ala–D-iGlu) (Glauner, Höltje, and Schwarz 1988). However, there are more variations in the composition of the peptides across the different Gram-positive bacteria (Sukhithasri *et al.*, 2013; Wright 2011). Stem peptide modifications facilitate immune system evasion (Sukhithasri *et al.*, 2013), and confer resistance to some antibiotics (Mainardi *et al.*, 2008). The carboxylic groups of D-iGlu, m-A₂pm and L-Lys can be amidated (Bernard *et al.*, 2011; Vollmer and Born 2010; Keglević and Derome 1989). D-iGlu can also be hydroxylated or substituted by Glycine (Gly), Glycine amide, D-Ala amide or polyamines (Vollmer and Born 2010). Instead of m-A₂pm or L-Lys at position 3 bacteria can present other diamino acids or monoamino acids (Schleifer and Kandler 1972), also, L-Lys can be substituted by D-Lys (Miyamoto *et al.*, 2019). The D-Ala at position 4 or 5 or L-Ala in

position 1 can be substituted by Gly impeding the formation of the peptide bond on it (Hammes *et al.*, 1973). Also, L-Ala in position 1 can be replaced by L-serine (L-Ser) (Schleifer and Kandler 1972) and the D-Ala at position 5 can be replaced by D-Lactate or D-Ser (Vollmer and Born 2010) (Fig.1.11).

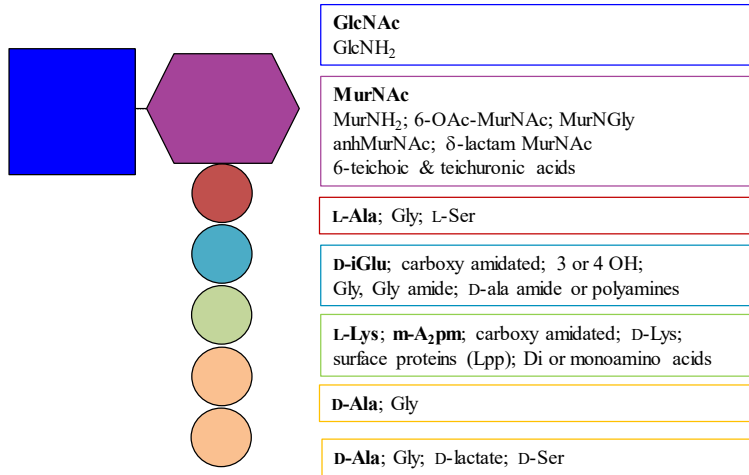


Figure 1.11. Variation in the structure of the PG on the carbohydrate backbone or the stem peptide. Glycan strands modifications confer PG resistance to lysozyme and other components of the innate immune system. Stem peptide modifications facilitate immune system evasion and confer resistance to some antibiotics.

The peptides protruding from different glycan strands can be cross-linked, to form the net-like structure of PG (Vollmer and Seligman 2010). The most prevalent cross-linkage is the 3→4 bond. DD-transpeptidases form amide bonds between D-Ala at position 4 of one peptide and m-A₂pm, L-Lys or the terminal amino acid of the branch at L-Lys of another peptide; the terminal D-Ala 5 is released in the transpeptidation reaction. This bond is either direct (Gram-negative) or through a peptide bridge (Gram-positive) (Rajagopal and Walker 2017). There are also LD-transpeptidases that connect the L-centre of m-A₂pm of one peptide and the D-centre of m-A₂pm of another peptide (3→3 bond) (Caparros *et al.*, 1992).

A mucopeptide is the disaccharide peptide fragment that is released from high-molecular weight PG by a muramidase, such as lysozyme or cellosyl (Fig.1.11).

Muramidases release the muropeptide monomers and cross-linked muropeptide oligomers from PG (Vollmer and Seligman 2010).

PG can covalently anchor proteins in Gram-negative and Gram-positive bacteria (Dramsı *et al.*, 2008). *E. coli* and other Gram-negatives possess the Braun's lipoprotein (Lpp) that tethers the OM to the PG (Braun and Wolff 1970). The ϵ -amino group of Lpp C-terminal Lysine is linked to the L-carboxyl group of the m-A₂pm of the PG. Specific LD-transpeptidases catalyse the attachment of Lpp to PG. Muropeptides with the L-lysine-L-arginine (L-Lys-L-Arg) dipeptide (at position 4) can be isolated by digesting Lpp-containing PG with pronase (Magnet *et al.*, 2007). Gram-positive bacteria have diverse surface proteins covalently and non-covalently anchored to PG. The sortases are transpeptidases that anchor surface proteins to the PG. Precursors of the surface proteins are synthesised in the cytoplasm and translocated across the CM where first the N-terminal signal peptide is cleaved off and then sortases cleave the membrane-anchored surface protein at the cell wall sorting signal near the C-terminus. Subsequently, the acyl enzyme intermediate (sortases-surface protein) is resolved by a nucleophilic attack of amino groups of PG precursors. Finally, surface proteins linked to PG precursors are incorporated into the PG (Marraffini *et al.*, 2006; Scott and Barnett 2006).

1.4.2. Host immune response to PG

PG is a MAMP and recognised by the innate immune system. The first interspecific defence against bacterial PG is lysozyme that lyse bacterial cells to prevent infections (*see* 1.4.4. PG hydrolysis). The receptors that recognise PG in humans are nucleotide oligomerisation domain proteins (NOD-1 and NOD-2), peptidoglycan recognition proteins (PGRP1, PGRP2, PGRP3, PGRP4) and the C-type lectins regenerating gene family protein III (RegIII) and mannose binding lectin (MBL). The recognition of PG from Gram-negative bacteria occurs despite

the presence of the OM because of the bacterial release of small PG fragments as a result of the normal metabolic recycling of cell wall components, without damage on the cell (Irazoki *et al.*, 2019).

Table 1.2. Specificity of the receptors involved in PG recognition: nucleotide oligomerisation domain proteins (NOD-1 and NOD-2), peptidoglycan recognition proteins (PGRP1, PGRP2, PGRP3, PGRP4) and the C-type lectins regenerating gene family protein III (RegIII) and mannose binding lectin (MBL).

Receptor	Ligand
NOD-1	MurNAc-L-Ala-D-iGlu-m-A ₂ pm
NOD-2	MurNA-L-Ala-D-iGlu
PGRP	PG different affinities for different amino acids
RegIII	GlcNAc Gram-positive bacteria
MBL	GlcNAc

NOD-1 intracellular receptor recognizes MurNAc-L-Ala-D-iGlu-m-A₂pm (muramyl tripeptide) which is present in almost all Gram-negative bacteria and the Gram-positive bacteria of the genus *Bacillus*, *Mycobacteria* and *L. plantarum* activating the transcription factor NF- κ B pathway (Girardin *et al.*, 2003). NOD-2 recognizes MurNA-L-Ala-D-iGlu (muramyl dipeptide) present in both types of PG (Schenk *et al.*, 2016).

Mammal PGRPs are secreted and interact with the stem peptide and glycan chains of the PG (Dziarski and Gupta 2006; Guan *et al.*, 2004). Different PGRPs discriminate between different amino acids (Royet *et al.*, 2011). PGRP-2 is secreted from the liver into the blood and has special affinity for MurNAc-L-Ala-D-iGlu-L-Lys muramyl tripeptide. PGRP-2 has acetylmuramoyl-L-alanine amidase activity and hydrolyses the lactoyl of MurNAc to separate it from the stem peptide (Guan *et al.*, 2004). Also, PGRP-1 (bone marrow) and PGRP-3 and PGRP-4 (skin, eyes, salivary glands, intestine, etc.) are antimicrobial proteins. The specific activity of PGRP-1, PGRP-3 and PGRP-4 has not been determined

yet (Sukhithasri *et al.*, 2013), but the structural similarities with PGRP-2 make likely that they have a similar amidase activity (Dziarski and Gupta 2006). PGRP directly kill the bacteria by interacting with the PG inducing membrane depolarisation and hydroxyl radical production. The systems employed are CssR–CssS system in Gram-positive bacteria and CpxA–CpxR system in Gram-negative bacteria (Sukhithasri *et al.*, 2013). In the fruit fly *Drosophila melanogaster* PGRP-LC and PGRP-LE detect Gram-negative PG and activate IMD pathway, whereas PGRP-SA and PGRP-SD detect Gram-positive PG and activate the Toll pathway. The IMD and Toll pathways control systemic immune responses and acquisition and maintenance of normal gut microorganisms (Royet *et al.*, 2011). Human PGRPs may also activate other immunity responses and play a role in the wellbeing of the gut microbiota (Guan *et al.*, 2004).

The C-type lectins RegIII and MBL recognize PG. RegIII receptors recognise the carbohydrate backbones of Gram-positive bacteria with a determinant specificity for GlcNAc. The binding depends as well of the saccharide chain length (Lehotzky *et al.*, 2010). RegIII α is secreted by Paneth cells and intestinal epithelial cells into the gut lumen and is involved in the agglutination of bacteria which may serve to control microbiota during inflammation (Chen *et al.*, 2019). MBL binds the carbohydrate backbone, having higher affinity for GlcNAc than for MurNAc. MBL inhibits production of proinflammatory cytokines while enhancing the production of chemokines by macrophages. MBL may regulate inflammation while enhancing phagocyte recruitment (Nadesalingam *et al.*, 2005).

In the past, TLR2 was considered to recognise PG (Schwandner *et al.*, 1999), however this has been recently probed wrong. TLR2 recognizes only lipoteichoic acids present in Gram-positive bacteria PG (Travassos *et al.*, 2004).

The host immune response differs in case of exposition to PG from pathogen or commensal bacteria. Pathogen PG activates direct antibacterial activity:

production of antimicrobial peptides, inflammation and immune responses. However, gut microbiota do not trigger such response. Moreover, gut microbiota muropeptides released during bacterial cell wall (Irazoki *et al.*, 2019) can reach the blood (Hergott *et al.*, 2016). These gut microbiota PG fragments may produce beneficial systemic effects by enhancing the innate immune function (Hergott *et al.*, 2016). For example, gut microbiota and its PG levels in sera correlate with neutrophil function. *In-vivo* administration of NOD-1 ligands is sufficient to restore neutrophil function after microbiota depletion caused by *Streptococcus pneumoniae* and *Staphylococcus aureus* (Clarke *et al.*, 2010). More information is necessary to fully understand the mechanisms and effects of the interaction between gut microbiota PG and its receptors to pave the way to develop medicines to induce microbiota PG benefits (Royet *et al.*, 2011) and antibiotics that target specifically the PG of pathogen bacteria without altering beneficial bacteria populations.

PG capacity to trigger an immune response makes it an excellent vaccine adjuvant (Garcia-Vello *et al.*, 2020) and a possible candidate to be used as vaccine antigen (Chen *et al.*, 2011). It could also be used to develop medication that mimic the positive effects of gut microbiota.

1.4.3. PG biosynthesis and transport

This chapter focusses on *E. coli* PG biosynthesis and transport, however the enzymatic machineries are largely conserved among Gram-negative bacteria (Radkov *et al.*, 2018; Typas *et al.*, 2012).

The first steps of PG synthesis occur in the cytoplasm. The nucleotide precursor UDP-GlcNAc is synthesised from fructose-6-phosphate by the Glm enzymes. Mur enzymes synthesize UDP-N-acetylmuramyl-pentapeptide (UDP – MurNAc – L-Ala – D-iGlu – m-A₂pm – D-Ala – D-Ala) (Liu and Breukink 2016). First, MurA transfers an enolpyruvate residue from phosphoenolpyruvate to position 3

of UDP-N-acetylglucosamine. Then, MurB catalyses the reduction of the enolpyruvate into D-lactate and liberates UDP-N-acetylmuramate. This is followed by the addition of the pentapeptide side-chain on the reduced D-lactate group by ATP-dependent amino acid ligases (MurC, MurD, MurE and MurF) (Zoeiby, Sanschagrín, and Levesque 2003) (Fig.1.12).

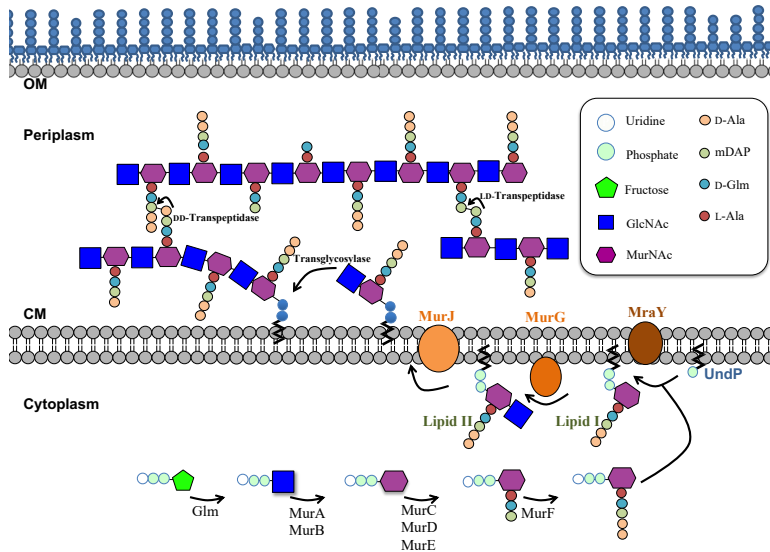


Figure 1.12. Synthesis of peptidoglycan. In the cytoplasm: The nucleotide precursor UDP-GlcNAc is synthesised from fructose-6-phosphate by the Glm enzymes. MurA, MurB, MurC, MurD, MurE and MurF synthesize UDP-N-acetylmuramyl-pentapeptide. MraY transfers the UDP-MurNAc-pentapeptide from UDP-Mpp to und-P, generating the lipid I. Afterwards, MurG transfers a GlcNAc from UDP-GlcNAc to Lipid I to produce the lipid II. MurJ flips lipid II from the inner to the outer leaflet of the CM. **In the periplasm:** transglycosilases transfer MurNAc of the nascent lipid-linked PG to the GlcNAc of a lipid II. Transpeptidases cross-link peptides protruding from different glycan strands to form a net-like structure. DD-transpeptidases form 3→4 bond and LD-transpeptidases form 3→3 bond. Modified from Typas et al., 2012.

D-amino acids are generated by racemases from the respective L-amino acids (Choi *et al.*, 1992). The enzyme MraY transfers the UDP-MurNAc-pentapeptide from UDP-Mpp to und-P, generating uridine-monophosphate and undecaprenyl-pyrophosphoryl-MurNAc-pentapeptide or lipid I. Afterwards, the glycosyltransferase MurG transfers a GlcNAc from UDP-GlcNAc to Lipid I to

produce undecaprenyl-pyrophosphoryl-MurNAc-pentapeptide-GlcNAc or lipid II. The MurJ flips lipid II from the inner to the outer leaflet of the CM (Liu and Breukink 2016; Typas *et al.*, 2012) (Fig.1.12).

The final steps of the PG synthesis occur in the periplasm. The glycan strand elongates by the trans-glycosyltransferase reaction, the reducing end of the MurNAc of the nascent lipid-linked PG strand is transferred to the C-4 of the GlcNAc of a lipid II molecule. This liberates the und-PP that is then dephosphorylated and recycled for further rounds of lipid I/II synthesis reactions. The transpeptidation cross-links peptides protruding from different glycan strands to form a net-like structure (Scheffers and Pinho 2005). DD-transpeptidases form 3→4 bond between the amino group of amino acid 3 (m-A₂pm or L-Lys) of the acyl-acceptor stem peptide and the carbonyl of amino acid 4 of a donor peptide; the terminal D-Ala 5 of the donor peptide is released in the reaction (Rajagopal and Walker 2017). The LD-transpeptidases LdtD and LdtE connect the L-centre of m-A₂pm of one peptide and the D-centre of m-A₂pm of another peptide (3→3 bond) (van Heijenoort 2011; Caparros *et al.*, 1992). The LD-transpeptidases LdtA, LdtB and LdtC anchor the Lpp to PG (van Heijenoort 2011). After transpeptidation other modifications occur, like the O-acetylation of C-6 of MurNAc catalysed by PG-O-acetyltransferases or the removal the terminal D-Ala by the D-Ala-D-Ala carboxypeptidases (Johnson *et al.*, 2013).

The Penicillin-binding proteins (PBPs) are transpeptidases that covalently bind β-lactams (*see* 1.6. Antibiotic resistance). PBPs are divided into class A (PBP1A, PBP1B and PBP1C), class B PBPs or DD-Transpeptidases (PBP2 and PBP3) and class C (PBP4, PBP5, PBP6, PBP6b, PBP7 and AmpH). PBPs' numbering is historically based on sodium dodecyl sulfate-polyacrylamide gel electrophoresis (SDS-PAGE) migration (Sauvage *et al.*, 2008), Class A and B PBPs are high-molecular-mass PBPs and Class C are low-molecular-mass PBPs. PBPs are regulated by other proteins (Walter and Mayer 2019). Some PBPs are semi-

redundant, ensuring cell survival in the absence of one of them (Pazos and Peters 2019; Vollmer and Bertsche 2008). Both, class A and class B PBPs are essential and have specific roles in the cell cycle. Class A PBPs are bifunctional and have a glycosyltransferase domain in addition to the transpeptidase domain. PBP1A (encoded by gene *mrcA*) participates in the synthesis of the PG during elongation and PBP1B (*mrcB*) during septation in cell division. PBP1A and PBP1B are semi-redundant (Amir *et al.*, 2019). PBP1C (*pbpC*) seems to be a transglycosylase only (Schiffer and Höltje 1999). Class B PBPs exhibit only transpeptidase activity. PBP2 (*pbpA*) participates on cell elongation to produce a spherical shape, and, PBP3 (*ftsI*) participates in septation generating rod shapes. Class C PBPs are PBP4 (*dacB*), PBP4b (*pbp4b*), PBP5 (*dacA*) PBP6 (*dacC*), PBP6b (*dacD*), PBP7 (*pbpB*) and AmpH (*ampH*) are very diverse and non-essential (Ropy *et al.*, 2015). In addition, they have hydrolytic activities and therefore will be mentioned in the subsequent section.

1.4.4. PG hydrolysis

PG is remodelled and cleaved during growth and cell division. PG hydrolases cleave covalent bonds in PG or PG turnover products. The glycosylases (N-acetylglucosaminidases, N-acetylmuramidases and lytic transglycosylases) hydrolyse the glycan backbone, the N-acetylmuramyl-L-alanine amidases remove peptide side chains from the carbohydrate polymer and the peptidases (carboxypeptidases and endopeptidases) cleave the peptides (Fig.1. 13).

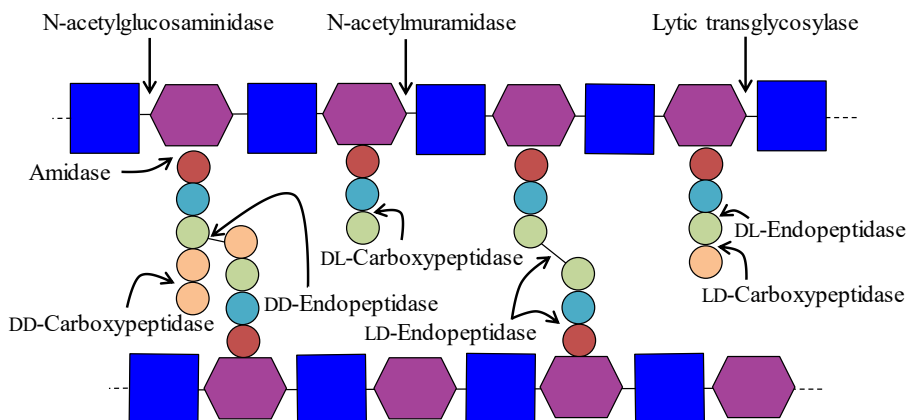


Figure 1.13. PG hydrolases action site. N-acetylglucosaminidases hydrolyse the terminal non-reducing GlcNAc. The N-acetylmuramidases hydrolyse the $\beta,1,4$ -bonds between MurNAc and GlcNAc. The lytic transglycosylases are N-acetyl muramidases that LTs recognise the bond between MurNAc and GlcNAc and catalyse the intramolecular cyclisation of MurNAc into anhMurNAc. The N-acetylmuramyl-L-Ala amidases or simply amidases cleave the amide bond between MurNAc and the L-Ala residue of the stem peptide. The endopeptidases hydrolyse the peptide cross-link in a non-terminal part of the peptide and can be DD, DL or LD. The carboxypeptidases can cleave the bond between terminal amino acids of the stem peptide and can be DD, DL or LD.

There are still many unanswered questions on hydrolases physiological roles. During cell division, hydrolases may be necessary for continued PG synthesis during septation and coordinators of septation and OM invagination with septal ingrowth (Haeusser and Margolin 2016; Typas *et al.*, 2012). In addition, hydrolases may be required to insert macromolecular structures such as flagella into or across the PG (Herlihey and Clarke 2017). However, it is difficult to assign the function to each hydrolase because of their high numbers, their redundant roles and that hydrolases may have more than one function (Vollmer *et al.*, 2008). PG synthesis and hydrolysis is controlled by the regulators of the divisome and the elongasome to avoid autolysis as the integrity of the sacculus can be compromised (Egan *et al.*, 2017; Szwedziak and Löwe 2013).

Glycosylases are divided into N-acetylglucosaminidases and N-acetylmuramidases. N-acetylglucosaminidases hydrolyse the terminal non-

reducing GlcNAc, like NagZ (Vermassen *et al.*, 2019). The N-acetylmuramidases like lysozyme hydrolyse the β ,1,4-bonds between MurNAc and GlcNAc. The lytic transglycosylases (LTs) are N-acetyl muramidases that catalyse the intramolecular cyclisation of MurNAc into anhMurNAc. LTs recognise the bond between MurNAc and GlcNAc of the PG strand in the periplasm. Afterwards, the new mucopeptide anhMurNAc-GlcNAc is transported to the cytoplasm by the CM protein AmpG, degraded and recycled (Dik *et al.*, 2017; van Heijenoort 2011).

The N-acetylmuramyl-L-Ala amidases cleave the amide bond between MurNAc and the L-Ala residue of the stem peptide. The N-acetylmuramyl-L-Ala amidases of *E. coli* are AmpD (cytoplasm) and AmiA, AmiB, AmiC and AmiD (periplasm) (van Heijenoort 2011). AmpD degrades the GlcNAc-1,6- anhMurNAc-peptide. The signal peptide in the N-termini of the periplasmatic amidases permits their transport across the CM. In the periplasm, when the signal peptide is cleaved AmiA, AmiB and AmiC become soluble, however AmiD is a lipoprotein anchored to the OM. AmiA, AmiB and AmiC are homologous LytC-type N-acetylmuramyl-L-alanine amidases and play major role in the splitting process, cleaving the septum after cell division (Yang *et al.*, 2012; Heidrich *et al.*, 2001). AmiD and AmpD are structurally similar. AmpD is specific for anhMurNAc-L-Ala and AmiD cleaves anhMurNAc-L-Ala and MurNAc-L-Ala (Uehara and Park 2007). One of the physiological functions of the amidases may be to facilitate invagination during septation. This would happen by elimination of the peptide side chains of a PG region to inhibit insertion of new monomers (Priyadarshini *et al.*, 2007).

The peptidases are divided into endopeptidases and carboxypeptidases. Endopeptidases hydrolyse the peptide cross-link in a non-terminal part of the peptide. The DD-endopeptidases (AmpH, PBP4, PBP7, MepA, MepH, MepM, and MepS) cleave 4 \rightarrow 3 amide bonds between D-Ala at position 4 of one peptide

and m-A₂pm, L-Lys or the terminal amino acid of the branch at L-Lys of another peptide (Singh *et al.*, 2012; van Heijenoort 2011). The LD-endopeptidases (MepA and MepK) (Chodisetti and Reddy 2019; Keck *et al.*, 1990) and DL-endopeptidases (Srikannathasan *et al.*, 2013; Garnier *et al.*, 1985) recognize L→D or D→L linkages present between the different amino acids of the stem peptide or between two different stem peptides. The enzymes DD- and/or LD-carboxypeptidases (PBP4, PBP4b, PBP5, PBP6, PBP6b, LdcA, AmpH and MepS) can cleave the bond between one or both terminal D-Ala from the peptides in the murein, although the objective of this action is not clear yet. DL-carboxypeptidases cleave DL-linkages between terminal peptides (Pazos and Peters 2019; Frirdich *et al.*, 2012; van Heijenoort 2011; González-Leiza *et al.*, 2011). In *E. coli*, no DL-endopeptidases nor DL-carboxypeptidases have been described. However, it is likely that an enzyme performs this activity since Diuropeptides are present in the PG (Glauner, Höltje, and Schwarz 1988)

During cell septation, new PG is synthesised. This new synthesis has an excess of 30% that is rapidly digested. In addition, 60% of the PG is hydrolysed each generation and efficiently recycled (Uehara and Park 2008; Park and Uehara 2008). The recycling pathways could involve the action of the oligopeptide permease Opp and the murein peptide permease Mpp (Vollmer and Bertsche 2008; Uehara *et al.*, 2005) or the AmpG permease (Jacobs *et al.*, 1994). Many enzymes are involved in this process, for example PBP4 and PBP5 are involved in the recycling of non-canonical D-amino acids (Miyamoto *et al.*, 2020) and AmpH bifunctional character and its wide substrate range has been associated with PG recycling (González-Leiza *et al.*, 2011).

1.5. Biogenesis of the cell envelope: elongasome and divisome

Bacterial elongate and then divide into two daughter cells which requires a coordinated elongation, invagination and division of the CM, PG and OM (Gray *et al.*, 2015).

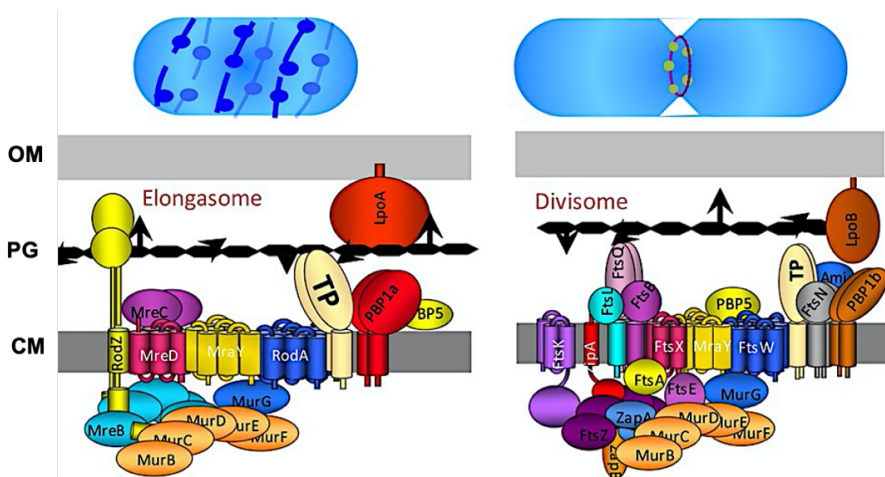


Figure 1.14. Elongasome and divisome of *E. coli*. PG sacculus is elongates and divides controlled by the bacterial cytoskeleton and associate proteins of the elongasome and the divisome. In addition, elongasome and divisome are somehow involved in the elongation and division of the OM and the CM (Hugonnet *et al.*, 2016).

PG sacculus is enlarged by insertion of PG precursors into the lateral wall and divided by a formation of a septum and constricted cell division and separation of the daughter cells (Typas *et al.*, 2012). This process is controlled by the bacterial cytoskeleton and associate proteins from inside the cell. The elongasome and the divisome are protein complexes that regulate PG synthesis during cell elongation and division. Numerous proteins involved in PG synthesis and hydrolysis (*see* 1. 4. Peptidoglycan) are part of the elongasome and the divisome protein complexes (Szwedziak and Löwe 2013). However, it is unknown how the cytoskeleton coordinates elongation and division of the OM. Some OM lipoproteins interact with the divisome and elongasome, but the details and factors remain to be disclosed (Berezuk *et al.*, 2018; Typas *et al.*, 2010).

The elongasome produces cylindrical growth or elongation in rod-shaped bacteria like *E. coli* by directing PG insertion into the lateral wall. It is composed by the proteins MreB, MreC, MreD, RodZ, RodA, PBP1A, PBP2, MurF, MurG and MraY amongst others (van den Ent *et al.*, 2014) (Fig.1.14). MreB forms filaments which move coordinated with the CM proteins MreC, MreD, and RodA/PBP2 and the PG synthesis proteins MraY and MurG (Shi *et al.*, 2018; Domínguez-Escobar *et al.*, 2011; Mohammadi *et al.*, 2007). Without MreB cells acquire an spherical shape (Karczmarek *et al.*, 2007).

The divisome assembles in two steps: The early proteins (FtsZ, FtsA, ZipA, EzrA and Zaps) monitor and recruit the late proteins (FtsE, FtsX, FtsK, FtsQ, FtsL, FtsB, FtsW, PBP3 (FtsI), FtsN MurJ and Tol-Pal) (den Blaauwen *et al.*, 2017; Du and Lutkenhaus 2017) (Fig.1.14). At some point the tubulin-like GTPase FtsZ starts the formation of a ring-like structure at midcell (the Z ring) (De Boer *et al.*, 1992). Afterwards, the proteins of the divisome localize in the Z ring starting by FtsBLQ, FtsIW and FtsN. FtsN bridges the early and late proteins, interacting with FtsA to stabilize the FtsBLQ complex. The FtsBLQ complex and FtsN regulate the initiation of septal PG synthesis. FtsBLQ can inhibit PBP1B and, so, the elongation, and PBP3 that participates in septation. The presence of FtsN or the OM lipoprotein LpoB suppresses FtsBLQ activating septation (Boes *et al.*, 2019; den Blaauwen *et al.*, 2017).

In *E. coli* and other Gram-negatives, AmiA, AmiB and AmiC (LytC-type N-acetylmuramyl-L-alanine amidases) play a major role separating daughter cells after cell division. These amidases need activation by proteins of the LytM family (EnvC, NlpD, YebA and YgeR). If the amidases or their regulators are inhibited severe cell separation defects occur (Uehara *et al.*, 2010; Uehara *et al.*, 2009; Heidrich *et al.*, 2001). EnvC regulates AmiA and AmiB and the OM lipoprotein NlpD regulates AmiC (Uehara *et al.*, 2010). If the regulators EnvC and NlpD are inactivated, cells cannot divide and form long chains of cells (Uehara *et al.*, 2009).

EnvC and NlpD localize in the septum before septal PG is synthesised. Later on, Ami B and AmiC translocate to the septum as well (Peters *et al.*, 2011). In *E. coli*, FtsN and FtsEX activate EnvC and NlpD respectively (Uehara *et al.*, 2010). YebA and YgeR are also required for cell septation, although they seem not to be recruited in the septum like EnvC and NlpD. It has been speculated that EnvC and NlpD are specialised division factors, while YebA and YgeR have a minor cell separation activity but other implications in PG biogenesis (Uehara *et al.*, 2009).

CM elongation and division is coordinated with PG. It is still unknown how this happens, the CM may invaginate by the contraction of the Z-ring in the cytoplasm and the boost of the septal PG synthesis (Cabr e *et al.*, 2013; MacAlister *et al.*, 1987).

Interestingly, many regulators of the PG elongation and septation are located in the OM. The essential glycosyltransferases and transpeptidases PBP1A and PBP1B are regulated by the OM lipoprotein LpoA and LpoB respectively. LpoB stimulates PBP1B transpeptidase activity (Egan 2018; Paradis-Bleau *et al.*, 2010; Typas *et al.*, 2010). In addition, LpoA together with RlpA (another OM lipoprotein from *E. coli* of unknown function) directly interacts with the divisome protein FtsK (Berezuk *et al.*, 2018).

The Tol-Pal system links the OM and PG layers and seem to promote OM constriction during cell division. The Tol-Pal system is composed by TolQ, TolR, TolA (TolQRA), TolB and Pal. TolQRA are proteins located in the CM. TolB, is a periplasmic protein and Pal is a PG-binding OM lipoprotein (Egan 2018; Gerding *et al.*, 2007). The Tol-Pal system may also have a direct role in promoting glycan cleavage at the septal site by enzymes localised in the OM, since TolA and CpoB interact directly with PBP1B-LpoB and modulate its activity (Gray *et al.*, 2015). Although, amidase activation is independent from the Tol-Pal system, the catalysis products from amidase activities cannot be efficiently processed without

the Pal-system and that impairs cell separation (Yakhnina and Bernhardt 2020). Other examples of coordination of PG and OM during division is the OM lipoprotein NlpD regulator of AmiC, that links PG remodelling and OM invagination during cell division (Tsang *et al.*, 2017). Also, in *Pseudomonas aeruginosa*, lytic transglycosylases are necessary for the OM integrity (Lamers *et al.*, 2015). As well, the OM protein NlpI is implicated in the degradation of the carboxy/endopeptidase MepS. NlpI interacts with DD-endopeptidases (PBP4, PBP7 and MepM) and may locate them by the OM and PG synthesis sites (Banzhaf *et al.*, 2020; Su *et al.*, 2017). Furthermore, PG synthesis machineries adapt to problems in the OM biosynthesis by producing PG with more LD-crosslinks. When OM synthesis is altered, *E. coli* responds by increasing the LD-crosslinks in the PG and the glycosyltransferase activity of PBP1B, its activator LpoB and the DD-carboxypeptidase PBP6B (Morè *et al.*, 2019).

1.6. Antibiotic resistance

1.6.1. Need for urgent action and new antibiotics

Antibiotics have played a crucial role in global development and are essential for modern medicine (IACG 2019). They are essential medicines (Hsia *et al.*, 2019; WHO 2017) which access is vital to treat severe communicable diseases. Vaccination and antimicrobial medication have changed the leading causes of death from communicable diseases to non-communicable diseases in high income countries. Also, significant progress in the prevention and treatment communicable diseases have been made in low income countries (WHO 2016).

The so called Antibiotic Era started in 1928 when Penicillin was discovered (Ligon 2004). Since then, bacteria have developed adaptation mechanisms to slowly become resistant to antibiotics in a natural fight for survival. However, misuse and overuse of antibiotics in human medicine and food production have accelerated the appearance of antibiotic resistant bacterial strains. Today we face an uncomfortable reality: the possibility of a time in which antibiotics are no longer effective (IACG 2019). The European Centre for Disease Prevention and Control (ECDC) calculate that about 33,000 people die each year in the EU due to infections with antibiotic-resistant bacteria (Cassini *et al.*, 2019). The World Bank estimates that the number of deaths caused by antibiotic resistant bacteria will quickly rise from the current 700,000 deaths per year to as many as 10 million deaths annually by 2050. This will specially affect the most vulnerable populations from low- and middle-income countries and areas affected by fragility, conflict and violence (World Bank 2019).

To address the worldwide antibiotic resistance crisis, the World Health Organisation (WHO) proposes five strategic objectives: 1) improve awareness and understanding on antibiotic resistance; 2) strengthen the knowledge and evidence base through surveillance and research; 3) reduce infections incidence

through effective sanitation, hygiene and prevention measures; 4) optimize the use of antimicrobials in human and animal health; and, 5) develop the economic case for sustainable investment that takes account of the needs of all countries and increase investment in new medicines, diagnostic tools, vaccines and interventions (WHO 2015).

However, the fulfilment of WHO strategic objectives is challenging, specially to encourage the development of new antibiotics. Most antibiotics were developed between 1940-1962 and many are still used nowadays. At present, the discovery of novel classes of antibiotics has slowed dramatically (Coates *et al.*, 2011). Pharmaceutical companies do not find profitable to develop new antibiotics because of their limited profit compared to the treatment of chronic diseases. Also, approval by the authorities is long and the research of non-toxicity and superiority to no treatment exigent. Once commercialised, benefits are still limited as novel antibiotics are usually reserved to be used in the case that no other treatment is possible. In addition, most new antibiotics have a very narrow spectrum, making necessary the application of diagnostic tools to identify the pathogen. Besides, new antibiotics may soon become ineffective and non-marketable since bacteria rapidly develop resistance to new small molecules (Fernandes and Martens 2017; Ventola 2015).

Gram-negative bacteria are Critical Priority Pathogens for which urgent new treatment is needed (WHO 2017b). Gram-negative bacteria present intrinsic resistance due to the presence of the OM, that gives bacteria the ability to resist small hydrophobic molecules, like most antibiotics, and large polar molecules (Silhavy *et al.*, 2010). But also, Gram-negative bacteria represent a tremendous challenge since they have developed diverse mechanisms for antibiotic resistance against medicines that were effective before. Some of these mechanisms of resistance are the acquisition of genes associated with mobile plasmids or transposons or mutations which alter bacterial targets for antibiotics, the

permeability of the OM, the regulation of innate efflux systems, etc. Treatment of infections caused by Gram-negative bacteria is becoming very difficult (Li *et al.*, 2015; Boucher *et al.*, 2009).

1.6.2. Antibiotics: targets and resistance

Antibiotics have diverse chemical structures and mechanism of action. Cationic peptides, polymyxins, β -hairpin peptidomimetics, anionic lipopeptides, β -lactams (penicillins, cephalosporins and carbapenems), β -lactamase inhibitors, glycopeptides, moenomycins aminoglycosides, tetracyclines, glycyliclones, amphenicols, oxazolidinones, pleuromutilins, lincosamides, macrolides, streptogramins, steroid antibacterials, rifamycins, quinolones, sulphonamides, and others are some of the families in which antibiotics are classified (Fig.1.15).

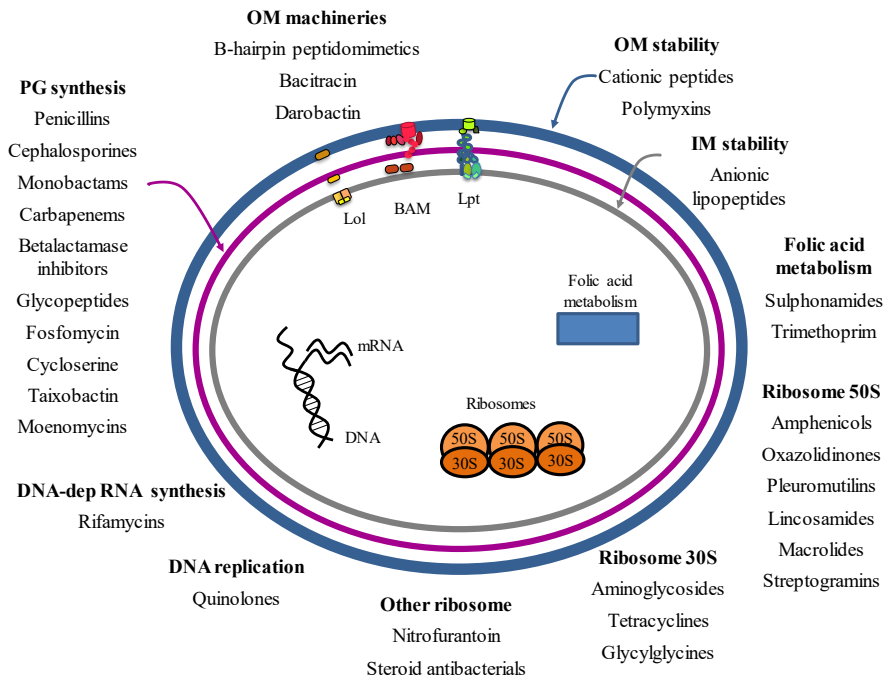


Figure 1.15. Antibiotics and their targets in the bacteria.

Main commercialised antibiotics against Gram-negative bacteria are β -lactams (especially β -lactam and β -lactamase inhibitor combinations, later-generation cephalosporins, and carbapenems), fluoroquinolones, and aminoglycosides.

Targeting the outer membrane

The OM is an intrinsic and essential component of Gram-negative bacteria. As an exacerbating agent for antibiotic resistance, the OM and its specific transport machineries: Lpt, BAM and Lol pathways, are potential targets for antibiotics that can either kill Gram-negative bacteria or make OM more permeable to antibiotics. Currently there are no antibiotics approved that target OM building machineries, but some promising molecules are under study.

Altering the OM

Cationic peptides are complex structures that can kill Gram-negative and Gram-positive bacteria, enveloped virus, fungi and cancer cells. Cationic peptides are natural products of the innate host defences from animals and plants such as defensins, cathelicidins and kinocidins. Despite their high structural diversity and large variability in peptide sequences, all cationic peptides share a three-dimensional arrangement, and the mechanism of action seems to be an interaction with the negatively charged membrane. Cationic peptides form transmembrane channels that depolarize and destabilize the membrane, in addition to their immunomodulatory effects (Peschel and Sahl 2006). Since the mode of action relies on charge–charge and hydrophobic interactions, resistances development against cationic peptides is unlikely (modifying the composition and structure is difficult). Also, the variability in peptide sequences implies that there is not a unique recognition site for protease cleavage. Bacteria would need to develop specific proteases for different peptide sequences and a combination of different cationic peptides could be used. Cationic peptides are a start point for the

development of new antimicrobials, like Pexiganan (MSI-78), MSI-367, MSI-594, and MSI-843 (Lee *et al.*, 2015) or the polymyxins (Trimble *et al.*, 2016).

Lipopeptides are linear or cyclic peptides with a fatty acid moiety covalently attached to the N-terminus, they can be positive or negatively charged (Straus and Hancock 2006). Polymyxins (Polymyxin B, Colistin) are positive charged lipopeptides. They are synthesised from cationic amphiphilic peptides with acetylated N-terminus (C8–C18 fatty acid chain length). Polymyxins interact with the phosphate residues of lipid A producing CM permeabilisation and death. Polymyxins' lipid tail increases the activity of the cationic peptide. However, they are neurotoxic and nephrotoxic (Trimble *et al.*, 2016). Although, polymyxins are used as last-line therapeutic option, bacteria have already developed resistances. Bacteria can modify their LPSs in order to reduce their negative charge and prevent polymyxins binding and also increase drug efflux, alter membrane proteins to decrease permeability to polymyxins and increase anionic capsular polysaccharide production (Moffatt *et al.*, 2019). Negatively charged or anionic lipopeptides (Amphomycin, Daptomycin, Echinocandins, Surfactin) target the CM of Gram-positive bacteria by producing a depolarisation. The mechanism of action are not clear yet, but it seems promising since resistances development is still rare (Straus and Hancock 2006).

Targeting OM building machineries

Table 1.3 summarises the molecules in development that target LPS synthesis, Lpt, BAM and Lol. The most promising molecules are the β -hairpin peptidomimetics (L27-11, Murepavidin, JB-95, LlpA) which are cationic peptides that disrupt OMPs of the Lpt and BAM complexes. Murepavidin is a 14 amino acid synthetic peptidomimetic that causes LptD inhibition, its activity is limited to *P. aeruginosa*, likely due to the extended N-terminal domain of LptD of *Pseudomonas* spp. (Andolina *et al.*, 2018). Murepavidin, however, caused kidney toxicity in phase III clinical trials (Lehman and Grabowicz 2019).

Table 1.3. Antibiotics that target OM building machineries.

Compound	Target	Mechanism
Compound 1 and 2	LpxA	1 substrate-competition; 2 targets LpxA-product complex. No acylation UDP-GlcAc (Han <i>et al.</i> , 2020)
BB-78485, Lpc-004, CHIR-090	LpxC	No de-acetylation of the UDP-GlcNAc precursor of lipid A (Erwin 2016)
Sulfonyl piperazine and pyrazole	LpxH	No UMP cleavage of the UDP-2,3-diacetylglucosamine (Nayar <i>et al.</i> , 2015)
Bacitracins (Bacitracin A)	Und-P	No Und-P dephosphorylation. No synthesis LPS nor PG (Manat <i>et al.</i> , 2014)
Hit compounds	Heptosyltransferase	No transfer of heptose to the Kdo during the building of the core (Panda, Saxena, and Guruprasad 2019)
Tetrahydrobenzothiopepenes and G907	MsbA	No ATPase activity, LPS translocation (Ho <i>et al.</i> , 2018)
4-phenylpyrrolcabazoles	LptBFGC	ATP-competitive kinase inhibitor (Sherman <i>et al.</i> , 2013)
Novobiocin	DNA gyrase Stimulate LptB.	Stimulation LptB - increase in LPS transport - synergism polymyxin (Mandler <i>et al.</i> , 2018)
Thanatin and its derivatives	LptCAD	Binds common β -strand domain and other mechanisms (Vetterli <i>et al.</i> , 2018)
IMB-881	LptA	Blocks interaction LptA-LptC (Zhang <i>et al.</i> , 2019)
L27-11 and Murepavidin	LptD	Binds extended N-terminal domain of LptD of Pseudomonas (Andolina <i>et al.</i> , 2018)
JB-95	β -barrel OMPs	Non-specific: BamA, LptD and others (Robinson 2019)
LlpA	BamA	Lectin-like bacteriocin (Robinson 2019)
Darobactin	BamA	Blocks BAM complex in a gate-closed conformation (Imai <i>et al.</i> , 2019)
MRL-494	BamA	Small molecule. No OMP folding (Hart <i>et al.</i> , 2019)
Chimeric peptides	BamA and LPS	β -hairpin peptide macrocycle linked to macrocycle of polymyxins (McLaughlin and Van Der Donk 2020)
Monoclonal antibodies (MAB1)	BamA	No OM proteins folding Only active if LPS truncated (Storek <i>et al.</i> , 2019)
Batimastat	RseP	Blocks cleavage of RseA, no σ^E activation: accumulation unfolded OMPs in periplasm (Konovalova <i>et al.</i> , 2018)
β -signal peptides	BamD	Interfere recognition of OMPs (Hagan <i>et al.</i> , 2015)
Globomycin	LspA peptidases Other	Hydrophobic cyclic peptide, mimic substrate (Lehman and Grabowicz 2019)
Myxovirescin	LspA	Prevents lipoproteins from being properly localised in the membrane (Kitamura <i>et al.</i> , 2018)
Benzamides	LspA	Prevents lipoproteins from being properly localised in the membrane (Kitamura <i>et al.</i> , 2018)
Pyridineimidazoles	LolCDE.	Inhibit the LolA-dependent release of Lpp (McLeod <i>et al.</i> , 2015)
G0507	LolCDE	Increase ATPase activity Accumulation of Lpp in CM (Nickerson <i>et al.</i> , 2018)
Thioureas, MAC13243, A22, S-4-chlorobenzyloisothiourea	LolA	Inhibits lipoprotein transport to the OM (Barker <i>et al.</i> , 2013)
Arylomycins (G0775)	LepB peptidase	Inhibit cleavage of the signal peptide and the release of mature β -barrel OMPs into periplasm (Smith <i>et al.</i> , 2018)
Trifolitoxin	Unknown	Gram-negative bacteria (Epand <i>et al.</i> , 2016)

1.7. Commensal bacteria

1.7.1. Commensal microbiota: an overview

The human body is inhabited by trillions of microorganisms, known as the human microbiota which is composed by Bacteria, Archaea, Eukarya and Virus (Cho and Blaser 2012; Human Microbiome Project Consortium 2012). The microbiota inhabits various niches in the human body, such as gut (Thursby and Juge 2017), oral cavity (Arweiler and Netuschil 2016), skin (Grice and Segre 2011), vagina (Martin 2012) and respiratory airways (Man *et al.*, 2017). The microbiota contains at least 100 times more genes than the human genome (Gill *et al.*, 2006) and commensal bacteria alone are as numerous as human cells (3.8×10^{13} in a 70 kg man) (Sender *et al.*, 2016). The microbiota plays crucial roles in the host immunity, metabolism, behaviour and disease development although more studies are necessary to fully understand its real involvement in human metabolism (Lloyd-Price *et al.*, 2017).

Different microbiota populations are associated with particular body niches (Lloyd-Price *et al.*, 2017; Human Microbiome Project Consortium 2012). In general, the human body is primarily colonised by bacteria and these are mainly part of the phyla Firmicutes, Bacteroidetes, Proteobacteria, Actinobacteria, Fusobacteria and Cyanobacteria (Lloyd-Price *et al.*, 2017; Sartor and Wu 2017; Cho and Blaser 2012). In the human intestine, instead, microbes of the phyla Firmicutes and Bacteroidetes predominate followed by bacteria belonging to the phyla Actinobacteria, Proteobacteria, Verrucomicrobia, Fusobacteria, Cyanobacteria and Tenericutes (Rinninella *et al.*, 2019). The dominating phyla and variability of bacterial microbiota in the different body sites together with the factors that alter microbiota populations are shown in figure 1.16 (Gupta *et al.*, 2017; Man *et al.*, 2017; Arweiler and Netuschil 2016; Rodríguez *et al.*, 2015; Human Microbiome Project Consortium 2012; Cho and Blaser 2012; Grice and Segre 2011).

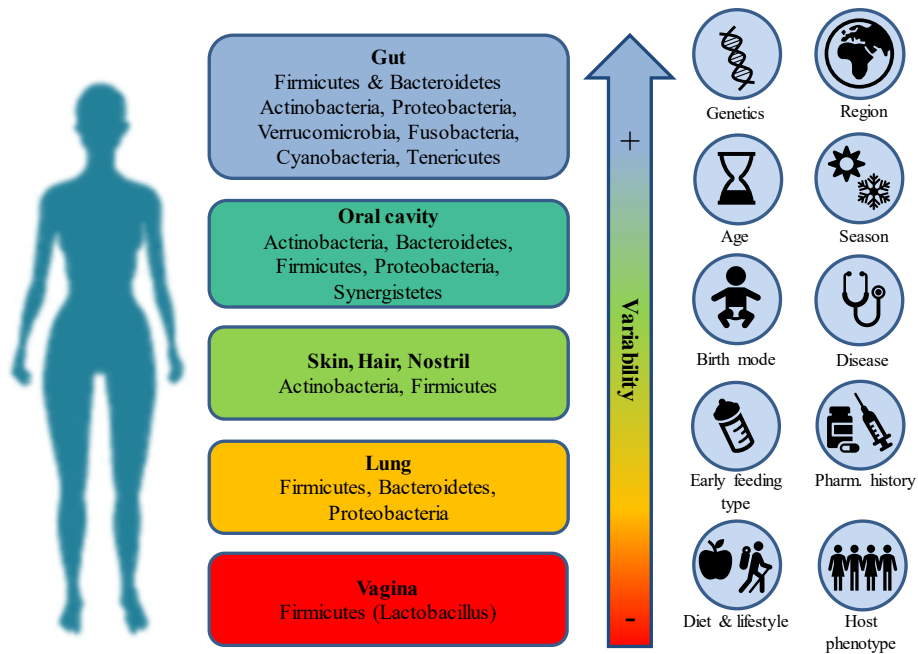


Figure 1.16. Main phyla and variability of bacterial microbiota in the different body sites and factors that alter microbiota populations.

The microbiota ecosystem with the highest diversity and highest level of personalisation is the gut (Lloyd-Price *et al.*, 2017), followed by the oral cavity and the skin (Fig.1.16). In addition, diversity increases among hunter-gatherer societies when compared to the rural agriculturalists and urban industrial populations (Gupta *et al.*, 2017).

1.7.2. Gut microbiota

The gut microbiota is an extremely complex ecosystem and it varies depending on diet, host genetics, antibiotic exposure (naturally produced or administered), maternal colonisation at birth, age, the metabolites that other gut microbiota produce and so forth (Fig.1.16) (Milani *et al.*, 2017; Thursby and Juge 2017). Moreover, bacterial composition also differs between organs and organ layers (Donaldson *et al.*, 2016).

Gut microbiota colonisation starts in the uterus where bacteria can enter the uterine environment through the bloodstream. Contextually, some species are correlated with negative pregnancy outcomes (Dunlop *et al.*, 2015; Han *et al.*, 2009). Afterwards, larger inocula are transferred during vaginal delivery and breastfeeding (Rodríguez *et al.*, 2015). The disruption of the normal balance of the gut microbiota is known as dysbiosis and it is associated with intestinal and extra-intestinal diseases such as obesity and cancer (Álvarez-Mercado *et al.*, 2019).

The gut microbiota signifies tremendous benefices for the host. Gut microbes protect the intestinal track from pathogenic colonisation by competing for adhesion sites and nutrients or by producing antimicrobials (Thursby and Juge 2017). In addition, the gut microbiota regulates host immunity, maintains the integrity of the mucosal barrier and produces nutrients like vitamins (Thursby and Juge 2017). It also produces different bioactive substances that interact with the host locally and through the blood. For example, members of the gut microbiota produce short fatty acid chains by fermentation of the dietary fibre, which might ultimately mediate microbiota-gut-brain communication (Dalile *et al.*, 2019).

The gut has a specialised mucosal immune system in which innate and adaptive immunity cooperate and balance each other to tolerate the gut microbiota. It has a physical barrier composed by the epithelial cells connected by intercellular tight junctions and covered by mucus which lubricates the intestinal tract. The mucus layer is mainly composed by gel-forming mucin glycoproteins. The small intestine has a single penetrable mucus layer protected by antibacterial mediators. The large intestine has a double mucus layer: the inner mucus layer is impenetrable and sterile, and the outer mucus layer is less dense and where mucus-associated bacteria live (Fig.1.17). The glycans present in the mucin glycoproteins are very diverse, offering bacteria many adhesion sites. Mucus is constantly produced, providing mucus-associated bacteria a place to live and

nutrients to grow. In summary, the mucus layer has a protective as well as prebiotic function. The integrity of the mucus is essential for a normal functioning of the intestine, integrity alterations are associated with disorders such as Crohn disease and ulcerative colitis (Johansson and Hansson 2016; Derrien *et al.*, 2010).

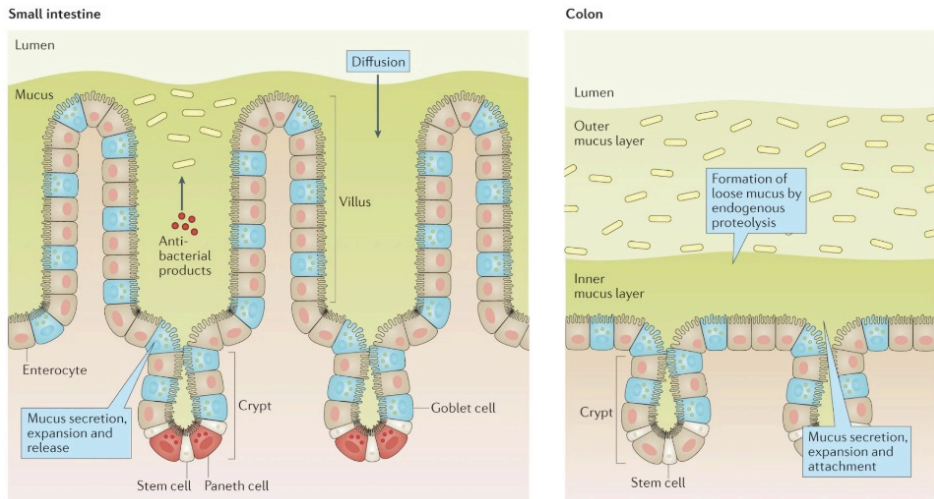


Figure 1.17. Schematic view of the small intestine and the colon (Johansson and Hansson 2016).

The chemical barrier relies on numerous cytokines and chemokines that are secreted to regulate immune cells (neutrophils, macrophages, basophils, and T-cells). In addition, the gut has some specialised cells from non-hematopoietic (epithelia, Paneth cells, goblet cells) and hematopoietic (macrophages, dendritic cells, T-cells) origin involved in the immune responses. Furthermore, intestinal cells express PRRs that recognize MAMPs, such as LPS and PG (Price *et al.*, 2018; Chassaing *et al.*, 2014; Oviedo-Boyso *et al.*, 2014), but how the immune system discriminates between gut microbiota and pathogens remains to be determined. From the host side, the transcription factor, nuclear factor kappa B (NF- κ B) is essential to activate and control immune responses (Lehman and Grabowicz 2019). It is plausible that the host down-regulates specific receptors and their expression, like TLRs (Price *et al.*, 2018). On the other side, commensal may achieve immune tolerance by evading immune recognition, modulating the

host immune response when recognition occurs or directly inhibiting the host response. The molecular communication between the symbionts and the host immune system is however very complex (Round and Mazmanian 2009; Sansonetti and Medzhitov 2009), briefly, certain gut bacteria can suppress unnecessary inflammatory responses, helping to maintain immune homeostasis (Kelly *et al.*, 2004) and this is performed through their MAMPs. Therefore, differences in the nature of MAMPs from gut microbiota bacteria and other bacteria may occur. More information about the degree of diversity of MAMPs in commensals compared to pathogens is necessary.

1.7.3. LPS and PG of gut microbiota

Some examples of gut microbiota bacteria with LPS and PG that elicit immune responses have been described. For example, the phylum Bacteroidetes achieves resistance to inflammation-associated cationic antimicrobial peptides by dephosphorylation of the lipid A (Cullen *et al.*, 2015). Moreover, pathogenic and commensal bacteria modify the PG to subvert the host defence by glycan backbone modifications and stem peptide modifications (especially m-A₂pm amidation) (Sukhithasri *et al.*, 2013). Recognition by receptors may determine their local effects, for example, increased epithelial TLR4 stimulation modulate intestinal microbiota and the susceptibility to colitis (Dheer *et al.*, 2016).

In addition, both LPS and PG from gut microbiota can be found in the blood stream (Laugerette *et al.*, 2011; Clarke *et al.*, 2010). They can be secreted by various ways, like the OMVs which are secreted by Gram-negative bacteria as a natural way to communicate with other bacteria and the host. OMVs can contain LPS and PG (Tan *et al.*, 2018; Bonnington and Kuehn 2016; Vanaja *et al.*, 2016). In addition, free PG is liberated during natural cell wall turnover (Johnson *et al.*, 2013). As well, LPS and its fragments may be freely liberated, although it has never been demonstrated. The remarkable diversity of PG and LPS structures in gut microbiota bacteria and their interaction with different host receptors pose the

question if their anatomy may play a role in the development of local and systemic beneficial effects as they reach the blood stream.

In healthy humans, not many LPS cross the intestinal barrier, with levels circulating in plasma remaining lower than 200 pg/mL (Benoit *et al.*, 1998; Hurley 1995). However, many diseases increase intestinal permeability (Luchetti *et al.*, 2020; Bischoff *et al.*, 2014; Teixeira *et al.*, 2012; Fasano 2011; Rapin and Wiernsperger 2010), as happens for *Clostridium* spp. that produce deoxycholic acid (Liu *et al.*, 2018). Also, blood endotoxic LPS levels are higher in humans with obesity, type 2 diabetes, non-alcoholic fatty liver disease, pancreatitis, amyotrophic lateral sclerosis, atherosclerosis, and Alzheimer's disease compared to healthy individuals. This suggests that an increase in gut permeability could favour LPS translocation into the blood stream (Loffredo *et al.*, 2020; Fuke *et al.*, 2019). Also, LPS levels greatly depend on diet (probiotics, prebiotics, polyphenols and dietary habits) and gut microbiota populations (Fuke *et al.*, 2019). Consequently, gut microbiota LPS might have, not only local, but systemic effects. For instance, total LPS produced by the healthy human gut microbiota potentially antagonizes TLR4-dependent cytokine production (d'Hennezel *et al.*, 2017). Same for PG that can be recognised by NOD-1 receptors (MurNAc-L-Ala-D-iGlu-m-A₂pm), activate the transcription factor NF-κB and restore neutrophil function (Clarke *et al.*, 2010). Also, PGRPs discriminate between symbionts and pathogens in many organisms. In mammals, the lack of PGRPs, favours the growth of pro-inflammatory and damaging microbiota (Saha *et al.*, 2010).

Within this frame, LPS and PG structures may be somehow implicated in the development of beneficial and negative effects of *Akkermansia muciniphila* and *Fusobacterium nucleatum*. *A. muciniphila* can reduce insulinemia, cholesterol, body weight and fat mass (Depommier *et al.*, 2019). The oral commensal *F. nucleatum* facilitates the formation of the dental plaque biofilm (Brennan and Garrett 2019). Conversely, when *F. nucleatum* spreads *extra-orally*, it is involved

in numerous diseases such as adverse pregnancy outcomes or colorectal cancer (Han 2015; Han and Wang 2013). Describing their LPS and PG architecture is crucial to fully understand these interactions and maybe, use bacterial MAMPs or develop analogues with clinical applications.

1.7.4. *Akkermansia muciniphila*

Akkermansia muciniphila is an oval non-spore forming Gram-negative bacteria. It is non-motile even if it presents pili proteins (Zhang *et al.*, 2019). It is anaerobic although it can grow in presence of some oxygen (Geerlings *et al.*, 2018). *A. muciniphila* is present in the intestines of humans and other animals and is one of the few bacteria that successfully inhabits the mucus layer; Its presence is associated with a healthy intestine (Zhang *et al.*, 2019).

A. muciniphila belongs to the phylum Verrucomicrobia, and it is the only member of this phylum that lives in the human intestine where it is one of the most abundant species (Zhang *et al.*, 2019). It is classified in the super-phylum PVC, together with Planctomycetes, Poribacteria, Lentisphaerae and Chlamydiae (Gupta *et al.*, 2012; Lee *et al.*, 2009) (Fig.1.18). At least eight different species of the *Akkermansia* genus live in the human intestinal tract, although it is not clear if they are niche-specific or not (Van Passel *et al.*, 2011).

The chromosome of *A. muciniphila* has a circular chromosome of $2,6 \cdot 10^6$ base pairs and only 65% of the protein-coding genes have been assigned to a putative function. *A. muciniphila* has specific genes that are absent in the other genomes of Verrucomicrobia members. Specific genes related to carbohydrate transport and metabolism and OM biogenesis are enriched. In contrast, specific genes related to ribosomal structure and biogenesis or nucleotide transport and metabolism are underrepresented (Van Passel *et al.*, 2011). Interestingly, *A. muciniphila* genome does not code for the enzyme Glm essential for PG synthesis

as it converts fructose-6-phosphate to glucosamine-6-phosphate. *A. muciniphila* synthesizes PG by using GlcNAc present in the mucin (van der Ark *et al.*, 2018).

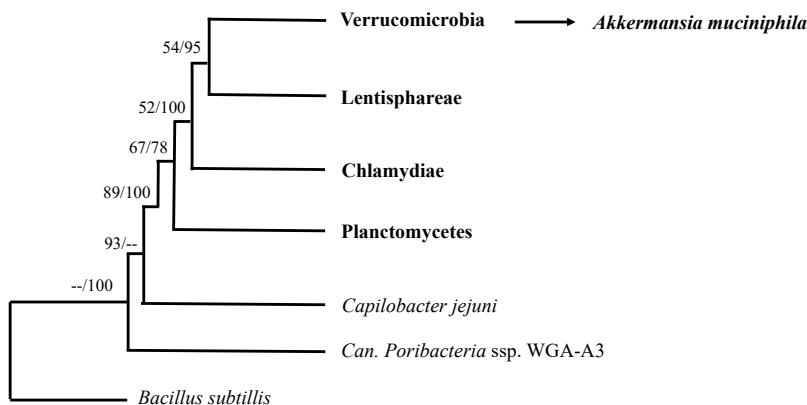


Figure 1.18. Phylogenetic profiling of *Akkermansia muciniphila*. The numbers on the node indicate the percentage of statistical support for different nodes using neighbour-joining / maximum likelihood algorithms of Gupta, Bhandari, and Naushad 2012.

There are various strains of *A. muciniphila* that inhabit the mucus layer (Van Passel *et al.*, 2011). Because of its mucus degradation capacity, *A. muciniphila* plays a crucial role in the natural mucus turn over, degrading mucine and stimulating mucine production (Derrien *et al.*, 2008).

A. muciniphila colonizes the human intestine very early in life and the amount of this bacterium quickly increases during the first year of life. It probably arrives to the human intestinal tract through breastfeeding since it has been detected in human milk. It has also been isolated from the oral cavity, pancreas, biliary system, small and large intestines, and appendix (Table 1.4). All these body sites have mucins or oligosaccharides with chemical composition similar to the intestinal mucus glycans. Interestingly the population levels of this bacterium are altered in disease and also slightly decreased in elderly (Geerlings *et al.*, 2018).

Table 1.4. Isolation sites of *A. muciniphila* in the digestive track. Modified from Geerlings et al 2018.

Low abundance	High abundance)
Oral cavity	Cecum
Pancreas	Appendix
Gallbladder	Ascending colon
Duodenum	Transverse colon
Common bile duct	Descending colon
Ileum	Sigmoid colon

The presence of *A. muciniphila* has been associated with a healthy intestine. Lowered population levels are associated with diseases such as ulcerative colitis, Crohn's disease, pre-diabetes, type 2 diabetes, obesity and other metabolic disorders. Many of these diseases alter the mucus layer and, therefore, the population levels are not enough to establish a causative effect. However, *A. muciniphila* population can be used as a biomarker for the pathological state of the intestine (Álvarez-Mercado *et al.*, 2019; Earley *et al.*, 2019; Geerlings *et al.*, 2018; Derrien *et al.*, 2017).

There is evidence of the beneficial effect of *A. muciniphila*. Studies in mice suggest that *A. muciniphila* reduces fat accumulation and body weight and regulates glycemia levels (Everard *et al.*, 2013). Also, a very recent clinical trial (NCT02637115) probed that the daily oral supplementation with live or pasteurised *A. muciniphila* is safe and improves insulin sensitivity and reduces insulinemia, cholesterol and blood markers for liver dysfunction and inflammation without affecting the rest of the microbiome structure. Also, it slightly decreases body weight and fat mass (Depommier *et al.*, 2019). Positive effects of *A. muciniphila* are maintained when the pasteurised bacterium is administered, but not after autoclaving (Cani and de Vos 2017). As well, specific

parts of the bacterium can produce positive effects. A specific pilus-associated protein isolated from the OM of *A. muciniphila* (Amuc_1100) interacts with TLR2 and has been linked to improvement of the gut barrier and reduction of fat mass development, insulin resistance and dyslipidaemia in mice (Plovier *et al.*, 2017).

There are still many open questions concerning its implications on health and disease. Likely, the strong effects of *A. muciniphila* administration are a consequence of its uniqueness (Derrien *et al.*, 2017). Deciphering structures inherent to *A. muciniphila* such as the LPS and PG will contribute to the understanding of their interaction with the host. It will also give key information for the development of new pharmaceutical molecules to prevent and treat metabolic diseases.

1.7.5. *Fusobacterium nucleatum*

Fusobacterium nucleatum is a non-spore forming, non-motile, rod shape, anaerobic Gram-negative bacterium. It is a commensal that inhabits the oral cavity and plays a crucial role in the formation of biofilms. It produces mainly butyric acid as product of the fermentation of glucose and peptone (Bolstad *et al.*, 1996) which seems to be relevant for the development of ulcerative colitis (Ohkusa *et al.*, 2003). It belongs to the phylum Fusobacteria which is divided into two families: *Leptotrichiaceae* and *Fusobacteriaceae* (Brennan and Garrett 2019) (Fig.1.19). The genus *Fusobacterium* is divided into five subspecies (spp.): *polymorphum*, *nucleatum*, *vincentii*, *fusiforme*, and *animalis* (Karpathy *et al.*, 2007). They are commensal or disease-associated (Brennan and Garrett 2019). The genome size of *F. nucleatum* is about $2,4 \cdot 10^6$ base pairs, and G+C content of 27 to 28 mol% (Bolstad 1994). Interestingly, *F. nucleatum* does not have sialidase activity and therefore sialic acid cannot be used as source of energy, carbon and nitrogen (Moncla, Braham, and Hillier 1990), not even as virulence factor to expose and use sialic acid for ligand binding (Sudhakara *et al.*, 2019). Sialic acid metabolism genes usually form clusters called Nan cluster and although *F. nucleatum* possess those genes, their activity is minimal (Yoneda *et al.*, 2014).

F. nucleatum is a ubiquitous member of the human oral flora. It is present in case of health and disease, although the population significantly increases in case of periodontitis (Bolstad *et al.*, 1996). As an oral commensal, *F. nucleatum* plays integral and beneficial roles. Thanks to its elongated shape and the expression of numerous adhesines, it can interact and connect with different bacterial species and human cells facilitating the formation of the dental plaque biofilm (Brennan and Garrett 2019).

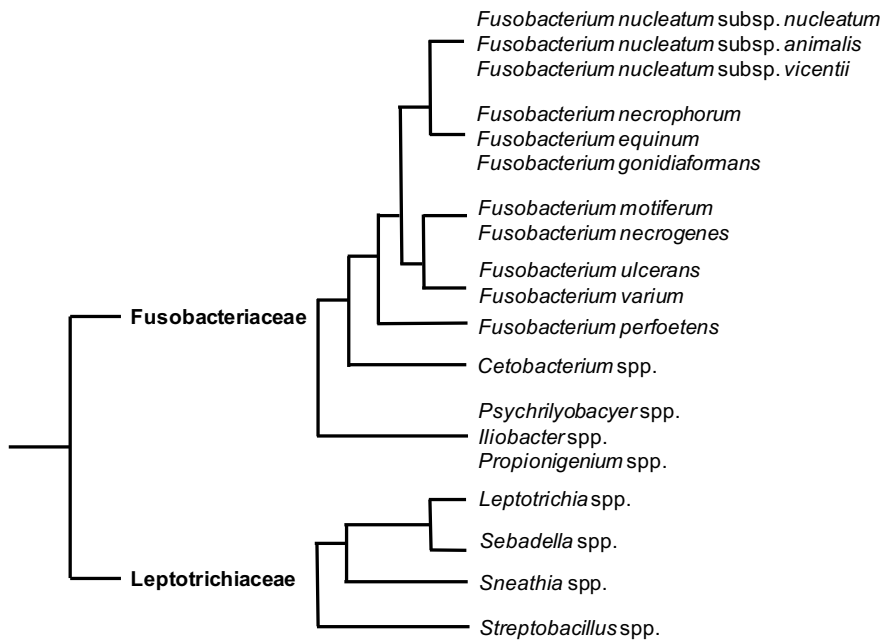


Figure 1.19. Phylogenetic profile of *Fusobacterium nucleatum*. Modified from Brennan and Garrett 2019.

Although it is an oral commensal, it is involved in periodontal diseases (Yang *et al.*, 2014) as well as extra-oral disorders such as adverse pregnancy outcomes (Han *et al.*, 2009), gastro intestinal disorders like colorectal cancer, ulcerative colitis, inflammatory bowel disease and appendicitis (Shang and Liu 2018), cardiovascular diseases like atherosclerosis (Velsko *et al.*, 2015), rheumatoid arthritis (Témoins *et al.*, 2012), respiratory tract infections (Brook 2013), Lemierre’s syndrome, organ abscesses (Brook 2013) and Alzheimer’s disease (Sparks Stein *et al.*, 2012). Its correlation with disease is clear since it is rarely detected in healthy tissues other than the mouth and in some disorders it is detected in significantly high proportions (Han and Wang 2013). For example, *F. nucleatum* has been isolated from infected respiratory tissue (Brook 2013) and oral hygiene has been proved to prevent pneumonia and respiratory tract infections (Sjögren *et al.*, 2008). *F. nucleatum* spp. *animalis* is the most involved in intrauterine infections (Han 2015) and colorectal cancer (Ye *et al.*, 2017; Gao *et al.*, 2017), reaching these extra-oral tissues through the blood (Abed *et al.*,

2016; Han *et al.*, 2004). *F. nucleatum* potentiates intestinal tumorigenesis mainly by selectively recruiting of tumour-infiltrating myeloid cells, predominantly myeloid-derived suppressor cells, with potent immunosuppressive activity (Ye *et al.*, 2017), and inhibits human T-cell response (Mima *et al.*, 2015), leading to colorectal neoplasia progression. Also the LPS from *F. nucleatum* has proved to stimulate the B lymphocytes (Hofstad *et al.*, 1993) and production of TNF α and IL-8 (Krisanaprakornkit *et al.*, 2000). However, the mechanisms underpinning the interaction of *F. nucleatum* with immune cells remain undefined.

LPSs and PG play a crucial role in immune system evasion and tissues invasion (Bartholomew *et al.*, 2019; Juan *et al.*, 2018; Sukhithasri *et al.*, 2013; Yan *et al.*, 2012; Kawasaki *et al.*, 2004; Edwards *et al.*, 2000) The dual behaviour commensal-pathogen of *F. nucleatum*, makes especially important the study of its LPS and PG. The structure of the OPS of the strains ATCC 23726 (Vinogradov *et al.*, 2018a), MJR 7757B (Vinogradov *et al.*, 2018b), 10953 (Vinogradov *et al.*, 2017; Okahashi *et al.*, 1988), 12230 (Vinogradov *et al.*, 2017a) and 25586 (Vinogradov *et al.*, 2017b) has been determined. Also, the composition of the LPS of the strain JCM 8535 (Onoue *et al.*, 1996) and Fev1 (Hofstad and Fredriksen 1979) and the structure of the lipid A of Fev-1 (Hase *et al.*, 1977). These data showed high diversity in carbohydrate composition among strains and common the presence of amino sugars, uronic acids and amino decorations. The composition of the PG of *Fusobacterium nucleatum* has only been described for Fev 1 which presents meso-lanthionine instead of m-A₂pm (Vasstrand 1981; Vasstrand *et al.*, 1979). Enhancing our understanding of the interaction commensal-host, pathogen-host and with other members of the microbiota of *F. nucleatum* and during disease development by LPS and PG characterisation is necessary.

1.8. Aims of the thesis

The overarching goal of this Ph.D. thesis is to characterize LPS and PG and their structural determinants when bound to major proteins involved in its transport across the periplasm. This way contributing to the understanding of the interaction of pathogen and commensal Gram-negative bacteria with the host through their MAMPs: LPS and PG; and deepening the understanding of the trans-envelope machineries to find new targets for antibiotics.

The specific objectives are:

1. To disclose the composition and structure of the LPS and the PG of *Akkermansia muciniphila* Muc^T (ATCC BAA-835) and *Fusobacterium nucleatum* spp. *animalis* ATCC 51191, contributing to phylogenetic and epidemiological knowledge.
2. To disclose the immunological properties of the LPS of *A. muciniphila* Muc^T (ATCC BAA-835) and *F. nucleatum*, contributing to the understanding of the interaction of pathogen and commensal bacteria with the host.
3. To study the effects of mutations of the essential β -barrel proteins assembly machinery (BAM) on the LPS synthesis, to deepen in the understanding of the relationship of different trans-envelope machineries.
4. To develop a tool for the study of the interaction between LPS with proteins such as Lpt or immune receptors by NMR.
5. To study the formation of the Lpt periplasmic bridge across the periplasm and the PG layer, contributing to the understanding on the functionality of the trans-envelope machineries.

Chapter 2

Results and discussion

Part 1. LPS and PG from commensal bacteria

2.1. The lipooligosaccharide of *Akkermansia muciniphila* Muc^T

2.1.1. Production and purification of the LOS of *A. muciniphila*

Akkermansia muciniphila Muc^T (ATCC BAA-835) freeze-dried cells (8 g) were treated through a combination of the phenol/chloroform/light petroleum (PCP) and the hot phenol/water extractions to isolate the LOS. The SDS-PAGE with silver staining evidenced the presence of LOS in both phases resulting from the PCP extraction and the water phase of the hot phenol/water extraction. Subsequently, the sample underwent an enzymatic digestion. SDS-PAGE evidenced the presence of LOS in the normal precipitate (**B**) and the precipitate of the ultra-centrifuge (UC) (**C**) resulting from the enzymatic digestion of the water phase of the hot phenol/water extraction (yield 16.2 mg LOS / 1 g dried cells) (Fig.2.1.1).

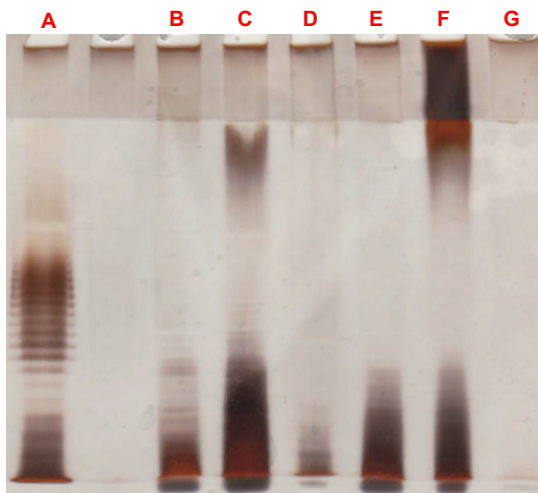


Figure 2.1.1. SDS-PAGE with silver staining 9 μ L sample. **A.** *E. coli* LPS; Hot phenol/water extraction; **B.** Precipitate after enzymatic digestion of aqueous phase; **C.** Precipitate UC after enzymatic digestion of aqueous phase; **D.** Supernatant UC after enzymatic digestion of aqueous phase; **E.** Precipitate centrifuge after enzymatic digestion phenol phase; **F.** Precipitate UC after enzymatic digestion phenol phase; **G.** Supernatant UC after enzymatic digestion phenol phase.

Mild acid hydrolysis was performed on the full LOS (16 mg) in order to separate the polysaccharidic chain from the lipid A. The lipid A was successfully isolated (5.6 mg, 35% of LOS). In the supernatant, however, a mix of different oligosaccharides was obtained and separated by High Performance Liquid Chromatography (HPLC) (Phenomenex C18 Reversed Phase). The HPLC resulted in a chromatogram with four different peaks (Fig.2.1.2). ^1H NMR experiments were performed for all the four fractions (Fig.2.1.3). The first and third peaks contained two oligosaccharides, a nonasaccharide (NONA) and a tetradecasaccharide (TETRAD) respectively as evidenced by MALDI analysis (Fig.2.1.4). The second peak presented a mix of the NONA and a TETRAD; last peak presented an impurity.

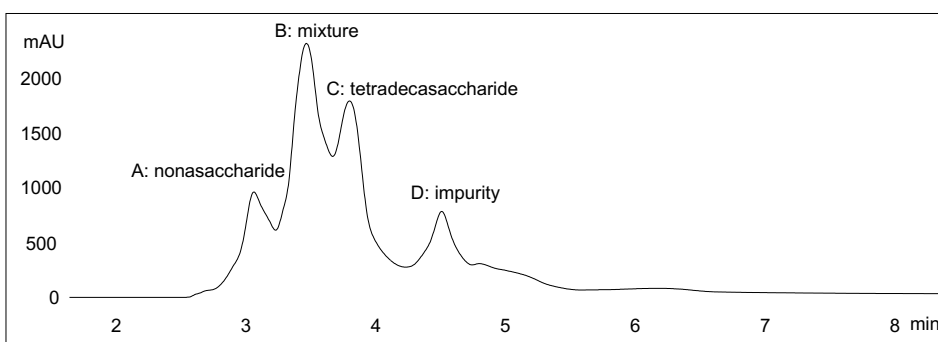


Figure 2.1.2. Mild acid hydrolysis was performed on the full LOS of *A. muciniphila* Muc^T (16 mg) in order to separate the polysaccharidic chain from the lipid A. In the supernatant, mix of different polysaccharides was obtained and separated by HPLC (High Performance Liquid Chromatography system Agilent 1100 Phenomenex C18 Reversed Phase in isocratic conditions; flow =0.8 mL/min and monitoring the eluate with a refractive index detector (206 nm). The HPLC resulted in a chromatogram with four differentiated peaks named from A to D. ^1H NMR experiments are presented in figure 2.1.3.

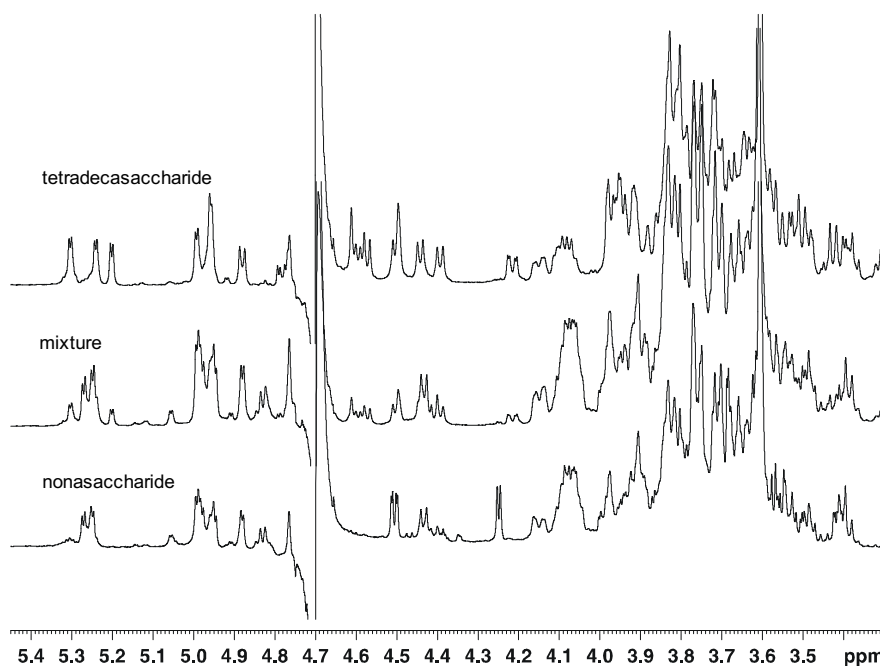


Figure 2.1.3. ^1H NMR spectra recorded for the fractions obtained by purification by HPLC of the polysaccharidic mix resulting from the acid hydrolysis of the crude LOS of *A. muciniphila* Muc^T (600 MHz). A and C contained two different polysaccharides respectively, B a mix of the polysaccharides from fractions A and C. Finally, D, presented an impure mix. The polysaccharides A and C were a nonasaccharide (NONA) and a tetradecasaccharide (TETRA) respectively.

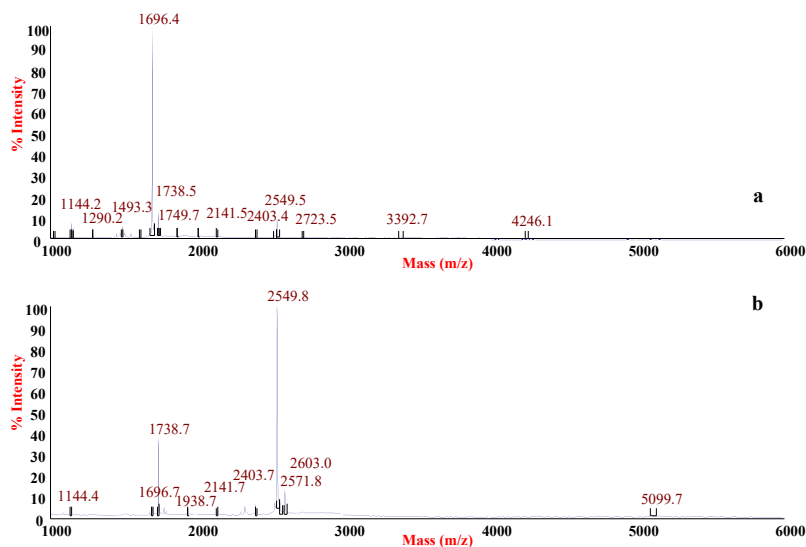


Figure 2.1.4. Negative-ion MALDI-TOF mass spectrum of the a. nonasaccharide and the b. tetradecasaccharide of *A. muciniphila* Muc^T.

2.1.2. Compositional analysis of the Nonasaccharide and the Tetradecasaccharide

Monosaccharide chemical analysis as acetylated *O*-methyl glycosides of the nonasaccharide detected the presence of fucose (Fuc), galactose (Gal), glucosamine (GlcNAc), galactosamine (GalNAc), *L-glycero-D-manno*-heptose (Hep) and 3-deoxy-*D-manno*-octulosonic acid (Kdo). The *O*-octylglycoside derivatives and the partially methylated alditol acetated methods, disclosed the presence of *t*-L-Fuc, 2,3-L-Fuc, 3,4-D-Gal, *t*-D-GlcNAc, *t*-D-GalNAc and 6-Hep (Fig.2.1.5.a).

Monosaccharide chemical analysis as acetylated *O*-methyl glycosides of the tetradecasaccharide detected the presence of Fuc, mannose (Man), Gal, glucose (Glc), GalNAc, GlcNAc, Hep and Kdo. The *O*-octylglycoside derivatives and the partially methylated alditol acetated methods, disclosed the presence of *t*-L-Fuc, 2-D-Man, 3,4-D-Gal, 2,3-D-Glc, 4-D-Glc, *t*-D-GlcNAc, 6-D-GalNAc, and 6-Heptose (Fig.2.1.5.b).

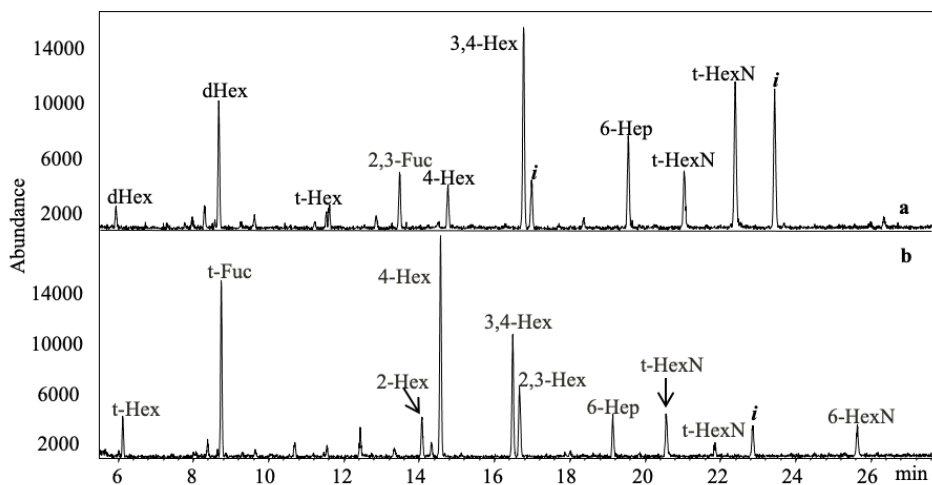


Figure 2.1.5. Partially methylated alditol acetated method results of **a.** nonasaccharide and **b.** tetradecasaccharide fractions obtained by purification by HPLC of the polysaccharidic mix resulting from the acid hydrolysis of the crude LOS of *A. muciniphila* Muc^T.

2.1.3. NMR analysis of the Nonasaccharide of *A. muciniphila*

The structure of the NONA was determined by analysing ^1H , ^1H homo- and ^1H , ^{13}C heteronuclear 2D NMR experiments recorded by dissolving this glycan in D_2O . ^1H , ^1H COSY and ^1H , ^1H TOCSY experiments were used to disclose the protons of each spin system; each carbon atom was identified through the analysis of the ^1H , ^{13}C HSQC and further confirmed by ^1H , ^{13}C HSQC-TOCSY. Finally, the primary sequence was inferred by analysis of *inter-residue* and long-range dipolar and scalar correlations from ^1H , ^1H TROESY and ^1H , ^{13}C HMBC spectra, respectively.

The HSQC spectrum presented eight main anomeric signals at ^1H 5.4-4.5 ppm that were labelled with a capital letter (A-I, Fig.2.1.6, Table 2.1.1).

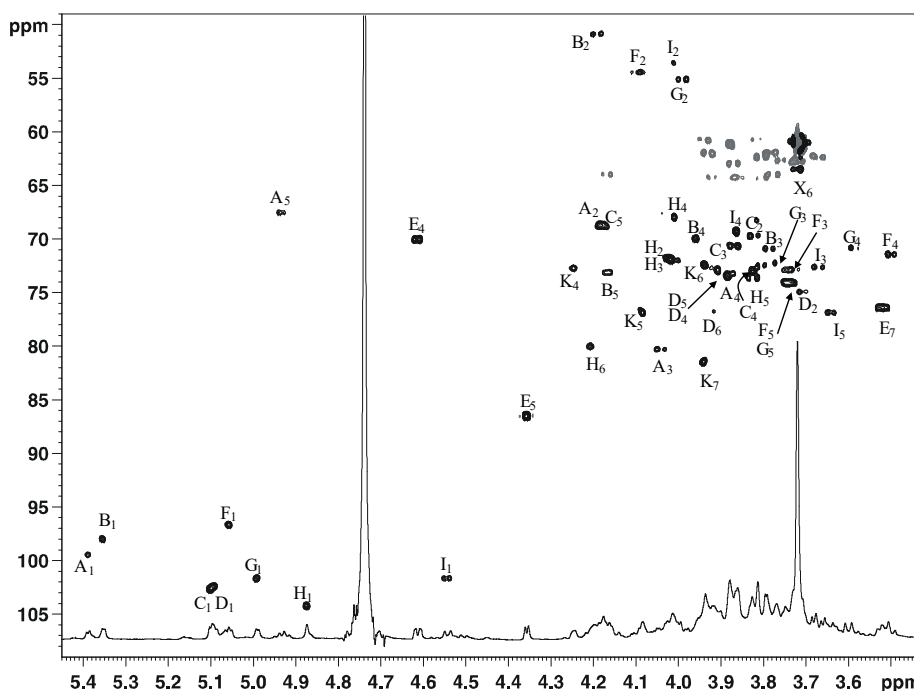


Figure 2.1.6. Expansion of HSQC spectrum recorded for NONA from *A. muciniphila* Muc^T (600 MHz, 32 °C). Grey densities correspond to “ CH_2 ” carbons. The structure is reported in figure 2.1.11 and labels refer to table 2.1.1.

NMR analysis started from H-1 of **A** (5.39 ppm) that displayed three correlations in the TOCSY spectrum (Fig.2.1.7), with that at 4.18 ppm in common with the COSY spectrum. Hence, this density was assigned to H-2, and by a similar approach H-3 (4.05 ppm) and H-4 (3.88 ppm). Lack of further correlations from H-1 enabled the recognition of **A** as a *galacto*-configured residue. Combination of TOCSY from H-3 (Fig.2.1.7) and HMBC from H-4 spectrum pointed to H-5 (4.93 ppm) (Fig.2.1.8) and it enabled the finding of H-6 via the corresponding COSY correlation (1.27 ppm). HSQC and the HSQC-TOCSY (Fig.2.1.8) spectra defined all the carbon chemical shifts of **A** (Table 2.1.1), an α -fucose based on the low chemical shift of C-6 (16.3 ppm), it is 2,3 *O*-substituted based on the low chemical shift of C-2 and C-3 (68.6 and 80.2 ppm).

Correlations on the TOCSY spectrum originating from H-1 of **B** (5.35 ppm), **C** (5.09 ppm), **D** (5.09 ppm) and **I** (4.54 ppm) had the same pattern of **A**, hence were *galacto*-configured residues. **C** was also a α -fucose, TOCSY spectrum (Fig.2.1.7), showed H-2 (3.81 ppm), H-3 (3.86 ppm) and H-4 (3.82) as overlapped, but HMBC and the HSQC-TOCSY (Fig.2.1.8) spectra allowed the unequivocal identification of both H and C chemical shifts.

B (5.35 ppm) and **D** (5.09 ppm) spin systems are α -galactoses based on the $^3J_{H1,H2}$ (3.4 Hz) value and COSY-TOCSY signals of H-5 with H-6, however, the specific identification of the H-6 was not possible because of the overlap of the signals in the CH₂ region. **B** residue was identified as a terminal α -galactosamine based on the chemical shift of C-2 (50.7 ppm). **D** residue was identified as a 3,4- α -galactose based on the values of C-3 and C-4 (76.4 and 72.8 ppm).

Table 2.1.1. Proton (^1H) (plain text) and carbon (^{13}C) (*italic*) NMR chemical shifts of the NONA polysaccharide from *A. muciniphila* Muc^T (600 MHz, 32 °C, D₂O).

	1	2	3	4	5	6	7	8
A	5.39	4.18	4.05	3.88	4.93	1.27		
2,3-α-Fuc	<i>99.4</i>	<i>68.6</i>	<i>80.2</i>	<i>73.2</i>	<i>67.2</i>	<i>16.3</i>		
B	5.35	4.19	3.79	3.96	4.17			
t-α-GalNAc	<i>98.1</i>	<i>50.7</i>	<i>70.7</i>	<i>69.9</i>	<i>72.9</i>			
C	5.09	3.81	3.86	3.82	4.18	1.27		
t-α-Fuc	<i>102.9</i>	<i>69.6</i>	<i>70.5</i>	<i>72.8</i>	<i>68.6</i>	<i>16.3</i>		
D	5.09	3.69	3.91	3.91	3.91			
3,4-α-Gal	<i>102.9</i>	<i>74.7</i>	<i>76.4</i>	<i>72.8</i>	<i>72.8</i>			
E			2.13/2.69	4.62	4.37	3.72	3.51	3.77/3.92
Free Kdof		<i>105.6</i>	<i>44.3</i>	<i>70.1</i>	<i>86.3</i>	<i>63.3</i>	<i>76.3</i>	<i>61.8</i>
F	5.06	4.10	3.72	3.50	3.74			
t-α-GlcNAc	<i>96.8</i>	<i>54.4</i>	<i>72.7</i>	<i>71.4</i>	<i>73.9</i>			
G	4.99	3.99	3.79	3.59	3.74			
t-α-GlcNAc	<i>101.8</i>	<i>55.2</i>	<i>72.3</i>	<i>70.6</i>	<i>73.9</i>			
H	4.87	4.03	4.03	4.01	3.82	4.21		
6-α-Hep	<i>104.1</i>	<i>71.7</i>	<i>71.7</i>	<i>68.0</i>	<i>73.6</i>	<i>79.9</i>		
I	4.54	2.02	3.67	3.86	3.64			
t-β-GalNAc	<i>101.5</i>	<i>53.5</i>	<i>72.6</i>	<i>69.1</i>	<i>76.7</i>			
K			1.89/1.98	4.25	4.09	3.94	3.94	3.87/3.76
4,5,7-Kdop		<i>97.75</i>	<i>34.96</i>	<i>72.6</i>	<i>76.6</i>	<i>72.4</i>	<i>81.5</i>	<i>62.7</i>

I residue (4.54 ppm) was β -galacto-configured based on the $^3J_{H1,H2}$ (8.5 Hz) value and COSY-TOCSY signals of H-5 with H-6, however, the specific identification of the H-6 was not possible because of the overlap of the signals in the CH₂ region. The chemical shift of the C-2 (53.5 ppm) highlighted the presence of an amino function. In conclusion, I was a terminal β -galactosamine.

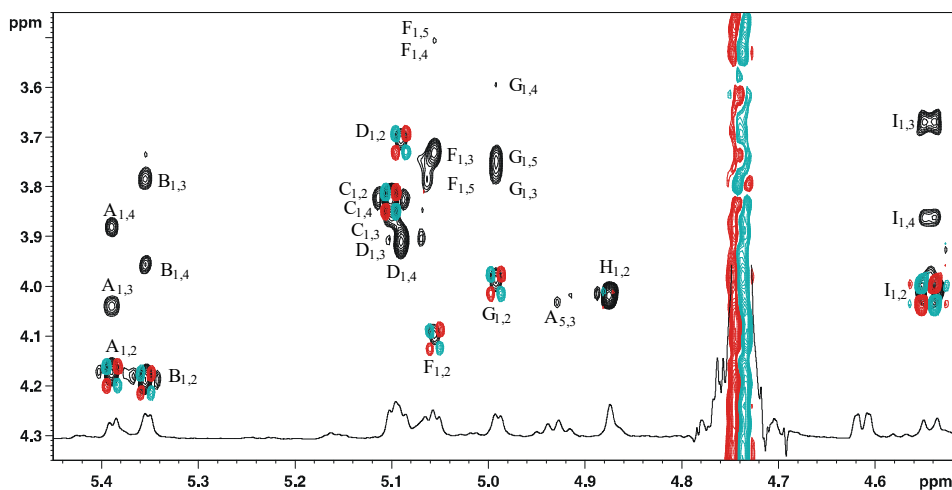


Figure 2.1.7. Expansion of TOCSY (black) and COSY (cyan/red) spectra of the NONA from *A. muciniphila* Muc^T (600 MHz, 32 °C). Labels refer to table 2.1.1.

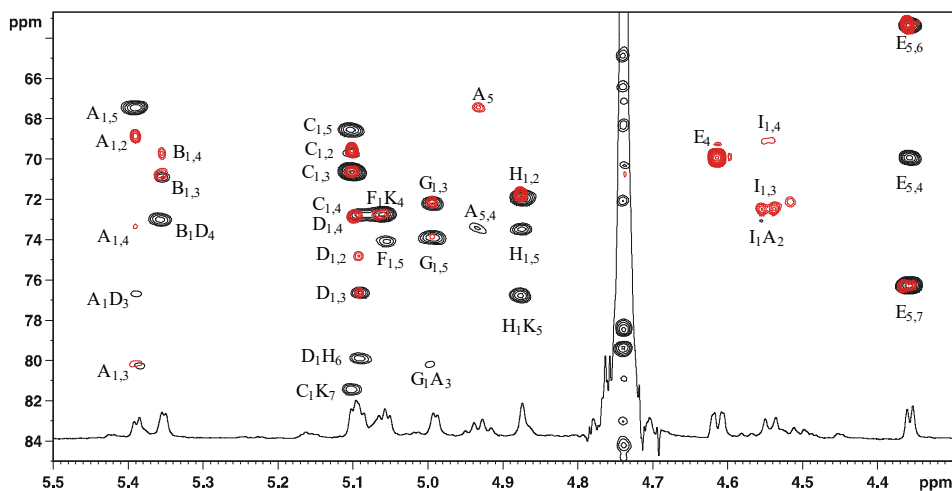


Figure 2.1.8. Expansion of HMBC (black) and HSQC-TOCSY (red) spectra of the NONA from *A. muciniphila* Muc^T (600 MHz, 32 °C). Labels refer to table 2.1.1.

H-1 of **F** (5.06 ppm) and **G** (4.99 ppm) TOCSY spectra displayed signals with all the carbons of the spin system (Fig.2.1.7), also, the $^3J_{H_1,H_2}$ value was 3.2 Hz, characterizing **F** and **G** as α -*gluco*-configured residues. They were identified as hexoses based on the COSY-TOCSY signals of H-5 with H-6; however, the specific identification of the H-6 was not possible because of the overlap of the signals in the CH₂ region. **F** and **G** showed a high field chemical shift of the C-2 (54.4 and 55.2 ppm) identifying them as terminal α -glucosamines.

H-1 of **H** (4.87 ppm) was recognised as *manno*-configured α -heptose residues, because of the lack of signals in the COSY and TOCSY spectra with other proton from the spin system other than H-2 (4.03 ppm) (Fig.2.1.7) and the low $^3J_{H_1,H_2}$ value, which is diagnostic for an equatorially oriented H-2. By TOCSY and ROESY spectra, from H-2 it was possible to assign all other cross-peaks up to H-7. It is identified as a 6 linked α -L-*glycero*-D-*manno*-heptose because of the high chemical shift of C-6 (73.6 ppm).

Finally, there were two different molecules of 3-deoxy-D-*manno*-octulosonic acid (Kdo) present in the sample named as **E** (H-4 4.62 ppm) and **K** (H-4 4.17 ppm). The analysis started from the H-3/C-3 methylene signals (4.62/70.1 and 4.17/72.3 ppm). The TOCSY connected these two protons to the H-4 (4.62 and 4.17 ppm) and H-5 (4.37 and 4.09 ppm), the COSY established the correct sequence between the two signals. **E** presented a COSY signal to H-6 (3.72 ppm) and this with H-7 (3.51 ppm). From H-5 of **K** there were overlapped TOCSY signals to H-6 (3.94 ppm) and H-7 (3.94 ppm). Note that the low resonances of H-4, H-5 and H-7 of **K** indicated that the positions were substituted). **E** was a furanose form of Kdo, as evidenced by the long-range correlation of C-2 with H-5 (Fig.2.1.9), and the chemical shift values of H-3s (2.13, 2.69 ppm), C-2 (105.6 ppm) and C-5 (86.3 ppm) (Table 2.1.1). This unit was not part of the nonasaccharide, it was co-eluted with it during the HPLC purification.

The combination of the HMBC (Fig.2.1.8) and TROESY (Fig.2.10) allowed the location of all carbohydrate residues in an oligosaccharide chain. Hence, the NONA from *A. muciniphila* is a nonasaccharide as reported in figure 2.1.11 and is consistent with the data from the GC-MS.

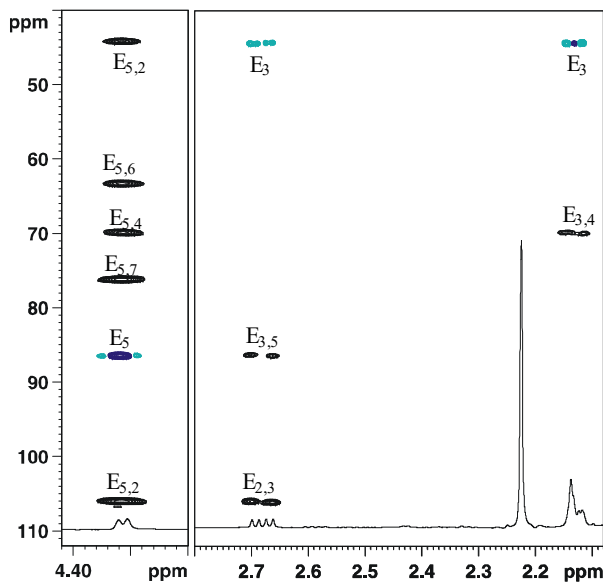


Figure 2.1.9. Expansion of HMBC (black) and HSQC (blue) spectra of the NONA from *A. muciniphila* Muc^T (600 MHz, 32 °C). Labels refer to table 2.1.1.

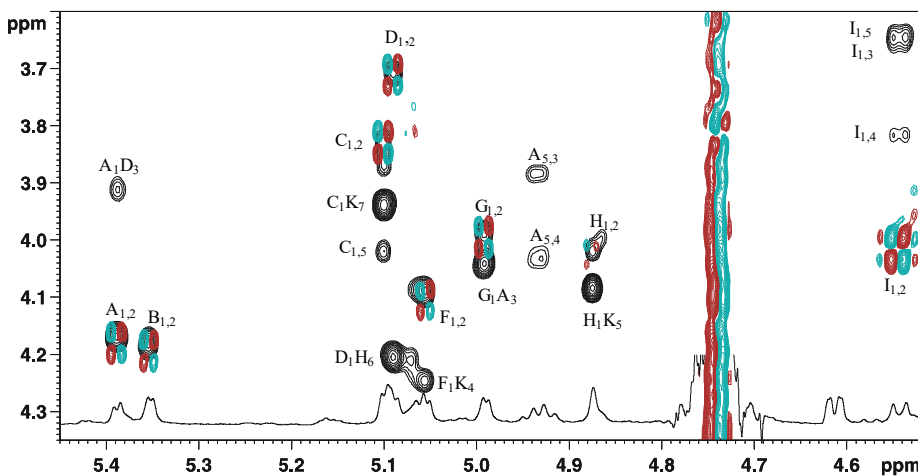


Figure 2.1.10. Expansion of TROESY (black) and COSY (cyan/red) spectra of the NONA from *A. muciniphila* Muc^T (600 MHz, 32 °C). Labels refer to table 2.1.1.

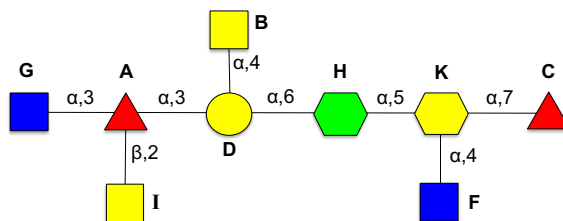


Figure 2.1.11. Structure of the NONA from *A. muciniphila* Muc^T using Symbol Nomenclature for Glycans (SNFG). Labels refer to table 2.1.1.

2.1.4. NMR analysis of the Tetradecasaccharide of *A. muciniphila*

The structure of the TETRAD was determined by NMR using the same approach reported for the nonasaccharide. ¹H,¹H COSY and ¹H,¹H TOCSY experiments were used to disclose the protons of each spin system; each carbon atom was identified through the analysis of the ¹H,¹³C HSQC and further confirmed by ¹H,¹³C HSQC-TOCSY. Finally, the primary sequence was inferred by analysis of *inter*-residue and long-range dipolar and scalar correlations from ¹H,¹H TROESY and ¹H,¹³C HMBC spectra, respectively.

The HSQC spectrum presented thirteen main anomeric signals at ¹H 5.4-4.5 ppm that were labelled with a capital letter (A-O, Fig.2.1.12, Table 2.1.2). NMR analysis started from H-1 of A (5.06 ppm) that displayed four correlations in the TOCSY spectrum (Fig.2.1.13), with the one at 4.08 ppm in common with the COSY spectrum. Hence, this density was assigned to H-2, and by a similar approach, H-3 (3.73 ppm), H-4 (3.48 ppm) and H-5 (3.74 ppm) were also assigned. These correlations from H-1 enabled the recognition of A as a *gluco*-configured monosaccharide. Combination of COSY and HMBC from H-5 spectrum pointed to the H-6 (3.77 and 3.93 ppm). The chemical shift of the C-2 (54.4 ppm) highlighted the presence of an amino function. HSQC and the HSQC-TOCSY (Fig.2.1.14) spectra defined all the carbon chemical shifts of A (Table 2.1.2) and based on the ³J_{H1,H2} (3.48 Hz) it was identified as a terminal t- α -2-GlcN. G was identified as a 4- α -Glc, following the same approach and based on the C-4 (79.6 ppm). H-1 of F, H and L (4.61, 4.55 and 4.98 ppm respectively)

also displayed four correlations in the TOCSY spectrum (Fig.2.1.13) and were identified as β -Glc based on their $^3J_{H1,H2}$ values (8.63, 8.04 and 7.7 Hz respectively). Both **F** and **H** were 4-substituted residues as evidenced from the high resonance of their C-4 (78.3 and 81.0 ppm respectively). **O** presented a similar signal arrangement with a C-2 at 54.6 ppm, indicative of a t- β -GlcN.

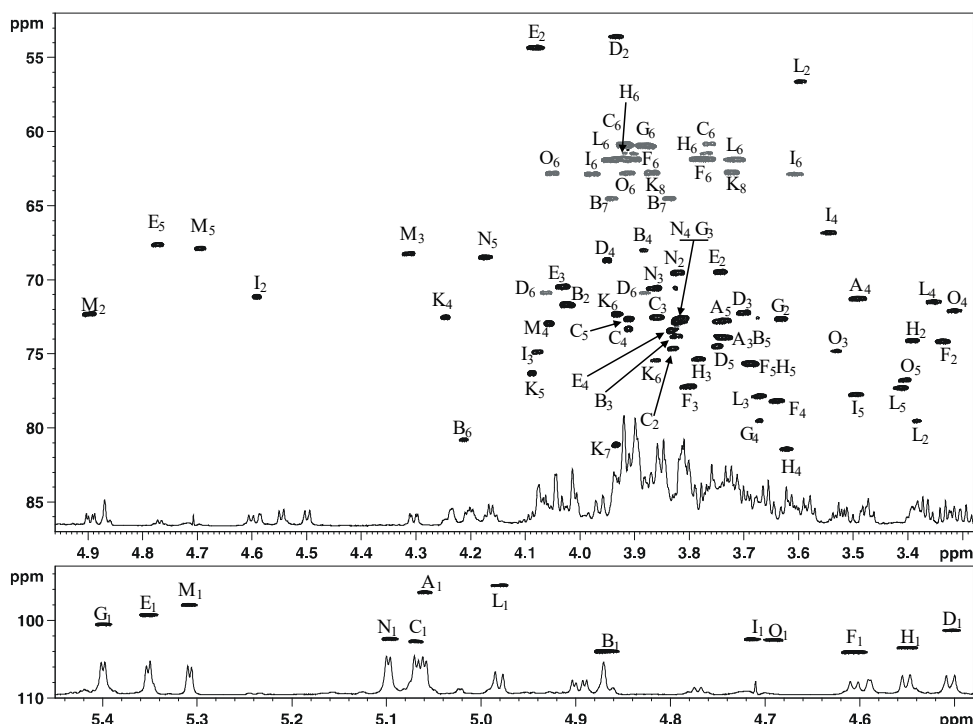


Figure 2.1.12. HSQC spectrum expansion of the TETRAD from *A. muciniphila* Muc^T (950 MHz, 27 °C) the structure is reported in figure 2.1.16. Labels refer to table 2.1.2.

Table 2.1.2. Proton (¹H) (plain text) and carbon (¹³C) (*italic*) NMR chemical shifts of the TETRAD polysaccharide from *A. muciniphila* Muc^T (950 MHz, 27 °C, D₂O).

	1	2	3	4	5	6	7	8
A	5.06	4.08	3.73	3.48	3.74	3.77/3.93		
t-α-GlcNAc	<i>96.6</i>	<i>54.4</i>	<i>73.9</i>	<i>71.3</i>	<i>72.8</i>	<i>61.9</i>		
B	4.87	4.02	3.83	3.88	3.74	4.21	3.94/3.83	
6-α-Hep	<i>104.1</i>	<i>71.7</i>	<i>73.8</i>	<i>68.1</i>	<i>73.8</i>	<i>80.8</i>	<i>64.5</i>	
C	5.97	3.83	3.86	3.91	3.91	3.77/3.92		
3,4-α-Gal	<i>102.7</i>	<i>74.7</i>	<i>72.6</i>	<i>73.3</i>	<i>72.7</i>	<i>60.8</i>		
D	4.50	3.93	3.71	3.95	3.75	3.86/4.07		
6-β-GalNAc	<i>101.3</i>	<i>53.6</i>	<i>72.4</i>	<i>68.6</i>	<i>74.5</i>	<i>70.9</i>		
E	5.35	3.74	4.03	3.83	4.77	1.23		
t-α-Fuc	<i>99.3</i>	<i>69.5</i>	<i>70.5</i>	<i>73.5</i>	<i>67.8</i>	<i>16.7</i>		
F	4.61	3.34	3.80	3.64	3.69	3.77/3.95		
4-β-Glc	<i>103.9</i>	<i>74.2</i>	<i>77.3</i>	<i>78.3</i>	<i>75.7</i>	<i>61.9</i>		
G	5.40	3.63	3.81	3.67	3.86	3.88		
4-α-Glc	<i>100.5</i>	<i>72.7</i>	<i>72.7</i>	<i>79.56</i>	<i>72.6</i>	<i>61.1</i>		
H	4.55	3.39	3.78	3.62	3.68	3.77/3.91		
4-β-Glc	<i>103.57</i>	<i>74.15</i>	<i>75.4</i>	<i>81.0</i>	<i>75.7</i>	<i>61.4</i>		
I	4.71	4.59	4.07	3.55	3.49	3.61/3.97		
2-β-Man	<i>102.5</i>	<i>71.2</i>	<i>74.8</i>	<i>66.9</i>	<i>77.8</i>	<i>62.87</i>		
K			1.90/2.22	4.25	4.09	3.93	3.93	3.87/3.72
4,5,7-Kdo	<i>174.7</i>	<i>97.9</i>	<i>34.6</i>	<i>72.6</i>	<i>76.2</i>	<i>72.3</i>	<i>81.0</i>	<i>62.8</i>
L	4.98	3.38	3.67	3.35	3.41	3.71/3.91		
2,3-β-Glc	<i>95.5</i>	<i>79.5</i>	<i>77.8</i>	<i>71.5</i>	<i>77.3</i>	<i>61.9</i>		
M	5.31	4.90	4.32	4.06	4.69	1.22		
t-α-Fuc	<i>97.97</i>	<i>74.4</i>	<i>68.3</i>	<i>73.0</i>	<i>69.9</i>	<i>16.4</i>		
N	5.10	3.81	3.86	3.82	4.17	1.19		
t-α-Fuc	<i>102.5</i>	<i>69.5</i>	<i>72.5</i>	<i>72.9</i>	<i>68.5</i>	<i>16.97</i>		
O	4.69	3.61	3.53	3.31	3.41	4.05/3.91		
t-β-GlcNAc	<i>102.5</i>	<i>54.6</i>	<i>74.8</i>	<i>72.1</i>	<i>76.8</i>	<i>63.0</i>		

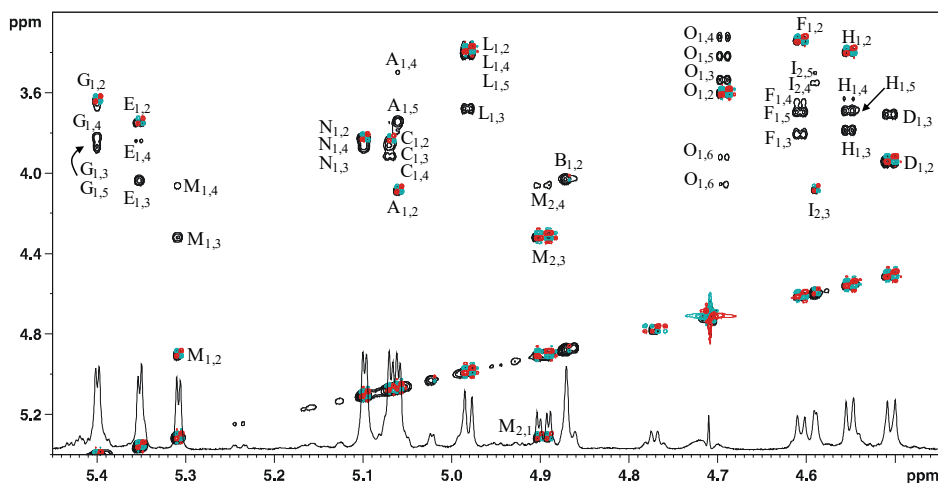


Figure 2.1.13. Expansion of TOCSY (black) and COSY (cyan/red) spectra of the TETRAD from *A. muciniphila* Muc^T (950 MHz, 27 °C). Labels refer to table 2.1.2.

The H-1 of **C** (5.07 ppm) displayed three correlations in the TOCSY spectrum (Fig.2.1.13), a pattern characteristic of a *galacto*-configured. The signal at 3.83 ppm was in common with the COSY spectrum, hence, this density was assigned to H-2. By a similar approach, H-3 (3.86 ppm) and H-4 (3.91 ppm) were also assigned. H-5 (3.91 ppm) was identified in the same way from H-4. It was identified as a t- α -Gal based on the $^3J_{H1,H2}$ value (4 Hz). **D** displayed three correlations in the TOCSY spectrum (Fig.2.1.13) as well. The chemical shift of the C-2 (53.6 ppm) highlighted the presence of an amino function and the $^3J_{H1,H2}$ (4 Hz) evidenced a t- β -GalN. In addition, **E**, **M** and **N** were also *galacto*-configured and H-2, H-3 and H-4 were identified in the same way as in **C**. The distinctive shift of H-2 of **M** (4.89 ppm) evidenced that this position was acetylated. H-1 of **E**, **M** and **N** (5.35, 5.31 and 5.10 ppm respectively) displayed HMBC signals with C-5 (67.8, 69.97 and 68.5 ppm respectively) (Fig.2.1.14) and TROESY signals from H-3 and H-4 to H-5 (4.77, 4.69 and 4.17 ppm respectively) (Fig.2.1.15). H-6 were identified through COSY signals from H-5 and disclosed that **E**, **M** and **N** were t- α -Fuc because of the values of the H-6 (1.23, 1.22 and 1.87 ppm respectively).

H-1 of **B** (4.87 ppm) was recognised as *manno*-configured α -heptose residue, because of the lack of signals in the COSY and TOCSY spectra with other protons from the spin system other than H-2 (4.02 ppm) (Fig.2.1.13). By TOCSY and ROESY spectra, from H-2 it was possible to assign all other cross-peaks up to H-7. It is identified as a 6 linked α -L-*glycero*-D-*manno*-heptose because of the high chemical shift of C-6 (80.8 ppm).

Finally, **K** was identified as Kdo (H-4 4.25 ppm). The analysis started from the H-3/C-3 methylene signals (1.90, 2.22 / 34.6 ppm). The TOCSY connected these two protons to the H-4 (4.25 ppm) and H-5 (4.09 ppm), the COSY established the correct sequence between the two signals. From H-5 HSQC-TOCSY signals and NOESY signals from H-4 to H-6 (3.91 ppm). H-7 (3.93 ppm) overlapped with H-6 in the 1D experiments but was identified using the HSQC-TOCSY and subsequently the H-8 (3.87/3.72 ppm). The low resonances of C-4, C-5 and C-7 of **K** indicated that the positions were substituted (72.6, 76.2 and 81.0 ppm respectively).

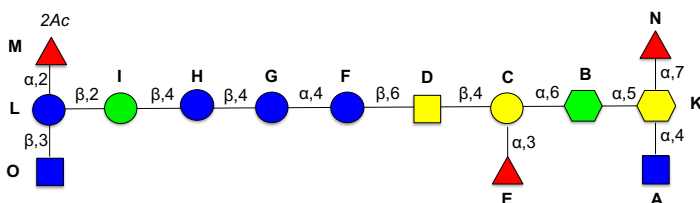


Figure 2.1.16. Structure of the TETRAD from *A. muciniphila* Muc^T using SNFG. Labels refer to table 2.1.2.

The combination of the HMBC (Fig.2.1.14) and ROESY (Fig.2.1.15) allowed the identification of the oligosaccharide chain sequence. Hence, the TETRAD from *A. muciniphila* is a tetradecasaccharide with high level of ramification by fucoses as reported in figure 2.1.16 and is consistent with the data from the GC-MS.

2.1.5. Structural characterisation of the Lipid A of *A. muciniphila*

The lipid compositional analysis of the LOS of *A. muciniphila* revealed the presence of *iso*-tetradecanoic acid (*i*-C14:0), *iso*-3-hydroxy pentadecanoic acid (*i*-C15:0 (3-OH)) and heptadecanoic acid (C17:0) amongst others (Fig.2.1.17). The negative-ion MALDI-TOF MS spectrum recorded in negative ion polarity of the lipid A from *A. muciniphila* isolated through mild acid hydrolysis of the LOS, is reported in figure 2.1.18.

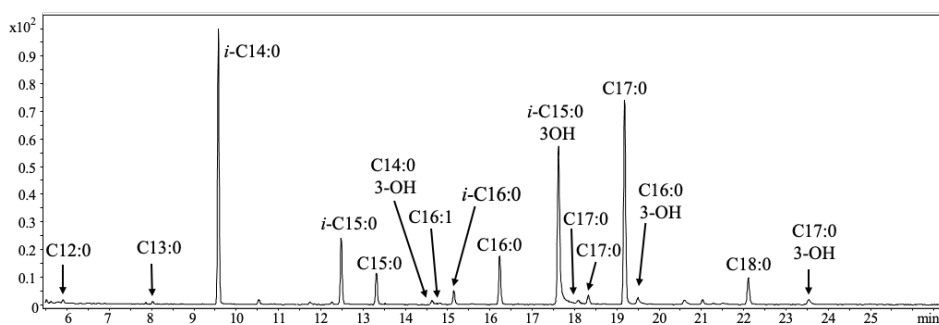


Figure 2.1.17. GC-MS profile of *A. muciniphila* MucT LOS lipid compositional analysis C16:0, C16:1 and C18:0 are impurities or cell derived fatty acids.

The spectrum showed in the m/z range 1332.1–1978.7, the presence of a heterogeneous pattern of signals relative to deprotonated $[M-H]^-$ lipid A species that differed in the nature and number of fatty acid chains and in the phosphate content. There were three main groups of signals at around m/z 1922.6, 1670.3 and 1430.1, identified as hexa-acylated, penta-acylated and tetra-acylated lipid A respectively. They all presented a *mono*-phosphorylated form at m/z 1842.8, 1590.4 and 1350.1 respectively (Table 2.1.3).

In particular, the main peak at m/z 1922.6 matched with a *bis*-phosphorylated lipid A carrying *i*-C15:0 (3-OH) as primary *O*-linked and *N*-linked fatty acids, whereas *i*-C14:0 and C17:0 residues corresponded to secondary acyl substituents. In addition, a cluster of peaks at about m/z 1670.3 was assigned to *bis*-phosphorylated penta-acylated lipid A species lacking one C17:0 unit, and the

family of peaks at about m/z 1430.1 were attributed to *bis*-phosphorylated tetra-acylated lipid A species because of the absence of both C17:0 and one of the primary *O*-linked *i*-15:0 (3-OH). Notably, the spectrum showed differences of 14 amu ($-\text{CH}_2-$ unit) diagnostic for the occurrence of lipid A species differing in the length of the acyl chains, further incrementing the heterogeneity of this lipid A. A negative-ion MS/MS analysis was conducted in order to establish the exact location of the acyl chains with respect to the glucosamine disaccharide backbone.

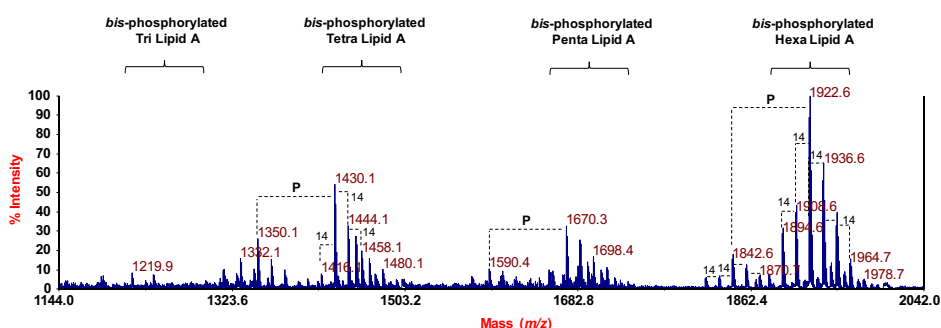


Figure 2.1.18. Negative ion MALDI mass spectrum of the lipid A from *A. muciniphila* Muc^T. Differences of 28 amu are reported in the spectrum. The families of lipid A species differing in the acylation degree were also indicated as “Hexa-acylated”, “Penta-acylated”, “Tetra-acylated” and “Tri-acylated”. P: phosphate group. The relevant ion peaks are described in the text and in table 2.1.3.

Table 2.1.3. The main MALDI-TOF MS ion peaks *A. muciniphila* Muc^T lipid A. Report of the predicted mass and the proposed interpretation of the substituting fatty acids and phosphates on the lipid A backbone. See figure 2.1.18 for full spectrum.

Predicted mass (Da)	Observed ion peaks (m/z)	Acyl substitution	Proposed fatty acid/phosphate composition
1923.3	1922.6	Hexa-acyl	HexN ₂ P ₂ [<i>i</i> -15:0(3-OH)] ₄ (17:0) (14:0)
1843.3	1842.6	Hexa-acyl	HexN ₂ P [<i>i</i> -15:0(3-OH)] ₄ (17:0) (14:0)
1671.1	1670.3	Penta-acyl	HexN ₂ P ₂ [<i>i</i> -15:0(3-OH)] ₄ (14:0)
1591.1	1590.4	Penta-acyl	HexN ₂ P [<i>i</i> -15:0(3-OH)] ₄ (14:0)
1430.9	1430.1	Tetra-acyl	HexN ₂ P ₂ [<i>i</i> -15:0(3-OH)] ₃ (14:0)
1350.9	1350.1	Tetra-acyl	HexN ₂ P [<i>i</i> -15:0(3-OH)] ₃ (14:0)

In particular, the MS/MS spectrum recorded on precursor ion at m/z 1922.6 relative to a *bis*-phosphorylated hexa-acylated lipid A species, showed, among others, an ion derived from the loss of a whole unit of a hydroxylated C15:0 bearing the secondary C17:0 substituent and one phosphate group matched peak at m/z 1314.3. It also showed an ion derived from the sequential loss of a C15:0 (3-OH) and a C17:0 at m/z 1394.4, and two ions originated from the sequential loss of a C15:0 (3-OH), a C17:0 and a phosphate group at m/z 1296.4 (Fig 2.1.19). Remarkably, the peak m/z 738.1 was attributed to an Y_1 -type ion derived from the cleavage of the glycosidic linkage (Domon and Costello 1988) which was essential to define the location of the two secondary acyl chains with respect to the glucosamine backbone. It suggested that the reducing glucosamine was acylated by two primary units of C15:0 (3-OH) (Fig 2.1.19) thus implying the location of the secondary acyl substituents on the non-reducing GlcN.

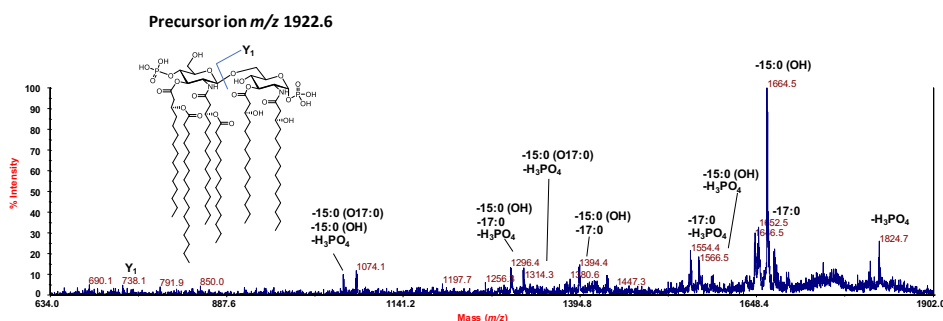


Figure 2.1.19. Negative ion MS/MS spectrum of m/z 1922.6 of the lipid from *A. muciniphila* Muc^T. This is a representative ion peak of the cluster ascribed to *bis*-phosphorylated hexa-acylated lipid A species. The main fragments' assignment is indicated in the spectrum. The proposed structure is reported in the inset.

In addition, to confirm the structural hypothesis a treatment of the lipid A with NH_4OH was performed to selectively remove the acyl and acyloxyacyl esters, while leaving the acyl and acyloxyacyl amides unaltered; this approach followed by a MALDI-TOF MS investigation of the related product is typically crucial in providing a clear indication of the location of the lipid A acyl chains. The negative-ion MS spectrum, recorded in reflectron mode, is shown in figure 2.1.20.

The peak at m/z 1189.8 was attributed to a *bis*-phosphorylated and tri-acylated lipid A product characterised by the occurrence of two units of C15:0 (3-OH) and one C14:0 (Fig.2.1.20). This information, complemented with those attained by MS/MS analysis, supported the hypothesis of C14:0 to be the substituent of the *N*-linked primary C15:0 (3-OH) of the non-reducing GlcN while C17:0 may be the substituent of the O-linked primary C15:0 (3-OH) of the same GlcN.

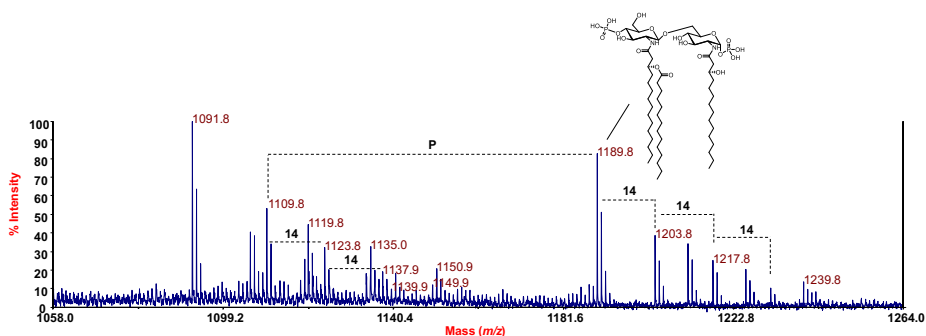


Figure 2.1.20. Reflectron negative ion spectrum of the NH_4OH -treated lipid A disclosing the location of the secondary acyl chains.

Therefore, by combining data from fatty acid compositional analysis and from MALDI MS and MS/MS, it was possible to establish the fine structure of the lipid A from *A. muciniphila* of which the main *bis*-phosphorylated forms are presented in figure 2.1.21.

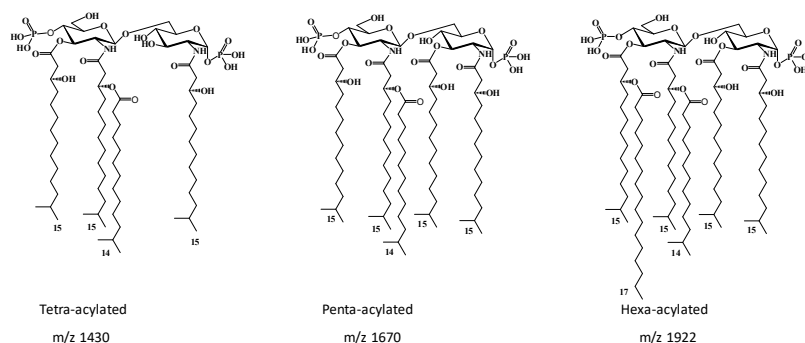


Figure 2.1.21. Proposed structure for the main *bis*-phosphorylated lipid A species of *A. muciniphila* Muc^T . The absolute configuration of the primary acyl chains and the anomeric configuration of the two GlcN residues are based on literature data.

2.1.6. Inner core determination of the LOS of *A. muciniphila*

Three pieces of the LOS were identified: the nonasaccharide, the tetradecasaccharide and the lipid A, to analyse how they were linked NMR experiments were performed. However, the NMR analysis was not conclusive due to the presence of numerous overlaps and the weak HMBC signals generated from the position 3 of the Kdo residues.

Therefore, Electrospray Ionisation Fourier Transform Ion Cyclotron Resonance Mass Spectrometry (ESI FT-ICR MS) was performed on the fully de-acylated molecule by Dr. Nicolardi from Leiden University (*see* Material and methods).

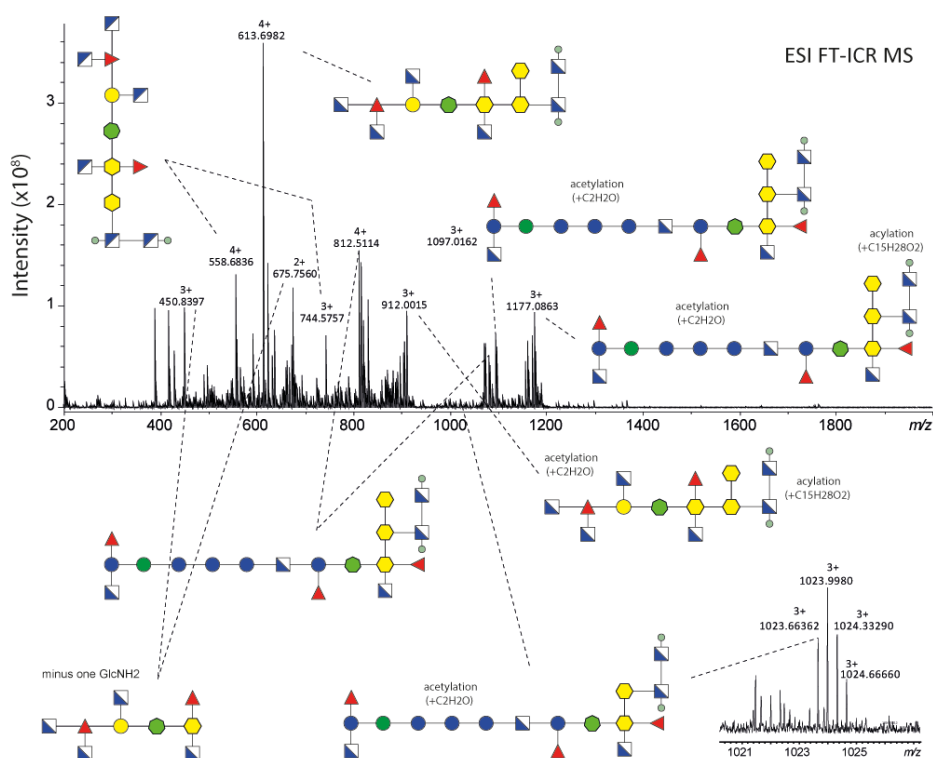


Figure 2.1.22. Positive mode ESI FT-ICR MS of de-acylated *A. muciniphila* MucT polysaccharide. The intact polysaccharide was not detected. Instead, the signals from intense protonated in-source fragment ions characterised the mass spectrum.

The intact polysaccharide was not detected while intense fragments, generated from in-source decay, were detected in the mass spectrum. Fragment ions with residual acylation and/or acetylation were also detected. In-source decay fragment ions were further characterised by ESI-CID FT-ICR MS (Fig.2.1.22). In the MS and MS/MS spectra, intense fragment ions from the loss of H₃PO₄ were observed (97.9769 Da) (data not shown). The identification of the specific monosaccharide residues was based in the results described above, since the identification of different isomers is not possible by this technique.

The existence of a central Kdo that links to the lipid A and a terminal Kdo instead of a linear sequence of 3 Kdos was established by the presence of TETRAD+lipidA+2Kdos and TETRAD+lipidA+3Kdos and was further confirmed by MS/MS. In addition, a complementary Kdo in-depth analysis is currently ongoing to confirm the presence of a terminal Kdo and gather more information on the central Kdo.

The results seemed to indicate the presence of a total of 4 Kdo residues (Fig.2.1.23). A central Kdo substituted with the NONA, the TETRAD, the lipid A and a terminal Kdo. However, the substitution site has not been determined yet.

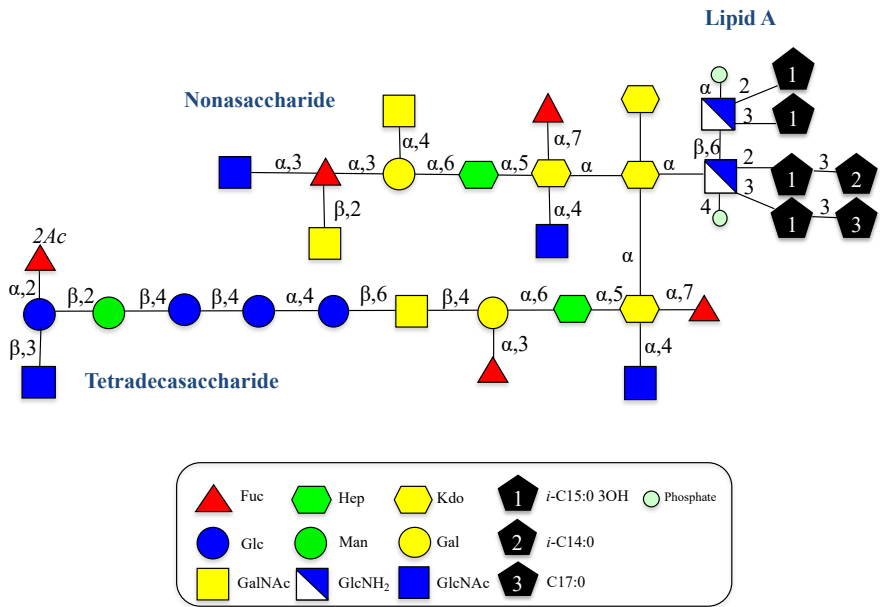


Figure 2.1.23. Preliminary results on the structure LOS of *A. muciniphila* MucT. The substitution pattern of the central Kdo remains to be disclosed.

2.1.7. Immunological properties of the LOS of *A. muciniphila*

The immunological properties of the LOS were evaluated by screening TLR2 and TLR4 activation in HEK-Blue hTLR2 and hTLR4 cell lines, by the team of Prof. De Vos at Wageningen University. In these cell lines, stimulation of TLR2 or TLR4 and subsequent activation of NF-κB and AP-1 induced the production of secreted embryonic alkaline phosphatase (SEAP), which was quantified spectrophotometrically. The full LOS were obtained and purified, the lipid and the saccharides obtained by PCP and subsequent hot phenol/water extractions and purified by enzymatic digestion and dialysis. The lipid A and the saccharide were the precipitate and the supernatant respectively after the mild acid treatment of the purified LOS. The synthetic TLR2 agonist Pam3CSK4, the TLR4 agonist hexa-acylated *Escherichia coli* O111:B4 LPS, the growth medium (Dulbecco's Modified Eagle Medium, DMEM) and the buffer (Phosphate-buffered saline PBS) were used as controls.

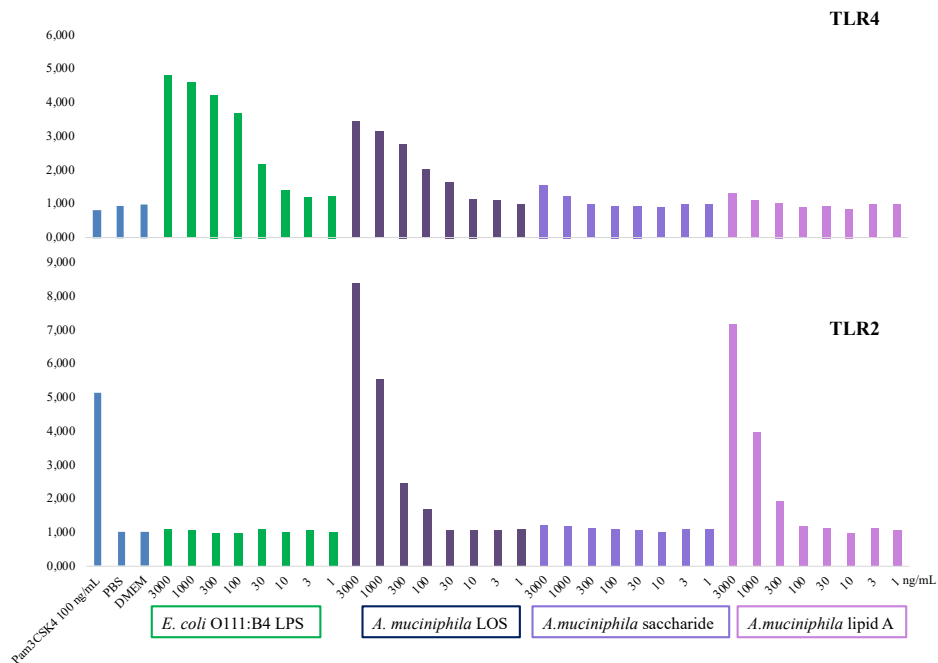


Figure 2.1.24. Analysis of the immune activity of LOS, saccharide and lipid A of *A. muciniphila* Muc^T on HEK-Blue hTLR4 and hTLR2 cells. NF- κ B and AP-1 induced the production of SEAP, which was quantified spectrophotometrically. Bars represent the median values from 3 independent replicates.

The purity of the LOS was established by Coomassie staining of the SDS-PAGE at University Federico II of Naples and MS analysis (not showed) at Wageningen University and proved the absence of contaminant proteins.

The test showed that the LOS, the saccharide and the lipid A of *A. muciniphila* Muc^T triggered a TLR4 activation significantly smaller than the LPS of *E. coli* at equal concentrations (Fig.2.1.24.TLR4). Remarkably, the LOS and the lipid A triggered a TLR2 response when *E. coli* LPS were silent and Pam3CSK4 was active (Fig.2.1.24.TLR2).

2.1.8. Discussion

The structure of the LOS of *A. muciniphila* Muc^T has almost entirely been solved, and the only point open regards the substitution pattern of the central Kdo

(Fig.2.1.23). The structure is totally unique as well as some of its characteristic features. Briefly, the saccharide is found to be composed by two chains (a nonasaccharide and a tetradecasaccharide) and a heterogeneous mixture of three species of lipid A characterised by the high presence of *iso*-acyl chains. This LOS has a high molecular weight and is very ramified compared to the LOS of other bacteria. The nonasaccharide and the tetradecasaccharide have characteristic features in common, like the substitution pattern of the Kdo and the high fucosylation level. The Kdo is substituted on position 4 by GlcNAc, on 5 by Hep and on 7 by Fuc. The presence of Hep on 5 is rather common, whether the presence of GlcNAc and Fuc are rather uncommon (Gronow *et al.*, 2010). LOS and LPS commonly possess two Kdo subunits, named inner and outer Kdo. The inner Kdo is directly linked to the lipid A, has a heptose in position five that in turn is further elongated with the saccharidic part of the LOS. Finally, the inner Kdo is normally substituted at position 4 with the outer Kdo, or with a phosphate in case this second unit is missing. The outer Kdo can be terminal or further substituted with other residues, as GlcN at position 4, as described for various bacteria of the genus *Pectinatus* (Helander *et al.*, 2004). Position 7 of both types of Kdos is normally free, although there are some examples of Kdo substituted at this position in nature, the query run on CSDB in December 2020 showed that Fuc has never been described on this position before. The high level of fucosylation could be related to the critical role that Fuc cell-surface moieties play on cells interactions (Li *et al.*, 2018). More importantly, our proposed structure contains more than two Kdo residues, which is very uncommon, although structures with three and four Kdo residues have been described (Kosma 1999). As for the lipid A, *iso*-acyl lipid A species have been described in some pathogenic and commensal bacteria and has been correlated to the lack of recognition by TLR4 (Di Lorenzo *et al.*, 2019).

The proposed LOS structure is the one that best fit the structural evidence collected. Indeed, the LOS must include at least 3 Kdo residues because: 1)

NONA and TETRAD are part of the full LOS because it was possible to separate them only after mild acid hydrolysis of the LOS and not from the fully de-acylated LOS (Wang and Cole 1996); 2) free Kdo was found in the NMR analysis of the NONA, suggesting the presence of at least 3 Kdo residues in the LOS; 3) the first Kdo linked to the lipid A normally has a Kdo linked to position 4 (Silipo and Molinaro 2010), so both the NONA and the TETRAD should not be linked to the lipid A because their position 4 has a GlcNAc, thus at least another Kdo should be present in the molecule; 4) LOS with 3 or 4 Kdo residues have been described in members of the phylum Chlamydiae (Fig.1.17) (Kosma 1999), taxonomically close to phylum Verrucomicrobia, to which *A. muciniphila* belongs to.

With regard to the immunological data, expressing the output of the assays (Fig.2.1.24) in mols, it seems that the LOS is a better immunostimulant than the isolated lipid A, which apparently contradicts the fact that the lipid A is the immunostimulant ligand of TLR4 (Molinaro *et al.*, 2015). Our explanation is that the reduced activity observed for the lipid A alone is due to its poor solubility in aqueous solvents, so that the amount administered to the cells is less than that calculated. Conversely, LOS is soluble in the buffer used, so that the amount of sample delivered to the cells is that expected. The structure of the lipid A is intrinsically related to the immune potency (Seydel *et al.*, 2000), the high presence of *iso*-acyl chains may be responsible for the reduced TLR4 stimulation, as showed in members of the genus *Bacteroides* and *Prevotella* (Di Lorenzo *et al.*, 2019). In addition, this study highlights the involvement of TLR2 in the recognition of the LOS of *A. muciniphila*. It has recently been demonstrated that some atypical LPS (like *Bacteroides vulgatus* or *Helicobacter pylori*) can also activate TLR2, with a synergic effect with the TLR4 for the production of nuclear factor- κ B (Di Lorenzo *et al.*, 2020; Chavarría-Velázquez *et al.*, 2018). The activation of TLR2 seems to be fundamental for the colonisation of the gut microbiota as it engenders mucosal tolerance (Round *et al.*, 2011). Coomassie staining of the SDS-PAGE and MS analysis confirmed that this activity is due to

the LOS and not because of contaminating proteins. However, it is still not known how the LOS-TLR2 interaction takes place, for this reason molecular modelling experiments are currently being conducted. Activation of TLR2 by a protein isolated from the OM of *A. muciniphila* (Amuc_1100) has been linked to improvement of the gut barrier and reduction of fat mass development, insulin resistance and dyslipidaemia in mice (Plovier *et al.*, 2017). Its LOS may also play a role in this effect. In addition, more assays should be performed to establish other interactions with immunologic receptors, for instance, the high degree of fucosylation may suggest the recognition by lectins and other receptors.

Studies in mice suggest that *A. muciniphila* reduces fat accumulation and body weight and regulates glycemia levels (Everard *et al.*, 2013). Also, a very recent clinical trial (NCT02637115) probed that the daily oral supplementation with live or pasteurised *A. muciniphila* is safe and improve insulin sensitivity and reduces insulinemia, cholesterol and blood markers for liver dysfunction and inflammation without affecting the rest of the microbiome structure. Also, it slightly decreases body weight and fat mass (Depommier *et al.*, 2019). Positive effects of *A. muciniphila* are maintained when pasteurised bacterium is administered, but not after autoclaving (Cani and de Vos 2017). Our results pave the way to the understanding of the mechanism involved in these beneficial effects.

2.2. The peptidoglycan composition of *Akkermansia muciniphila* Muc^T

2.2.1. Purification and analysis of the peptidoglycan of *A. muciniphila*

A. muciniphila Muc^T cells were pelleted, resuspended in ice-cold water, boiled in the presence of 4% SDS and treated with Pronase E. The purified PG was treated with cellosyl and the resulting muropeptides were reduced with sodium borohydride. This was performed by the author of this Ph.D. thesis under the guidance of Dr. Biboy and Dr. Daniela Vollmer at Newcastle University, during a secondment. The reduced muropeptides were applied to a micro-C₁₈ reversed-phase HPLC column which was directly coupled to a Thermo LTQ ion trap Mass Spectrometer (*see* Material and methods) by Dr. Gray from Newcastle University.

The chromatogram is shown in figure 2.2.1 and its preliminary interpretation is presented in table 2.2.1.

Interestingly, the muropeptide profile revealed changes in the acetylation pattern of the glycan chains. Some MurNAc residues were *O*-acetylated and some GlcNAc residues were de-acetylated to N-acetylglucosamine (GlcNH₂). The two major peaks corresponded to the muropeptide Tetra (GlcNAc-MurNAc-L-Ala-D-iGlu-m-A₂pm-D-Ala) (peak 4) and its *O*-6-acetylated form (GlcNAc-MurNAc(Ac)-L-Ala-D-iGlu-m-A₂pm-D-Ala) (peak 5), and the de-*N*-acetylated Tetra (GlcNH₂-MurNAc-L-Ala-D-iGlu-m-A₂pm-D-Ala) (peak 3), de-*N*-acetylated TetraTetra dimer (peak 6) and the TetraTetra (peak 8). Peaks 2a, 4 and 8 had the same structures as the corresponding muropeptides from *E. coli*, the Tri (GlcNAc-MurNAc-L-Ala-D-iGlu-m-A₂pm), Tetra (GlcNAc-MurNAc-L-Ala-D-iGlu-m-A₂pm-D-Ala) and TetraTetra (Glauner 1988).

None of the major peaks of *A. muciniphila* Muc^T corresponded to anhydro (Anh) muropeptides, which originate from glycan chain ends, or muropeptide trimers or

tetramers. It is possible that these muuropeptides exist in the PG of *A. muciniphila* Muc^T, but they were not detected due to their low abundance.

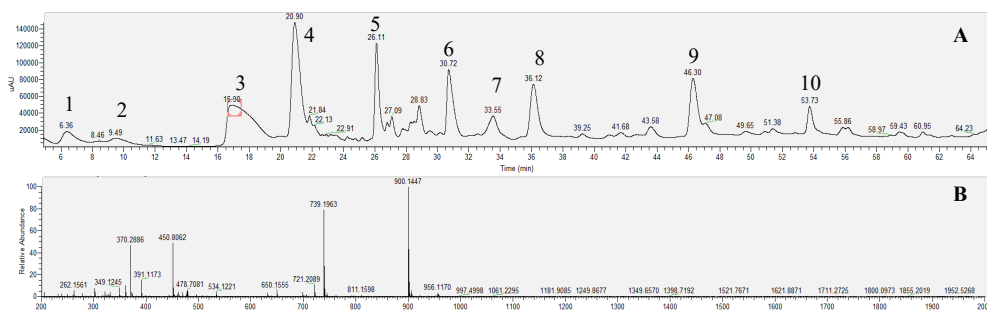


Figure 2.2.1. A. Separation of muuropeptides *A. muciniphila* Muc^T. Muuropeptides were released from PG by cellosyl, reduced using sodium borohydride, and separated by C₁₈ reversed-phase HPLC. The interpretation of the labelled peaks is in table 2.2.1. **B.** MS spectrum of peak 3 corresponding to the de-*N*-acetylated Tetra-muuropeptide.

Table 2.2.1. Reduced muuropeptides detected in *A. muciniphila* Muc^T. Peak numbers refer to the labels of figure 2.2.1.

Peak	Rt (min)	Mass/charge (m/z)	Neutral mass (amu)	Theoretical mass (amu)	Muuropeptide*
1	6.36	829.16 (1+)	828.16	828.34	GlcNH ₂ -MurAc-Ala-iGlu-A ₂ pm
2a	9.49	871.09 (1+)	870.09	869.35	GlcNAc-MurNAc-Ala-iGlu-A ₂ pm
2b	9.49	930.17 (1+)	929.17	--	GlcNAc-MurNAc-Ala-iGlu-A ₂ pm-X
3	15.00	900.14 (1+)	899.14	899.38	GlcNH ₂ -MurAc-Ala-iGlu-A ₂ pm-Ala
4	20.90	942.14 (1+)	941.14	941.39	GlcNAc-MurNAc-Ala-iGlu-A ₂ pm-Ala
5	26.11	984.12 (1+)	983.12	983.40	GlcNAc-MurNAc(Ac)-Ala-iGlu-A ₂ pm-Ala
6	30.72	891.18 (2+)	1780.36	1780.74	Dimer of GlcNH ₂ -MurNAc-Ala-iGlu-A ₂ pm-Ala
7	33.55	912.15 (2+)	1822.40	1822.75	Dimer of GlcNH ₂ -MurNAc-Ala-iGlu-A ₂ pm-Ala and GlcNAc-MurNAc-Ala-Glu-A ₂ pm-Ala
8	36.12	933.30 (2+)	1864.60	1864.76	Dimer of GlcNAc-MurNAc-Ala-iGlu-A ₂ pm-Ala
9	46.30	954.32 (2+)	1906.64	1906.77	Dimer of GlcNAc-MurNAc(Ac)-Ala-iGlu-A ₂ pm-Ala and GlcNAc-MurNAc-Ala-Glu-A ₂ pm-Ala
10	53.73	975.34 (2+)	1948.68	1948.78	Dimer of GlcNAc-MurNAc(Ac)-Ala-iGlu-A ₂ pm-Ala

* Ac means acetyl group at position O-6 of the MurNAc.

2.2.2. Discussion

The preliminary results of the muropeptide composition of *A. muciniphila* Muc^T reveal its difference compared to the typical Gram-negative PG in *E. coli* (Glauner 1988). The lack of peaks of *A. muciniphila* Muc^T corresponding to Anh-muropeptides, muropeptide trimers or tetramers is probably due to their low abundance (Vollmer *et al.*, 2008; Glauner 1988) and these muropeptides are probably represented by some of the unidentified minor peaks.

The PG of *A. muciniphila* Muc^T is unusual because a de-*N*-acetylated glucosamine (GlcNH₂) has not been described before in the PG of Gram-negative bacteria, except for *Helicobacter pylori* (Wang *et al.*, 2009) which, however, was not confirmed in other studies (Chaput *et al.*, 2016). Some Gram-positive bacteria have been described to contain GlcNH₂ in their PG like *Streptococcus pneumoniae* (Vollmer and Tomasz 2000) and *Listeria monocytogenes* (Boneca *et al.*, 2007). Other bacteria, like *Bacillus subtilis*, possess de-*N*-acetylated muramic acid (MurNH₂) (Blair and Van Aalten 2004) and one, *Bacillus anthracis*, has both GlcNH₂ and MurNH₂ in its PG (Zipperle, *et al.*, 1984). Both the de-*N*-acetylation of the GlcNAc and the MurNAc are factors for resistance against lysozyme (Bera *et al.*, 2005; Zipperle *et al.*, 1984).

The enzyme responsible of the formation of GlcNH₂ from GlcNAc in *S. pneumoniae* and *L. monocytogenes* is the peptidoglycan GlcNAc deacetylase (PgdA) (Q8DP63-1 and B3VUE6-1 respectively)(Boneca *et al.*, 2007; Vollmer and Tomasz 2000). The enzyme responsible of the formation of MurNH₂ from MurNAc in *Bacillus subtilis* is the peptidoglycan-*N*-acetylmuramic acid deacetylase (PdaA) (O34928-1) (Blair and Van Aalten 2004). Therefore, a query using tBlastp was performed to confront these enzymes against the proteome of *Akkermansia muciniphila* Muc^T (taxid: 349741). For both PgdA the percentage of identity is 39% and 40% respectively and the similarity 61% and 64%

respectively with the protein Amuc_1500. PdaA presents a percentage of identity of 34% and a similarity of 54% (Table 2.2.2).

Interestingly, *A. muciniphila* genome does not encode for the enzyme Glm essential for PG synthesis as it converts fructose-6-phosphate to glucosamine-6-phosphate. *A. muciniphila* synthesizes PG by using GlcNAc present in the mucin (van der Ark *et al.*, 2018).

Table 2.2.2. Summary of the results of the alignment search between *Akkermansia muciniphila* Muc^T (taxid: 349741) and PG modifying enzymes of different microorganism.

Enzyme	Microorganism of origin	Identification number	E value	Identity* (%)	Similarity* (%)	Region length (amino acids)	Enzyme of <i>A. muciniphila</i>
PgdA	<i>S. pneumoniae</i>	Q8DP63.1	8e-44	39	61	185	WP_012420537 Amuc_1500
PgdA	<i>L. monocytogenes</i>	B3VUE6.1	1e-41	40	64	153	WP_012420537 Amuc_1500
PdaA	<i>B. subtilis</i>	O34928.1	3e-36	34	54	190	WP_012420537 Amuc_1500
PatA	<i>N. gonorrhoeae</i>	A0A5K1KKD4.1	--	n.s.	n.s.	--	
PatB/Ape	<i>N. gonorrhoeae</i>	SCW06924.1	--	n.s.	n.s.	--	
OatA	<i>S. aureus</i>	Q2FV54.1	4e-28	39	60	168	WP_012419812.1 Amuc_0761

* n.s. means no significant identity/similarity found.

De-*N*-acetylation has been demonstrated to be an evasion mechanism from immune responses in Gram-positive bacteria since it is not recognised by NOD-1 receptor (Boneca *et al.*, 2007). NOD-1 recognizes MurNAc-L-Ala-D-iGlu-m-A₂pm (muramyl tripeptide) which is present in almost all Gram-negative bacteria and the Gram-positive bacteria of the genus *Bacillus*, *Mycobacteria* and *L. plantarum* activating the transcription factor NF-κB pathway (Girardin *et al.*, 2003). Once the definitive compositional analysis of *A. muciniphila* Muc^T PG is known, it will be interesting to perform immunological assays on them.

MurNAc *O*-acetylation (also here reported as component of *A. muciniphila* Muc^T muuropeptides) is found in many Gram-positive and Gram-negative bacteria and has been demonstrated to be an evasion mechanism from immune detection by

the lysozyme and the inflammasome, but without impairing NOD-2 recognition (Brott and Clarke 2019). The addition of an acetyl group on the hydroxyl group of C-6 of MurNAc is catalysed by the PG *O*-acetyltransferases PatA and PatB (or Ape2) in Gram-negative bacteria as described for *Neisseria gonorrhoeae* (Weadge *et al.*, 2005). PatA transports the acetyl groups from the cytoplasm to the periplasm and then PatB introduces it in the MurNAc residues of the PG. For Gram-positives the *O*-acetyltransferase OatA has been described in *S. aureus* and *S. pneumoniae* (Bera *et al.*, 2005), called Adr in the latter species (Crisóstomo *et al.*, 2006). Therefore, a query using Blastp was performed of these enzymes against the genome of *A. muciniphila* Muc^T (taxid: 349741). For PatA (A0A5K1KKD4-1) and PatB (or Ape, SCW06924.1) no significant similarity was found. For OatA of *S. aureus* (Q2FV54-1) percentage of identity was 39% and the similarity was 60% (Table 2.2.2). Although the most significant hit of OatA of *S. aureus* was found with the protein Amuc_0761 from *A. muciniphila*, there were also matches with the acetyl transferases Amuc_2098, Amuc_0773 and Amuc_1793 with a smaller percentage of identity and a higher the E-value.

Hence, the identified homologs of PgdA and OatA are candidates for the PG GlcNAc deacetylase (Amuc_1500) and *O*-acetyltransferase (Amuc_0761) in *A. muciniphila*, which could be tested in further studies.

2.3. The lipopolysaccharide of *Fusobacterium nucleatum* ATCC 51191

2.3.1. Production and purification of the LPS of *F. nucleatum*

LPS from *F. nucleatum* spp. *animalis* ATCC 51191 cells was isolated by hot water/phenol extraction (*see* Material and methods). LPS was further purified by enzymatic treatment, centrifugation and ultracentrifugation steps. SDS-PAGE analysis of the water layer of the extract showed the presence of two main groups of bands, suggesting that this bacterium produces smooth(S)-type LPS (LPS with O-polysaccharide) and rough(R)-type LPS (composed only by lipid A and core region). The apparent molecular weight of the smooth(S)-type LPS was estimated between 25-35 kDa (Fig.2.3.1 left).

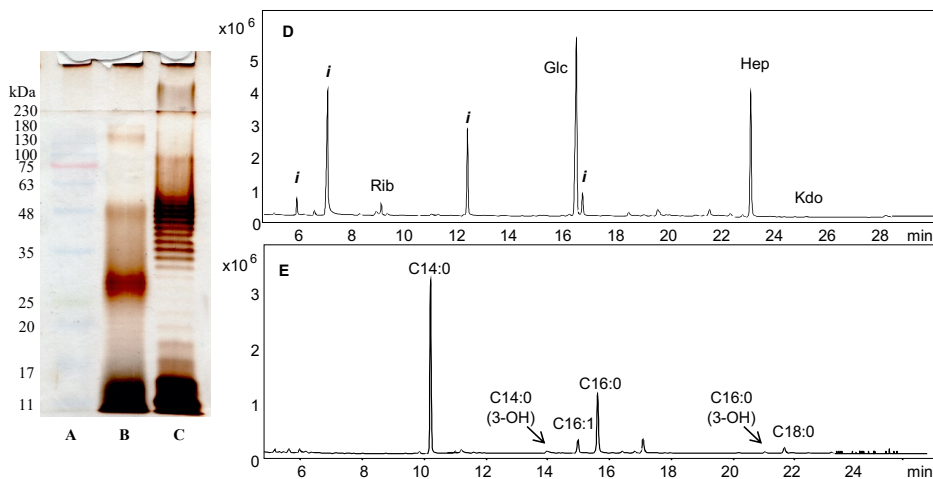


Figure 2.3.1. On the left: electrophoresis analysis: **A.** *E. coli* O111:B4 LPS (8 μ g). **B.** *F. nucleatum* ATCC 51191 LPS (8 μ g) **C.** BlueEye protein standard. (12% SDS-PAGE and visualised by silver staining). On the right: GC-MS profile of *F. nucleatum* ATCC 51191 LPS: **D.** acetylated methyl glycosides, **E.** lipid compositional analysis. *i*: impurities; C16:1 and C18:0 are impurities or cell derived fatty acids.

Monosaccharide compositional analysis of purified LPS was performed via derivatisation to acetylated *O*-methyl glycosides and revealed the presence of Glc, Hep, and traces of Kdo; no other monosaccharides could be detected using this approach, probably due to the resistance to cleavage of the aminuronic acids

composing the OPS. These units, along with the 2,4-diamino-2,4,6-trideoxydeoxy-galactose (FucpN4N) were detected during the NMR analysis. The fatty acid analysis revealed the presence of C14:0, 3-hydroxytetradecanoic acid (C14:0 3-OH), hexadecanoic acid (C16:0) and 3-hydroxyhexadecanoic acid (C16:0 (3-OH)) (Fig.2.3.1 right).

A mild acid hydrolysis of the purified LPS was then carried out in order to analyse separately the lipid A and the OPS fraction. The lipid A, obtained as a precipitate after centrifugation of the acid hydrolysis product, was analysed via MALDI-TOF MS and MS/MS, while the polysaccharide part was further purified by size exclusion chromatography and the purified polysaccharide (yield 55.5%) was analysed by 1D and 2D NMR (Fig.2.3.2). The first fraction did not produce relevant signals in the proton NMR spectrum, which suggested that it could be a minor fraction of LPS that survived to the mild acidic treatment. The material eluted after the OPS, contained carbohydrate material with several anomeric signals with no apparent stoichiometric ratio, which suggested that it was a mixture of oligosaccharides deriving from the core region of the rough component of the LPS. This fraction was not investigated further.

2.3.2. Structural characterisation of the O-polysaccharide of *F. nucleatum*

The structure of the OPS of *F. nucleatum* ATCC 51191 LPS was determined by analysing homo- and heteronuclear 2D NMR experiments recorded by dissolving this glycan in D₂O. ¹H, ¹H COSY and ¹H, ¹H TOCSY experiments were used to disclose the protons of each spin system; each carbon atom was identified through the analysis of the ¹H, ¹³C HSQC. Finally, the primary sequence was inferred by analysis of inter-residue and long-range dipolar and scalar correlations from ¹H, ¹H NOESY and ¹H, ¹³C HMBC spectra, respectively.

The ¹H NMR spectrum (Fig.2.3.2) presented six main anomeric signals in the range 5.5 - 4.4 ppm and a crowded carbinolic region (4.3 - 3.4 ppm); furthermore,

eight signals in the region of the methyl groups were detected (2.1 - 1.0 ppm). These were identified as the methyl groups of acetyl groups (2.1 - 1.8 ppm), of alanine (1.43 ppm) and of two 6-deoxy sugars (1.23 and 1.04 ppm) (Fig.2.3.2). In the HMBC spectrum, several signals were observed in the region of the carbonyl groups between 172 - 176 ppm, consistent with the presence of the alanine group, two uronic acid residues and several acetyl moieties.

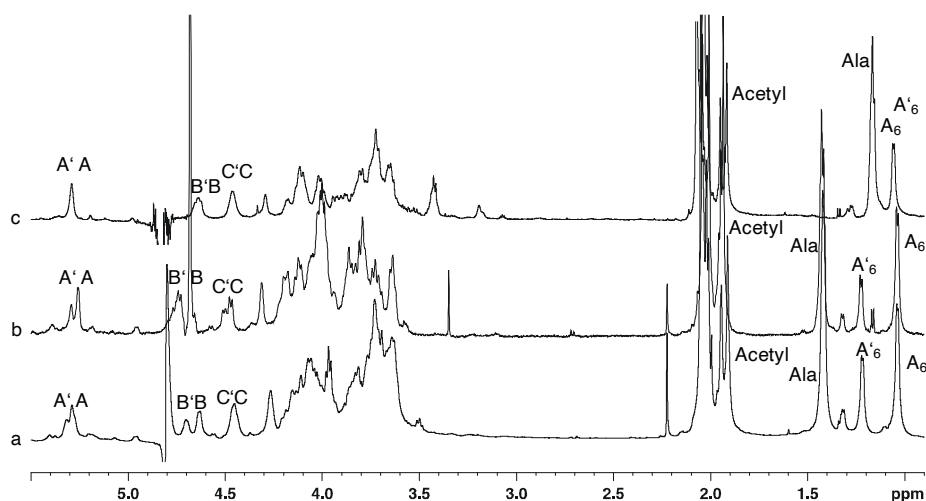


Figure 2.3.2. ^1H NMR spectrum (600 MHz) of the OPS of *F. nucleatum* ATCC 51191. The analysis was carried out at (a) neutral pH (550 μL D_2O , 25°C); (b) acid pH (550 μL D_2O + 4 μL of DCl conc, 37°C), and (c) alkaline pH (550 μL D_2O + 4 μL of NaOD 4 M, 25°C).

Three different monosaccharide residues were found to compose the *F. nucleatum* ATCC 51191 OPS repeating unit: i.e. $\beta\text{-D-GlcpNAcA}$, $\beta\text{-D-GlcpNAc3NA}1\text{aA}$ and $\alpha\text{-D-FucpNAc4NAc}$. However, the anomeric region of the spectrum presented six relevant signals indicative of non-stoichiometric substitutions; the spin systems were labelled in couples as **A-A'**, **B-B'** and **C-C'** (Figs. 2.3.2, 2.3.3 and Table 2.3.1).

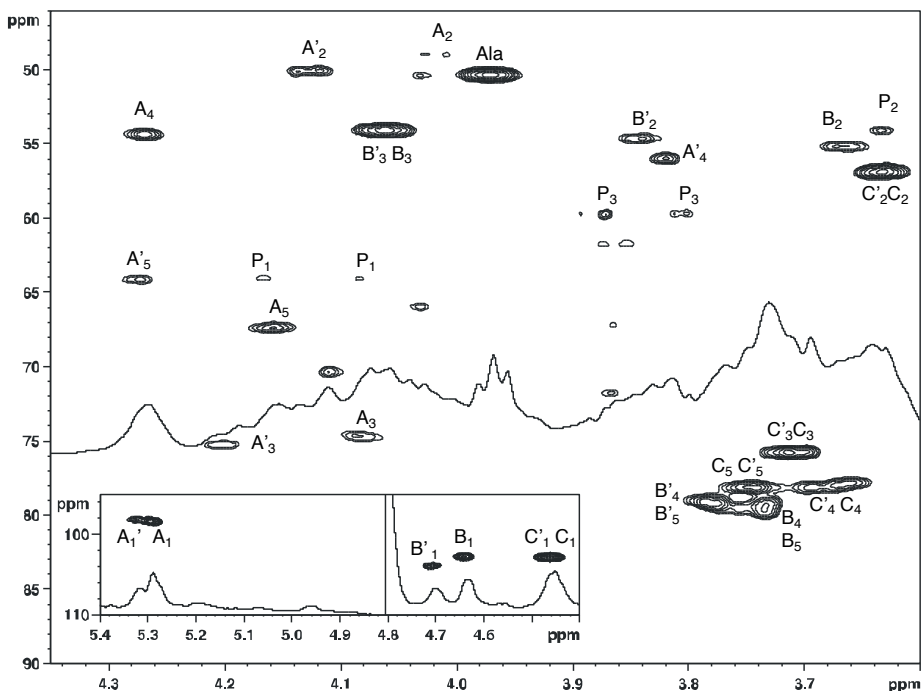


Figure 2.3.3. ^1H , ^{13}C HSQC spectrum of the OPS of *F. nucleatum* ATCC 51191 (600 MHz, 25 °C, 550 μL of D_2O , neutral pH). P₁ and P₃ are not relevant signals related to minor species.

The NMR analysis of residue **A'**, whose anomeric proton (5.32 ppm) correlated with H-2, H-3 and H-4 in the TOCSY spectrum (Fig.2.3.4), suggested a *galacto*-configured residue. Combining the analysis of the TOCSY and COSY spectra with those of the HSQC spectrum, the corresponding carbon chemical shifts were identified (Table 2.3.1). Identification of the C-4 value allowed assignment of the methyl group at 1.24 ppm, based on the corresponding long-range correlation in the HMBC and also provided information about H-5/C-5 chemical shifts. Thus, **A'** was identified as a FucpN4N based on the diagnostic carbon chemical shifts of C-2 and C-4 (48.8 and 55.9 ppm, respectively) characteristic of nitrogen bearing carbon atoms. Based on the H-2 and H-4 chemical shifts, it was possible to establish that the amino group at C-2 was acetylated (H-2 at 4.02 ppm) while the C-4 was not (H-4 at 3.82 ppm). The α configuration of the anomeric centre was inferred by the chemical shift of the anomeric proton, by the presence of a

NOE correlation between H-1 and H-2 of A', and further confirmed by comparison with literature data (Vinogradov *et al.*, 2017b; Wang *et al.*, 2009). The analysis of residue A, conducted as above for A', indicated that it also corresponded to an α -D-Fucp2N4N. However, there was a significant difference in the proton chemical shifts between H-4 of A' (3.82 ppm) and H-4 of A (4.27 ppm), indicating that N-4 of A was acetylated.

Table 2.3.1. Proton (^1H) and carbon (^{13}C) (*italic*) NMR chemical shifts of the OPS of *F. nucleatum* ATCC 51191 (600 MHz, 25 °C, 550 μL of D_2O , neutral pH). The chemical shifts of the methyl protons belonging to the N-acetyl groups resonated at about ^1H 2.1-1.8 ppm.

Residue	1	2	3	4	5	6
A'	5.32	4.02	4.20	3.82	4.27	1.24
3-α-D-FucpNAc4N	<i>98.2</i>	<i>48.9</i>	<i>75.2</i>	<i>56.0</i>	<i>64.1</i>	<i>16.2</i>
A	5.29	4.13	4.09	4.27	4.17	1.04
3-α-D-FucpNAc4NAc	<i>98.4</i>	<i>50.1</i>	<i>74.6</i>	<i>54.3</i>	<i>67.3</i>	<i>16.5</i>
B'	4.71	3.84	4.08	3.78	3.78	
β-D-GlcpNAc3NAlaA	<i>103.9</i>	<i>54.5</i>	<i>54.0</i>	<i>79.1</i>	<i>79.1</i>	<i>176.5</i>
B	4.64	3.67	4.06	3.73	3.73	
β-D-GlcpNAc3NAlaA	<i>102.8</i>	<i>55.2</i>	<i>54.0</i>	<i>79.3</i>	<i>79.3</i>	<i>176.5</i>
C'	4.47	3.65	3.73	3.69*	3.75	
β-D-GlcpNAcA	<i>102.0</i>	<i>56.9</i>	<i>75.5</i>	<i>78.1*</i>	<i>78.0</i>	<i>176.5</i>
C	4.46	3.63	3.71	3.67*	3.75	
β-D-GlcpNAcA	<i>102.9</i>	<i>56.7</i>	<i>75.5</i>	<i>77.9*</i>	<i>78.0</i>	<i>176.5</i>
Alanine	--	3.98	1.43			
	<i>172.6</i>	<i>50.2</i>	<i>18.1</i>			

*C4 and C'4 attribution can be exchanged.

The analysis of the NOESY spectrum showed that the anomeric proton of **A** and **A'** had one correlation at about 3.73 ppm, an area of the spectrum which contained several proton signals, belonging to residues **C** (and **C'**) and to **B** (or **B'**) (Fig.2.3.4). However, the linkage of **A'** to **B'** was ruled out because **B** was connected to **A** as inferred by the NOE effect between H-1 of **B** with H-3 of **A** (*vide infra*). For this reason, **A** (or **A'**) was connected to **C** (or **C'**). The exact point of substitution was confirmed in a further NMR analysis by varying the pH (as described below), which decreased the overlap between the signals in that region of the proton spectrum.

The anomeric proton **C'** (4.47 ppm) was almost coincident with that of **C** (4.46 ppm) at neutral pH (Fig.2.3.2a), while it appeared at a distinct chemical shift when the spectra were recorded at acidic pH (Fig.2.3.2b). For both **C** and **C'**, the correlation pattern in the TOCSY spectrum suggested a β -*gluco*-configured residue (Fig.2.3.4), with all the ring protons next to each other at 3.77-3.61 ppm. Identification of H-2 protons was inferred by analysing the COSY spectrum, while identification of H-3 and H-5 protons was possible by observing the H-1/H-3 and H-1/H-5 NOE's effects, with the sorting between H-3 and H-5 driven from the correlation in the COSY spectrum, then the density left out in the TOCSY spectrum was assigned to H-4.

The HSQC showed a chemical shift for C-2 at 56.9 ppm evidencing the presence of an amino function, and the HMBC related H-4 and H-5 to a C-6 at 176.5 ppm thus disclosing its nature as an uronic acid. Therefore, based on this information, **C'** and **C** were identified as two units of glucosaminuronic acid (Glc ρ NA). However, due to the crowded region of signals in the HSQC spectrum, the assignment of the C-3, C-4 and C-5 values of this residue was confirmed by analysing the spectra recorded at acidic pH.

The analysis of the NOESY spectrum (Fig.2.3.4) was not resolute, because **C'** and **C** had a very intense NOE in a region where their H-3 and H-5 appeared along

with the protons of **B'** and **B**. The information that **C'** (or **C**) was linked to O-4 of **B'** (or **B**) was inferred by analysing the spectra at acidic pH.

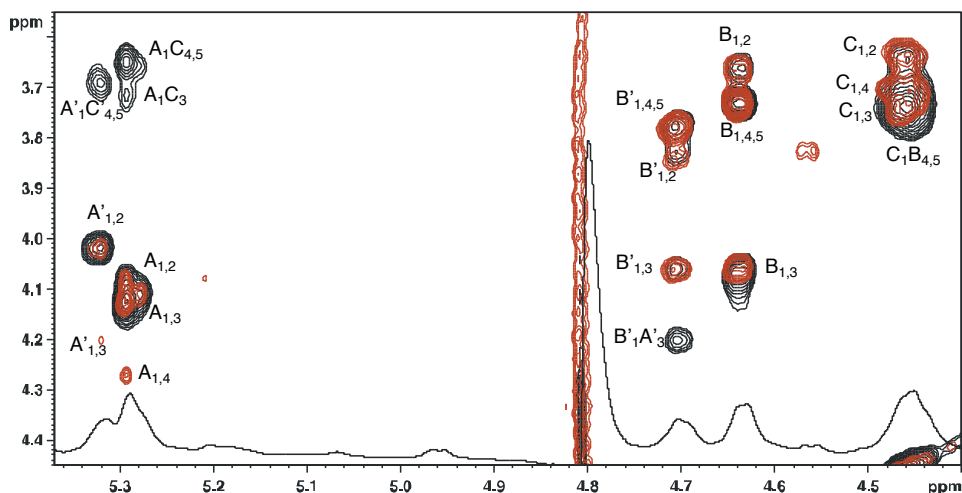


Figure 2.3.4. ^1H TOCSY (red) and ^1H NOESY (black) spectra of the OPS of *F. nucleatum* ATCC 51191 (600 MHz, 25 °C, 550 μL of D_2O , neutral pH).

Residues **B** and **B'** were analysed in a similar way to **C** and identified these as a β -*gluco* configured unit. However, **B** (or **B'**) presented amino functions on both C-2 and C-3, with N-3 bearing an alanine as proved by the correlation in the HMBC spectrum between H-3 and a carbonyl at 172.6 ppm (Kocharova *et al.*, 2001). According to the Carbohydrate Structure Database (CSDB) (Toukach and Egorova 2016; Toukach 2011), GlcN3NA is present in different bacterial LPS and with the amino group at position C-3 bearing different types of groups including L-alanine (and never D-) which is instead, further decorated by a formyl group. The lack of signal at about 8.0 ppm in the proton spectrum indicated that in the *F. nucleatum* ATCC 51191 OPS the formyl moiety was not present.

Finally, residue **B'** was proposed to be linked to O-3 of **A'** based on the NOE correlation between the anomeric proton signal of **B'** and H-3 of **A'** (Fig.2.3.4); the same connectivity was assumed between **B** and **A** because the corresponding NOE was not visible since it overlapped with that between H-1 of **B** and its H-3.

Together, the above NMR analysis identified two partial sequences: β -D-GlcNAc3NAlaA-(1 \rightarrow 3)- α -D-FucNAc4N (**B'** \rightarrow **A'**), and β -D-GlcNAc3NAlaA-(1 \rightarrow 3)- α -D-FucNAc4NAc (**B** \rightarrow **A**), respectively. The absolute configuration for these three units was assumed to be D since this is the only isomer reported for each of them in the CSDB database (Toukach and Egorova 2016). Similarly, the absolute configuration of Ala was assumed as L, since the CSDB database reported only L-Ala and never D-Ala attached to GlcN3NA (last query placed in October 2020). However, at neutral pH, it was not possible to locate **C** (or **C'**) in the sequence due to the overlap occurring for some of the proton signals.

In order to determine the full sequence of the OPS repeating unit, NMR spectra were acquired at acidic and alkaline pH, with the one at acid pH being the most resolutive (Table 2.3.2). Following the same approach as above, the analysis of the NMR spectra led to the unequivocal identification of the C-3, C-4 and C-5 of **C'** and **C** (Fig.2.3.5, Table 2.3.2) that, combined with the results from the NOESY spectrum, showed that **A'** (or **A**) was linked to O-4 of **C'** (or **C**) (Fig.2.3.5). The NOESY spectrum revealed the presence of a glycosidic bond between C-1 of **C'** and the O-4 of **B'**. The same connectivity was proposed for **C** and **B** as the corresponding NOE overlapped with that of the H-3 of **C** and, therefore, was not visible (Fig.2.3.5).

Moreover, the evident change of the H-5 chemical shifts of **B** and **C** at acidic pH (**B**: 3.75 vs 4.02 ppm; **C**: 3.67 vs 3.98 ppm), confirmed that the carboxylic groups (residues **B/C** and **B'/C'**) were free and not amidated.

The sample solved in alkaline condition (Fig.2.3.2c) was not further investigated because of the strong overlap between the two sets of anomeric signals. However, the spectrum in alkaline condition reported a shift at high field for the methyl group of alanine, which suggested that the amino function of this amino acid was not capped with any acyl but present in the free form.

Table 2.3.2. Proton (^1H) and carbon (^{13}C) (*italic*) NMR chemical shifts of the OPS of *F. nucleatum* ATCC 51191(600 MHz, 37 °C, 550 μL D_2O + 4 μL of DCl conc).

Residue	1	2	3	4	5	6
A'	5.30	4.07	4.19	3.79	4.22	1.22
3-α-D-FucpNAc4N	<i>98.5</i>	<i>48.8</i>	<i>75.0</i>	<i>55.8</i>	<i>64.0</i>	<i>16.3</i>
A	5.26	4.19	4.01	4.32	4.06	1.04
3-α-D-FucpNAc4NAc	<i>98.8</i>	<i>49.5</i>	<i>71.5</i>	<i>53.6</i>	<i>67.3</i>	<i>16.7</i>
B'	4.74	3.87	4.13	3.82	4.02	
4-β-D-GlcpNAc3NAlaA	<i>102.4</i>	<i>54.2</i>	<i>53.7</i>	<i>75.9</i>	<i>75.9</i>	<i>176.1</i>
B	4.74	3.71	4.13	3.82	4.02	
4-β-D-GlcpNAc3NAlaA	<i>102.4</i>	<i>54.6</i>	<i>53.7</i>	<i>75.9</i>	<i>75.9</i>	<i>176.1</i>
C'	4.51	3.64	3.97	3.73	3.98	
4-β-D-GlcpNAcA	<i>102.3</i>	<i>56.7</i>	<i>75.5</i>	<i>77.9</i>	<i>78.0</i>	<i>176.1</i>
C	4.48	3.64	3.97	3.73	3.98	
4-β-D-GlcpNAcA	<i>102.5</i>	<i>56.7</i>	<i>75.5</i>	<i>77.9</i>	<i>78.0</i>	<i>176.1</i>
Alanine		3.99	1.42			
	<i>172.6</i>	<i>50.1</i>	<i>18.0</i>			

In conclusion, the OPS repeating unit of *F. nucleatum* ATCC 51191 has been identified as $[\rightarrow 4)\text{-}\beta\text{-D-GlcpNAcA-(1}\rightarrow 4)\text{-}\beta\text{-D-GlcpNAc3NAlaA-(1}\rightarrow 3)\text{-}\alpha\text{-D-FucpNAc4NR-(1}\rightarrow]$, R = Acetyl or H (Fig.2.3.6).

Hence, the amino function at C-4 of the $\alpha\text{-D-Fucp2NAc,4N}$ (**A-4** and **A'-4**) is acetylated in a non-stoichiometric fashion, and the integration of the HSQC densities of **A** and **A'** revealed that acetylation occurs for approximately 60% of the residues. The presence (or absence) of the acetyl units influences the chemical

shifts of the other sugars, so that two different repeating units are identified by NMR.

2.3.3. Structural characterisation of the lipid A of *F. nucleatum*

The negative-ion MALDI-TOF MS spectrum of the lipid A from *F. nucleatum* ATCC 51191 (Fig.2.3.7) showed in the m/z range 1346.7–1909.2, the presence of a heterogeneous pattern of signals relative to deprotonated $[M-H]^-$ lipid A species that differed in the nature and number of fatty acid chains and in the phosphate content. Two main groups of signals at around m/z 1801.1 and 1881.1 were identified as hexa-acylated lipid A species substituted by one or two phosphate groups, respectively (Table 2.3.3). In particular, as described below, the main peak at m/z 1881.1 matched with a *bis*-phosphorylated lipid A carrying C14:0 (3-OH) and C16:0 (3-OH) as primary *O*-linked and *N*-linked fatty acids, whereas two C14:0 residues corresponded to secondary acyl substituents. In addition, a cluster of peaks at about m/z 1670.9 and 1590.9 was assigned to *bis*- and *mono*-phosphorylated penta-acylated lipid A species lacking one C14:0 unit, whereas peaks at m/z 1444.7 and 1364.7 were attributed to *bis*- and *mono*-phosphorylated tetra-acylated lipid A species devoid of both one C14:0 and one C14:0 (3-OH).

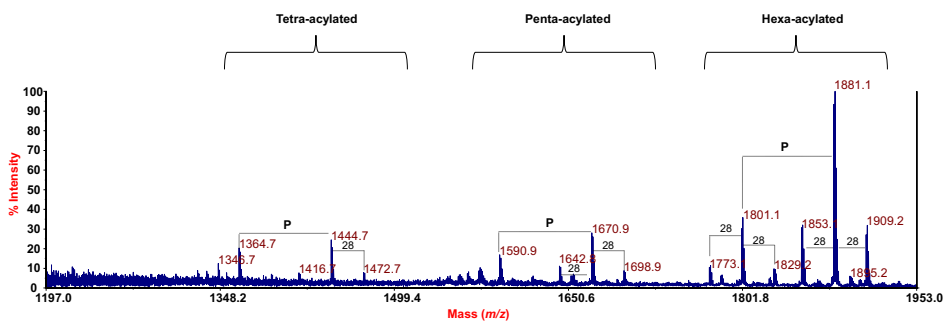


Figure 2.3.7. Negative-ion MALDI-TOF (reflectron mode) mass spectrum of the lipid A of *F. nucleatum* ATCC 51191. Differences of 28 amu are reported in the spectrum. The families of lipid A species differing in the acylation degree were also indicated as “Hexa-acylated”, “Penta-acylated” and “Tetra-acylated”. P: phosphate group.

Notably, the spectrum clearly showed differences of 28 amu ($-\text{CH}_2\text{CH}_2-$ unit) diagnostic for the occurrence of lipid A species differing in the length of the acyl chains. A negative-ion MS/MS analysis was conducted in order to establish the exact location of the acyl chains, as well as of the phosphate decorations of the *mono*-phosphorylated lipid A species, with respect to the glucosamine disaccharide backbone. In particular, the MS/MS spectrum recorded on the precursor ion at m/z 1801.1 relative to a *mono*-phosphorylated hexa-acylated lipid A species, is reported in figure 2.3.8.

The spectrum clearly showed the presence of two main peaks matching with ions originated from the loss of one C14:0 (m/z 1573.0) and one C14:0 (3-OH) (m/z 1557.0) unit, respectively.

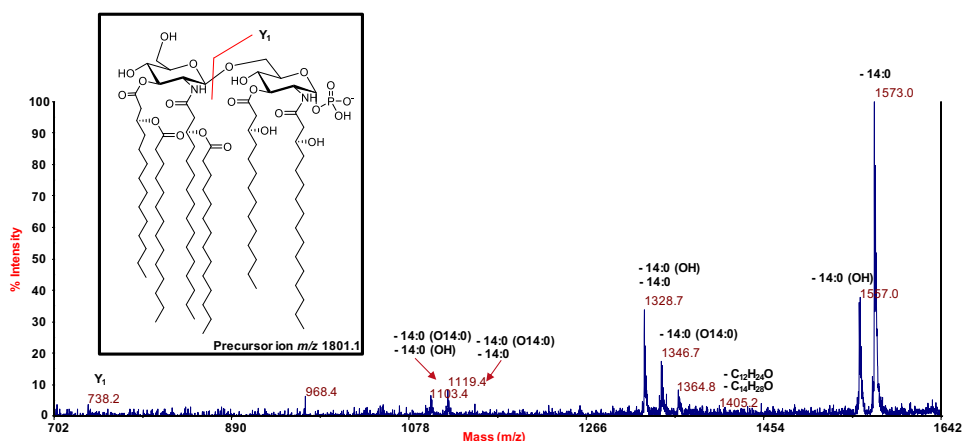


Figure 2.3.8. Negative-ion MALDI MS/MS spectrum of precursor ion at m/z 1801.1 of the lipid A of *F. nucleatum* ATCC 51191. This is a representative ion peak of the cluster ascribed to hexa-acylated and *bis*-phosphorylated lipid A species. The main fragments are indicated in the spectrum. The proposed structure is reported in the inset. The loss of $\text{C}_{12}\text{H}_{24}\text{O}$ (184 mass units) and $\text{C}_{14}\text{H}_{28}\text{O}$ (212 mass units) indicated was due to a rearrangement on primary acyl chains when their 3-OH group is free, thus contributing to the establishment of the secondary acyl substitution.

Table 2.3.3. The main MALDI-TOF MS ion peaks *F. nucleatum* ATCC 51191 lipid A. Report of the predicted mass and the proposed interpretation of the substituting fatty acids and phosphates on the *F. nucleatum* ATCC 51191 lipid A backbone. See figure III.3.6 for full spectrum.

Predicted mass (Da)	Observed ion peaks (<i>m/z</i>)	Acyl substitution	Proposed fatty acid/phosphate composition
1364.96	1364.68	Tetra-acyl	HexN ₂ P [14:0(3-OH)] [16:0(3-OH)] ₂ (14:0)
1444.92	1444.69	Tetra-acyl	HexN ₂ P ₂ [14:0(3-OH)] [16:0(3-OH)] ₂ (14:0)
1591.15	1590.86	Penta-acyl	HexN ₂ P [14:0(3-OH)] ₂ [16:0(3-OH)] ₂ (14:0)
1671.11	1670.87	Penta-acyl	HexN ₂ P ₂ [14:0(3-OH)] ₂ [16:0(3-OH)] ₂ (14:0)
1801.35	1801.15	Hexa-acyl	HexN ₂ P [14:0(3-OH)] ₂ [16:0(3-OH)] ₂ (14:0) ₂
1881.31	1881.15	Hexa-acyl	HexN ₂ P ₂ [14:0(3-OH)] ₂ [16:0(3-OH)] ₂ (14:0) ₂

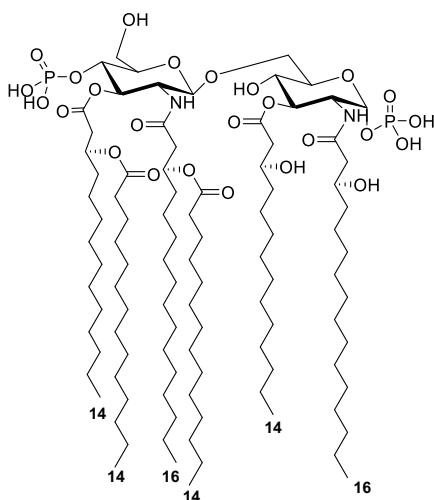


Figure 2.3.9. Proposed structure for the main bis-phosphorylated hexa-acylated lipid A species of *F. nucleatum* ATCC 51191. The absolute configuration of the primary acyl chains and the anomeric configuration of the two GlcN residues are based on literature data.

An ion derived from the loss of a whole unit of a hydroxylated C14:0 bearing the secondary C14:0 substituent matched peak at *m/z* 1346.7; in contrast, an ion originated from the sequential loss of one C14:0 (3-OH) and one C14:0 was attributed to peak at *m/z* 1328.7. Importantly, a peak that was crucial to define the location of the two secondary C14:0 acyl chains with respect to the glucosamine backbone was detected at *m/z* 738.2; this was attributed to an Y₁-type ion derived from the cleavage of the glycosidic linkage (Domon and Costello 1988), which demonstrated that the phosphate group was on the reducing glucosamine that in turn was acylated by one C14:0 (3-OH) and one C16:0 (3-OH). In parallel, the presence of this fragmentation-derived ion demonstrated that the secondary acyl

substitutions occurred on the primary acyl chains of the sole non-reducing glucosamine. Finally, the absence of any peak matching with the loss of a C16:0 (3-OH) unit suggested that this fatty acid was present only as an acyl amide moiety. Therefore, by combining data from fatty acid compositional analysis and from MALDI MS and MS/MS, it was possible to establish the fine structure of the lipid A from *F. nucleatum* ATCC 51191 LPS of which the main form is bis-phosphorylated hexa-acylated (Fig.2.3.9).

2.3.4. Immunological properties of the LPS of *F. nucleatum*

Monocyte-derived dendritic cells (moDCs) and monocyte-derived macrophages (moMφs) were stimulated with the LPS of *F. nucleatum* ATCC 51191 (Fig.2.3.10) by Dr. Lamprinaki at Quadram Institute Bioscience.

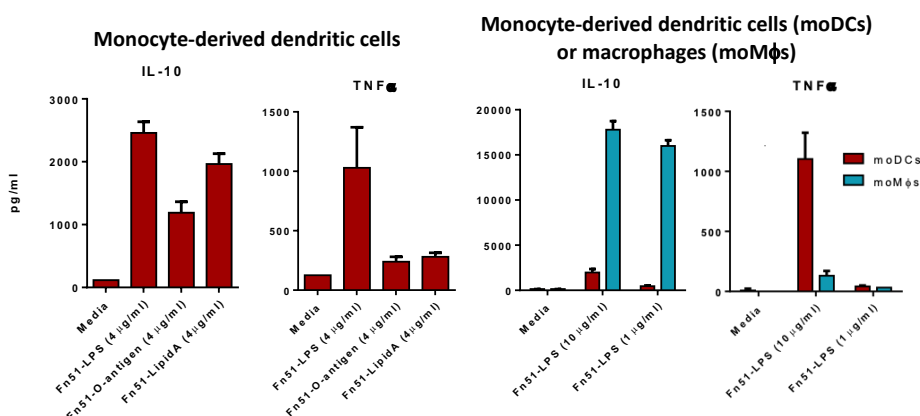


Figure 2.3.10. Immunostimulation of monocyte-derived dendritic cells (moDCs) and monocyte-derived macrophages (moMφs) when exposed to the LPS of *F. nucleatum* ATCC 51191. Bars represent the median values from 3 replicates.

Stimulation of moDCs with *F. nucleatum* LPS resulted in a marked increased production of IL-10 and TNFα. A different profile was observed with moMφs where stimulation led to a significant induction of IL-10 production and low levels of TNFα production. The response was concentration dependant.

2.3.5. Discussion

Using a combination of chemical, MS and NMR approaches, the structure of the OPS $[\rightarrow 4)\text{-}\beta\text{-D-GlcpNAcA-(1}\rightarrow 4)\text{-}\beta\text{-D-GlcpNAc3NAlaA-(1}\rightarrow 3)\text{-}\alpha\text{-D-FucpNAc4NR-(1}\rightarrow]$, (R= Acetylated 60%) and the heterogenous lipid A moiety of the LPS from *F. nucleatum* spp. *animalis* ATCC 51191 were determined adding to the knowledge on the high variability of OPS structures characterised to date on *F. nucleatum* strains (Okahashi *et al.*, 1988; Vinogradov *et al.*, 2018a; 2018b; Vinogradov *et al.*, 2017; 2017a; 2017b; Onoue *et al.*, 1996; Hofstad and Fredriksen 1979). According to the Bacterial Carbohydrate Structure Database (Toukach 2011; Egorova and Toukach 2014), *F. nucleatum* ATCC 51191 LPS represents a novel OPS structure for bacterial LPS. The tool was used in the “composition” mode, by searching for a glycan containing the three units. This search produced no results, even though the queries with the single monosaccharides returned several hits: 63 results for $\beta\text{-D-GlcpNAcA}$, 132 for $\beta\text{-D-GlcpNAc3NAcA}$, and 167 for $\alpha\text{-D-FucpNAc4NAc}$. Importantly, $\alpha\text{-D-FucpNAc4NAc}$ was described for other strains of *F. nucleatum* such as MJR 7757 B (Vinogradov *et al.*, 2018b) and strain 10953 (Vinogradov *et al.*, 2017). Such uncommon structural features of *F. nucleatum* ATCC 51191 OPS raise questions on the immunomodulatory properties of this polysaccharide.

Moreover, *F. nucleatum* ATCC 51191 lipid A consists of a mixture of species with a certain degree of heterogeneity in both the acyl chains and phosphate content. In particular, the main species detected by negative-ion MALDI-TOF MS were identified as *bis*-phosphorylated and hexa-acylated with C14:0 (3-OH) and C16:0 (3-OH) as primary acyl chains, and two C14:0 as secondary fatty acids distributed in a 4+2 symmetry (Fig.2.3.9). This analysis is in agreement with the lipid A structure reported for *F. nucleatum* spp. *nucleatum* strains, (Wollenweber *et al.*, 1984; Hase *et al.*, 1977) although no C12:0 fatty acid residue has been

detected in *F. nucleatum* ATCC 51191 compared to data previously reported for *F. nucleatum* spp. *nucleatum* JCM 8532 (Asai *et al.*, 2007).

Our immunological assays shows that the LPS is immunogenic, stimulating the production of TNF α in dendritic cells (moDCs), but immunomodulatory on macrophages (moM ϕ s) producing much higher levels of IL-10 and low levels of TNF α . *F. nucleatum* ATCC 51191 lipid A is similar to that of *E. coli* in terms of acylation degree and distribution of the acyl chains (4+2), however, the length of the acyl chains (12 and 14 in *E. coli* vs 14 and 16 in *F. nucleatum* ATCC 51191) is different and may influence its immunopotency (Molinaro *et al.*, 2015). Furthermore, *Burkholderia cenocepacia* has the same acylation pattern than the lipid A of *F. nucleatum*, but only tetra- and penta-acylated lipid A species, and it strongly activates human TLR4/MD-2 signalling partly through the occurrence of the C16:0 (3-OH) acyl chains (Di Lorenzo *et al.*, 2015), producing inflammatory cytokines TNF- α and IL-6 when presented to macrophages (Shimomura *et al.*, 2001) and dendritic cells (Guadalupe Cabral *et al.*, 2017). The different stimulation between moDCs and moM ϕ s by *F. nucleatum* LPS must likely reside in the OPS and suggested that moDCs stimulated with *F. nucleatum* strains show a pro-inflammatory profile while moM ϕ s acquire a tumour associated profile. This is further discussed in 3.4. Comparative analysis of *F. nucleatum* strains. Therefore, the acylation profile of *F. nucleatum* ATCC 51191 lipid A and OPS unique structure may significantly contribute to the immunostimulatory potency of this strain.

2.4. The role of the LPS of *F. nucleatum* in colorectal cancer development

F. nucleatum ssp. *polymorphum* ATCC 10953, *F. nucleatum* ssp. *animalis* ATCC 51191 and *F. nucleatum* ssp. *nucleatum* ATCC 25586 strains full cells, LPS and outer membrane vesicles (OMVs) were tested against sialic acid-binding immunoglobulin-like lectins (Siglecs) expressed on innate immune cells to test how *F. nucleatum* promotes colorectal cancer progression by facilitating immune evasion in the tumour microenvironment. The OMV compositional analysis was performed by the author of this Ph.D. thesis at University Federico II of Naples and the Siglecs assays were performed by Dr. Lamprinak at Quadram Institute Bioscience and Dr. Hellmich at Norfolk and Norwich University Hospitals.

2.4.1. Outer membrane vesicles compositional analysis

The OMVs are secreted by Gram-negative bacteria as a natural way to communicate with other bacteria and the host. The external membrane of the OMVs, as the bacterial OM, contains LPSs and phospholipids. The composition of the OMVs depend, of course, of the bacterial specie and strain, but also of the environmental conditions (Tan *et al.*, 2018; Bonnington and Kuehn 2016; Vanaja *et al.*, 2016).

The OMVs of three different strains of *F. nucleatum* were studied to determine the proportion of LPSs versus phospholipids by measuring the content of three fatty acids: C14:0, C16:0 and C18:0.

C14:0 was considered the reporter group of the LPS of *Fusobacterium*. Indeed, the most abundant species of lipid A contain two units of this lipid (Fig.2.3.9), as found by our MALDI analysis (Fig.2.3.7) and in the literature (Hase *et al.*, 1977). C16:0 and C18:0 were considered reporters of the phospholipids. Each phospholipid has, in good approximation, two units of C16:0, because the amount of C18:0 seems rather low in our analysis and in the literature (Sadek *et al.*, 1998).

A semiquantitative analysis of C14:0, C16:0 and C18:0 was performed via GC-MS, by analysing them as methylesters. The analysis was semiquantitative because it did not estimate the amount of these lipids in the sample, but the amount of each component (in this case C14:0) versus the other (C16:0 and C18:0) by means of a corrective (or response) factor.

As for the response factor, C14:0 versus C16:0 and C18:0 versus C16:0 were calculated by preparing a series of standards for the calibration (Fig.2.4.1). This information was used to calculate the proportion of C14:0 in comparison with C16:0 and C18:0. A good correlation by linear regression was found (Fig.2.4.1) and was used to relate the amount of C14:0 versus that of C16:0 and C18:0 in the OMV.

A blank was used to quantify C16:0 and C18:0 derived from the solvents/reactives used. In the analysis of 5 mg of dried weight of OMVs, the error caused from the contaminants on the evaluation of the response factor was about 1-5%. Therefore, the contribute of the contaminants to the area of the peak was not significant.

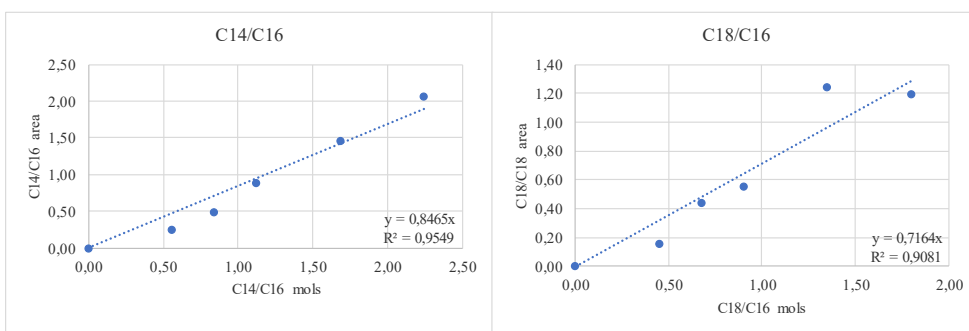


Figure 2.4.1. Response factor calculated for C14:0 versus C16:0 (in mol) (on the left) and C18:0 versus C16:0 (on the right).

The OMVs (5 mg) underwent the monosaccharide chemical analysis as acetylated *O*-methyl glycosides and total fatty acid composition analysis by methanolysis (De Castro *et al.*, 2010). The monosaccharide content (Fig.2.4.2). was consistent

with the already described LPS of *F. nucleatum* 10953 (Vinogradov *et al.*, 2017), *F. nucleatum* 25586 (Vinogradov *et al.*, 2017b) and *F. nucleatum* 51191 (see section 3.3). The total fatty acid composition analysis by methanolysis (Fig.III.4.3) was used for the elaboration of the semiquantitative analysis of C14:0, C16:0 and C18:0 (Table 2.4.1).

For *F. nucleatum* 10953 the calculations showed that C14:0 is 1.47 times more abundant than C16:0 + C18:0 (in mols) and this same number relates the mols of LPS to those of phospholipids. Thus, the ratio LPS/phospholipids is 1.47 or 59.5% (approx. 60%).

For *F. nucleatum* 25586 the calculations showed that C14:0 is 1.86 times more abundant than C16:0 + C18:0 (in mols) and this same number relates the mols of LPS to those of phospholipids. Thus, the ratio LPS/phospholipids is 1.86 or 65,07% (approx. 65%).

For *F. nucleatum* 51191 the calculations showed that C14:0 is 2,76 times more abundant than C16:0 + C18:0 (in mols) and this same number relates the mols of LPS to those of phospholipids. Thus, the ratio LPS/phospholipids 2,76 or 73.4% (approx. 70%).

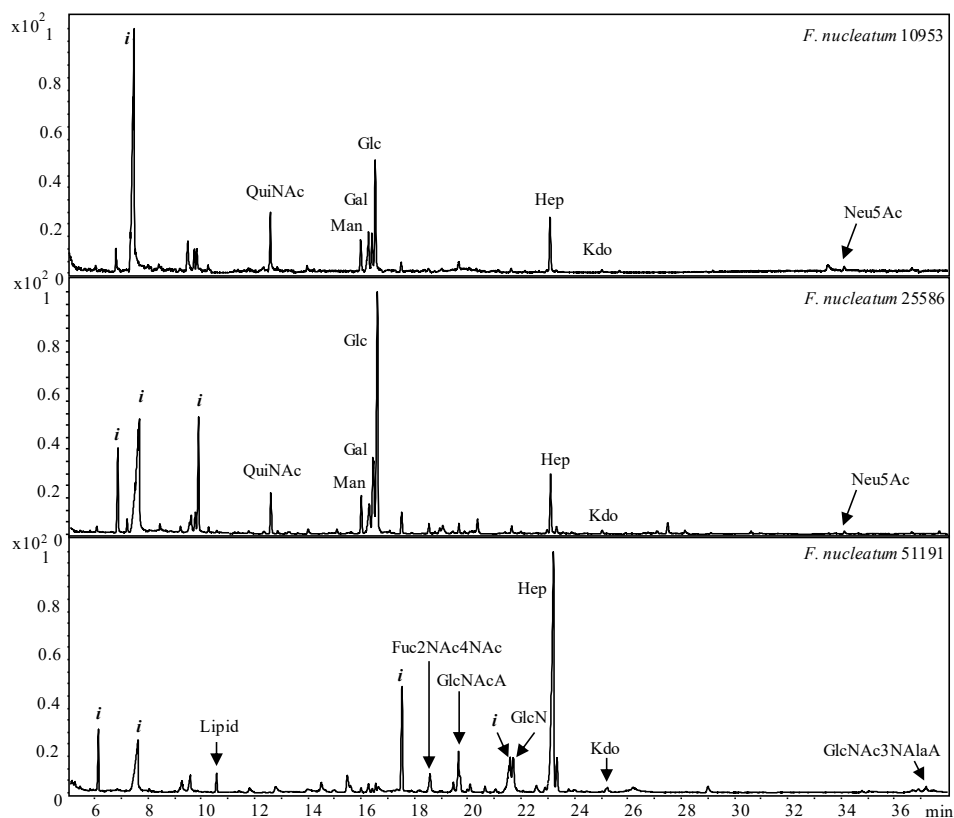


Figure 2.4.2. Acetylated *O*-methyl glycosides results of the OMVs of *F. nucleatum* 10953, *F. nucleatum* 25586 and *F. nucleatum* 51191. QuiNAc: N-Acetylquinovosamine, Neu5Ac: N-Acetylneuraminic acid, Fuc2NAc4NAc: 2,4-diaminofucose, GlcNAc3NAlaA: 2,3-diamino-3N-alanine-glucuronic acid, *i*: unknown.

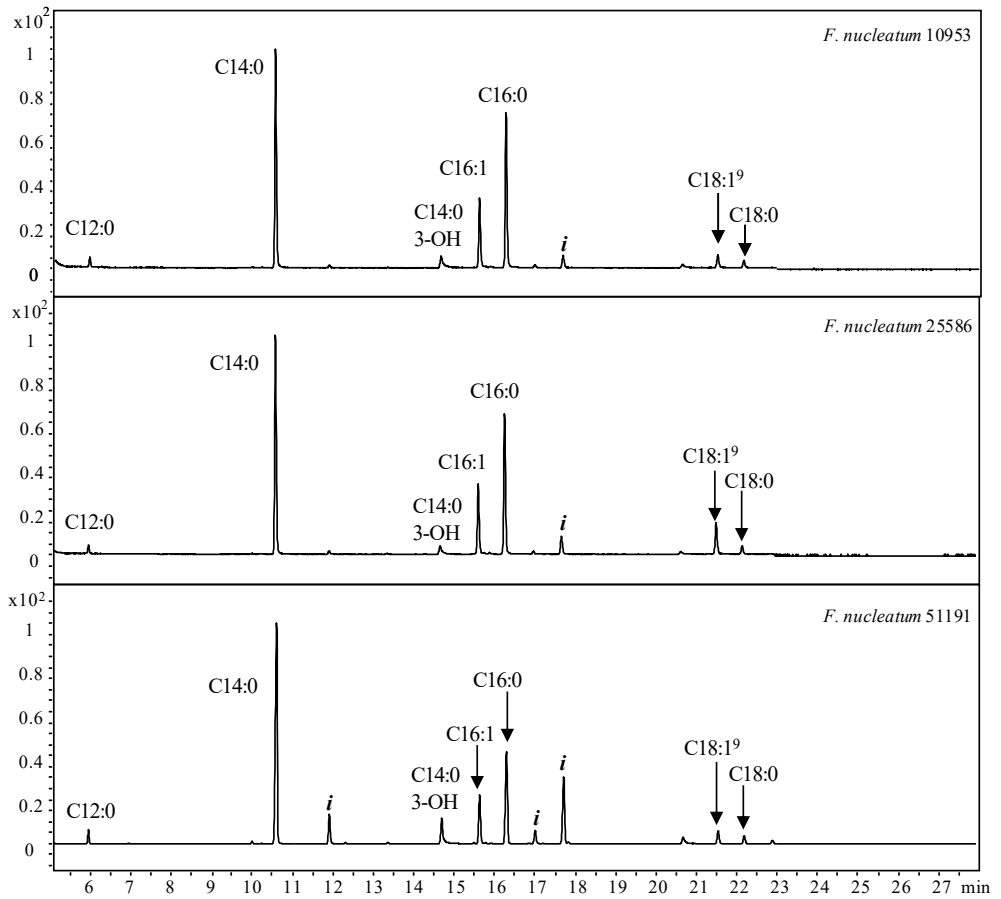


Figure 2.4.3. Total fatty acid composition analysis by methanolysis of the OMVs of *Fusobacterium nucleatum* 10953, *F. nucleatum* 25586 and *F. nucleatum* 51191.

Table 2.4.1. Fatty acids methylesters of OMVs.

Peak	Retention time	Area (blank corrected)	Area rel. /C16	Mol/molC16+C18
<i>F. nucleatum</i> 10953				
C12:0	5.96	264223.6	0.05225065	--*
C14:0	10.58	6728494.6	1.33057058	1.465
C14:0 (3-OH)	14.68	698521.5	0.13813375	--*
C16:1	15.63	2407438.7	0.47607485	--*
C16:0	16.28	5056849.1	1	0.932
C18:1 ⁹	21.53	542252.7	0.10723133	--*
C18:0	22.18	261938.3	0.05179871	0.067
<i>F. nucleatum</i> 25586				
C12:0	5.96	430037.5	0.05345365	--*
C14:0	10.58	13787707.2	1.71381145	1.863
C14:0 (3-OH)	14.68	93346.,3	0.1160297	--*
C16:1	15.63	4974225.8	0.61829606	--*
C16:0	16.28	8045054.9	1	0.920
C18:1 ⁹	21.53	2340011.8	0.29086337	--*
C18:0	22.18	500442.9	0.06220504	0.079
<i>F. nucleatum</i> 51191				
C12:0	5.96	4588147.1	0.05345365	--*
C14:0	10.58	106043639.1	1.71381145	2.762
C14:0 (3-OH)	14.68	13422740.4	0.1160297	--*
C16:1	15.63	22076192.2	0.61829606	--*
C16:0	16.28	40868873.7	1	0.901
C18:1 ⁹	21.53	4319881.5	0.29086337	--*
C18:0	22.18	3208850.6	0.06220504	0.098

* not calculated because the response factor is not available.

2.4.2. Immunological properties of *F. nucleatum* derived LPS and OMVs

A series of assays were performed using full cells, OMVs and LPS from *F. nucleatum* at Quadram Institute Bioscience by Prof. Juge's team.

F. nucleatum strains ATCC 51191, ATCC 25586 and ATCC 10953 full cells showed to bind to Siglec-7 when tested by flow cytometry and to investigate whether the binding of *F. nucleatum* ssp. to Siglec-7 was due to cell surface sialic acid (Neu5Ac), the bacterial cells were treated with Neuraminidase A, a sialidase with broad specificity to (α 2-3,6,8,9) sialylated linkages, cleaving linear and branched non-reducing terminal sialic acid residues from glycoconjugates. The sialidase treatment led to a small reduction in the binding of *F. nucleatum* ssp. to Siglec-7. Also, OMV and LPS showed to bind Siglec-7 by ELISA-type assay (not showed).

To investigate the impact of *F. nucleatum* ssp. on the immune response, myeloid cells moDCs and moM ϕ s were stimulated with *F. nucleatum* strains, *F. nucleatum*-derived OMVs and LPS. Stimulation of moDCs with *F. nucleatum* strains resulted in a marked increase in cytokine production of TNF α , IL-8, IL-6 across all strains (Fig.2.4.4). A different profile was observed with moM ϕ s where stimulation with *F. nucleatum* strains led to a significant induction of IL-10, IL-6 and IL-8 production and low levels of TNF α (Fig.2.4.4). These results were consistent throughout all strains and the response was dose dependent. This tendency was similar when isolated LPS were tested (Fig.2.4.5).

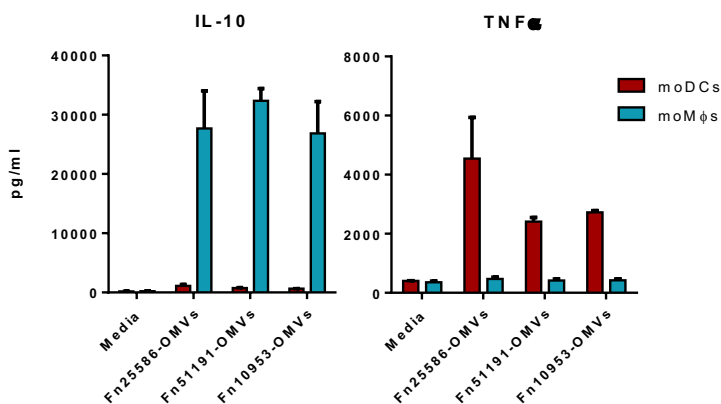


Figure 2.4.4. *F. nucleatum*-derived OMVs mediated moDC and moM ϕ cytokine induction. Bars represent the median values from 3 independent replicates.

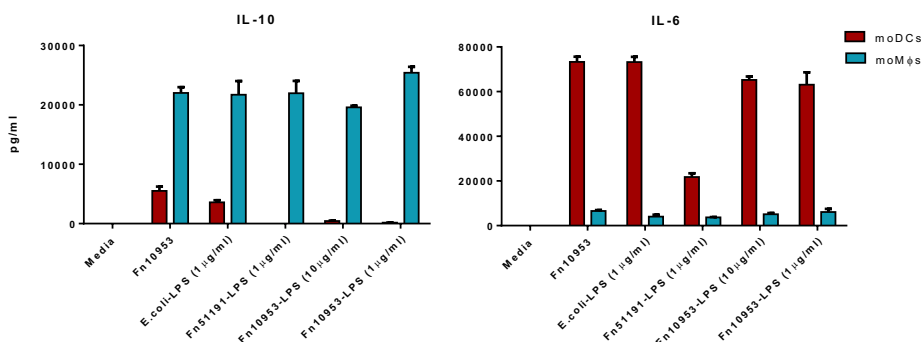


Figure 2.4.5. *F. nucleatum* LPS mediated moDC and moM ϕ cytokine induction. Bars represent the median values from 3 independent replicates.

Overall, our results suggest that moDCs stimulated with *F. nucleatum* strains show a pro-inflammatory profile while moM ϕ s acquire a tumour associated profile and that Siglect-7 may be involved in it.

2.4.3. Discussion

The approach used to analyse the LPS content on OMVs enabled the semiquantitative determination of the lipids in the sample, because disclosed the relative amount of each component (in this case C14:0 and C18:0) versus C16:0, by means of a corrective (or response) factor. Our contribute to this work shows that the proportion of LPS in the OMVs seems unrelated to the immunopotency

of each OMVs, suggesting that this depends on specific structural differences, yet to be defined.

Siglec-7 shows to be involved in the interaction of *F. nucleatum* with immune cells. Human NK cells, macrophages, DCs and CD8⁺ T cells constitutively express inhibitory Siglec-7 (Miyazaki *et al.*, 2012). While the most Siglec-7 positive cells in blood are NK cells among leukocytes, this differs in colonic lamina propria cells where monocytes and macrophages are the major Siglec-7 positive populations (Miyazaki *et al.*, 2012). These results show that *F. nucleatum* ssp. induces a pro-inflammatory profile in moDCs and a tumour associated profile in moM ϕ characterised by the induction of IL-10, IL-6, IL-8 cytokines characteristic of *F. nucleatum*-associated macrophage type 2 polarisation (Kostic *et al.*, 2013; Chen *et al.*, 2018). This phenotype could be recapitulated using *F. nucleatum* derived OMV or LPS, implicating LPS as a potential ligand of the interaction with Siglec-7. The interaction of *F. nucleatum* derived LPS with surface receptors like TLR4 expressed on epithelial cells also lead to polarisation of macrophages that is associated with tumour cell proliferation and metastasis (Chen *et al.*, 2018). These data suggest that *F. nucleatum* strains and OMVs can promote immune evasion by hijacking glycan-lectin responses.

To date Siglec-7 has been reported to bind to terminal sialic acid moieties with diverse underlying glycan structures. The sialidase treatment led to a small reduction in the binding of *F. nucleatum* ssp. to Siglec-7. This may suggest that some of the Neu5Ac residues are not accessible to or are not recognised by the sialidase, as shown for *F. nucleatum* ATCC 10953 LPS containing internal Neu5Ac residues (Vinogradov *et al.*, 2017). In addition, this may suggest that other monosaccharides are involved in the recognition: the strain *F. nucleatum* ATCC 25586 contains a novel sialic acid-like molecule named as fusaminic acid (Vinogradov *et al.*, 2017b). Since binding to Siglec-7 was also observed using LPS and OMVs derived from all 3 strains, it is likely that the LPS glycans in *F.*

nucleatum ATCC 51191, that is devoid of sialic acid, realizes the observed binding to Siglec-7 by a different mechanism. Enzymatic removal of sialic acids from cancer cell surfaces enhanced immune cell-mediated clearance of those cells through loss of Siglec-7 and Siglec-9 binding although the physiological ligands of Siglec-7 and Siglec-9 remain to be identified (Fraschilla and Pillai 2017). Our results reporting the interaction of *F. nucleatum* strains and their OMVs with Siglec-7, open a new dimension in our understanding of the role of sialic acid–Siglec interactions in cancer progression and provide mechanistic insights into how *F. nucleatum* promotes colorectal tumour progression by facilitating immune evasion in the tumour microenvironment. Targeted glycan interventions to displace Siglec-7 interactions with *F. nucleatum* OMVs as a potential checkpoint inhibition strategy could prove to be an effective way of improving current approaches for the treatment of cancer without compromising the rest of the gut microbiome or inducing antimicrobial resistance.

2.5. The peptidoglycan composition of *F. nucleatum* ATCC 51191

2.5.1. Purification and analysis of the peptidoglycan of *F. nucleatum*

In a first approach, PG of *F. nucleatum* ATCC 51191 was extracted from the cell pellet after PCP and hot phenol/water extractions for LPS (*see* Material and methods). The pellet was boiled in the presence of SDS and treated with Pronase E to remove contaminant proteins. Then, the PG was treated with the muramidase cellosyl to liberate the muropeptides and these were reduced with sodium borohydride. Finally, the reduced muropeptides were applied to a micro-C₁₈ reversed-phase HPLC. Simultaneously, *E. coli* D456 cells were treated in the same way to be used as a standard. This was performed by the author of this Ph.D. thesis under the guidance of Dr. Biboy and Dr. Daniella Vollmer at Newcastle University, in occasion of the secondment of the author of this Ph.D. thesis.

Figure 2.5.1 presents the HPLC chromatographic profiles of the muropeptides of *E. coli* D456 and *F. nucleatum* ATCC 51191. Both profiles were very different, and the retention times could not be used to assign a preliminary identity of the peaks. In addition, to verify that this diversity was not caused by the method used (starting from phenol treated and freeze-dried cells), in the next experiment the standard approach was followed before the HPLC and MS analysis.

F. nucleatum ATCC 51191 cells were pelleted, boiled in the presence of SDS and treated with Pronase E. Then, the PG was treated with cellosyl and reduced with sodium borohydride. The reduced muropeptides were applied to a micro-C₁₈ reversed-phase HPLC column which was directly coupled to an Thermo LTQ ion trap Mass Spectrometer (*see* Material and methods) by Dr. Gray from Newcastle University.

The chromatogram is shown in figure 2.5.2 and its preliminary interpretation is presented in table 2.5.1.

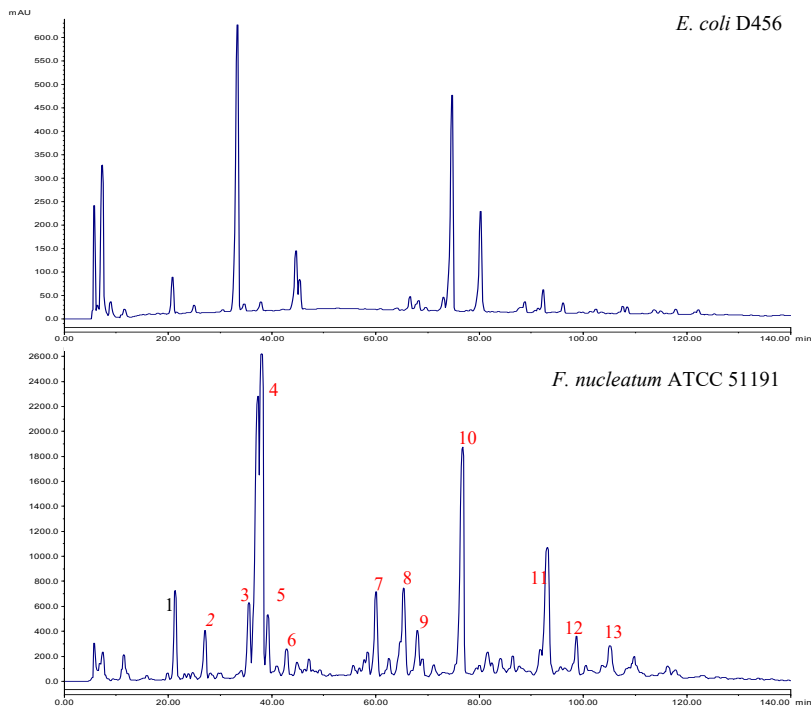


Figure 2.5.1. Separation of mucopeptides of *E. coli* D456 and *F. nucleatum* ATCC 511191 (first preparation). Mucopeptides were released from PG by cellosyl, reduced with sodium borohydride and separated by C₁₈ reversed-phase HPLC.

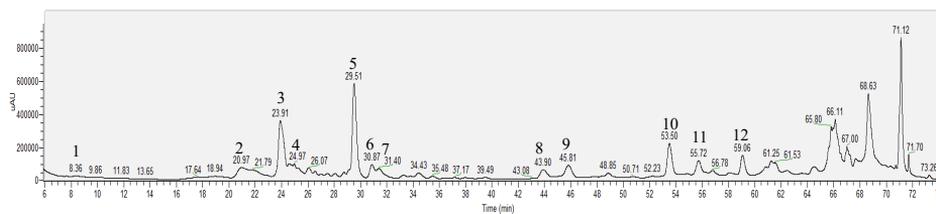


Figure 2.5.2. Separation of mucopeptides *F. nucleatum* ATCC 511191 (second preparation). Mucopeptides were released from PG by cellosyl, reduced using sodium borohydride, and separated by C₁₈ reversed-phase HPLC. The interpretation of the labelled peaks is in table 2.5.1.

Mucopeptides of *F. nucleatum* ATCC 51191 with L-meso-diaminopimelic acid (m-A₂pm) were not identified, it was instead substituted by the sulfur-containing diamino acid, lanthionine (Lnt) or an unknown amino acid (peaks 7 and 9). Lnt was identified because of its mass (208.23 amu), its presence was in agreement with previous compositional analysis reported, although the configuration

remains to be disclosed (Kato *et al.*, 1979). None of the major peaks of *F. nucleatum* ATCC 51191 corresponded to anhydro (Anh) muropeptides which originate from glycan chain ends nor muropeptide trimers or tetramers. It is possible that these muropeptides exist in the PG of *F. nucleatum*, but they were not detected due to their low abundance.

The two major peaks corresponded to GlcNAc-MurNAc-L-Ala-D-iGlu-Lnt-D-Ala (TetraLnt) and the acetylated version of the TetraLnt, followed by mono- and di-acetylated TetraLntTetraLnt (Tetra 3→4 bonded dimer). Only peak 2 corresponded with a muropeptide isolated in *E. coli*, the Di-muropeptide (GlcNAc-MurNAc- L-Ala-D-iGlu) (Glauner 1988).

Table 2.5.1. Reduced muropeptides detected in *F. nucleatum* ATCC 511191. Peak numbers refer to the labels of figure 2.5.2.

Peak	Rt (min)	Mass/charge (m/z)	Neutral mass (amu)	Theoretical mass (amu)	Muropeptide *
1	8.4	889.08 (1+)	888.08	888.31	GlcNAc-MurNAc-Ala-iGlu-Lnt
2	20.9	698.99 (1+)	697.99	696.29	GlcNAc-MurNAc-Ala-iGlu
3	23.9	960.15 (1+)	959.15	959.35	GlcNAc-MurNAc-Ala-iGlu-Lnt-Ala
4	24.9	857.04 (1+)	856.04	--	GlcNAc-MurNAc-Ala-iGlu-X-Ala
5(a)	29.5	1002.14 (1+)	1001.14	1001.36	GlcNAc-MurNAc(Ac)-Ala-iGlu-Lnt-Ala
5(b)	29.5	741.00 (1+)	740.00	--	Possible MurNAc(Ac)-Ala-iGlu-Lnt-Ala
6	30.9	841.04 (1+)	840.04	--	Unknown
7	31.4	899.04 (1+)	898.04	--	GlcNAc-MurNAc(Ac)-Ala-iGlu-X-Ala
8	43.9	883.03 (1+)	882.03	--	Unknown
9	45.8	951.44 (2+)	1900.88	1900.68	Dimer of GlcNAc-MurNAc-Ala-iGlu-Lnt-Ala
10	53.5	972.39 (2+)	1942.78	1942.69	Dimer of GlcNAc-MurNAc(Ac)-Ala-iGlu-Lnt-Ala and GlcNAc-MurNAc-Ala-iGlu-Lnt-Ala
11	55.7	920.66(2+)	1839.32	--	Unknown
12	59.1	993.79 (2+)	1985.58	1984.70	Dimer made of two GlcNAc-MurNAc(Ac)-Ala-iGlu-Lnt-Ala

*Ac means acetyl group at position O-6 of the MurNAc.

2.5.2. Discussion

The preliminary results of the composition of *F. nucleatum* ATCC 51191 revealed its difference compared to the typical Gram-negative PG composition in *E. coli* (Glauner 1988).

Most Gram-negative species contain m-A₂pm at position 3 of the stem peptide, although some species have described to have other amino acids like *Thermotoga maritima* (L- and D-Lys) or A₂pm enantiomers *Myxococcus xanthus* (meso- and LL-A₂pm) (Desmarais *et al.*, 2013) and *Micromonospora olivoasterospora*, *Micromonospora sagamiensis* and related organisms (3-hydroxy-A₂pm) (Kawamoto *et al.*, 1981). The muropeptides identified in *F. nucleatum* ATCC 51191 have no m-A₂pm, that is instead substituted by Lnt and, in lower abundance, another yet unknown amino acid (possible serine (Ser)). Others already reported that Lnt was one of the major constituents of *F. nucleatum* PG, which was the first time that Lnt was reported as natural constituent of wild PG. However, those authors could not determine the optical configuration of the Lnt due to the small amount of biological sample available (Kato *et al.*, 1979; Vasstrand *et al.*, 1979). Another work showed that it is possible to suppress auxotrophy for m-A₂pm in *E. coli* mutants by exogenous cystathionine or Lnt. Most of the Lnt incorporated into the precursors and sacculi was meso-lanthionine (Mengin-Lecreulx *et al.*, 1994). A complementary chemical analysis is necessary to identify the optical configuration of Lnt in *F. nucleatum*. The unknown amino acid (peaks 7 and 9) could be Ser because of its molecular weight (105.09 amu) and that has already been identified as a component of *F. nucleatum* PG (Kato *et al.*, 1979). However, Ser has never been described to be present in position 3 of the PG stem peptide in Gram-negative bacteria (Vollmer *et al.*, 2008).

The lack of major peaks of *F. nucleatum* ATCC 51191 corresponding to Anh-muropeptides nor muropeptide trimers or tetramers is probably due to their low

abundance (Vollmer, *et al.*, 2008; Glauner 1988) and these muropeptides are probably represented by some of the unidentified minor peaks.

Once the definitive compositional analysis of *F. nucleatum* ATCC 51191 is known, it will be interesting to perform immunological assays on them. NOD-1 intracellular receptor recognizes MurNAc-L-Ala-D-iGlu-m-A₂pm (muramyl tripeptide) which is present in almost all Gram-negative bacteria, this recognition may be altered by the absence of m-A₂pm and its substitution by m-Lnt and other amino acids (Tosoni *et al.*, 2019). Interestingly, NOD-1 is highly expressed in human colorectal cancer and seems to augment colorectal cancer cell adhesion, migration and metastasis (Jiang *et al.*, 2020) although more research is necessary to fully understand their role in the immune response to bacterial infection and colorectal tumour development.

In addition, it is important to note that the chromatographic profile obtained from PG extracted from the cell pellet after PCP and hot phenol/water extractions for LPS (first approach) was significantly different from the standard approach (second approach). This is probably caused by the contact of PG with cytoplasmic components since the hot phenol/water extractions compromises cell integrity (Westphal and Jann 1965). Therefore, these results seem to indicate that the PG compositional analysis on phenol treated cells may not be a recommendable approach.

Part 2. Study of trans-envelope machineries

2.6. Effects BAM complex mutations on LPS production

BAM system is a fundamental structure for the building of the OM. To date, it is unknown if any failure in this system induces changes in the LPS component, with a possible impairment of the membrane integrity. Presently, it has been addressed how mutations in some components of the BAM system (BamB, BamC and BamE) and three periplasmic chaperones (SurA, Skp and DegP) impact on the structure of the LOS, taking *E. coli* K12 as model bacterium (Fig.2.6.1).

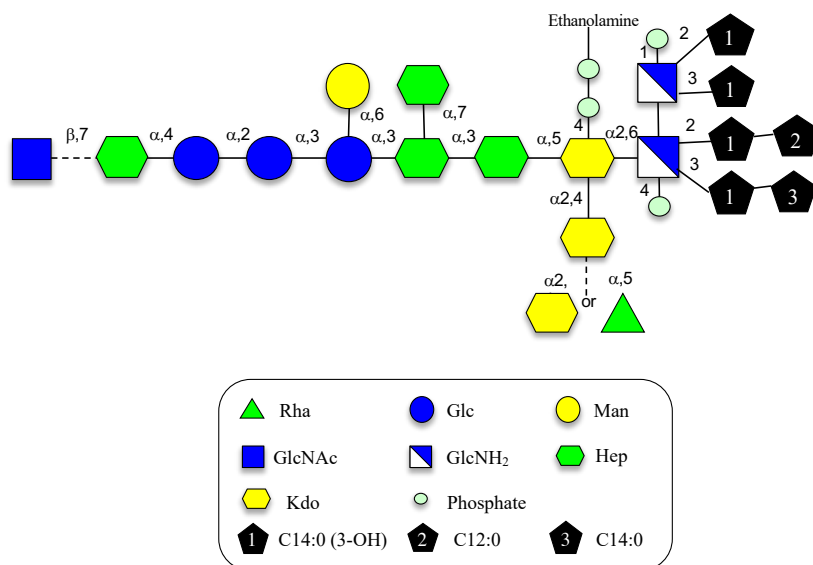


Figure 2.6.1. Wild form LOS along with the structure of the glycan part. Dotted lines mean a not stoichiometric substitution.

Therefore, mutants $\Delta surA$, Δskp , $\Delta degP$, $\Delta bamB$, $\Delta bamC$, and $\Delta bamE$ were created and grew by University of Birmingham and their LOS extracted and analysed to verify if differences occurred by the author of this Ph.D. thesis at University Federico II of Naples.

2.6.1. Isolation and purification of the LOS of *E. coli* mutants

All mutants were constructed via allele transference from the Keio library into the parent strain at the University of Birmingham. Then the kanR cassette was removed using the pCP20 plasmid. Dried cells of *E. coli* K12 BW25113 (wild type or WT) and of the mutants $\Delta surA$, Δskp , $\Delta degP$, $\Delta bamB$, $\Delta bamC$, and $\Delta bamE$ were treated through the PCP extraction to isolate the LOS (see Material and methods). The SDS-PAGE with silver staining evidenced the presence of LOS in the precipitate of the PCP from all mutants (Fig.2.6.2). WT and Δskp displayed some tailing, however this was related to a major amount of the sample loaded in the well and not to significant structural variations (Fig.2.6.2). Yields of all bacteria were comparable around 40%.

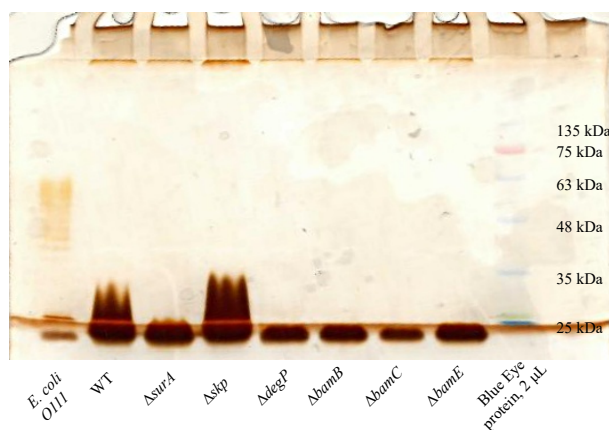


Figure 2.6.2. SDS-PAGE profiles of *E. coli* mutants, as specify in the picture. Each sample is about 8 μ g, 12% SDS-PAGE and visualised by silver staining.

2.6.2. Monosaccharide compositional analysis of the LOS

The acetylated methyl glycosides analysis was performed in order to identify the monosaccharides that compose each mutant. The seven samples had the same chromatographic profile (Fig.2.6.3 shows that of the WT as example for all the others), whose peaks were attributed to Rha, Man, Gal, Glc, GlcN, Hep and Kdo.

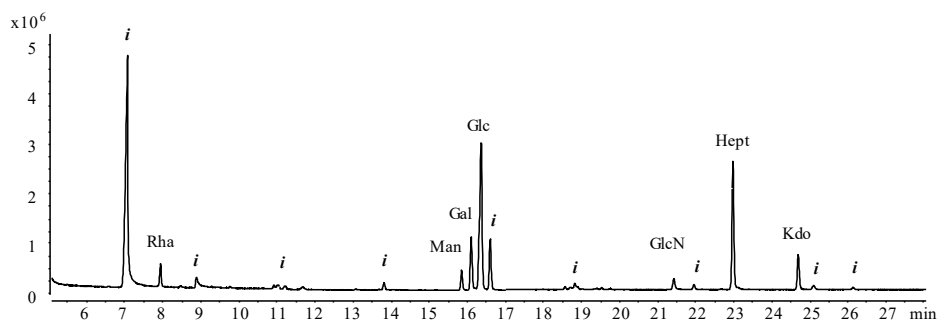


Figure 2.6.3. Monosaccharide of *E. coli* K12 WT. Rhamnose (Rha), mannose (Man), galactose (Gal), glucose (Glc), glucosamine (GlcN), L-glycero-D-manno-Heptose (Hep), 3-deoxy-D-manno-octulosonic acid (Kdo), impurities (*i*).

The comparison of the areas of each monosaccharide (Fig.2.6.4) and percentual areas (Fig.2.6.5) demonstrated no significant differences between the seven samples.

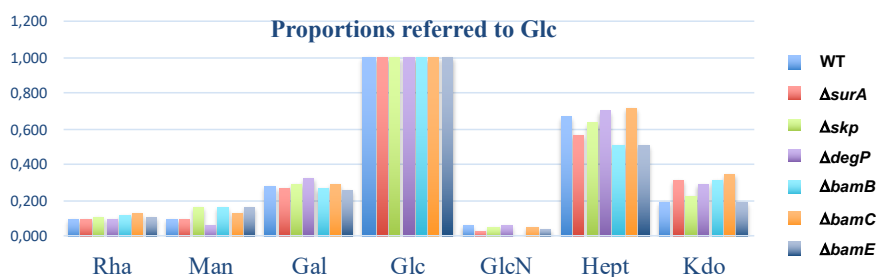


Figure 2.6.4. Monosaccharide composition of *E. coli* WT and mutants. Areas are normalised with respect to that of Glc and are not corrected with a response factor.

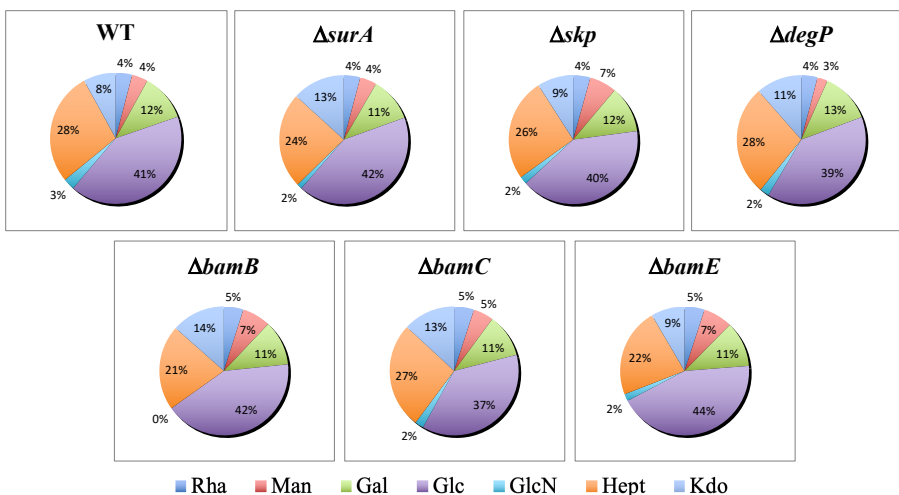


Figure 2.6.5. Monosaccharide percentual area of *E. coli* WT and of its mutants.

2.6.3. ^1H NMR profiling of the core of LOS of *E. coli* mutants

Hence, to confirm that the minor differences between the different monosaccharides were not relevant, the saccharide portion was also profiled by ^1H NMR. In detail, the core region of each LOS was cleaved from the lipid A moiety by mild acid treatment (Wang and Cole 1996) and separated by centrifugation and checked via ^1H NMR (Fig.2.6.6).

In agreement with the monosaccharide chemical analysis, the profiles of each glycan resembled to that of the WT strain of *E. coli* K12 (Fig.2.6.1), leading to the conclusion that these mutations had no effect on the glycan part of the LOS.

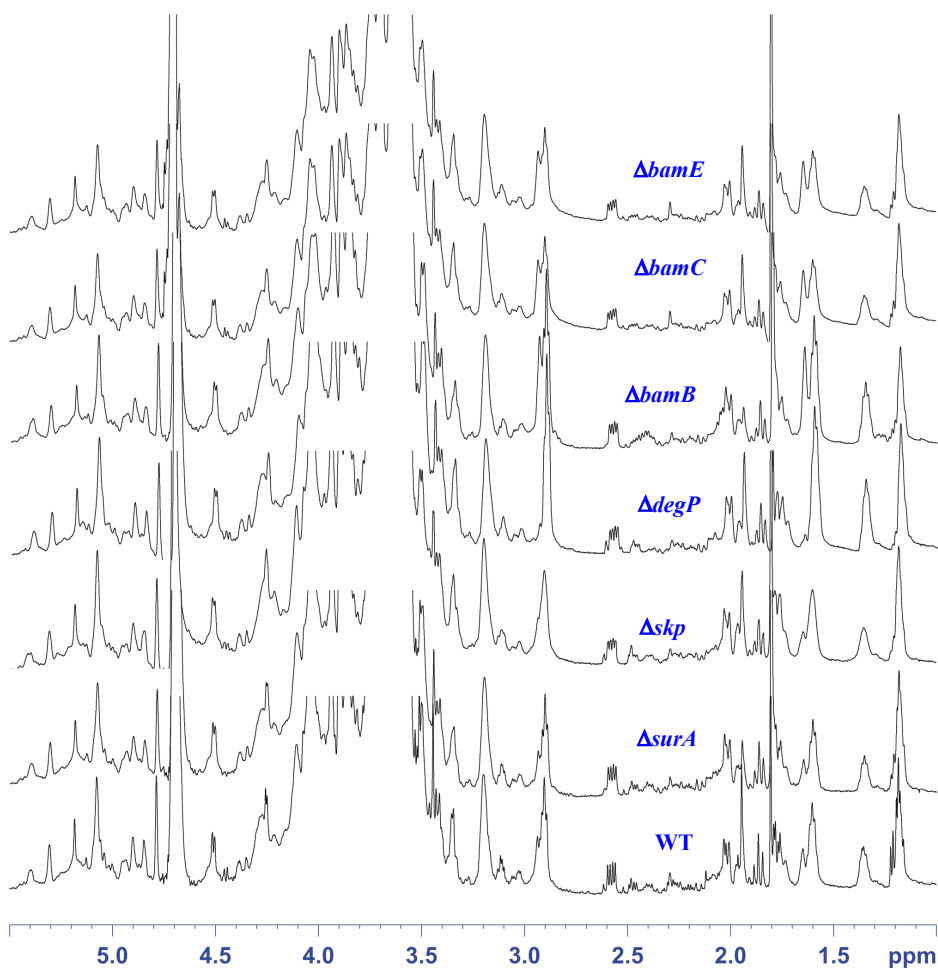


Figure 2.6.6. ^1H NMR profile of the oligosaccharides derived from mild acid hydrolysis of the LOS (600 MHz, 25 °C, 550 μL D_2O).

2.6.4. Lipid profiling by GC-MS of the LOS of *E. coli* mutants

The procedure used for the analysis of the monosaccharides was extended to evaluate the lipid content of each sample. Hence, the fatty acids were recovered as ester derivatives after methanolysis by extracting the crude reaction with hexane (De Castro *et al.*, 2010). The fatty acid analysis revealed the presence of C12:0, C13:0, C14:0, C14:0 (3-OH), C15:0, C16:0, C17:0^A and C18:0 (Fig.2.6.7). The low abundance of C14:0 (3-OH) can be due to the retention by the column of 3-hydroxylated fatty acids. This procedure reports all the lipids present in the

sample, along with those of the phospholipids that are co-extracted with LOS at some extent by the PCP method.

Thus, each LOS contained all the lipids expected based on the structure reported for *E. coli*, namely: C12:0, C14:0, and C14:0 3-OH (in green in Fig.2.6.7), along with those expected for the phospholipids (C16:0, C18:0, and α -C17:0 in red in Fig.2.6.7). However, all the samples (including the WT) presented two additional fatty acids with an odd number of carbon atoms, C13:0 and C15:0 (in blue in Fig.2.6.7). While this finding is unusual, it does not seem related to any kind of mutation, since these two fatty acids appear in the WT bacterium as well.

Comparison of the areas of each fatty acid (Fig.2.6.8) and percentual areas (Fig.2.6.9) focused on those of the lipid A, including C13:0 and C15:0 demonstrated no significant differences between the samples.

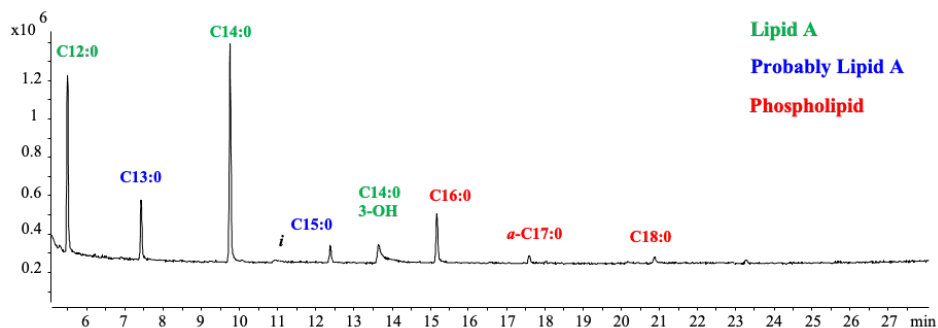


Figure 2.6.7. Chromatogram of the fatty acid compositional analysis. The colour code corresponds to: **Green:** fatty acids that belong to the lipid A; **Blue:** fatty acids that probably belong to the lipid A; and, **Red:** fatty acids from phospholipids.

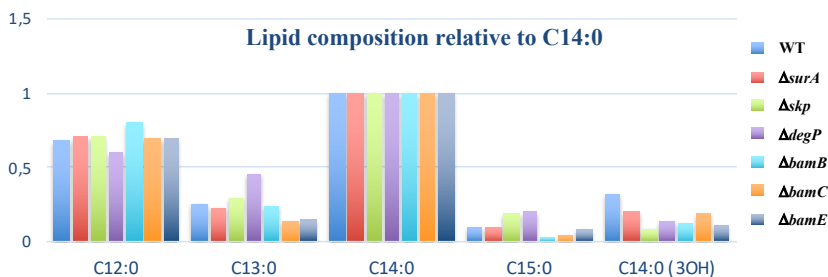


Figure 2.6.8. Fatty acids composition of *E. coli* WT and of its mutants. Areas were normalised with respect to that of C14:0 and not corrected with a response factor.

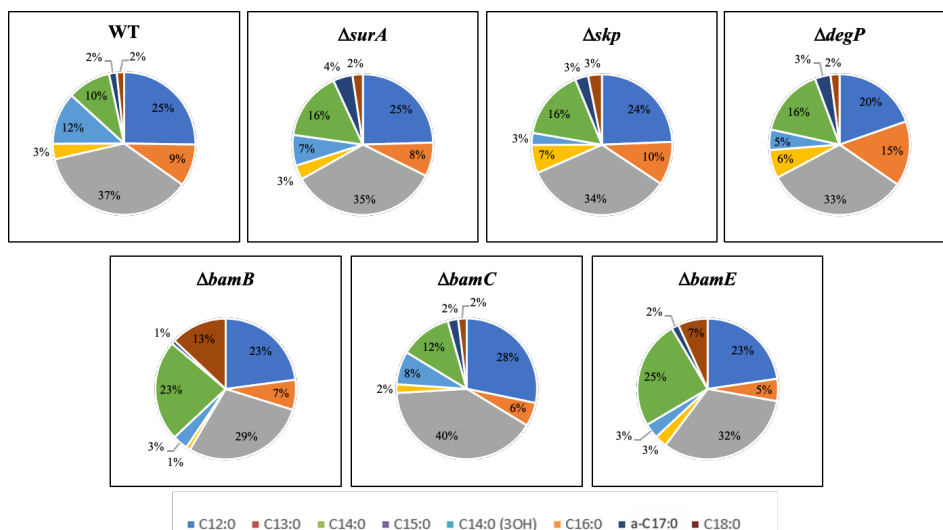


Figure 2.6.9. Fatty acids percentual area of *E. coli* WT and of its mutants.

2.6.5. MALDI analysis of the lipid A of *E. coli* mutants

To prove the similarity between the lipid contents of the different strains and to evaluate if minor modifications existed, especially phosphate appendages and the stoichiometry of substitution of the fatty acids, that may have escaped in the previous analysis, a further analysis on the lipid A obtained from each strain was performed. Briefly, the lipid A was isolated by mild acid hydrolysis of the LOS, as described before, and analysed via MALDI spectrometry.

The structure of the lipid A of *E. coli* consists of a glucosamine disaccharide backbone, phosphorylated at position 1 and 4', and acylated with six fatty acids,

which are classified as primary or secondary depending on their location (*see* Introduction). Primary fatty acids are hydroxylated at C-3 and are directly connected to the glucosamine disaccharide backbone, while secondary fatty acids are never hydroxylated at C-3 (eventually at C-2 or not at all) and are linked at the hydroxyl function of the primary fatty acid. The fatty acid distribution is not symmetric, indeed the non-reducing glucosamine on the left has four fatty acids, while the other has only two. It is an asymmetric 4+2 lipid A with composition: 2×GlcN, 2×P, 4×C14:0 (3-OH), 1×C14:0, 1×C12:0 (Fig.2.6.1).

Importantly, bacteria generally do not produce a unique lipid A, but a family of molecules that differ for the non-stoichiometric presence of phosphates and lipids (Mattsby-Baltzer *et al.*, 1984), and this heterogeneity is easily detected by MALDI spectrometry. Accordingly, MALDI spectra (Fig.2.6.10) displayed that each lipid A had a discrete heterogeneity, as expected.

Analysis of these spectra disclosed that peaks within the same family were separated by 14 u, namely by a methylene unit. For instance, taking into account the base peak (1715.9 u) of the WT (Fig.2.6.10), this corresponded to the composition: 1×P, 2×GlcN, 4×C14:0 (3-OH), 1×C14:0 and 1×C12:0, implying that the species at -14 u (1701.9 u) had one fatty acid replaced with another fatty acid shorter by one carbon atom. Hence, the specie at 1701.9 u was consistent with the replacement of C14:0 with C13:0. In this same way, the appearance of the peak at 1729.9 u implied the substitution of C14:0 with C15:0 or of C12:0 with C13:0.

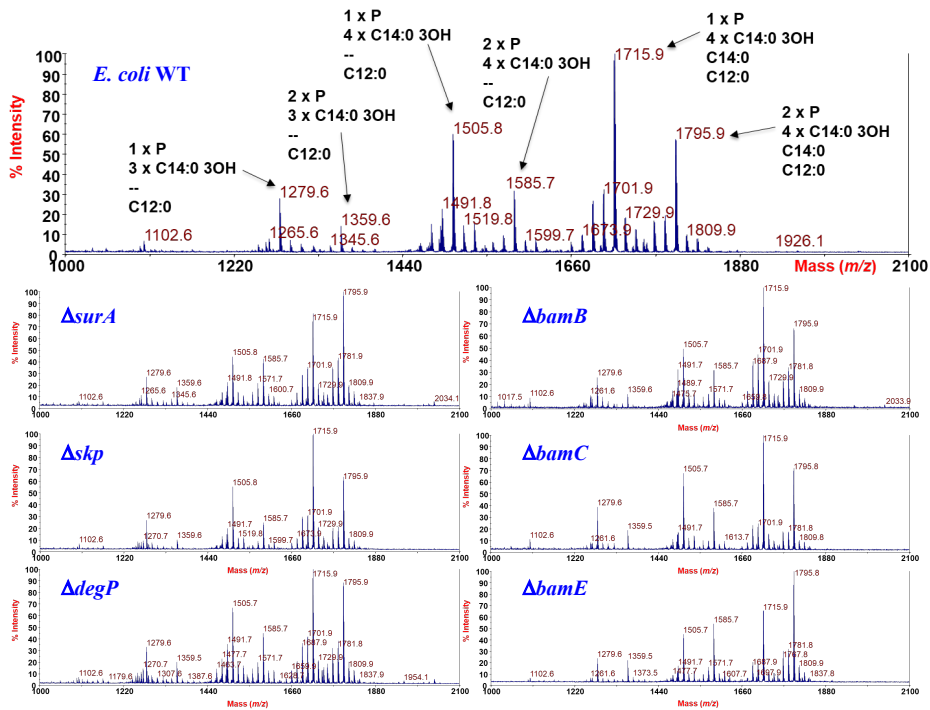


Figure 2.6.10. MALDI spectra in negative mode measured for the different lipid As. In the short notation reported for the WT, the presence of two GlcN units is omitted.

This same pattern was present in all the other groups of peaks, and in all the tested strains. In general, this pattern is unusual for *E. coli*, as it produces exclusively even numbered fatty acids. Nevertheless, this pattern is not related to the kind of mutations done because this characteristic is also present in the WT strain.

As second point, the WT produces both mono- and disphosphorylated lipid A (Fig.2.6.10) with the monophosphorylated being slightly more abundant than the other form; this same pattern with minor variation is conserved for most of the mutants, except for two of them ($\Delta surA$ and $\Delta bamE$) where this proportion is reversed.

2.6.6. Discussion

The LOS from six different mutants $\Delta surA$, Δskp , $\Delta degP$, $\Delta bamB$, $\Delta bamC$, and $\Delta bamE$ have been analysed by chemical and spectroscopical/spectrochemical techniques and compared to the WT strain of *E. coli* K12. The profiling obtained by the different approaches shows that the mutants are very similar to the WT and that the differences, if any, are not significant.

The only variation is minor, and it regards the phosphorylation pattern of the lipid A moiety of the LOS, that for $\Delta surA$ and $\Delta bamE$ consists of an increased content of the diphosphoryl species. Considering that all the procedures (extraction and acid hydrolysis) have been conducted in parallel, it is very likely that this is a true difference between the samples and not an artifact.

Concluding, these preliminary results show that variations in the LOS structure are minimal and may not be enough to change significantly the properties of the OM. From this evidence it can be foreseen that the permeability to drugs of the mutants should be comparable to that of the WT strain. However, targeting BAM may alter OMP folding and compromise membrane integrity by an unknown mechanism (Storek *et al.*, 2018). As β -barrel protein, LptD transport and folding may be compromised, altering in unknown ways the LPS transport.

2.7. New NMR tool for the study LPS-protein interaction

The study of the interactions of LPS with proteins by NMR is difficult because of the complexity of both molecules. Therefore, our idea was to create a new tool for the study of the interactions of LPS with proteins that recognize the lipid A and/or the core, such as Lpt or receptors of the immune system. In detail, the attempt was to introduce some active nuclei in the LPS that would give typical and recognizable signals when close to the interaction protein regions.

Active nuclei could be bound to the acid groups (-COOH) of the Kdo or to the free amino functions (-NH₂) of the glucosamine (GlcN) of the lipid A (Fig.2.7.1).

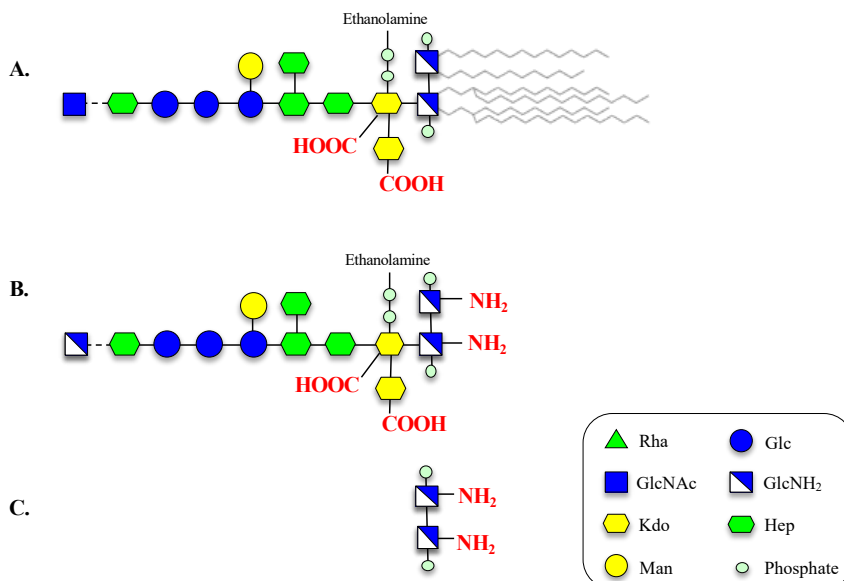


Figure 2.7.1. LOS derived molecules to be used as substrate for the introduction of active nuclei. **A.** LOS from *E. coli* K12. **B.** Fully de-acylated LOS from *E. coli* K12. **C.** Fully de-acylated lipid A from *E. coli* K12.

Therefore, first the above-mentioned substrates were obtained and consequently functionalised with the active nuclei. Details of each step will be explained in the following paragraphs. The LOS from *E. coli* K12 was chosen as starting point due to the fair amount of existing literature about the interaction of the LPS of *E. coli* and Lpt and immune proteins.

2.7.1. LOS production and purification

Escherichia coli K12 dried cells (20 g) were treated through the PCP method (see Material and methods) to yield 18 mg LOS per 1 g dried cells. To confirm the identity of the LPS and the quality of the sample, a monosaccharide and lipid compositional analysis was performed by GC-MS (Fig.2.7.2). The lack of ribose indicated that there was no contamination with nucleic acids. In addition, the lipid compositional analysis showed the presence of C14:0 3-OH, C14:0 and C12:0, all characteristic of the LOS of *E. coli*, while C16:0 and C18:0 denoted the presence of some phospholipids.

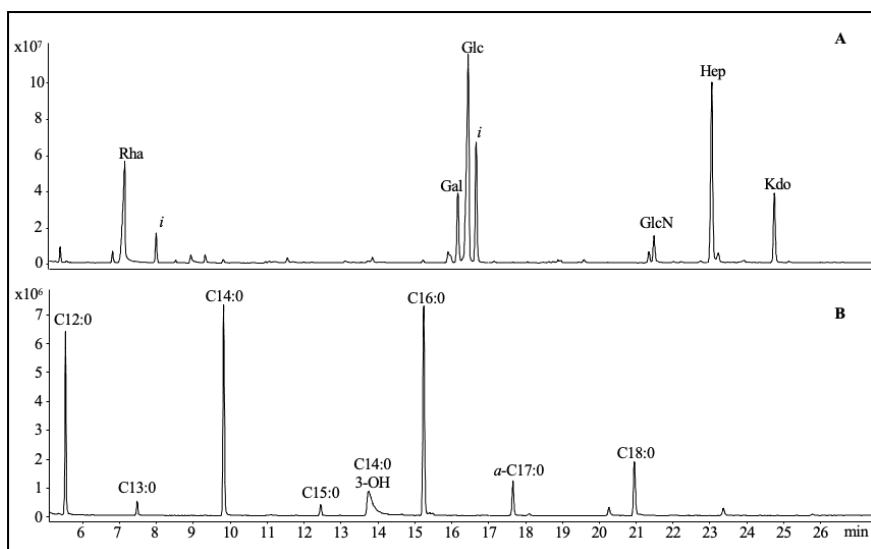


Figure 2.7.2. A. Acetylated methyl glycosides (AMG) of the crude LOS of *E. coli* K12. B. Fatty acid analysis of the crude LOS of *E. coli* K12. *i*: impurities.

2.7.2. Fully de-acylated LOS production and purification

Escherichia coli K12 LOS (40 mg) was treated first with methylhydrazine to remove the *O*-acyl chains and then, with potassium hydroxide (KOH) to remove the *N*-acyl chains. The fully de-acylated LOS (DODN-LOS) underwent a chloroform extraction to remove the acyl chains and a desalting by G10

chromatography (yield 20% w/w of DODN-LOS versus LOS). The quality of the sample was verified via ^1H NMR (Fig.2.7.3).

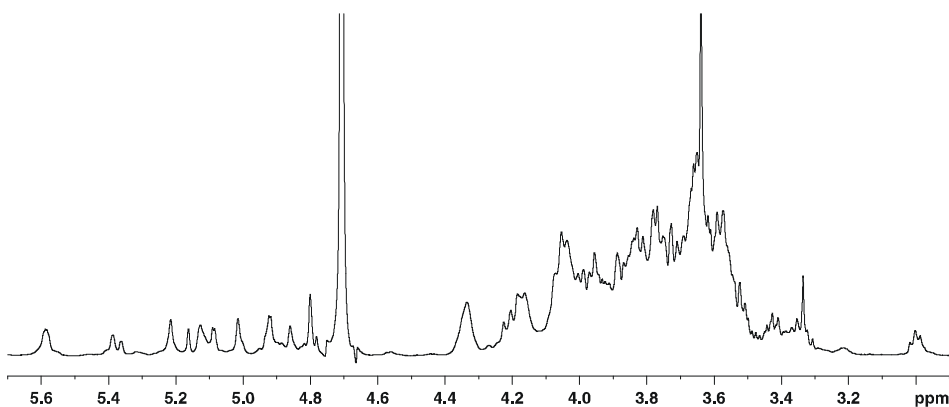


Figure 2.7.3. ^1H NMR of the DODN-LOS of *E. coli* K12 after purification by chromatography (600 MHz, 25 °C).

2.7.3. Fully de-acylated lipid A production and purification

In order to obtain the fully de-acylated lipid A, 125 mg of *E. coli* K12 LOSs were treated with methylhydrazine and subsequently with 1% acetic acid. In this way the Kdo was cleaved and, therefore, the de-*O*-acylated lipid A and the core were separated. Finally, the de-*O*-acylated lipid A was de-*N*-acylated with potassium hydroxide.

The fully de-acylated lipid A (DODN-lipid A) was subjected to an extraction with chloroform to remove the lipids and then, desalted by G10 chromatography (yield 32 mg DODN-lipid A / 1 g LOS). To verify the identity and purity of the DODN-lipid A the ^1H NMR, ^1H , ^{13}C HSQC (Fig.2.7.4 and Table 2.7.1) and MALDI-TOF-TOF (Fig.2.7.5) experiments were performed. Both experiments disclosed the occurrence of slightly heterogenic molecules (for example anomeric carbons in NMR). This is due to: 1) partial de-phosphorylation, consequence of the natural heterogeneity that occur in nature (Mattsby-Baltzer *et al.*, 1984) (and because of the treatments (phosphate group at position 1 is labile and easily removed in acid

media) (Wang and Cole 1996); 2) partial de-acylation, some of the lipid chains may still be present; and 3) some by-products resulting from the reactions.

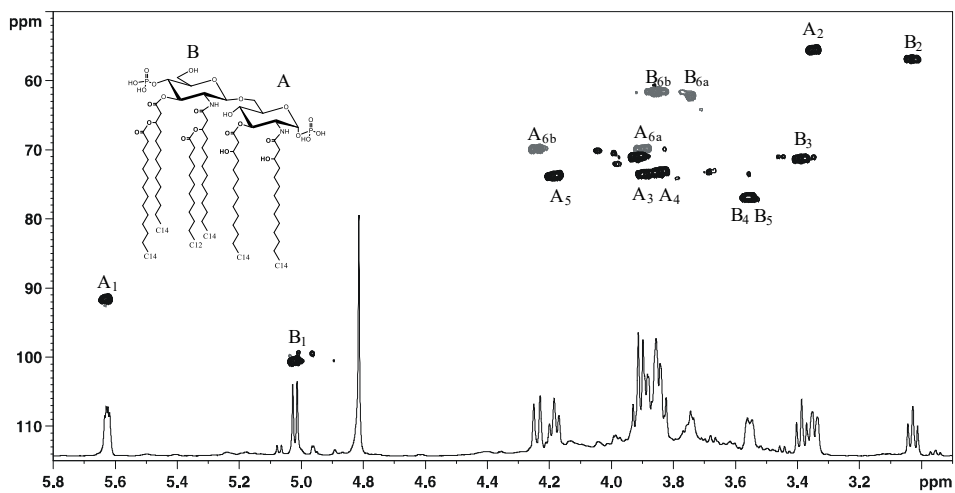


Figure 2.7.4. ^1H NMR and $^1\text{H},^{13}\text{C}$ HSQC spectra of the DODN-lipid A of *E. coli* K12 (600 MHz, 25 °C, 550 μL D_2O).

Table 2.7.1. Proton (^1H) (plain text) and carbon (^{13}C) (*italic*) NMR chemical shifts of the DODN-lipid A of *E. coli* K12 (600 MHz, 25 °C, 550 μL D_2O).

	1	2	3	4	5	6a	6b
A	5.63	3.37	3.90	3.84	3.84	3.91	4.25
6-α-GlcN1P	<i>91.6</i>	<i>55.4</i>	<i>73.4</i>	<i>73.3</i>	<i>73.3</i>	<i>70.0</i>	<i>70.0</i>
B	5.03	3.04	3.39	3.58	3.55	3.75	3.85
t-β-GlcN4P	<i>100.4</i>	<i>56.9</i>	<i>71.3</i>	<i>76.5</i>	<i>77.1</i>	<i>61.6</i>	<i>61.6</i>

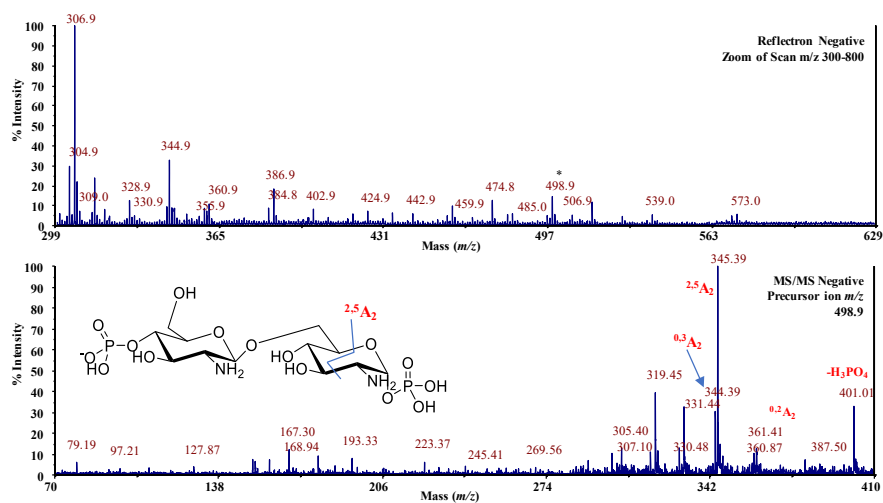


Figure 2.7.5. MALDI-TOF-TOF and MS/MS in negative polarity of the DODN-lipid A obtained from *E. coli* K12.

2.7.4 Active nuclei insertion into the fully-deacylated lipid A

For the NMR interaction studies, glycans can be labelled with isotopes or tags of fluorine or paramagnetic groups (Gimeno *et al.*, 2020). Fluorine is an NMR sensitive nucleus, whose chemical shift strongly depends on the environment (Dalvit and Vulpetti 2019). A paramagnetic group instead causes the fast relaxation of the nuclei in the neighbourhoods (Tesch and Nevzorov 2014), therefore, the signals of atoms in close contact with the LPS are expected to disappear in the spectrum giving an indication of which amino acids are involved in the interaction. To our knowledge, the LPS labelling with tags of fluorine and/or paramagnetic groups has never been performed. Therefore, it was decided to amidate in dimethylformamide (DMF) using the dicyclohexylcarbodiimide (DCC) as activating reagent.

2.7.4.1. Lipid A amidation with fluoropropanoyl chloride

DODN-lipid A was treated with DCC and 3-fluoropropanoyl chloride in DMF and pyridine, in argon atmosphere (*see* Material and methods).

The product was purified by P10 chromatography in water and all fractions were checked via ^1H NMR. Based on the ^{19}F -NMR experiment recorded at the CNRS of Grenoble by Prof. Simorre's team and myself during my secondment in his laboratory (Fig.2.7.6.c), it could be speculated that the reaction was successful based on the ^{19}F NMR analysis of the product which disclosed the presence of two fluorine signals at -122.3 and -130.0 ppm (Fig.2.7.6.c) that could belong to the two insertions at the two NH_2 of the DODN-lipid A and by the ^{13}C chemical shifts of the C-2 of the non-reducing GlcN (**B**) of the lipid A (3.04 to 3.4 and 3.6 ppm) (Fig.2.7.6.a and d).

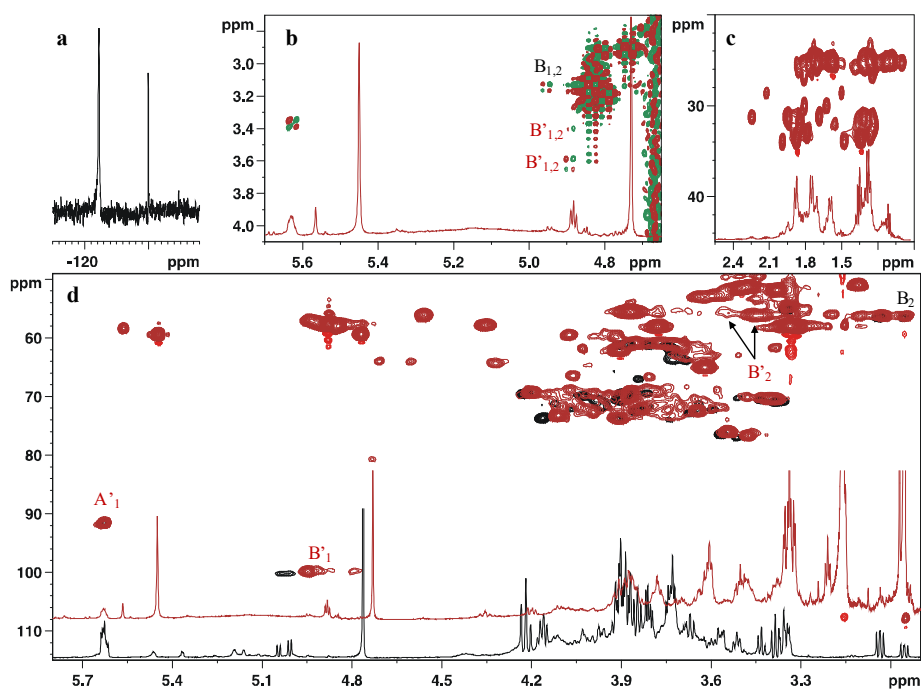


Figure 2.7.6 **a.** ^{19}F -NMR of the N,N' -difluoropropanoyl-DODN-lipid A (700 MHz, 27 °C, 550 μL D_2O). **b.** ^1H NMR and $^1\text{H},^1\text{H}$ COSY dqf of N,N' -difluoropropanoyl-DODN-lipid A (positive red, negative green) (600 MHz, 27 °C, 550 μL D_2O). **c.** ^1H NMR and $^1\text{H},^{13}\text{C}$ HSQC of the N,N' -difluoropropanoyl-DODN-lipid A extension of the dicyclohexylisourea (850 MHz, 27 °C, 550 μL D_2O). **d.** ^1H NMR and $^1\text{H},^{13}\text{C}$ HSQC of the DODN-Lipid A of *E. coli* K12 (black) N,N' -difluoropropanoyl-DODN-lipid A (red) (850 MHz, 27 °C, 550 μL D_2O).

However, both ^1H NMR and $^1\text{H},^{13}\text{C}$ HSQC spectra showed large amounts of dicyclohexylisourea (around 1,52-29.9 ppm) and other contaminants. In order to

eliminate all the contaminants to enable the NMR interpretation and the use of the sample to measure its interaction with the protein(s), the sample underwent a subsequent purification with HiTrap column and CaptoQ 1 mL. Nevertheless, the dicyclohexylisourea was impossible to eliminate, thus preventing any further use of the sample (Fig.2.7.6.b).

2.7.4.2. Lipid A amidation with doxyl stearic acid

By a similar approach, the DODN-lipid A was treated with DCC and 5-doxyl stearic acid in DMF and pyridine, in argon atmosphere, to produce N,N'-doxyl stearate-DODN-lipid A. The N,N'-doxyl stearate-DODN-lipid A was treated with ascorbate in order to eliminate the paramagnetic effect and make the product visible by NMR at the CNRS of Grenoble by Prof. Simorre's team and me.

Despite the numerous attempts, the reaction was not successful. The ^1H , ^{13}C -HSQC shows that there are no significant changes between the spectra of DODN-lipid A (substrate) and the N,N'-doxyl stearate-DODN-lipid A after the ascorbate treatment (Fig.2.7.7).

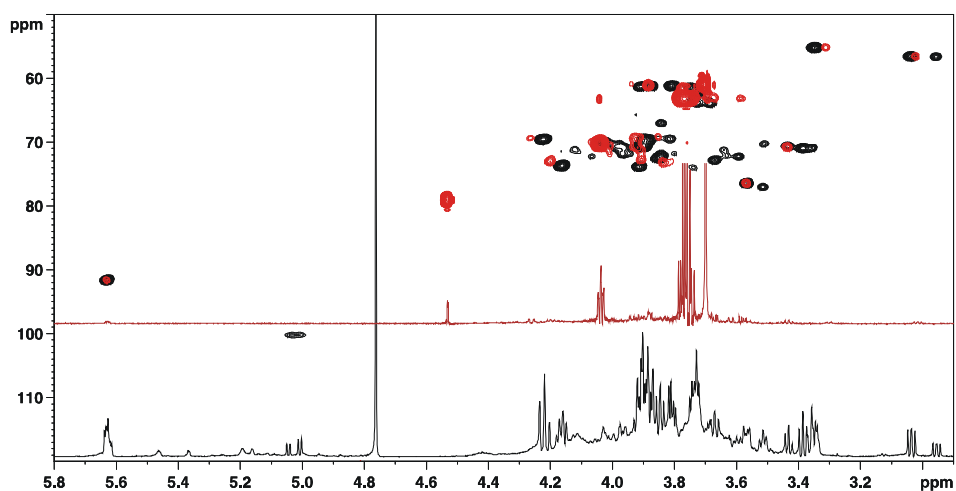


Figure 2.7.7. ^1H NMR and ^1H , ^{13}C HSQC of the DODN-lipid A (black) and the N,N'-doxyl stearate-DODN-lipid A after ascorbate treatment (red) (850 MHz, 27 °C).

2.7.5. Discussion

An uncommon sequence of known reactions was performed to isolate the fully de-acylated lipid A consisting on: the methylhydrazine to remove the *O*-linked fatty acids (Haishima *et al.*, 1992), mild acid hydrolysis to cleave the Kdo linkage (Wang and Cole 1996) and the de-*N*-acylation with potassium hydroxide (Holst *et al.*, 1994), with the idea to use it as initial substrate for the insertion of the fluorine group.

Therefore, the fully de-acylated lipid A was treated with DCC and 3-fluoropropanoyl chloride in order to functionalised it with the fluorine. ¹⁹F NMR analysis of the product discloses the presence of two fluorine signals at -122.3 and -130.0 ppm that do not correspond to any of the expected subproducts like 3-fluoropropanoyl chloride in D₂O (-218 ppm) nor F⁻ (-125 ppm). In addition, H-2 of **B** (t-β-GlcN4P) seems to shift from 3.04 to 3.4 and 3.6 ppm. Thus, suggesting that the expected reaction was successful.

It could be argued that one of the fluorine signals belongs to the *O*-acylurea intermediate and the other to the N,N'-difluoropropanoyl-DODN-lipid A with two fluorines equivalent and converging in only one signal. However, this hypothesis was discarded because of the instability of the *O*-acylurea intermediate (with respect the dicyclohexylisourea). Moreover, the finding of two fluorine signals is reasonable, because the two fluorine nuclei on the DODN disaccharide differ for the chemical and the magnetic environment in which they are, in particular for their distance from the phosphate group.

Nevertheless, it was not possible to further purify the developed compound, as evidenced by the heavy contamination with the dicyclohexylisourea by-product (1,52-29.9 ppm).

Hence, these experiments demonstrate that this kind of insertions are possible. Other ways of purification must be pursued, and also, a new synthetic approach that could produce a purer final compound. One solution could be the amidation of the sample N-ethyl-N'-(3-(dimethylamino)propyl)carbodiimide (EDC) and N-hydroxysuccinimide (NHS) in a approach similar to that of Johnson *et al.*, 2011, which avoids the formation of the dicyclohexylisourea by-product, facilitating its purification.

Also, this approach can be tried in bigger molecules such as the fully de-acylated LOS from *E. coli* K12 or the LOS from *E. coli* K12 (Fig.2.7.1). The obtained tool would be closer to the molecule that performs the interaction in nature, remarkably the Kdo and Hep monosaccharides, that play a role in some LPS-protein interactions (Cochet and Peri 2017). However, these approaches pose other challenges. For fully de-acylated LOS from *E. coli* K12 active nuclei could be bound to the acid groups (-COOH) of the Kdo or the free amino functions (-NH₂) of the glucosamine (GlcN), but also have crossed reactions in which the acid and amino groups of different LOS react between them. Protection steps should be added to the reaction strategy. In addition, there will be another free -NH₂ at the GlcN of the outer core where the active nuclei would also be introduced, however, it is far from the interaction side and it would only be considered from a stoichiometry point of view. For the LOS from *E. coli* K12, the presence of acyl changes drastically decreases the solubility of the molecule in aqueous solvents, detergents should be added and may interfere with the reaction and their traces would also interfere with protein interactions.

2.8. LptA interaction with PG hydrolysis machineries

The Lpt transportation machinery extracts the LPS from the external leaflet of the CM, transports it across the periplasm and the PG, flips it across the OM and locates the LPS in its external face. The known as periplasmic bridge is composed by one LptC, one LptD and a multimer of LptA, which sequesters the lipid A to allow the LPS diffusion through the aqueous periplasm compartment and the PG. However, it is not known how the bridge is built (Laguri *et al.*, 2017; Schultz and Klug 2017). Here, we hypothesised that LptA may somehow interact with the PG hydrolysis enzymes in order to open a hole across it.

2.8.1. LptA as amidase activator

LptA could be an amidase regulator itself, this way, amidases would recognize LptA before the bridge is formed opening a “hole” in the PG. Therefore, amidase activity tests (*see* Material and methods) on AmiA, AmiB and AmiC with LptAHis or LptAmHis (truncated version of LptA at its C-terminus part ($\Delta_{160-185}$ unable to oligomerize in solution) were performed. Moreover, AmiA and AmiB were tested with their regulator EnvC, as positive control, and AmiC was tested with EnvC (instead of its regulator NlpD) as negative control.

After incubation of the different combinations, reaction was stopped by boiling and muuropeptides were digested with cellosyl and prepared for HPLC analysis. Activity is measured by the decrease in Tetra (GlcNAc-MurNAc-L-Ala-D-iGlu-m-A₂pm-D-Ala, indicated with **a** in the Fig.2.8.1) and TetraTetra (dimer of Tetras 3→4 bonded, named **b** in Fig.2.8.1) muuropeptides and the emergence of amidase products (**c** and **d** peaks in the Fig.2.8.1) (*see* Material and methods).

No decrease in Tetra and TetraTetra muuropeptides was detected for either of the combinations of LptA proteins with amidases. This suggests that LptA does not activate amidases (Fig.2.8.1). As expected, there was decrease in Tetra and

TetraTetra muuropeptides and occurrence of amidase products for the controls
 AmiA + EnvC and AmiB + EnvC.

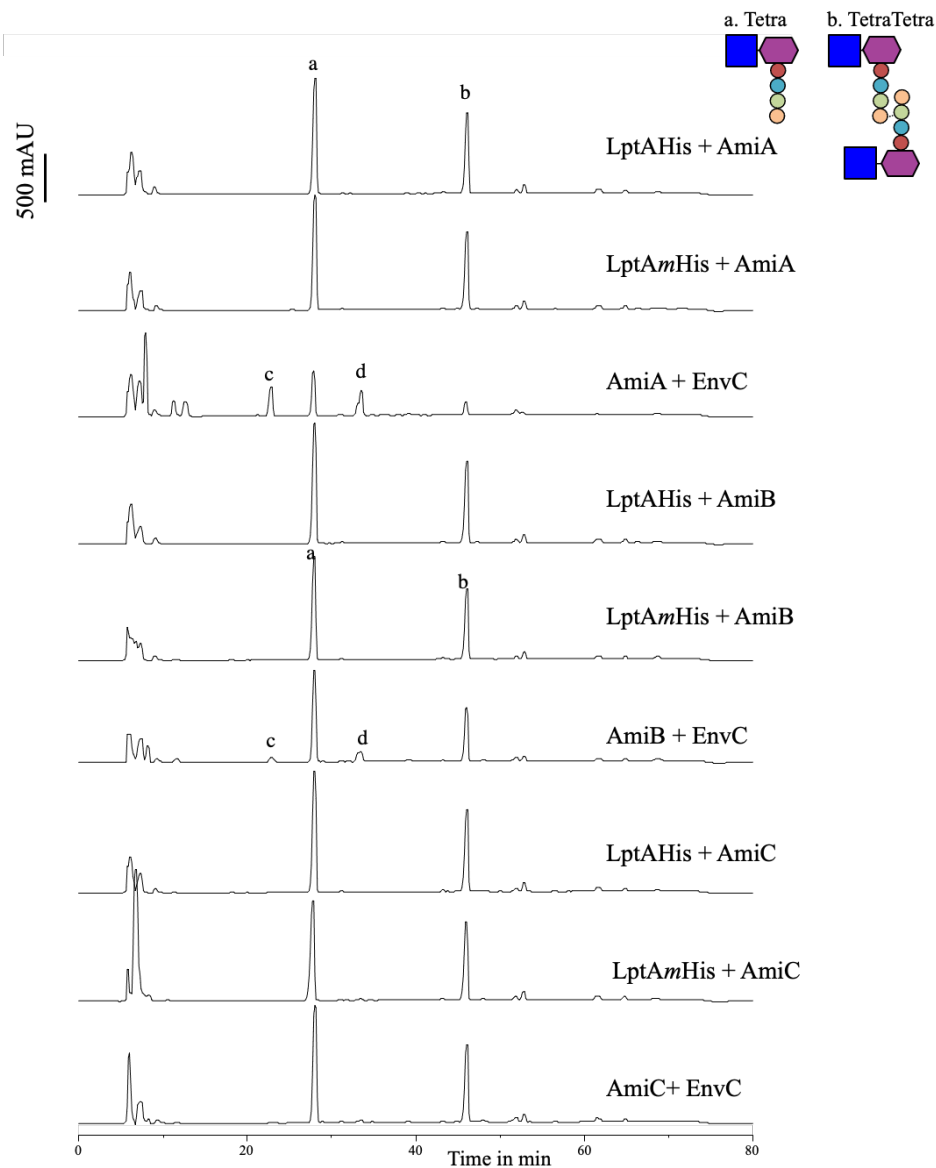


Figure 2.8.1. HPLC chromatogram of the activity test of the amidases AmiA, AmiB and AmiC with amidase regulators or LptAHis or LptAmHis. Muuropeptides: a. Tetra, b. TetraTetra. c and d are amidase products.

2.8.2. Interaction LptA and amidase regulators

LptA could physically interact with the amidase regulators in order to locate the opening of the hole. To test this possibility, an *in-vitro* pull down assay was performed between the soluble His-tagged LptAHis or LptAmHis and the two amidase activators YgeR or NlpD.

LptAHis and LptAmHis were incubated with the amidase activators YgeR or NlpD (fraction A, Fig.2.8.2.A), and the mixture was incubated with Ni²⁺-NTA beads for the *in-vitro* pull-down assay (fraction E, Fig.2.8.2.A) (*see* Material and methods). The same procedure was also performed with the four proteins separately (LptAHis, LptAmHis, YgeR, NlpD), as control (Fig.2.8.2.B).

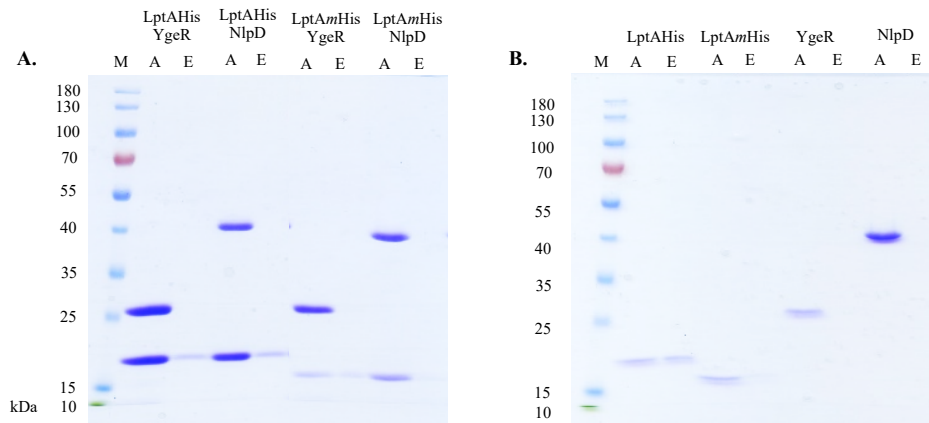


Figure 2.8.2. Electrophoresis of the *in-vitro* pull-down assay. (12% acrylamide, 5 μ l marker, 10 μ l sample, preheated 10 min 100 $^{\circ}$ C, 120 V, Coomassie staining). **A.** LptAHis with YgeR or NlpD and LptAmHis with YgeR or NlpD. The no visualisation of YgeR nor NlpD in fraction E evidences that no interaction occurs. **B.** Control: LptAHis, LptAmHis, YgeR and NlpD separately. LptAHis and LptAmHis bind the Ni²⁺-NTA beads thanks to the His-tag but not YgeR nor NlpD. M: Protein marker PageRulerTM; A: Applied fraction; E: eluate.

The control shows a band at around 20 kDa for both fractions (A and E) of the LptAHis and LptAmHis meaning that they bind the Ni²⁺-NTA beads, thanks to the His-tag, contrary to what found for YgeR and NlpD which appeared only in A (Fig.2.8.2.A). Regarding the protein combinations, there were no interactions

as two bands were visualised in fractions A, while only LptAHis or LptAmHis were visualised in fraction E. This suggests that YgeR and NlpD did not interact with any of the two forms of LptA (Fig.2.8.2.A).

2.8.3. Discussion

Lpt system is composed by seven essential proteins named Lpt A-G, one LptC, one LptD and a multimer of LptA form the periplasmic bridge that forms a continuous β -jellyroll across the periplasm and the PG (Laguri *et al.*, 2017; Schultz and Klug 2017). PG hydrolases may be necessary to insert macromolecular structures into or across the PG layer (Priyadarshini *et al.*, 2007). To explore how the periplasmic bridge is built, the role of LptA as amidase regulator or its capacity to interact with the amidase regulators YgeR or NlpD was tested.

LptA is a periplasmic protein formed by 16 consecutive antiparallel β -strands, folded to resemble a slightly twisted β -jellyroll (Suits *et al.*, 2008). LptA tends to form polymers in a head-to-tail fashion in solution. The presented experiments were performed both with LptA (that probably formed multimers of unknown length) and LptAm that is unable to polymerize to avoid challenges related to the polymerisation. It has been probed that the Lpt transport can successfully occur with only one subunit of LptA, although the affinity for the LPS decreases (Laguri *et al.*, 2017; Schultz *et al.*, 2017). In addition, the use of LptAm for experiments related the periplasmic bridge presents another advantage. LptA binds LptDE with higher affinity than LptC, suggesting that during Lpt assembly, LptA joins LptD/E in the OM and then polymerise until reaching LptC in the CM (Chng *et al.*, 2010). Differences in activity between LptA and LptAm could support this hypothesis and that the C-terminus needs to be exposed for the construction of the PG hole.

The performed assays showed that LptA does not act as an amidase regulator as disclosed by the activity test. On the other hand, results suggested that it does not interact with the amidase regulators YgeR or NlpD either. However, it would be interesting to continue the investigation about LptA's interaction with amidase regulators, the pull-down assay could be performed between LptA and EnvC, YebA and YgeR as they also have implications in PG biogenesis (Uehara *et al.*, 2009). In addition, the assay could be repeated with milder washes, as interaction may occur but with low affinity. More research is necessary to disclose how LptA is built across the PG.

Chapter 3

General conclusion

The main focus of this Ph.D. thesis is to characterize the LPS and PG and their structural determinants when bound to major proteins involved in its transport across the periplasm. The characterised LPS and PG of *Akkermansia muciniphila* and *Fusobacterium nucleatum* reported in the first five sections of the results chapter contribute to the understanding of the interaction of pathogen and commensal Gram-negative bacteria with the host. The assays on the trans-envelope machineries using *E. coli* as model bacterium are reported in the last three sections of the results chapter.

The structure of the LPS and the muuropeptides composition of the PG reveal novel structures with striking immunological features that in case of *A. muciniphila* might play a key role in the protection from metabolic diseases, while for *F. nucleatum* may play a role in the development of the colorectal tumour microenvironment.

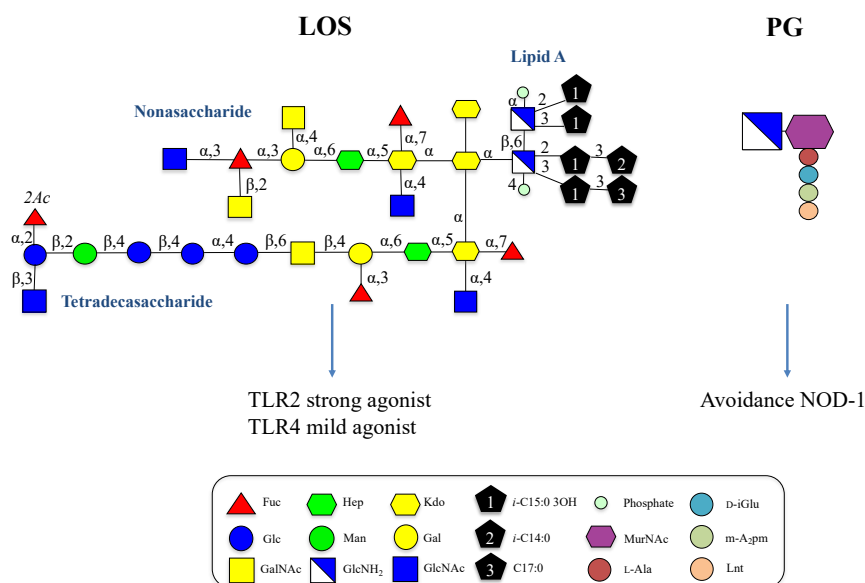


Figure 3.1. Summary findings on the LOS and PG of *A. muciniphila* Muc^T.

The structure of the LOS of *A. muciniphila* Muc^T is highly complex: it includes more than the two canonical units of Kdo, is rich in fucose units and most of the

fatty of the lipid A are branched at the penultimate carbon (Fig.3.1). The LOS shows to be a mild agonist of TLR4 and relevant activator of TLR2 which may play a role in the development of its beneficial effects as it has been linked to protection from diet-induced obesity, increased mucosal barrier function and reduced insulin resistance and inflammation. Also, *A. muciniphila* Muc^T is the first case of a Gram-negative bacterium with a de-*N*-acetylated glucosamine in the PG, a modification found so far in some Gram-positive bacteria and linked to the avoidance of NOD-1 immune receptors (Fig.3.1).

The LPS of *F. nucleatum* ATCC 51191 is composed by a trisaccharide repeating unit rich in amino- and aminuronic monosaccharides and a lipid A similar to that of *Burkholderia cenocepacia* (Fig.3.2). In addition, *F. nucleatum* ssp. *polymorphum* ATCC 10953, *F. nucleatum* ssp. *animalis* ATCC 51191 and *F. nucleatum* ssp. *nucleatum* ATCC 25586 full cells, OVMs and LPSs denote a pro-inflammatory profile in moDCs and a tumour associated profile in moMφs which seems to be mediated by Siglec-7 receptors, being monocytes and macrophages the major Siglec-7 positive populations in colonic lamina propria. This provides further information on the working of this receptor, up to date thought to interact with sialic acid only. The PG of *F. nucleatum* ssp. *animalis* ATCC 51191 presents an alteration of the most common stem peptide by substitution of the L-meso-diaminopimelic acid by the sulfur-containing diamino acid lanthionine or another amino acid (Fig.3.2). This may be crucial to avoid the recognition by NOD-1 immune receptors potentiating colorectal cancer development.

The results on *A. muciniphila* and *F. nucleatum* pave the way to the development of new molecules with clinical applications such as analogues of the LOS of *A. muciniphila* that may mimic its beneficial effects or inhibitors of the Siglect-7 receptors to treat colorectal cancer without altering the microbiota nor contributing to the development of antibiotic resistances.

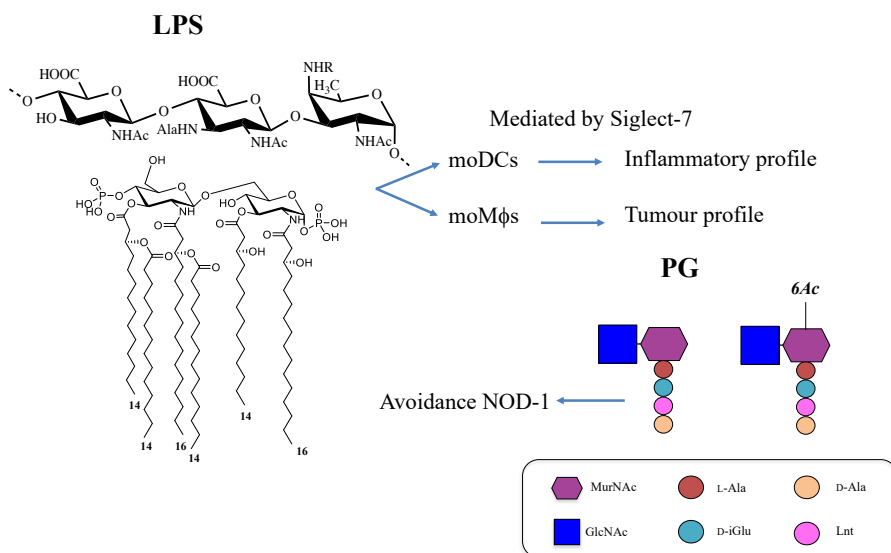


Figure 3.2. Summary findings on the LPS and PG of *F. nucleatum* ATCC 51191.

Remarkably, the second part of the thesis is dedicated to the study of the trans-envelope machineries in order to find new targets for antibiotics. Interestingly, the elucidation of the LPS structure of *E. coli* BAM mutants $\Delta surA$, Δskp , $\Delta degP$, $\Delta bamB$, $\Delta bamC$, and $\Delta bamE$ shows that the alterations in the different structures of the BAM machinery do not alter the composition nor structure of the LPS (Fig.3.3). This provides an insight on the mechanism by which the alteration of the BAM machinery may alter the integrity of the OM.

In addition, in order to study the interaction sites of the Lpt proteins with LPS, the development of a semi-synthetic lipid A with active nuclei instead of acyl chains was attempted. The introduction of a paramagnetic group on the fully deacylated lipid A failed, while that of fluoropropanoyl chloride seems to be partially successful (Fig.3.3). Although, the process needs serious improvements, it paves the way to the development of semi-synthetic LPS NMR tools.

Also, two hypotheses on role of PG hydrolases on the formation of the periplasmic bridge were tested disclosing that LptA does not act as an amidase regulator for AmiA, AmiB nor AmiC nor as a ligand for the amidase activators

YgeR or NlpD (Fig.3.3). Leaving unanswered the question on how the hole on the PG is open to the building of the Lpt bridge.

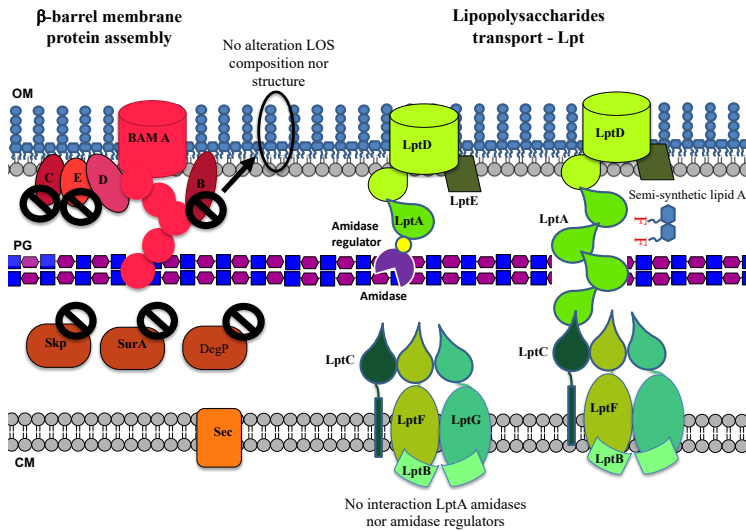


Figure 3.3. Study of the trans-envelope machineries. From left to right: Mutations in BAM do not alter LOS composition; LptA do not act as amidase regulator nor interact with the tested amidase regulators; and the first attempts for the development of a semi-synthetic lipid A with active nuclei were performed.

In conclusion, the architecture of bacterial envelope is crucial for the interaction with the host and the knowledge of the structure of its components is a fundamental prerequisite to proceed with functional studies, and to dissect the role of each component.

In this frame, the knowledge of the molecular determinants of the bacteria of the microbiota is preliminary. This Ph.D. thesis demonstrates that their LPS and PG have unexpected structures and activities. Likewise, the biogenesis of OM, dissected on model organisms, still presents many gaps to be filled. Thus, our understanding of the cell envelope and of its metabolism is still in an early stage. However, it is mature enough to devise alive bacteria and/or synthetic analogues of their surface structures in clinical practice.

Chapter 4

Material and methods

4.1. Strains, plasmids, primers, bacterial and growth conditions

4.1.1. BAM mutants

4.1.1.1. P1 phage transduction

At University of Birmingham, Prof. Henderson's team performed P1 transduction to produce a mutant where the gene of interest was replaced by a kanamycin cassette from Keio collection in the BW25113 strain. P1vir stock was added to the donor culture and incubated for ~3 h or until culture lysis. Chloroform (100 μ L) was added to the culture for complete cell lysis. The recipient cell pellets were suspended in 750 μ L P1 salts (10 mM CaCl₂ and 5 mM MgSO₄). 100 μ L of cells/P1 salts were mixed with 100 μ L of the donor P1 lysate. Cells were incubated for 30 min at 37 °C. Following which, 1 mL of LB and 200 μ L 1 M sodium citrate were added to each sample and the culture was incubated for 1 h at 37 °C with aeration. The cells were harvested by centrifugation at 4,000 g for 2 min and re-suspended in 100 μ L of LB. The cells were then plated onto agar plates containing 50 μ g/mL kanamycin, and 5 mM sodium citrate. The plates were incubated overnight at 37 °C. The mutants were confirmed by check PCR and re-streaked on plates supplemented with 50 μ g/mL kanamycin, and 5 mM sodium citrate. This step was repeated three times to ensure P1 phage absence.

4.1.1.2. Removal of the Kanamycin cassette

At University of Birmingham, Prof. Henderson's team used some mutant strains that contained no resistance cassette in place of a gene. This kanamycin cassette contains two FRT sites either side of the resistance gene which allows the resistance gene to be flipped out, producing a scar region of around ~100 bp. Firstly, the strain of interest was transformed with the plasmid pCP20 and incubated at 30 °C. This plasmid is a temperature sensitive and does not replicate at 37 °C. The pCP20 plasmid codes for the yeast recombinase Flp, which,

recombines the FRT sites either side of the kanamycin cassette (Cherepanov and Wackernagel 1995). The transformants were selected on 100 µg/mL carbenicillin plates. In an attempt to remove the pCP20 plasmid, the transformants were re-streaked on LB only plates and incubated overnight at 37 °C. Individual colonies were then selected and re-streaked onto LB agar plates, LB agar supplemented with kanamycin (to confirm deletion) and LB agar supplemented with carbenicillin (to confirm plasmid loss). The colonies that grew on the LB plate were screened by colony PCR to confirm the deletion. This method was utilised in the construction of mutants: $\Delta surA$, Δskp , $\Delta degP$, $\Delta bamB$, $\Delta bamC$, and $\Delta bamE$. Mutants were grown in LB media 37 °C, overnight at University of Birmingham.

4.1.2. LptA and LptAm mutant

At the University of Milan, Prof. Polissi's team obtained LptA with a C-terminal His6 tag in the Plasmid pGS109 by PCR (external primers: AP55-AP64; *lptA* open reading frames from genomic MG1655 DNA). The DNA fragment was then digested with *EcoRI* and *XbaI* and cloned in the corresponding sites of pGS100 plasmid. Finally, *lptA* $\Delta_{160-185}$ *lptB* operon was excised from the plasmid and subcloned into *EcoRI-HindIII* sites of pWSK29 (Sperandeo *et al.*, 2007).

The *lptA* $\Delta_{160-185}$ *lptB* DNA region was obtained by two-step PCR using (external primers: AP55-AP35; templates: the *lptA* region encoding for amino acids 1–159 of LptA (LptA_m)). It was PCR-amplified from pGS105 using AP55-AP295 primers. The DNA fragment was then digested with *EcoRI* and *XbaI* and cloned in the corresponding sites of pGS100 plasmid (pGS105 $\Delta_{160-185}$). Finally, *lptA* $\Delta_{160-185}$ *lptB* operon was excised from the plasmid and subcloned into *EcoRI-HindIII* sites of pWSK29 (Laguri *et al.*, 2017).

4.1.3. *Akkermansia muciniphila* Muc^T

At Wageningen University, Prof. De Vos' team grew *Akkermansia muciniphila* Muc^T (ATCC BAA-835) in anaerobic serum bottles sealed with butyl-rubber stoppers at 37 °C with N₂:CO₂ (80:20 ratio) in the headspace at 1.5 atm. The bacterial pre-cultures were prepared by overnight growth in: minimal media supplemented with type III hog gastric mucin (Sigma-Aldrich, St. Louis, USA) (Derrien *et al.*, 2004). Growth was measured by spectrophotometer as optical density at 600 nm (OD₆₀₀) (OD₆₀₀ DiluPhotometer™, IMPLEN, Germany).

4.1.4. *Fusobacterium nucleatum*

At Quadram Institute Bioscience, Prof. Juge's team isolated *F. nucleatum* ssp. *polymorphum* ATCC 10953, *F. nucleatum* ssp. *animalis* ATCC 51191 and *F. nucleatum* ssp. *nucleatum* ATCC 25586 strains from clinical isolates were obtained from ATCC in partnership with LGC standards ltd. All *F. nucleatum* strains were cultured in tryptic soy broth media (Becton Dickinson) supplemented with 5 µg/mL hemin (Sigma) and 1 µg/mL menadione (Sigma).

4.1.5. *Escherichia coli* K12

Both at University Federico II of Naples (wild type for 3.7 New NMR tool for the study LPS-protein interaction) and at University of Birmingham (wild type and BAM mutants for 3.6. Effects of BAM complex mutations on LPS production) *Escherichia coli* K12 was grown at 37 °C in aerobic condition in Nutrient Broth 4 from Sigma (meat extract, 3 g/L; meat peptone, 5 g/L). After 18 h cells were harvested by centrifugation 20 min, 15000 g, 4 °C.

4.2. LPS, LOS and OMV isolation procedures

The first step for the study of lipopolysaccharides is their extraction from intact bacterial cells and purification. The lipopolysaccharides extraction is usually

performed by the application of two complementary techniques: the phenol-chloroform-petroleum ether protocol (PCP) for R (rough)-form LPS or lipooligosaccharide (LOS) and hot phenol-water method for smooth-type LPS. The separated extraction of the different types of LPS is based on the different chemical properties, the LOS are more liposoluble. Also, it is remarkable to say that the PCP method extracts the LOS maintaining intact the cellule, whole the phenol water extraction breaks it. Both techniques should be performed when the bacterium phenotype is unknown.

4.2.1. PCP extraction

Dry cells were stirred for 30 min at room temperature (RT) in a mixture containing liquid phenol, chloroform and light petroleum in proportion 2:5:8 (v/v/v). Afterwards, the sample was centrifuged, and the supernatant extracted. This step was repeated twice, and all the supernatants collected together. Consecutively, the low boiling solvents were eliminated by rotary evaporation. Then, drops of water were slowly added to the sample with remaining traces of phenol and water until LOS precipitated. It needed some hours at low temperature to precipitate. The precipitate was separated by centrifugation, dialysed to eliminate the traces of phenol and then lyophilised (Galanos *et al.* 1969).

4.2.2. Hot water-phenol extraction and enzymatic digestion

The pellet resulting from the PCP was stirred in water at 65 °C. Once equilibrated, the same amount of warm phenol was added and left at 65 °C for 30 min. The mix was then centrifuged at 4 °C producing the separation of the phenol layer at the bottom and the water layer at the top. The water layer was extracted and replaced with the same amount of warm water to repeat the extraction twice. The water supernatants pulled together and the phenol phase was dialysed to eliminate the phenol and lyophilised (Westphal and Jann 1965).

LOS obtained by PCP extraction were not further purified since the material was already very pure. On the other hand, the rupture of the cells during the hot water-phenol extraction, produce nucleic acids and proteins to be present in the sample and samples were treated through an enzymatic digestion. The material was dissolved in a buffer (100 mM Tris, 50 mM NaCl, 10 mM MgCl₂, pH 7.5) at a concentration 5.5 mg/mL. Then, RNase and DNase were added (100 µg/mL) and left at 37 °C 18 h under stirring. Amylase and pullulanase were added in this step for the purification of *Akkermansia muciniphila* and *Fusobacterium nucleatum* material. Consecutively, proteinase K was added at a concentration 100 µg/mL at 37 °C, 4 h under stirring. Subsequently the resulting material was dialysed during 48 h to eliminate the nitrogenous bases and amino acids. After lyophilizing the resulting material, it was resuspended in water and underwent a step of centrifugation and ultracentrifugation that concluded in the separation, if present, of LOS, LPS and capsule (De Castro *et al.* 2010).

4.2.3. SDS-PAGE

Screening to detect the presence and length of LPS in polyacrylamide electrophoresis gel, by using the denaturing agent sodium dodecyl sulfate (SDS) in a PolyAcrylamide Gel Electrophoresis (PAGE) with silver staining (Kittelberger and Hilbink 1993; Tsai and Frasch 1982).

4.2.4. Outer membrane vesicles isolation

At Quadram Institute Bioscience, Prof. Juge's team cultured bacterial cells until reaching OD₆₀₀ of approximately 1.2 and centrifuged cells at 8,500 g for 15 min at 4 °C. The supernatant was collected, and vacuum filtered in 0.22 µm membrane. The filtered supernatant was ultra-centrifuged at 200,500 g for 2 h at 4 °C using Type 45 Ti rotor (Beckman Coulter). The filtered supernatant was concentrated by spin-filtration using 100,000 MW cut-off filter unit (Sartorius). OMVs were recovered from the filter using sterile DPBS and further purified by

density gradient ultra-centrifugation. For the gradient, Optiprep media (60% w/v, Sigma) was diluted in 0.85% w/v NaCl and 10 mM Tricine-NaOH pH 7.4 solution to make 35%, 30%, 25% and 20% density solutions. The OMVs were mixed with 40% Optiprep solution and placed at the bottom of a 13.2 mL Ultra-clear tube (Beckman Coulter) and Optiprep (2 mL) was added subsequently by density-decreasing order. The preparation was ultracentrifuged at 135,000 g for 16 h at 4°C with minimum acceleration and deceleration using a SW41 Ti rotor (Beckman Coulter). From the top to the bottom, 1 mL fractions were collected and analysed by SDS-PAGE in 4–15% Mini-PROTEAN® TGX™ Precast Protein Gel (BIO-RAD). The OMV-containing fractions were diluted with sterile DPBS and ultracentrifuged at 200,500 g for 2 h at 4°C using a Type 45 Ti rotor (Beckman Coulter). OMVs were resuspended in sterile DPBS and then filtered using a 0.22 mm membrane (Liu *et al.*, 2019).

Purified OMVs were quantified and measured for their particle size by diluting 100 times in 1 mL DPBS and loading onto a NanoSight LM12 (Malvern Panalytical) chamber by a syringe and the sample were slowly released. The considered particle size of each OMV sample were the mean of triplicates. Instrument settings used: camera shutter 1035, camera gain 680, capture duration 60 sec.

4.2.5. De-acylated LPS isolation

The full polysaccharidic part can be studied by NMR after performing a complete de-acylation on the LPS to remove the lipids, leaving intact the glucosamine disaccharide. LPS were treated with anhydrous methylhydrazine (37 °C, 90 min, cooled under stirring). After wards de-*O*-acylated LPS were precipitated with ice-cold acetone. The precipitate was centrifuged, washed with ice-cold acetone, dried, dissolved in water and lyophilised. LPS were de-*N*-acylated with KOH (4 M, 120 °C, 16 h), followed by a neutralisation with HCl at room temperature. The free fatty acids were extracted with chloroform thrice and then passed through a

G10 column to eliminate salts (Di Lorenzo *et al.*, 2016; Holst *et al.*, 1994; Kaczyński *et al.*, 2007).

4.2.6. Isolation of the lipid A

The ketosidic bond between Kdo and lipid A ($\alpha 2 \rightarrow 6$) is especially susceptible to acid cleavage. Therefore, mild acid hydrolysis (1% acetic acid, 100 °C, 2 h) was used to cleave the Lipid A and the OPS that were separated by centrifugation (Wang and Cole 1996).

4.2.7. De-acylated lipid A isolation

An uncommon sequence of known reactions to isolate the fully de-acylated lipid A was performed consisting on: the methylhydrazine to remove the O-linked fatty acids (Haishima *et al.*, 1992), mild acid hydrolysis to cleave the Kdo linkage (Wang and Cole 1996) and the de-*N*-acylation with potassium hydroxide (Holst *et al.*, 1994), with the idea to use it as initial substrate for the insertion of the fluorine group.

4.3. LPS composition and structure determination

A combination of various techniques is required to determine LPS structure. First, a compositional analysis of the monosaccharides and lipids is performed by using chemical derivatisations and gas chromatography - mass spectrometry (GC-MS). Consecutively, the structure of different LPS fractions is analysed by Nuclear Magnetic Resonance (NMR), Matrix-Assisted Laser Desorption/Ionisation Mass Spectrometry (MALDI-TOF MS), and Electrospray Ionisation Fourier Transform Ion Cyclotron Resonance Mass Spectrometry (ESI FT-ICR MS) (Fig.4.1).

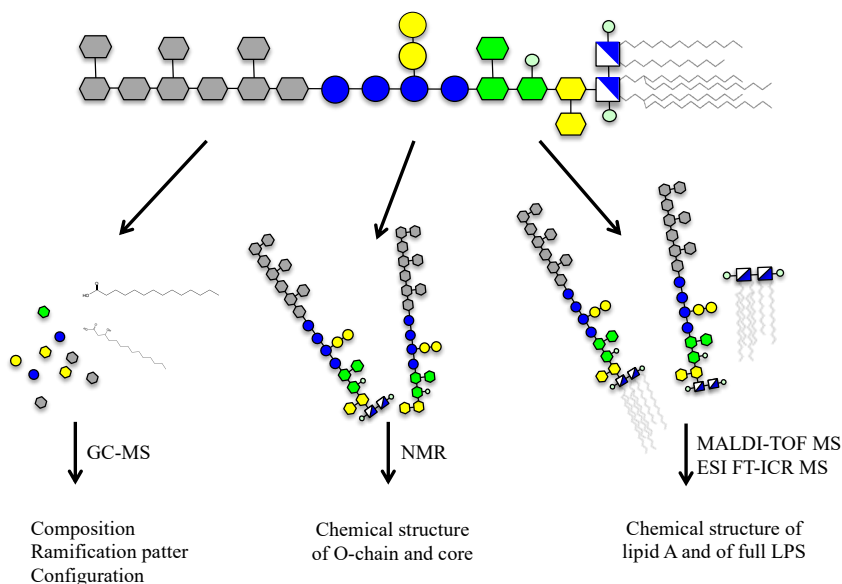


Figure 4.1. Schematic view of the techniques used for the LPS structural characterisation.

4.3.1. GC-MS

In order to study the monosaccharide composition of a sample, it is necessary to make the monosaccharide volatile through derivatisation. For the purpose of this research the acetylated methyl glycosides (AMG), octyl-glycosides and partially methylated alditols acetates (PMAA) methods were used (De Castro *et al.*, 2010).

All chemical derivatives were analysed by using a GC-MS Agilent Technologies 7820A (Santa Clara, CA, USA) equipped with a mass selective detector 5977B, equipped with the automatic injector 7693A and HP-5ms capillary column Agilent, Italy (30 m x 0.25 mm i.d., 0.25 μm as film thickness, flow rate 1 mL/min, He as carrier gas). Electron impact mass spectra were recorded with ionisation energy of 70 eV and an ionizing current of 0.2 mA. The temperature program used was: 150 $^{\circ}\text{C}$ for 5 min, 150 up to 300 $^{\circ}\text{C}$ at 10 $^{\circ}\text{C}/\text{min}$, 300 $^{\circ}\text{C}$ for 12 min (De Castro *et al.*, 2010).

4.3.1.1. Acetylated methyl glycosides (AMG)

The monosaccharide content was established by the acetylated O-methyl glycoside derivatives method. For this purpose, the capsule (0.5 mg) was treated with HCl/MeOH (1.25 M, 80 °C, 16 h) followed by an acetylation step with acetic anhydride in pyridine (80 °C, 30 min) (De Castro *et al.*, 2010).

4.3.1.2. Octyl-glycosides

This protocol allows the determination of the absolute configuration of a sample. Pure LPS were treated with 200 µL of 2-(-)- octanol and 14 µL acetyl chloride at 60 °C for 16 h. Octanol excess was eliminated under air flux. Consecutively, the octyl glycosides underwent a treatment with 100 µL of pyridine and 50 µL of acetic anhydride at 80 °C for 30 min to acetylate the sample (Leontein *et al.*, 1978). After drying the sample, an extraction with water and chloroform was performed. Afterwards, the organic phase was dried and analysed by GC-MS.

4.3.1.3. Partially methylated alditols acetates (PMAA)

The sugar linkage pattern was defined by the partially methylated alditol acetated method. The sample (0.5 mg) was solved in DMSO, methylated with CH₃I, hydrolysed with trifluoroacetic acid (2 M, 100 °C, 1 h), carbonyl-reduced with NaBD₄, and acetylated with acetic anhydride and pyridine (Di Lorenzo *et al.*, 2016).

4.3.1.4. Fatty acid compositional analysis by methanolysis

Fatty acids present in LPS could have different length and be saturated simple or C-2 or C-3 hydroxylated as well as unsaturated lipids. Their abundance and conformation are factors that determines how much the lipid A stimulates the immune system. The LPS underwent a treatment with HCl/MeOH (1.25 M, 80 °C, 16 h) as for the MGA and subsequently lipids were extracted with hexane

thrice. Afterwards volume was adjusted, and the sample injected into the GC-MS (De Castro *et al.*, 2010).

4.3.1.5. Semiquantitative analysis of LPS in OMVs

The OVMs were treated by HCl/MeOH (1.25 M, 80 °C, 16 h) and lipids were extracted with hexane and analysed by GC-MS (*see* Material and methods). The content of LPS versus phospholipids was done by measuring the integration of the chromatographic profiles of three fatty acids: C14:0, C16:0 and C18:0. C14:0 (or myristic acid) was considered as the reporter of LPS of *Fusobacterium nucleatum*. C16:0 (or palmitic acid) and C18:0 (or stearic acid), were considered reporter of phospholipids. The analysis estimated the amount of each component (in this case, C14:0 versus C16:0 and C18:0) by means of a corrective factor calculated by preparing a series of standards for the calibration. The correlation was done by linear regression: C14/C16 area= 0.846 C14/C16 mols ($R^2= 0,9549$) and C18/C16 area= 0.7164 C18/C16 mols ($R^2= 0,9081$). Then the proportion LPS/phospholipids was calculated by (C14/C16 mols)/(C16+C18/C16 mols) proportions were approximately 1.5-2.5 (60-70%).

4.3.2. NMR

For structural assignments of the OPS ^1H NMR and 2D NMR spectra were recorded using a Bruker 600 (University Federico II of Naples), 850 and 950 MHz (CNRS Grenoble, Prof. Simorre) spectrometers equipped with a reverse cryoprobe with gradients along the z axis. In addition, ^{19}F -NMR experiment was recorded 550 μL D_2O , 27 °C, at 700 MHz (CNRS Grenoble, Prof. Simorre). The sample was solved at a concentration of 1 mg in 550 μL of D_2O and the spectra were calibrated with internal acetone ($\delta_{\text{H}} = 2.225$ ppm; $\delta_{\text{C}} = 31.45$ ppm). The conditions were as follows: for *A. muciniphila* the NONA was recorded 550 μL D_2O , 32 °C at 600 MHz and the TETRAD 550 μL D_2O , 27 °C at 950 MHz; for *F. nucleatum* and *E. coli* in neutral conditions 550 μL D_2O , 25°C at 600 MHz;

for *F. nucleatum* alkaline conditions by adding 4 μL of NaOD 4 M to 550 μL of D_2O , 25 $^\circ\text{C}$ and in acid conditions by adding 4 μL of DCl conc. to 550 μL of D_2O , 37 $^\circ\text{C}$ at 600 MHz; for the $\text{N,N}'$ -difluoropropanoyl-DODN-lipid A were recorded 550 μL D_2O , 27 $^\circ\text{C}$ at 850 MHz.

Total Correlation Spectroscopy (TOCSY) experiments were performed with spinlock times of 100 ms using data sets ($t_1 \times t_2$) of 2048×512 points. Nuclear Overhauser Enhancement Spectroscopy (NOESY) experiments were performed using data sets ($t_1 \times t_2$) of 2048×512 points with mixing times of 200 ms. Heteronuclear Single-Quantum Coherence (HSQC), and Heteronuclear Multiple-Bond Correlation (HMBC) experiments were performed in the ^1H -detection mode by single-quantum coherence with proton decoupling in the ^{13}C domain using data sets of 2048×512 points. HSQC was performed using sensitivity improvement and the phase-sensitive mode using echo/antiecho gradient selection, with multiplicity editing during the selection step (States *et al.*, 1982). HMBC was optimised on long-range coupling constants, with a low-pass J filter to suppress one-bond correlations, using gradient pulses for selection. Moreover, a 60 ms delay was used for the evolution of long-range correlations. HMBC spectra were optimised for 6–15 Hz coupling constants. The data matrix in all the heteronuclear experiments was extended to 4092×2048 points and transformed by applying a qsine or a sine window function (Stern *et al.*, 2002).

4.3.3. MALDI-TOF MS and MS/MS

MALDI-TOF MS and MS/MS analysis were performed on an ABSCIEX TOF/TOFTM 5800 Applied Biosystems mass spectrometer equipped with a Nd:YLF laser with a λ of 345 nm, a 500-ps pulse length and a repetition rate of up to 1000 Hz. The lipid A was dissolved in $\text{CHCl}_3/\text{MeOH}$ (1:1, v/v), as previously described (Larrouy-Maumus *et al.*, 2016; Di Lorenzo 2017). The matrix was the trihydroxyacetophenone dissolved in methanol/ 0.1%

trifluoroacetic acid/acetonitrile (7:2:1, v/v/v) at a concentration of 75 mg/mL. The lipid A solution (0.5 μ L) and the matrix solution (0.5 μ L) were deposited on the MALDI plate and dried at room temperature. All spectra were a result of the accumulation of 2000 laser shots, whereas 6000–7000 shots were summed for the MS/MS data acquisitions as described previously (Di Lorenzo *et al.*, 2017). Each experiment was performed in triplicate. In addition, Prof. Garozzo performed this approach on the NONA and the TETRADECA of *A. muciniphila* at CNR of Catania. Alternatively, the lipid A was treated with concentrated NH_4OH (RT, 16 h) and analysed by MALDI (Silipo *et al.*, 2002).

4.3.4. ESI FT-ICR MS

At University Leiden University, Dr. Nicolardi performed measurements on a 15 T solariX XR FT-ICR mass spectrometer (Bruker Daltonics) equipped with a CombiSource and a ParaCell. The system was operated using fimsControl software (Bruker Daltonics). A 20 $\mu\text{g/mL}$ solution of the DODN LOS in water/ACN (v/v 50%:50%) was infused at a 2 $\mu\text{L/min}$ into the ESI source. The ESI dry gas flow rate, drying temperature, nebulizer gas pressure and capillary voltage were 4.0 L/min, 200 $^{\circ}\text{C}$, 1.0 bar, and -4500 V respectively. Mass spectra were acquired in the m/z -range 93-5000 with 2 M data points. For collision-induced dissociation (CID) experiments, precursor ions were selected in the quadrupole and fragmented in the hexapole cell. Collision energies were optimised for each precursor ion to improve the fragmentation efficiency.

Fragment ions detected in the ESI-CID mass spectra were exported as a peak list of $[\text{M}+\text{H}]^+$ species. Each list was then loaded into GlycoWorkbench 2 and tested against hypothesised polysaccharide fragment structures. Fragment ions were assigned within 10 ppm error and allowing a maximum of up to 3 glycosidic cleavages. For each fragment ion, only one isomeric structure out of those possible was illustrated in the figures (Müller-Loennies *et al.*, 2003).

4.4. LPS amidation treatment

A novel approach on LPS derivatisation was tried to introduce active nuclei such as fluorine or paramagnetic groups. This reaction was done using carbodiimide conjugation, by activating carboxyl groups to react with amines via amide bond formation.

The fully de-acylated lipid A of *E. coli* K12 was treated with 3-fluoropropanoyl chloride (Enamine) or 5-doxyyl stearic acid (Avanti), N,N'-Dicyclohexylcarbodiimide (DCC) (Sigma-Aldrich) and pyridine (Sigma-Aldrich) (2 equivalents, 60 °C, 18 h, under stirring) in a Dimethylformamide (DMF) solution (10 mg lipid A/ 1 mL DMF). The DMF and pyridine were dried with Aw300 400 Å seeds for 2 h (Giordano *et al.*, 1991; Jones *et al.*, 2014). It was purified by gel filtration in a HiTrap™ Capto™ Q, 5 mL (Fig.4.2).

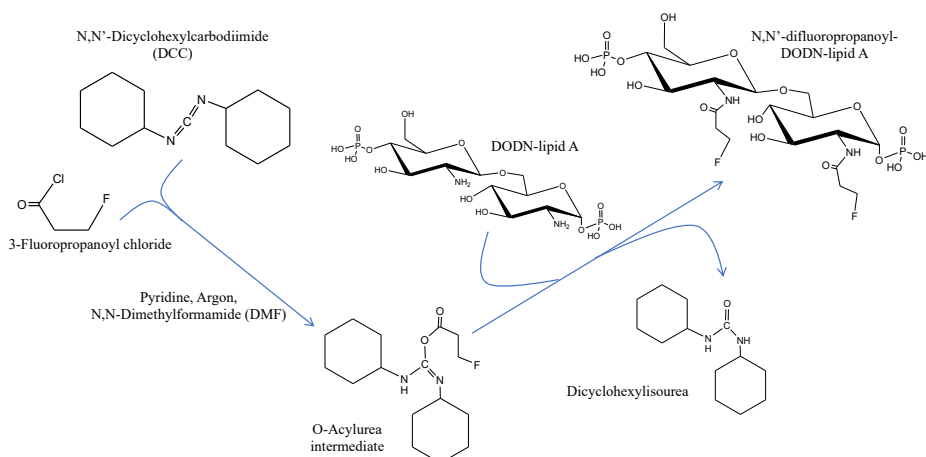


Figure 4.2. Reaction mechanism of the amidation of the DODN-lipid A using the DCC and 3-fluoropropanoyl chloride in pyridine, argon and DMF.

4.5. Peptidoglycan isolation

Bacterial culture (2 L, OD₆₀₀ of 0.4, resulting in a CFU of about 1.4 10⁸ cells/ mL) was centrifuged. The cell pellet was resuspended in 40 mL of ice-cold 50 mM Tris-HCl (pH 7.0). The cell suspension was added dropwise into a flask with 150

mL of boiling 5% SDS solution, boiled 30 min and pelleted by ultracentrifugation (Wageningen University or Quadram Institute). At Newcastle University, Dr. Biboy, Dr. Daniela Vollmer, Dr. Atkinson and I repeatedly washed the pellet with deionised water until it was SDS free (Hayashi test). The pellet was resuspended in 900 μ L of 10 mM Tris/HCl with 10 mM NaCl pH 7.0 + 100 μ L of 3.2 M imidazole pH 7.0 and hydrolysed with α -amylase (15 μ L, 10 mg/mL, 37 $^{\circ}$ C, 2 h). Afterwards, it was treated with Pronase E (20 μ L, 10 mg/mL, 60 $^{\circ}$ C, 1 h) and subsequently treated with SDS 4% (1 mL, 100 $^{\circ}$ C, 15 min) and washed SDS free with deionised water (Glauner 1988).

4.6. Peptidoglycan muropeptides compositional analysis

At Newcastle University, Dr. Biboy and I prepared and reduced muropeptides for HPLC and MS study. First, the muropeptides were mixed with 100 μ L of sample with 50 μ L of 80 mM NaPO₄ 4 \times Buffer pH 4.8, and 50 μ L of water and treated with cellosyl (20 μ L, 0.500 μ g/mL, 37 $^{\circ}$ C, ON). The enzyme was then inactivated by 10 min at 100 $^{\circ}$ C and the resulting pellet collected. The supernatant volume was reduced in the speed vac to 100 μ L and treated with sodium borate (100 μ L, 0.5 M pH 9.0) and solid sodium borohydride (spatula tip, 30 min). The pH was adjusted to 3.5 - 4.5 with 20% phosphoric acid and injected in the HPLC (Glauner 1988). Reversed-phase column (Prontosil 120-3-C18-AQ 3 μ m, Bischoff, Germany) using an Agilent HPLC1220 infinity series with binary pump. HPLC was performed with a column temperature of 55 $^{\circ}$ C using a linear 135-min gradient from 100% buffer A (50 mM NaPO₄-pH 4.31+ 10 μ L of 10% NaN₃) to 100% buffer B (75 mM NaPO₄- pH 4.95 + 15% MeOH (MS grade) at a flow rate of 0.5 mL/min. Muropeptide fractions detected at 205 nm were collected separately for its analysis by Liquid Chromatography - Mass Spectrometry (LC-MS). The LC-MS setup consisted of a Waters Acquity Ultra-Performance Liquid Chromatography (UPLC) system (Waters, Milford, MA) and an LTQ ion trap Mass Spectrometer (Thermo Fisher Scientific, Waltham, MA) equipped with an

Ion Max electrospray source. Chromatographic separation consisted of an Acquity UPLC HSS T3 C18 column (1.8 μm , 100 \AA , 2.1 mm by 100 mm). Mobile phase A (99.9% H_2O and 0.1% formic acid) and mobile phase B (95% acetonitrile, 4.9% H_2O , and 0.1% formic acid). Flow rate 0.5 mL/min and gradient program consisted of 1 min 98% A, 12 min from 98% A to 85% A, and 2 min from 85% A to 0% A, 3 min 100% B, the gradient was then set to 98% A, and the column was equilibrated for 8 min (30 $^\circ\text{C}$ and the injection volume 5 μL). The temperature of the autosampler tray was set to 8 $^\circ\text{C}$. Samples were run in triplicates. MS/MS was performed on the full chromatogram and on specific peaks by Dr. Gray from Newcastle University. The activation type was CID. MS/MS experiments in the ion trap were carried out with relative collision energy of 35%, the trapping of product ions was carried out with a false-discovery rate (q value) of 0.25, and the product ions were analysed in the ion trap. Data were collected in the positive electrospray ionisation (ESI) mode (scan range of m/z 500 to 3,000 in high-range mode). The resolution was set to 15,000 (at m/z 400) (Van Der Aart *et al.*, 2018).

In another approach, at Newcastle University, Dr. Biboy and I treated 100 μL of mucopeptides with 10 μL of 50 mM Ammonium formate buffer pH 4.8 and 20 μL of cellosyl (0.5 mg/mL, prepared in 5 mM Ammonium formate, 10 mM Ammonium chloride buffer pH 4.8) (900 rpm, 37 $^\circ\text{C}$, ON). Afterwards, enzymes were inactivated (100 $^\circ\text{C}$, 10 min), cooled and centrifuged (14,000 rpm, 10 min). The supernatant was collected and dried in the speed vac. The material was then resuspended (25 μL of MilliQ water and 25 μL of 0.5 M Ammonium buffer pH 9.0 adjusted with formic acid). Then it was reduced (few crystals Tetra methyl ammonium borohydride, RT, 30 min). The pH was adjusted to 3.5-4.5 using 5% Formic acid and injected in the LC-MS (Bui *et al.*, 2009). LC-MS was performed by Dr. Gray from Newcastle University.

4.7. LptA and LptAm production and purification

At CNRS of Grenoble LptA was expressed in BW25113 cells containing plasmid pGS109 and at Newcastle University, Dr. Winkle and I transformed LptAm in a pET21b vector into BL21 cells growth in M9 minimal media 20 °C overnight (ON) with ampicillin (100 µg/ml). Induced when OD₆₀₀ 0.6 with 0.5 mM isopropyl β-D-1-thiogalactopyranoside (IPTG) (ON at 20 °C, 220 rpm). Cells were harvested and resuspended 20 ml Buffer A (50 mM NaPO₄, pH 8.0, 300 mM NaCl, 10 mM imidazole, 10% glycerol). Then, sonicated (2 min, 25%, 2 sec on, 2 sec off) and centrifuged, (20,000 rpm, 30 min, 4 °C). Proteins were purified by using a Histrap 5 mL column. Mobile buffer A (50 mM NaPO₄, pH 8.0, 300 mM NaCl, 10 mM imidazole, 10% glycerol) and mobile buffer B (50 mM NaPO₄, pH 8.0, 300 mM NaCl, 500 mM imidazole, 10% glycerol). Flowrate: 1 mL/min, isocratic flow, 96% Buffer A + 4% Buffer B, 10 mL, 96% Buffer A + 4% Buffer B to 100% Buffer B, 30 mL, isocratic flow, 100% Buffer B, 10 mL, isocratic flow, 100% Buffer A, 10 mL (collection in column, 1.5 mL/well) (Laguri *et al.*, 2017; Oliver and Beckwith 1982; Sperandeo *et al.*, 2007).

4.8. LptA, LptAm and PG assays

4.8.1. Amidase activity test

At Newcastle University, Dr. Winkle and I performed the assay. Each protein had a final concentration of 2 µM in a Buffer 20 mM Hepes, 1 mM ZnCl₂, 100 mM NaCl, 0.05% Tx-100, pH 7.5. 10 µL of peptidoglycan suspension were added to each protein mix simultaneously and incubated at 37 °C for 1 h (Peters *et al.*, 2016). Reaction was stopped by boiling for 10 min. Followed by digestion with cellosyl at 37 °C overnight and preparation as described for muuropeptides study on the HPLC (*see* Material and methods). Activity is measured by the decrease in the original muuropeptides and the emergence of amidase products.

4.8.2. Ni²⁺-NTA beads *in-vitro* pull-down assay

At Newcastle University, Dr. Winkle and I performed the assay. A 2 µM of ultracentrifuged protein in a final volume of 200 µL of binding buffer (final concentration 10 mM Hepes/NaOH (pH 7.5), 150 mM NaCl, 10 mM MgCl₂, 0.05% TX-100). The cocktail was incubated at RT for 15 min. 20 µL of the sample were removed, labelled as applied and stored at 4 °C. The rest of the sample was added to Ni²⁺-NTA beads (110 µL, previously washed) and incubated (gentle agitation, 4 °C, 3 h). Part of the sample (2 mL) was labelled as “applied” and conserved at 4 °C. The mix was then placed in a spin column and centrifuged (1 min, 4 °C, 3,000 rpm). The beads were rinsed with 400 µL of washing buffer (10 mM Hepes/NaOH (pH 7.5), 150 mM NaCl, 10 mM MgCl₂, 0.05% TX-100, 30 mM imidazole) and centrifuged ten times (3,000 rpm, 1 min, 4 °C). Then 30 µL 4×SDS loading buffer were added to the spin tube (100 °C, 10 min) and centrifuged (10,000 rpm, 5 min) and labelled as “eluate”. Also, 20 µL of 4×SDS loading buffer was added to the applied samples (100 °C, 10 min). All collected fractions were analysed by SDS-PAGE and Coomassie staining (Egan *et al.*, 2015; Gray *et al.*, 2015).

All experiments were confirmed using in parallel a negative control with protein alone to check that the apparition of the protein in fraction E was not due to the formation of aggregates.

4.9. Immunological assays

4.9.1. HEK-Blue cells

At Wageningen University, Prof. De Vos’ team used HEK-Blue hTLR2 and hTLR4 cells to screen for TLR2 and TLR4 activation, respectively. In these cell lines, stimulation of TLR2 or TLR4 and subsequent activation of NF-κB and AP-1 induces the production of secreted embryonic alkaline phosphatase (SEAP),

which can be quantified spectrophotometrically. Cell lines were grown and subpassaged according to InvivoGen instructions. Cells were subpassaged at 70–80% of confluency in a maintenance medium of Dulbecco's Modified Eagle Medium (DMEM) supplemented with GlutaMAX™ and 4.5 g/L D-glucose), 1x MEM non-essential amino acids, 100 U/mL penicillin, 100 µg/mL streptomycin, 100 µg/mL normocin, 10% (v/v) of heat-inactivated Fetal Calf Serum and 1x HEK-Blue™ Selection. Cells were maximally maintained until passage 25. Receptor activation was tested by seeding cells at 280.000 and 140.000 cells/mL, respectively, in flat-bottom 96-well plates in maintenance medium without HEK-Blue™ Selection in a total volume of 180 µL/well. After 1 day, cells were stimulated by addition of 20 µL of the stimulant of interest (up to 3 µg/mL) in triplicate. Plates were incubated for 14-20 h at 37 °C under 5% CO₂ with *A. muciniphila*'s LPS, O-chain or lipid A. The receptor ligand Pam3CSK4 (100 ng/mL) and Ultrapure LPS from *E. coli* O111:B4 (up to 3 µg/mL) was used as control for TLR2 and TLR4 respectively. PBS and culture medium without antibiotics were used as a negative control. SEAP activity was detected by measuring the absorbance at 600 nm at 1 h after addition of 20 µL of induced HEK-Blue hTLR2 supernatant to 180 µL of QUANTI-Blue. Signals were normalised to negative controls (cell culture medium).

4.9.2. Recombinant Siglec-Fc proteins

At Quadram Institute Bioscience, Prof. Juge's team cultured CHO-Siglec-7-Fc cells in Glasgow Modified Essential Medium (GMEM) without L-glutamine media supplemented with 10% FBS, 100 U/mL penicillin and 100 µg/mL streptomycin and 50xGS supplements. Adherent CHO-Siglec-7-Fc cells (80-90% confluence) were washed twice with DPBS and protein expression was induced by culturing the cells with GMEM without L-glutamine media supplemented with 200x FetalClone II, 100 U/mL penicillin and 100 µg/mL streptomycin, 50xGS

supplements and 100 µg/mL MSX. After 4 days, supernatant was collected gravity-flow column was used for Siglec-7-Fc purification.

For the flow cytometry binding assays between *F. nucleatum* spp. and recombinant Siglecs. Bacteria (10^7 cells) were incubated with the pre-complex of recombinant Siglec-Fc (4 µg/mL) and mouse α -Fc-PE Ab (anti-Fc domain of Siglec-7-fluorescence labelled antibody) (1 µg/mL) in DPBS for 1 h at 37 °C. Following centrifugation at 14,000 g for 4 min, bacterial cells were washed with DPBS and analysed by Fortessa.

For the ELISA-based binding assays, bacteria (10^7 cells) or bacteria-derivatives (10 µg/ml LPS or lipid A or OPS or 10^8 OMV particles) in DPBS solution were coated in a 96-well plate, o/n at 4°C. Following a washing step with 0.05% tween in PBS (washing buffer) the plates were incubated with 1% bovine serum albumin (BSA) (1 h, RT). Followed by 3 times washing the plate were incubated with pre-complexed Siglec-Fc and α -Fc-HRP for 2 h at RT. Colour development was stopped by the addition of 2N H₂SO₄ and the absorbance was measured at 450 nm with reference at 570 nm.

4.9.3. Human primary immune cells

Human peripheral blood was obtained from haemochromatosis patients undergoing a therapeutic venesection at the Norfolk and Norwich University Hospital (Norwich, UK). Blood collection in this study was approved by the Faculty of Medicine and Health Sciences Research Ethics Committee REC reference number 2013/2014 -14HT (University of East Anglia). For monocyte-derived dendritic cell (moDC) and macrophage (moM ϕ) generation, peripheral blood mononuclear cells (PBMCs) were isolated from whole blood following centrifugation using Ficoll-Paque gradient media at Quadram Institute Bioscience. Monocytes (CD14⁺ cells) were isolated from PBMCs using CD14 positive selection microbeads. Freshly isolated CD14⁺ monocytes (10^6 cells/ml

cells) grown in Mercedes medium supplemented with 25 mM HEPES, 10% FBS, 55 μ M 2-mercaptoethanol, 100 U/mL penicillin and 100 μ g/mL streptomycin, 2 mM glutamine, 1 mM non-essential amino acids and 1 mM Sodium Pyruvate, were incubated with granulocyte-macrophage colony-stimulating factor and IL-4 (25 ng/mL) for differentiation of monocytes to moDCs or with macrophage colony-stimulating factor (25 ng/mL) for differentiation of monocytes to moM ϕ s. The cells were incubated for 7 days at 37 °C, with addition of the cytokines on day 3 (Ohradanova-Repic *et al.*, 2016). Human TNF α , IL-10, IL-6 production in the supernatant was monitored by ELISA.

4.11. Image flow cytometry

At Quadram Institute Bioscience, Prof. Juge's team incubated monocyte-derived human cells at 5 10^6 cells/mL with 5×10^7 FITC-stained *F. nucleatum* ssp. for 4 h. Cells were washed with FACS buffer and analysed by ImageStreamx Mk II (Amnis). On INSPIRE software a total of 5000 positive to FITC cells were collected.

Acknowledgements

I would like to express my deepest appreciation to my principal investigators Prof. De Castro and Prof Molinaro from University Federico II of Naples for choosing, trusting and guiding me through this adventure. Our alliance goes beyond professional. *Grazie mille!*

As well, I cannot begin to express my sincere thanks to all the Synthesis and Structure of Carbohydrates in Naples group (SSCN), especially Prof. Silipo, Dr. Di Lorenzo, Dr. Speciale and Dr. Notaro for their direct input in this thesis and their unrelenting support. Also, I would like to extend my gratitude to Prof. Lanzetta, Prof. Lombardi, Prof. Bedini, Prof. Iadonisi, Prof. Marchetti, Dr. Casillo, Dr. Ziaco, Dr. Traboni, Dr. Pallach, Dr. Barrau, Dr. Forgione, Dr. Vessella, Dr. Pither, Dr. Di Carluccio, Dr. Nieto, Dr. Di Guida and Dr. Vanacore, it was a pleasure working with each of you and will always have a very special place in my heart.

In addition, I would like to thank my Innovative Training Network (ITN): Train2Target. Specially, I'm deeply indebted to Prof. Vollmer, Dr. Biboy, Dr. Daniella Vollmer, Dr. Atkinson, Dr. Pazos, Dr. Wrinkle, Dr. Corona and Dr. Lopez from Newcastle University and Prof. Simorre, Dr. Laguri, Dr. Bougault and Dr. Baeta from the National Centre of Scientific Research (CNRS) of Grenoble for hosting and training me during my secondments and performing additional experiments afterwards. Remarkably, Prof. Vollmer significantly contributed to the correction process of this thesis. In addition, I'd like to acknowledge the assistance of Prof. Henderson from Birmingham University and Prof. Polissi from the University of Milan for providing some of the mutants and plasmids necessary for my research. I am extremely grateful as well to the European Commission as this project has received funding from the European Union's Horizon 2020 research and innovation programme under the Marie Skłodowska-Curie grant agreement No 721484.

I very much appreciate Prof. De Vos, Dr. Tytgat, Dr. Plovier and Dr. Elzinga from Wageningen University, Prof. Juge and Dr. Lamprinaki from Quadram Institute Bioscience, and Dr. Nicolardi from Leiden University Medical Centre which inputs through the collaborations we hold played a decisive role in the thesis.

Last, but not least, I wish to thank my family, especially my parents, sisters and aunts, for blindly and unquestioningly supporting me in the pursuit of my dreams, up to the point of learning what a lipopolysaccharide is.

References

- Aart, LT an der, GK Spijksma, A Harms, W Vollmer, T Hankemeier, and GP Van Wezel. 2018. "High-resolution analysis of the peptidoglycan composition in *Streptomyces coelicolor*." *Journal of Bacteriology* 200 (20): e00290-18. <https://doi.org/10.1128/JB.00290-18>.
- Abed, J, JEM Emgård, G Zamir, M Faroja, G Almogy, A Grenov, A Sol, *et al.* 2016. "Fap2 mediates *Fusobacterium nucleatum* colorectal adenocarcinoma enrichment by binding to tumor-expressed Gal-GalNAc." *Cell Host and Microbe* 20 (2): 215–25. <https://doi.org/10.1016/j.chom.2016.07.006>.
- Adinolfi, M, MM Corsaro, C De Castro, A Evidente, R Lanzetta, P Lavermicocca, and M Parrilli. 1996. "Analysis of the polysaccharide components of the lipopolysaccharide fraction of *Pseudomonas caryophylli*." *Carbohydrate Research* 284 (1): 119–33. [https://doi.org/10.1016/0008-6215\(96\)00019-5](https://doi.org/10.1016/0008-6215(96)00019-5).
- Álvarez-Mercado, AI, M Navarro-Oliveros, C Robles-Sánchez, J Plaza-Díaz, MJ Sáez-Lara, S Muñoz-Quezada, L Fontana, and F Abadía-Molina. 2019. "Microbial population changes and their relationship with human health and disease." *Microorganisms* 7 (3): pii: E68E68. <https://doi.org/10.3390/microorganisms7030068>.
- Amir, A, J Männik, CL Woldringh, and A Zaritsky. 2019. "Editorial: the bacterial cell: coupling between growth, nucleoid replication, cell division, and shape. Volume 2." *Frontiers in Microbiology*. 10:2056. <https://doi.org/10.3389/fmicb.2019.02056>.
- Anandan, A, and A Vrieling. 2020. "Structure and function of lipid A-modifying enzymes." *Annals of the New York Academy of Sciences* 1459 (1): 19–37. <https://doi.org/10.1111/nyas.14244>.
- Andolina, G, LC Bencze, K Zerbe, M Müller, J Steinmann, H Kocherla, M Mondal, *et al.* 2018. "A peptidomimetic antibiotic interacts with the periplasmic domain of LptD from *Pseudomonas aeruginosa*." *ACS Chemical Biology* 13 (3): 666–75. <https://doi.org/10.1021/acscembio.7b00822>.
- Ark, KCH van der, S Aalvink, M Suarez-Diez, PJ Schaap, WM de Vos, and C Belzer. 2018. "Model-driven design of a minimal medium for *Akkermansia muciniphila* confirms mucus adaptation." *Microbial Biotechnology* 11 (3): 476–485. <https://doi.org/10.1111/1751-7915.13033>.
- Arweiler, NB, and L Netuschil. 2016. "The oral microbiota." *Advances in Experimental Medicine and Biology*, 902:45-60. https://doi.org/10.1007/978-3-319-31248-4_4.
- Asai, Y, Y Makimura, A Kawabata, and T Ogawa. 2007. "Soluble CD14 discriminates slight structural differences between lipid As that lead to distinct host cell activation." *The Journal of Immunology* 179 (11): 7674–83. <https://doi.org/10.4049/jimmunol.179.11.7674>.
- Atrih, A, P Zöllner, G Allmaier, and SJ Foster. 1996. "Structural analysis of *Bacillus subtilis* 168 endospore peptidoglycan and its role during differentiation." *Journal of Bacteriology* 178 (21): 6173–6183. <https://doi.org/10.1128/jb.178.21.6173-6183.1996>.
- Banzhaf, M, HCL Yau, J Verheul, A Lodge, G Kritikos, A Mateus, B Cordier, *et al.* 2020. "Outer Membrane Lipoprotein NlpI scaffolds peptidoglycan hydrolases within multi-enzyme complexes in *Escherichia coli*." *The EMBO Journal* 39 (5): e102246. <https://doi.org/10.15252/embj.2019102246>.
- Barker, CA, SE Allison, S Zlitni, ND Nguyen, R Das, G Melacini, AA Capretta, and ED Brown. 2013. "Degradation of MAC13243 and studies of the interaction of resulting Thiourea compounds with the lipoprotein targeting chaperone LolA." *Bioorganic and Medicinal Chemistry Letters* 197 (10): 1726–34. <https://doi.org/10.1016/j.bmcl.2013.02.005>.
- Bartholomew, TL, TJ Kidd, J Sá Pessoa, R Conde Álvarez, and JA Bengoechea. 2019. "2-Hydroxylation of *Acinetobacter Baumannii* Lipid a Contributes to Virulence." *Infection and Immunity* 87 (4): e00066-19. <https://doi.org/10.1128/IAI.00066-19>.
- Benoit, R, S Rowe, SC Watkins, P Boyle, M Garrett, S Alber, J Wiener, MI Rowe, and HR Ford. 1998. "Pure endotoxin does not pass across the intestinal epithelium *in vitro*." *Shock*, 10 (1): 43–48. <https://doi.org/10.1097/00024382-199807000-00008>.
- Bera, A, S Herbert, A Jakob, W Vollmer, and F Götz. 2005. "Why are pathogenic Staphylococci so lysozyme resistant? The peptidoglycan O-acetyltransferase OatA is the major determinant for lysozyme resistance of *Staphylococcus aureus*." *Molecular Microbiology* 55 (3): 778-87. <https://doi.org/10.1111/j.1365-2958.2004.04446.x>.
- Berezuk, AM, S Glavota, EJ Roach, MC Goodyear, JR Krieger, and CM Khursigara. 2018. "Outer

- Membrane Lipoprotein RlpA is a novel periplasmic interaction partner of the cell division protein FtsK in *Escherichia coli*.” *Scientific Reports* 8 (1): 12933. <https://doi.org/10.1038/s41598-018-30979-5>.
- Bernard, E, T Rolain, P Courtin, P Hols, and MP Chapot-Chartier. 2011. “Identification of the amidotransferase AsnB1 as being responsible for meso-diaminopimelic acid amidation in *Lactobacillus plantarum* peptidoglycan.” *Journal of Bacteriology* 193 (22): 6323–30. <https://doi.org/10.1128/JB.05060-11>.
- Bi, Y, and J Zimmer. 2020. “Structure and ligand-binding properties of the O-antigen ABC transporter carbohydrate-binding domain.” *Structure* 28 (2): 252-258.e2. <https://doi.org/10.1016/j.str.2019.11.020>.
- Bischoff, SC, G Barbara, W Buurman, T Ockhuizen, JD Schulzke, M Serino, H Tilg, A Watson, and JM Wells. 2014. “Intestinal permeability - a new target for disease prevention and therapy.” *BMC Gastroenterology*. 14: 189. <https://doi.org/10.1186/s12876-014-0189-7>.
- Bishop, RE. 2019. “Ratcheting up lipopolysaccharide transport.” *Nature* 567 (7749): 471–72. <https://doi.org/10.1038/d41586-019-00802-w>.
- Blaauwen, T den, LW Hamoen, and PA Levin. 2017. “The Divisome at 25: the road ahead.” *Current Opinion in Microbiology* 36: 85-94. <https://doi.org/10.1016/j.mib.2017.01.007>.
- Blair, DE, and DMF van Aalten. 2004. “Structures of *Bacillus subtilis* PdaA, a family 4 carbohydrate esterase, and a complex with N-acetyl-Glucosamine.” *FEBS Letters* 570 (1–3): 13-19. <https://doi.org/10.1016/j.febslet.2004.06.013>.
- Boags, A, F Samsudin, and S Khalid. 2019. “Details of hydrophobic entanglement between small molecules and Braun’s lipoprotein within the cavity of the bacterial chaperone LolA.” *Scientific Reports* 9 (1): 3717. <https://doi.org/10.1038/s41598-019-40170-z>.
- Boer, P De, R Crossley, and L Rothfield. 1992. “The essential bacterial cell-division protein FtsZ is a GTPase.” *Nature* 359 (6392): 254–56. <https://doi.org/10.1038/359254a0>.
- Boes, A, S Olatunji, E Breukink, and M Terrak. 2019. “Regulation of the peptidoglycan polymerase activity of PBP1b by antagonist actions of the core divisome proteins FtsBLQ and FtsN.” *MBio* 10 (1): e01912-18. <https://doi.org/10.1128/mBio.01912-18>.
- Bolstad, AI, HB Jensen, and V Bakken. 1996. “Taxonomy, biology, and periodontal aspects of *Fusobacterium nucleatum*.” *Clinical Microbiology Reviews* 9 (1): 55-71. <https://doi.org/10.1128/cmr.9.1.55>.
- Bolstad, AI. 1994. “Sizing the *Fusobacterium nucleatum* genome by pulsed-field gel electrophoresis.” *FEMS Microbiology Letters* 123 (1-2): 145–152. <https://doi.org/10.1111/j.1574-6968.1994.tb07214.x>.
- Boneca, IG, O Dussurget, D Cabanes, MA Nahori, S Sousa, M Lecuit, E Psylinakis, *et al.* 2007. “A critical role for peptidoglycan N-deacetylation in *Listeria* evasion from the host innate immune system.” *Proceedings of the National Academy of Sciences of the United States of America* 104 (3): 997–1002. <https://doi.org/10.1073/pnas.0609672104>.
- Boneca, IG, ZH Huang, DA Gage, and A Tomasz. 2000. “Characterization of *Staphylococcus aureus* cell wall glycan strands, evidence for a new β -N-acetylglucosaminidase activity.” *Journal of Biological Chemistry* 275 (14): 9910–18. <https://doi.org/10.1074/jbc.275.14.9910>.
- Bonnington, KE, and MJ Kuehn. 2016. “Outer Membrane Vesicle production facilitates LPS remodeling and Outer Membrane maintenance in *Salmonella* during environmental Transitions.” *MBio* 7 (5): e01532-16. <https://doi.org/10.1128/mBio.01532-16>.
- Botos, I, N Majdalani, SJ Mayclin, JG McCarthy, K Lundquist, D Wojtowicz, TJ Barnard, JC Gumbart, and SK Buchanan. 2016. “Structural and functional characterization of the LPS transporter LptDE from Gram-negative pathogens.” *Structure* 24 (6): 965–976. <https://doi.org/10.1016/j.str.2016.03.026>.
- Boucher, HW, GH Talbot, JS Bradley, JE Edwards, D Gilbert, LB Rice, M Scheld, B Spellberg, and J Bartlett. 2009. “Bad bugs, no drugs: No ESKAPE! An update from the infectious diseases society of America.” *Clinical Infectious Diseases* 48 (1): 1–12. <https://doi.org/10.1086/595011>.
- Braun, V, and H Wolff. 1970. “The murein-lipoprotein linkage in the cell wall of *Escherichia coli*.” *European Journal of Biochemistry* 14 (2): 387–91. <https://doi.org/10.1111/j.1432-1033.1970.tb00301.x>.
- Brennan, CA, and WS Garrett. 2019. “*Fusobacterium nucleatum* — Symbiont, opportunist and oncobacterium.” *Nature Reviews Microbiology* 17(3):156-166. <https://doi.org/10.1038/s41579->

018-0129-6.

- Brook, I. 2013. "Fusobacterial infections in children." *Current Infectious Disease Reports* 15 (3): 288–294. <https://doi.org/10.1007/s11908-013-0340-6>.
- Brott, AS, and AJ Clarke. 2019. "Peptidoglycan O-acetylation as a virulence factor: its effect on lysozyme in the innate immune system." *Antibiotics* 8 (3): 94. <https://doi.org/10.3390/antibiotics8030094>.
- Bui, NK, J Gray, H Schwarz, P Schumann, D Blanot, and W Vollmer. 2009. "The peptidoglycan sacculus of *Myxococcus xanthus* has unusual structural features and is degraded during glycerol-induced *Myxospore* development." *Journal of Bacteriology* 191 (2): 494–505. <https://doi.org/10.1128/JB.00608-08>.
- Cabré, EJ, A Sánchez-Gorostiaga, P Carrara, N Ropero, M Casanova, P Palacios, P Stano, M Jiménez, G Rivas, and MI Vicente. 2013. "Bacterial division proteins FtsZ and ZipA induce vesicle shrinkage and cell membrane invagination." *Journal of Biological Chemistry* 288 (37): 26625–26634. <https://doi.org/10.1074/jbc.M113.491688>.
- Cani, PD, and WM de Vos. 2017. "Next-generation beneficial microbes: the case of *Akkermansia muciniphila*." *Frontiers in Microbiology* 8:1765. <https://doi.org/10.3389/fmicb.2017.01765>.
- Caparros, M. AG Pisabarro, and MA De Pedro. 1992. "Effect of D-amino acids on structure and synthesis of peptidoglycan in *Escherichia coli*." *Journal of Bacteriology* 174 (17): 5549–5559. <https://doi.org/10.1128/jb.174.17.5549-5559.1992>.
- Cassini, A, L Diaz Högberg, D Plachouras, A Quattrocchi, A Hoxha, G Skov Simonsen, M Colomb-Cotinat, et al. 2019. "Attributable deaths and disability-adjusted life-years caused by infections with antibiotic-resistant bacteria in the EU and the European economic area in 2015: a population-level modelling analysis." *The Lancet Infectious Diseases* 19 (1): 56–66. [https://doi.org/10.1016/S1473-3099\(18\)30605-4](https://doi.org/10.1016/S1473-3099(18)30605-4).
- Castro, C De, M Parrilli, O Holst, and A Molinaro. 2010. "Microbe-Associated Molecular Patterns in innate immunity. Extraction and chemical analysis of Gram-negative bacterial lipopolysaccharides." In *Methods in Enzymology*, 480:89-115. [https://doi.org/10.1016/S0076-6879\(10\)80005-9](https://doi.org/10.1016/S0076-6879(10)80005-9).
- Cava, F, H Lam, MA De Pedro, and MK Waldor. 2011. "Emerging knowledge of regulatory roles of D-amino acids in bacteria." *Cellular and Molecular Life Sciences* 68(5):817-31. <https://doi.org/10.1007/s00018-010-0571-8>.
- Chaput, C, C Ecobichon, N Pouradier, JC Rousselle, A Namane, and IG Boneca. 2016. "Role of the N-acetylmuramoyl-L-alanyl amidase, AmiA, of *Helicobacter pylori* in peptidoglycan metabolism, daughter cell separation, and virulence." *Microbial Drug Resistance* 22 (6): 477–486. <https://doi.org/10.1089/mdr.2016.0070>.
- Chassaing, B, M Kumar, MT Baker, V Singh, and M Vijay-Kumar. 2014. "Mammalian gut immunity." *Biomedical Journal* 37 (5): 246–258. <https://doi.org/10.4103/2319-4170.130922>.
- Chavarría-Velázquez, CO, A. Torres-Martínez, LF Montaño, and EP Rendón-Huerta. 2018. "TLR2 activation induced by *H. pylori* LPS promotes the differential expression of Claudin-4, -6, -7 and -9 via either STAT3 and ERK1/2 in AGS cells." *Immunobiology* 223 (1): 38–48. <https://doi.org/10.1016/j.imbio.2017.10.016>.
- Chen, T, Q Li, J Wu, Y Wu, W Peng, H Li, J Wang, X Tang, Y Peng, and Xi Fu. 2018. "*Fusobacterium nucleatum* promotes M2 polarization of macrophages in the microenvironment of colorectal tumours via a TLR4-dependent mechanism." *Cancer Immunology, Immunotherapy* 67 (10): 1635–1646. <https://doi.org/10.1007/s00262-018-2233-x>.
- Chen, Y, B Liu, D Yang, X Li, L Wen, P Zhu, and N Fu. 2011. "Peptide mimics of peptidoglycan are vaccine candidates and protect mice from infection with *Staphylococcus aureus*." *Journal of Medical Microbiology* 60 (Pt7): 995–1002. <https://doi.org/10.1099/jmm.0.028647-0>.
- Chen, Z, S Downing, and ES Tzanakakis. 2019. "Four decades after the discovery of regenerating islet-derived (Reg) proteins: current understanding and challenges." *Frontiers in Cell and Developmental Biology* 7:235. <https://doi.org/10.3389/fcell.2019.00235>.
- Cherepanov, PP, and W Wackernagel. 1995. "Gene disruption in *Escherichia coli*: Tc^R and Km^R cassettes with the option of Flp-catalyzed excision of the antibiotic-resistance determinant." *Gene* 158 (1): 9–14. [https://doi.org/10.1016/0378-1119\(95\)00193-A](https://doi.org/10.1016/0378-1119(95)00193-A).
- Chng, SS, LS Gronenberg, and D Kahne. 2010. "Proteins required for lipopolysaccharide assembly in *Escherichia coli* form a transenvelope complex." *Biochemistry* 49 (22): 4565–4567.

- <https://doi.org/10.1021/bi100493e>.
- Cho, I, and MJ Blaser. 2012. "The human microbiome: at the interface of health and disease." *Nature Reviews Genetics* 13(4):260-70. <https://doi.org/10.1038/nrg3182>.
- Cho, SH, J Szewczyk, C Pesavento, M Zietek, M Banzhaf, P Roszczenko, A Asmar, *et al.* 2014. "Detecting envelope stress by monitoring β -barrel assembly." *Cell* 159 (7): 1652–64. <https://doi.org/10.1016/j.cell.2014.11.045>.
- Chodiseti, PK, and M Reddy. 2019. "Peptidoglycan hydrolase of an unusual cross-link cleavage specificity contributes to bacterial cell wall synthesis." *Proceedings of the National Academy of Sciences of the United States of America* 116 (16): 7825–30. <https://doi.org/10.1073/pnas.1816893116>.
- Choi, SY, N Esaki, T Yoshimura, and K Soda. 1992. "Reaction mechanism of glutamate racemase, a pyridoxal phosphate-independent amino acid racemase." *Journal of Biochemistry* 112 (1): 139–42. <https://doi.org/10.1093/oxfordjournals.jbchem.a123853>.
- Clarke, T., KM Davis, ES Lysenko, AY Zhou, Y Yu, and JN Weiser. 2010. "Recognition of peptidoglycan from the microbiota by Nod1 enhances systemic innate immunity." *Nature Medicine* 16 (2): 228–231. <https://doi.org/10.1038/nm.2087>.
- Coates, AR, G Halls, and Y Hu. 2011. "Novel classes of antibiotics or more of the same?" *British Journal of Pharmacology* 163(1):184-94. <https://doi.org/10.1111/j.1476-5381.2011.01250.x>.
- Cochet, F, and F Peri. 2017. "The role of carbohydrates in the lipopolysaccharide (LPS)/Toll-like receptor 4 (TLR4) signalling." *International Journal of Molecular Sciences* 18 (11): 2318. <https://doi.org/10.3390/ijms18112318>.
- Coico, R. 2005. "Gram staining tutorial." *Current Protocols in Microbiology*. <https://doi.org/10.1002/9780471729259.mca03cs00>.
- Crisóstomo, MI, W Vollmer, AS Kharat, S Inhülsen, F Gehre, S Buckenmaier, and A Tomasz. 2006. "Attenuation of penicillin resistance in a peptidoglycan O-acetyl transferase mutant of *Streptococcus pneumoniae*." *Molecular Microbiology* 61 (6): 1497–1509. <https://doi.org/10.1111/j.1365-2958.2006.05340.x>.
- Crocker, PR, JC Paulson, and A Varki. 2007. "Siglecs and their roles in the immune system." *Nature Reviews Immunology* 7 (4): 255–266. <https://doi.org/10.1038/nri2056>.
- Cullen, TW, WB Schofield, NA Barry, EE Putnam, EA Rundell, MS Trent, PH Degnan, CJ Booth, H Yu, and AL Goodman. 2015. "Antimicrobial peptide resistance mediates resilience of prominent gut commensals during inflammation." *Science* 347 (6218): 170–175. <https://doi.org/10.1126/science.1260580>.
- d’Hennezel, E, S Abubucker, LO Murphy, and TW Cullen. 2017. "Total lipopolysaccharide from the human gut microbiome silences Toll-like receptor signaling." *MSystems* 2 (6): e00046–17. <https://doi.org/10.1128/mSystems.00046-17>.
- Dalbey, RE, and A Kuhn. 2012. "Protein traffic in Gram-negative bacteria - how exported and secreted proteins find their way." *FEMS Microbiology Reviews* 36(6):1023-45. <https://doi.org/10.1111/j.1574-6976.2012.00327.x>.
- Dalile, B, L van Oudenhove, B Vervliet, and K Verbeke. 2019. "The role of short-chain fatty acids in microbiota–gut–brain communication." *Nature Reviews Gastroenterology and Hepatology* 16 (8): 461–478. <https://doi.org/10.1038/s41575-019-0157-3>.
- Dalvit, C, and A Vulpetti. 2019. "Ligand-based Fluorine NMR screening: principles and applications in drug discovery projects." *Journal of Medicinal Chemistry* 62 (5): 2218–2244. <https://doi.org/10.1021/acs.jmedchem.8b01210>.
- Depommier, C, A Everard, C Druart, H Plovier, M van Hul, S Vieira-Silva, G Falony, *et al.* 2019. "Supplementation with *Akkermansia muciniphila* in overweight and obese human volunteers: s proof-of-concept exploratory study." *Nature Medicine* 25(7):1096-1103. <https://doi.org/10.1038/s41591-019-0495-2>.
- Derrien, M, C Belzer, and WM de Vos. 2017. "*Akkermansia muciniphila* and its role in regulating host functions." *Microbial Pathogenesis* 106:171-181. <https://doi.org/10.1016/j.micpath.2016.02.005>.
- Derrien, M, MC Collado, K Ben-Amor, S Salminen, and WM De Vos. 2008. "The mucin degrader *Akkermansia muciniphila* is an abundant resident of the human intestinal tract." *Applied and Environmental Microbiology* 74 (5): 1646–48. <https://doi.org/10.1128/AEM.01226-07>.
- Derrien, M, MWJ van Passel, JHB van de Bovenkamp, RG Schipper, WM de Vos, and J Dekker. 2010.

- “Mucin-bacterial interactions in the human oral cavity and digestive tract.” *Gut Microbes* 1 (4): 254–68. <https://doi.org/10.4161/gmic.1.4.12778>.
- Derrien, M, EE Vaughan, CM Plugge, and WM de Vos. 2004. “*Akkermansia muciniphila* gen. nov., sp. nov., a human intestinal mucin-degrading bacterium.” *International Journal of Systematic and Evolutionary Microbiology* 54 (Pt 5): 1469–1476. <https://doi.org/10.1099/ijs.0.02873-0>.
- Desmarais, SM, MA De Pedro, F Cava, and KC Huang. 2013. “Peptidoglycan at its peaks: how chromatographic analyses can reveal bacterial cell wall structure and assembly.” *Molecular Microbiology* 89(1):1-13. <https://doi.org/10.1111/mmi.12266>.
- Dheer, R, R Santaolalla, JM Davies, JK Lang, MC Phillips, C Pastorini, MT Vazquez-Pertejo, and MT Abreu. 2016. “Intestinal epithelial Toll-like receptor 4 signaling affects epithelial function and colonic microbiota and promotes a risk for transmissible colitis.” *Infection and Immunity* 84 (3): 798–810. <https://doi.org/10.1128/IAI.01374-15>.
- Dik, DA, DR Marous, JF Fisher, and S Mobashery. 2017. “Lytic transglycosylases: concinnity in concision of the bacterial cell wall.” *Critical Reviews in Biochemistry and Molecular Biology* 52(5):503-542. <https://doi.org/10.1080/10409238.2017.1337705>.
- Domínguez-Escobar, J, A Chastanet, AH Crevenna, V Fromion, R Wedlich-Söldner, and R Carballido-López. 2011. “Processive movement of MreB-associated cell wall biosynthetic complexes in bacteria.” *Science* 333 (6039): 225–28. <https://doi.org/10.1126/science.1203466>.
- Domon, B, and CE Costello. 1988. “A systematic nomenclature for carbohydrate fragmentations in FAB-MS/MS spectra of glycoconjugates.” *Glycoconjugate Journal* 5: 397–409. <https://doi.org/10.1007/BF01049915>.
- Donaldson, GP, S Lee, and SK Mazmanian. 2016. “Gut biogeography of the bacterial microbiota.” *Nature Reviews Microbiology* 14(1):20-32. <https://doi.org/10.1038/nrmicro3552>.
- Dong, H, X Tang, Z Zhang, and C Dong. 2017. “Structural insight into lipopolysaccharide transport from the Gram-negative bacterial Inner Membrane to the Outer Membrane.” *Biochimica et Biophysica Acta - Molecular and Cell Biology of Lipids* 1862 (11): 1461–67. <https://doi.org/10.1016/j.bbalip.2017.08.003>.
- Dong, H, Z Zhang, X Tang, S Huang, H Li, B Peng, and C Dong. 2016. “Structural insights into cardiolipin transfer from the Inner Membrane to the Outer Membrane by PbgA in Gram-Negative Bacteria.” *Scientific Reports* 6: 30815. <https://doi.org/10.1038/srep30815>.
- Dong, H, Z Zhang, X Tang, NG Paterson, and C Dong. 2017. “Structural and functional insights into the lipopolysaccharide ABC transporter LptB2FG.” *Nature Communications* 8 (1): 222. <https://doi.org/10.1038/s41467-017-00273-5>.
- Dramsi, S, S Magnet, S Davison, and M Arthur. 2008. “Covalent attachment of proteins to peptidoglycan.” *FEMS Microbiology Reviews* 32 (2): 307–20. <https://doi.org/10.1111/j.1574-6976.2008.00102.x>.
- Du, S, and J Lutkenhaus. 2017. “Assembly and activation of the *Escherichia coli* divisome.” *Molecular Microbiology* 105(2):177-187. <https://doi.org/10.1111/mmi.13696>.
- Dunlop, AL, JG Mülle, EP Ferranti, S Edwards, AB Dunn, and EJ Corwin. 2015. “Maternal microbiome and pregnancy outcomes that impact infant health: a review.” *Advances in Neonatal Care* 15 (6): 377–385. <https://doi.org/10.1097/ANC.0000000000000218>.
- Dziarski, R, and D Gupta. 2006. “The peptidoglycan recognition proteins (PGRPs).” *Genome Biology* 7(8):232. <https://doi.org/10.1186/gb-2006-7-8-232>.
- Earley, H, G Lennon, Á Balfe, JC Coffey, DC Winter, and PR O’Connell. 2019. “The abundance of *Akkermansia muciniphila* and its relationship with sulphated colonic mucins in health and ulcerative colitis.” *Scientific Reports* 9 (1): 15683. <https://doi.org/10.1038/s41598-019-51878-3>.
- Edwards, NJ, MA Monteiro, G Faller, EJ Walsh, AP Moran, IS Roberts, and NJ High. 2000. “Lewis X structures in the O-antigen side-chain promote adhesion of *Helicobacter pylori* to the gastric epithelium.” *Molecular Microbiology* 35 (6): 1530–1539. <https://doi.org/10.1046/j.1365-2958.2000.01823.x>.
- Egan, AJF. 2018. “Bacterial Outer Membrane constriction.” *Molecular Microbiology* 107(6):676-687. <https://doi.org/10.1111/mmi.13908>.
- Egan, AJF, J Biboy, I van’t Veer, E Breukink, and W Vollmer. 2015. “Activities and regulation of peptidoglycan synthases.” *Philosophical Transactions of the Royal Society B: Biological Sciences* 370 (1679): 20150031. <https://doi.org/10.1098/rstb.2015.0031>.
- Egan, AJF, RM Cleverley, K Peters, RJ Lewis, and W Vollmer. 2017. “Regulation of bacterial cell wall

- growth.” *FEBS Journal* 284(6):851-867. <https://doi.org/10.1111/febs.13959>.
- Egorova, KS, and PV Toukach. 2014. “Expansion of coverage of Carbohydrate Structure Database (CSDB).” *Carbohydrate Research* 389: 112–14. <https://doi.org/10.1016/j.carres.2013.10.009>.
- Ekiert, DC, G Bhabha, GL Isom, G Greenan, S Ovchinnikov, IR Henderson, JS Cox, and RD Vale. 2017. “Architectures of lipid transport systems for the bacterial Outer Membrane.” *Cell* 169 (2): 273–85. <https://doi.org/10.1016/j.cell.2017.03.019>.
- Ent, F van den, T Izoré, TAM Bharat, CM Johnson, and J Löwe. 2014. “Bacterial actin MreB forms antiparallel double filaments.” *ELife* 3: e02634. <https://doi.org/10.7554/eLife.02634>.
- Eband, RM, C Walker, RF Eband, and NA Magarvey. 2016. “Molecular mechanisms of membrane targeting antibiotics.” *Biochimica et Biophysica Acta - Biomembranes* 1858 (5): 980–87. <https://doi.org/10.1016/j.bbamem.2015.10.018>.
- Erridge, C, E Bennett-Guerrero, and I R. Poxton. 2002. “Structure and function of lipopolysaccharides.” *Microbes and Infection* 4 (8): 837–51. [https://doi.org/10.1016/S1286-4579\(02\)01604-0](https://doi.org/10.1016/S1286-4579(02)01604-0).
- Erwin, AL. 2016. “Antibacterial drug discovery targeting the lipopolysaccharide biosynthetic enzyme LpxC.” *Cold Spring Harbor Perspectives in Medicine* 6 (7): a025304. <https://doi.org/10.1101/cshperspect.a025304>.
- Everard, A, C Belzer, L Geurts, JP Ouwerkerk, C Druart, LB Bindels, Y Guiot, *et al.* 2013. “Cross-talk between *Akkermansia muciniphila* and intestinal epithelium controls diet-induced obesity.” *Proceedings of the National Academy of Sciences of the United States of America* 110 (22): 9066–71. <https://doi.org/10.1073/pnas.1219451110>.
- Fasano, A. 2011. “Zonulin and its regulation of intestinal barrier function: the biological door to inflammation, autoimmunity, and cancer.” *Physiological Reviews* 91 (1): 151–75. <https://doi.org/10.1152/physrev.00003.2008>.
- Ferain, T, JN Hobbs, J Richardson, N Bernard, D Garmyn, P Hols, NE Allen, and J Delcour. 1996. “Knockout of the two *ldh* genes has a major impact on peptidoglycan precursor synthesis in *Lactobacillus plantarum*.” *Journal of Bacteriology* 178 (18): 5431–37. <https://doi.org/10.1128/jb.178.18.5431-5437.1996>.
- Fernandes, P, and E Martens. 2017. “Antibiotics in late clinical development.” *Biochemical Pharmacology* 133:152-163. <https://doi.org/10.1016/j.bcp.2016.09.025>.
- Fraschilla, I, and S Pillai. 2017. “Viewing siglecs through the lens of tumor immunology.” *Immunological Reviews* 276 (1): 178–191. <https://doi.org/10.1111/imr.12526>.
- Freeze, Hudson H., Gerald W. Hart, and Ronald L. Schnaar. 2015. *Glycosylation Precursors. Essentials of Glycobiology*. <https://doi.org/10.1101/glycobiology.3e.005>.
- Freinkman, E, S Okuda, N Ruiz, and D Kahne. 2012. “Regulated assembly of the transenvelope protein complex required for lipopolysaccharide export.” *Biochemistry* 51 (24): 4800–4806. <https://doi.org/10.1021/bi300592c>.
- Frirdich, E, J Biboy, C Adams, J Lee, J Ellermeier, LD Giolda, VJ DiRita, SE Girardin, W Vollmer, and EC Gaynor. 2012. “Peptidoglycan-modifying enzyme Pgp1 is required for helical cell shape and pathogenicity traits in *Campylobacter jejuni*.” *PLoS Pathogens* 8 (3): e1002602. <https://doi.org/10.1371/journal.ppat.1002602>.
- Fuke, N, N Nagata, H Sukanuma, and T Ota. 2019. “Regulation of gut microbiota and metabolic endotoxemia with dietary factors.” *Nutrients* 11(10):2277. <https://doi.org/10.3390/nu11102277>.
- Galanos, C, O Lüderitz, and O Westphal. 1969. “A new method for the extraction of R lipopolysaccharides.” *European Journal of Biochemistry* 9 (2): 245–49. <https://doi.org/10.1111/j.1432-1033.1969.tb00601.x>.
- Gamian, A, C Jones, T Lipiński, A Korzeniowska-Kowal, and N Ravenscroft. 2000. “Structure of the Sialic acid-containing O-specific polysaccharide from *Salmonella enterica* serovar Toucra O48 lipopolysaccharide.” *European Journal of Biochemistry* 267 (11): 3160–67. <https://doi.org/10.1046/j.1432-1327.2000.01335.x>.
- Gao, R, C Kong, L Huang, H Li, X Qu, Z Liu, P Lan, J Wang, and H Qin. 2017. “Mucosa-associated microbiota signature in colorectal cancer.” *European Journal of Clinical Microbiology and Infectious Diseases* 36 (11): 2073–2083. <https://doi.org/10.1007/s10096-017-3026-4>.
- Garcia-Vello, P, I Speciale, F Chiodo, A Molinaro, and C De Castro. 2020. “Carbohydrate-based adjuvants.” *Drug Discovery Today: Technologies* 35-36:57-68. <https://doi.org/10.1016/j.ddtec.2020.09.005>.
- Garnier, M, MJ Vacheron, M Guinand, and G Michel. 1985. “Purification and partial characterization

- of the extracellular gamma-D-glutamyl-(L)meso-diaminopimelate endopeptidase I, from *Bacillus sphaericus* NCTC 9602.” *European Journal of Biochemistry* 148 (3): 539–543. <https://doi.org/10.1111/j.1432-1033.1985.tb08873.x>.
- Geerlings, S, I Kostopoulos, W de Vos, and C Belzer. 2018. “*Akkermansia muciniphila* in the human gastrointestinal tract: when, where, and how?” *Microorganisms* 6 (3): E75. <https://doi.org/10.3390/microorganisms6030075>.
- Gerding, MA, Y Ogata, ND Pecora, H Niki, and PAJ De Boer. 2007. “The trans-envelope Tol-Pal complex is part of the cell division machinery and required for proper Outer Membrane invagination during cell constriction in *E. coli*.” *Molecular Microbiology* 63 (4): 1008–1025. <https://doi.org/10.1111/j.1365-2958.2006.05571.x>.
- Gill, SR, M Pop, RT DeBoy, PB Eckburg, PJ Turnbaugh, BS Samuel, JI Gordon, DA Relman, CM Fraser-Liggett, and KE Nelson. 2006. “Metagenomic analysis of the human distal gut microbiome.” *Science* 312 (5778): 1355–1359. <https://doi.org/10.1126/science.1124234>.
- Gimeno, A, P Valverde, A Ardá, and J Jiménez-Barbero. 2020. “Glycan structures and their Interactions with proteins. A NMR view.” *Current Opinion in Structural Biology* 62: 22–30. <https://doi.org/10.1016/j.sbi.2019.11.004>.
- Giordano, C, C Gallina, V Consalvi, and R Scandurra. 1991. “Synthesis and properties of D-Glucosamine N-peptidyl derivatives as substrate analog inhibitors of Papain and Cathepsin B.” *European Journal of Medicinal Chemistry* 26 (8): 753–62. [https://doi.org/10.1016/0223-5234\(91\)90001-4](https://doi.org/10.1016/0223-5234(91)90001-4).
- Girardin, SE, IG Boneca, LAM Carneiro, A Antignac, M Jéhanno, J Viala, K Tedin, *et al.* 2003. “Nod1 detects a unique muropeptide from Gram-negative bacterial peptidoglycan.” *Science* 300 (5625): 1584–87. <https://doi.org/10.1126/science.1084677>.
- Glauner, B, and JV Höltje. 1990. “Growth pattern of the murein sacculus of *Escherichia coli*.” *Journal of Biological Chemistry* 265 (31): 18988–96.
- Glauner, B. 1988. “Separation and quantification of muropeptides with High-Performance Liquid Chromatography.” *Analytical Biochemistry* 172 (2): 451–64. [https://doi.org/10.1016/0003-2697\(88\)90468-X](https://doi.org/10.1016/0003-2697(88)90468-X).
- Glauner, B, JV Höltje, and U Schwarz. 1988. “The composition of the murein of *Escherichia coli*.” *Journal of Biological Chemistry* 263 (21): 10088–96. PMID: 3292521.
- González-Leiza, SM, MA de Pedro, and JA Ayala. 2011. “Amph, a bifunctional DD-endopeptidase and DD-carboxypeptidase of *Escherichia coli*.” *Journal of Bacteriology* 193 (24): 6887–94. <https://doi.org/10.1128/JB.05764-11>.
- Gray, AN, AJF Egan, IL van’t Veer, J Verheul, A Colavin, A Koumoutsis, J Biboy, *et al.* 2015. “Coordination of peptidoglycan synthesis and Outer Membrane constriction during *Escherichia coli* cell division.” *ELife* 4: e07118. <https://doi.org/10.7554/eLife.07118>.
- Green, ER, and J Meccas. 2016. “Bacterial secretion systems: an overview.” *Microbiology Spectrum* 4 (1): 10. <https://doi.org/10.1128/microbiolspec.vmbf-0012-2015>.
- Greenfield, LK, and C Whitfield. 2012. “Synthesis of lipopolysaccharide O-antigens by ABC transporter-dependent pathways.” *Carbohydrate Research* 356: 12–24. <https://doi.org/10.1016/j.carres.2012.02.027>.
- Grice, EA, and JA Segre. 2011. “The skin microbiome.” *Nature Reviews Microbiology* 9(4):244-53. <https://doi.org/10.1038/nrmicro2537>.
- Gronow, S, G Xia, and H Brade. 2010. “Glycosyltransferases involved in the biosynthesis of the inner core region of different lipopolysaccharides.” *European Journal of Cell Biology* 89 (1): 3–10. <https://doi.org/10.1016/j.ejcb.2009.10.002>.
- Guadalupe CM, M Pereira, Z Silva, I Iria, C Coutinho, A Lopes, I Sá-Correia, and PA Videira. 2017. “Using dendritic cells to evaluate how *Burkholderia cenocepacia* clonal isolates from a chronically infected cystic fibrosis patient subvert immune functions.” *Medical Microbiology and Immunology* 206 (2): 111–23. <https://doi.org/10.1007/s00430-016-0488-4>.
- Guan, R, A Roychowdhury, B Ember, S Kumar, G Jan Boons, and R A. Mariuzza. 2004. “Structural basis for peptidoglycan binding by peptidoglycan recognition proteins.” *Proceedings of the National Academy of Sciences of the United States of America* 101 (49): 17168–17173. <https://doi.org/10.1073/pnas.0407856101>.
- Gupta, RS, V Bhandari, and HS Naushad. 2012. “Molecular signatures for the PVC clade (Planctomycetes, Verrucomicrobia, Chlamydiae, and Lentisphaerae) of bacteria provide insights

- into their evolutionary relationships.” *Frontiers in Microbiology* 3: 327. <https://doi.org/10.3389/fmicb.2012.00327>.
- Gupta, VK, S Paul, and C Dutta. 2017. “Geography, ethnicity or subsistence-specific variations in human microbiome composition and diversity.” *Frontiers in Microbiology* 8:1162. <https://doi.org/10.3389/fmicb.2017.01162>.
- Haeusser, DP, and W Margolin. 2016. “Splitsville: structural and functional insights into the dynamic bacterial Z ring.” *Nature Reviews Microbiology* 14(5):305-19. <https://doi.org/10.1038/nrmicro.2016.26>.
- Hagan, CL, JS Wzorek, D Kahne, and RT Sauer. 2015. “Inhibition of the β -Barrel Assembly Machine by a peptide that binds BamD.” *Proceedings of the National Academy of Sciences of the United States of America* 112 (7): 2011–16. <https://doi.org/10.1073/pnas.1415955112>.
- Haishima, Y, O Holst, and H Brade. 1992. “Structural investigation on the lipopolysaccharide of *Escherichia coli* rough mutant F653 representing the R3 core type.” *European Journal of Biochemistry* 203(1-2):127-34. <https://doi.org/10.1111/j.1432-1033.1992.tb19837.x>.
- Hammes, W, KH Schleifer, and O Kandler. 1973. “Mode of action of glycine on the biosynthesis of peptidoglycan.” *Journal of Bacteriology* 116 (2): 1029–1053. <https://doi.org/10.1128/jb.116.2.1029-1053.1973>.
- Han, W, X Ma, CJ Balibar, CM Baxter Rath, B Benton, A Bermingham, F Casey, *et al.* 2020. “Two distinct mechanisms of inhibition of LpxA acyltransferase essential for lipopolysaccharide biosynthesis.” *Journal of the American Chemical Society* 142 (9): 4445–55. <https://doi.org/10.1021/jacs.9b13530>.
- Han, YW. 2015. “*Fusobacterium nucleatum*: a commensal-turned pathogen.” *Current Opinion in Microbiology* 23:141-7. <https://doi.org/10.1016/j.mib.2014.11.013>.
- Han, YW, RW Redline, M Li, L Yin, GB Hill, and TS McCormick. 2004. “*Fusobacterium nucleatum* induces premature and term stillbirths in pregnant mice: implication of oral bacteria in preterm birth.” *Infection and Immunity* 72 (4): 2272–2279. <https://doi.org/10.1128/IAI.72.4.2272-2279.2004>.
- Han, YW, T Shen, P Chung, IA Buhimschi, and CS Buhimschi. 2009. “Uncultivated bacteria as etiologic agents of intra-amniotic inflammation leading to preterm birth.” *Journal of Clinical Microbiology* 47 (1): 38–47. <https://doi.org/10.1128/JCM.01206-08>.
- Han, YW, and X Wang. 2013. “Mobile microbiome: oral bacteria in extra-oral infections and inflammation.” *Journal of Dental Research* 92(6):485-91. <https://doi.org/10.1177/0022034513487559>.
- Hart, EM, AM Mitchell, A Konovalova, M Grabowicz, J Sheng, X Han, FP Rodriguez-Rivera, *et al.* 2019. “A small-molecule inhibitor of BamA impervious to efflux and the Outer Membrane permeability barrier.” *Proceedings of the National Academy of Sciences of the United States of America* 116 (43): 21748–57. <https://doi.org/10.1073/pnas.1912345116>.
- Hase, S, T Hofstad, and ET Rietschel. 1977. “Chemical structure of the lipid A component of lipopolysaccharides from *Fusobacterium nucleatum*.” *Journal of Bacteriology* 129 (1): 9–14. <https://doi.org/10.1128/jb.129.1.9-14.1977>.
- Hayhurst, EJ, L Kailas, JK Hobbs, and SJ Foster. 2008. “Cell wall peptidoglycan architecture in *Bacillus subtilis*.” *Proceedings of the National Academy of Sciences of the United States of America* 105: 14603–8. <https://doi.org/10.1073/pnas.0804138105>.
- Heidrich, C, MF Templin, A Ursinus, M Merdanovic, J Berger, H Schwarz, MA De Pedro, and J Volker Hölte. 2001. “Involvement of N-acetylmuramyl-L-alanine amidases in cell separation and antibiotic-induced autolysis of *Escherichia coli*.” *Molecular Microbiology* 41 (1): 167–178. <https://doi.org/10.1046/j.1365-2958.2001.02499.x>.
- Heijenoort, J van. 2011. “Peptidoglycan hydrolases of *Escherichia coli*.” *Microbiology and Molecular Biology Reviews* 75 (4): 636–663. <https://doi.org/10.1128/mmbr.00022-11>.
- Heikema, AP, MP Bergman, H Richards, PR Crocker, M Gilbert, JN Samsom, WJB van Wamel, Hubert P. Endtz, and Alex Van Belkum. 2010. “Characterization of the specific interaction between sialoadhesin and sialylated *Campylobacter jejuni* lipooligosaccharides.” *Infection and Immunity* 78 (7): 3237–46. <https://doi.org/10.1128/IAI.01273-09>.
- Helander, IM, A Haikara, I Sadovskaya, E Vinogradov, and MS Salkinoja-Salonen. 2004. “Lipopolysaccharides of anaerobic beer spoilage bacteria of the genus *Pectinatus* - lipopolysaccharides of a Gram-positive genus.” *FEMS Microbiology Reviews* 28 (5): 543–552.

- <https://doi.org/10.1016/j.femsre.2004.05.001>.
- Hergott, CB, AM Roche, E Tamashiro, TB Clarke, AG Bailey, A Laughlin, FD Bushman, and JN Weiser. 2016. "Peptidoglycan from the gut microbiota governs the lifespan of circulating phagocytes at homeostasis." *Blood* 127 (20): 2460–71. <https://doi.org/10.1182/blood-2015-10-675173>.
- Herlihey, FA, and AJ Clarke. 2017. "Controlling autolysis during flagella insertion in Gram-negative bacteria." In *Advances in Experimental Medicine and Biology*, 925:41-56. https://doi.org/10.1007/5584_2016_52.
- Hicks, G, and Z Jia. 2018. "Structural basis for the lipopolysaccharide export activity of the bacterial lipopolysaccharide transport system." *International Journal of Molecular Sciences* 19 (9): pii: E2680. <https://doi.org/10.3390/ijms19092680>.
- Ho, H, A Miu, MK Alexander, NK Garcia, A Oh, I Zilberleyb, M Reichelt, *et al.* 2018. "Structural basis for dual-mode inhibition of the ABC transporter MsbA." *Nature* 557 (7704): 196–201. <https://doi.org/10.1038/s41586-018-0083-5>.
- Hobot, JA, E Carlemalm, W Villiger, and E Kellenberger. 1984. "Periplasmic gel: new concept resulting from the reinvestigation of bacterial cell envelope ultrastructure by new methods." *Journal of Bacteriology* 160 (1): 143–152. <https://doi.org/10.1128/jb.160.1.143-152.1984>.
- Hofstad, T, and G Fredriksen. 1979. "Immunochemical studies of partially hydrolyzed lipopolysaccharide from *Fusobacterium nucleatum* Fev1." *European Journal of Biochemistry* 94 (1): 59–64. <https://doi.org/10.1111/j.1432-1033.1979.tb12871.x>.
- Hofstad, T, N Skaug, and K Sveen. 1993. "Stimulation of B lymphocytes by lipopolysaccharides from anaerobic bacteria." *Clinical Infectious Diseases* 16 (4): S200-2. https://doi.org/10.1093/clinids/16.Supplement_4.S200.
- Holst, O. 2002. "Chemical structure of the core region of lipopolysaccharides - an update." *Trends in Glycoscience and Glycotechnology* 14 (76): 87–103. <https://doi.org/10.4052/tigg.14.87>.
- Holst, O, and A Molinaro. 2010. "Core region and lipid A components of lipopolysaccharides." In *Microbial Glycobiology*, 29–55. <https://doi.org/10.1016/B978-0-12-374546-0.00003-1>.
- Holst, O, JE Thomas-Oates, and H Brade. 1994. "Preparation and structural analysis of oligosaccharide monophosphates obtained from the lipopolysaccharide of recombinant strains of *Salmonella minnesota* and *Escherichia coli* expressing the genus-specific epitope of Chlamydia lipopolysaccharide." *European Journal of Biochemistry* 222 (1): 183–94. <https://doi.org/10.1111/j.1432-1033.1994.tb18856.x>.
- Höltje, JV, D Mirelman, N Sharon, and U Schwarz. 1975. "Novel type of murein transglycosylase in *Escherichia coli*." *Journal of Bacteriology* 124 (3): 1067–76. <https://doi.org/10.1128/jb.124.3.1067-1076.1975>.
- Hong, Y, MA Liu, and PR Reeves. 2018. "Progress in our understanding of Wzx Flippase for translocation of bacterial membrane lipid-linked oligosaccharide." *Journal of Bacteriology* 200 (1): e00154-17. <https://doi.org/10.1128/JB.00154-17>.
- Hsia, Y, BR Lee, A Versporten, Y Yang, J Bielicki, C Jackson, J Newland, H Goossens, N Magrini, and M Sharland. 2019. "Use of the WHO access, watch, and reserve classification to define patterns of hospital antibiotic use (AWaRe): an analysis of paediatric survey data from 56 countries." *The Lancet Global Health* 18 (1): 18–20. [https://doi.org/10.1016/S2214-109X\(19\)30071-3](https://doi.org/10.1016/S2214-109X(19)30071-3).
- Hugonnet, JE, D Mengin-Lecreux, A Monton, T den Blaauwen, E Carbonnelle, C Veckerlé, V Brun Yves, *et al.* 2016. "Factors essential for L,D-transpeptidase-mediated peptidoglycan cross-linking and β -lactam resistance in *Escherichia coli*." *ELife* 5:e19469. <https://doi.org/10.7554/eLife.19469>.
- Human Microbiome Project Consortium. 2012. "Structure, function and diversity of the healthy human microbiome." *Nature* 486 (7402): 207–214. <https://doi.org/10.1038/nature11234>.
- Hurley, JC. 1995. "Endotoxemia: methods of detection and clinical correlates." *Clinical Microbiology Reviews*, 268–92. <https://doi.org/10.1128/cmr.8.2.268>.
- Hussein, NA, S Hyun Cho, G Laloux, R Siam, and JF Collet. 2018. "Distinct domains of *Escherichia coli* IgaA connect envelope stress sensing and down-regulation of the Rcs phosphorelay across subcellular compartments." *PLoS Genetics* 14 (5): e1007398. <https://doi.org/10.1371/journal.pgen.1007398>.
- IACG. 2019. "No time to wait: infections from drug-resistant securing the future from drug-resistant infections." *Artforum International*.

- Imai, Y, KJ Meyer, A Inishi, Q Favre-Godal, R Green, S Manuse, M Caboni, *et al.* 2019. “A new antibiotic selectively kills Gram-negative pathogens.” *Nature* 576 (7787): 459–464. <https://doi.org/10.1038/s41586-019-1791-1>.
- Irazoki, O, SB Hernandez, and F Cava. 2019. “Peptidoglycan muropeptides: release, perception, and functions as signaling molecules.” *Frontiers in Microbiology* 10:500. <https://doi.org/10.3389/fmicb.2019.00500>.
- Islam, ST, and JS Lam. 2014. “Synthesis of bacterial polysaccharides via the Wzx/Wzy-dependent pathway.” *Canadian Journal of Microbiology* 60 (11): 697–716. <https://doi.org/10.1139/cjm-2014-0595>.
- Isom, GL, N Coudray, MR MacRae, CT McManus, DC Ekiert, and G Bhabha. 2020. “LetB structure reveals a tunnel for lipid transport across the bacterial envelope.” *Cell* 181 (3): 653–664.e19. <https://doi.org/10.1016/j.cell.2020.03.030>.
- Jacobs, C, LJ Huang, E Bartowsky, S Normark, and JT Park. 1994. “Bacterial cell wall recycling provides cytosolic muropeptides as effectors for beta-lactamase induction.” *The EMBO Journal* 13 (19): 4684–94. <https://doi.org/10.1002/j.1460-2075.1994.tb06792.x>.
- Jiang, HY, S Najmeh, G Martel, E MacFadden-Murphy, R Farias, P Savage, A Leone, *et al.* 2020. “Activation of the pattern recognition receptor NOD1 augments colon cancer metastasis.” *Protein and Cell* 3 (11): 187–201. <https://doi.org/10.1007/s13238-019-00687-5>.
- Johansson, MEV., and GC Hansson. 2016. “Immunological aspects of intestinal mucus and mucins.” *Nature Reviews Immunology* 16(10):639–49. <https://doi.org/10.1038/nri.2016.88>.
- Johnson, JW, JF Fisher, and S Mobashery. 2013. “Bacterial cell-wall recycling.” *Annals of the New York Academy of Sciences* 1277 (1): 54–75. <https://doi.org/10.1111/j.1749-6632.2012.06813.x>.
- Johnson, RK, A Zink-Sharp, and WG Glasser. 2011. “Preparation and characterization of hydrophobic derivatives of TEMPO-oxidized nanocelluloses.” *Cellulose* 18: 1599–1609. <https://doi.org/10.1007/s10570-011-9579-y>.
- Jones, NC, and MJ Osborn. 1977. “Translocation of phospholipids between the Outer and Inner Membranes of *Salmonella typhimurium*.” *Journal of Biological Chemistry* 252 (20): 7405–12.
- Jones, RA, Y Thillier, SS Panda, N Rivera Rosario, CD Hall, and AR Katritzky. 2014. “Synthesis and characterisation of Glucosamine-NSAID bioconjugates.” *Organic and Biomolecular Chemistry* 12 (41): 8325–35. <https://doi.org/10.1039/c4ob01681e>.
- Juan, C, G Torrens, IM Barceló, and A Olivera. 2018. “Interplay between peptidoglycan biology and virulence in Gram-negative pathogens.” *Microbiol Mol Biol Rev* 82 (4): e00033-18. <https://doi.org/10.1128/MMBR.00033-18>.
- Kaczyński, Z, S Braun, B Lindner, K Niehaus, and O Holst. 2007. “Investigation of the chemical structure and biological activity of oligosaccharides isolated from rough-type *Xanthomonas campestris* Pv. *campestris* B100 lipopolysaccharide.” *Journal of Endotoxin Research* 13 (2): 101–8. <https://doi.org/10.1177/0968051907079121>.
- Karczmarek, A, R Martínez Arteaga Baselga, S Alexeeva, FG Hansen, M Vicente, N Nanninga, and T Den Blaauwen. 2007. “DNA and origin region segregation are not affected by the transition from rod to sphere after inhibition of *Escherichia coli* MreB by A22.” *Molecular Microbiology* 65 (1): 51–63. <https://doi.org/10.1111/j.1365-2958.2007.05777.x>.
- Karpathy, SE, X Qin, J Gioia, H Jiang, Y Liu, JF Petrosino, S Yerrapragada, *et al.* 2007. “Genome sequence of *Fusobacterium nucleatum* subspecies *polymorphum* - A genetically tractable *Fusobacterium*.” *PLoS ONE* 2 (8): e659. <https://doi.org/10.1371/journal.pone.0000659>.
- Kato, K, T Umemoto, H Sagawa, and S Kotani. 1979. “Lanthionine as an essential constituent of cell wall peptidoglycan of *Fusobacterium nucleatum*.” *Current Microbiology* 3: 147–151. <https://doi.org/10.1007/BF02601857>.
- Kawahara, K, H Brade, ET Rietschel, and U Zähringer. 1987. “Studies on the chemical structure of the core-lipid A region of the lipopolysaccharide of *Acinetobacter calcoaceticus* NCTC 10305: Detection of a new 2-octulosonic acid interlinking the core oligosaccharide and lipid A component.” *European Journal of Biochemistry* 163 (3): 489–495. <https://doi.org/10.1111/j.1432-1033.1987.tb10895.x>.
- Kawamoto, I, T Oka, and T Nara. 1981. “Cell wall composition of *Micromonospora olivoasterospora*, *Micromonospora aagamiensis*, and related organisms.” *Journal of Bacteriology* 146: 527–34. <https://doi.org/10.1128/jb.146.2.527-534.1981>.
- Kawasaki, K, RK Ernst, and SI Miller. 2004. “Deacylation and palmitoylation of lipid A by *Salmonellae*

- Outer Membrane enzymes modulate host signaling through Toll-like receptor 4.” *Journal of Endotoxin Research* 10 (6): 439–44. <https://doi.org/10.1179/096805104225006264>.
- Keck, W, AM Van Leeuwen, M Huber, and E Wm Goodell. 1990. “Cloning and characterization of MepA, the structural gene of the Penicillin-insensitive murein endopeptidase from *Escherichia coli*.” *Molecular Microbiology* 4 (2): 209–19. <https://doi.org/10.1111/j.1365-2958.1990.tb00588.x>.
- Keglević, D, and AE Derome. 1989. “Synthesis and reactions of O-acetylated benzyl α -glycosides of 6-O-(2-acetamido-2-deoxy- β -D-glucopyranosyl)-N-acetylmuramoyl-L-alanyl-D-isoglutamine esters: The base-catalysed isoglutamine \rightleftharpoons Glutamine rearrangement in peptidoglycan-related structures.” *Carbohydrate Research* 186 (1): 63–75. [https://doi.org/10.1016/0008-6215\(89\)84005-4](https://doi.org/10.1016/0008-6215(89)84005-4).
- Kelly, D, JI Campbell, TP King, G Grant, EA Jansson, AGP. Coutts, S Pettersson, and S Conway. 2004. “Commensal anaerobic gut bacteria attenuate inflammation by regulating nuclear-cytoplasmic shuttling of PPAR- γ and RelA.” *Nature Immunology* 5 (1): 104–12. <https://doi.org/10.1038/ni1018>.
- Kenneth, JR, and CG Ray. 2004. *Sherris Medical Microbiology (4th Ed.)*. McGraw Hill. Vasa. <https://doi.org/10.1036/0838585299>.
- Kitamura, S, A Owensby, D Wall, and DW Wolan. 2018. “Lipoprotein signal peptidase inhibitors with antibiotic properties identified through design of a robust in vitro HT platform.” *Cell Chemical Biology* 25 (3): 301–8. <https://doi.org/10.1016/j.chembiol.2017.12.011>.
- Kittelberger, R, and F Hilbink. 1993. “Sensitive silver-staining detection of bacterial lipopolysaccharides in polyacrylamide gels.” *Journal of Biochemical and Biophysical Methods* 26 (1): 81–86. [https://doi.org/10.1016/0165-022X\(93\)90024-I](https://doi.org/10.1016/0165-022X(93)90024-I).
- Kocharova, NA, AV Perepelov, GV Zatonsky, AS Shashkov, YA Knirel, PE Jansson, and A Weintraub. 2001. “Structural studies of the O-specific polysaccharide of *Vibrio cholerae* O8 Using Solvolysis with Triflic Acid.” *Carbohydrate Research* 330 (1): 83–92. [https://doi.org/10.1016/S0008-6215\(00\)00271-8](https://doi.org/10.1016/S0008-6215(00)00271-8).
- Komandrova, NA, VV Isakov, SV Tomshich, LA Romanenko, AV Perepelov, and AS Shashkov. 2010. “Structure of an acidic O-specific polysaccharide of the Marine bacterium *Pseudoalteromonas agarivorans* KMM 232 (R-Form).” *Biochemistry (Moscow)* 63 (10): 1200–1204. <https://doi.org/10.1134/S0006297910050123>.
- Kong, Q, DA Six, Q Liu, L Gu, S Wang, P Alamuri, CH Raetz, and R Curtiss. 2012. “Phosphate groups of lipid a are essential for *Salmonella enterica* serovar Typhimurium virulence and affect innate and adaptive immunity.” *Infection and Immunity* 80 (9): 3215–3224. <https://doi.org/10.1128/IAI.00123-12>.
- Konovalova, A, M Grabowicz, CJ Balibar, JC Malinverni, RE Painter, D Riley, PA Mann, *et al.* 2018. “Inhibitor of intramembrane protease RseP blocks the Σ E response causing lethal accumulation of unfolded outer membrane proteins.” *Proceedings of the National Academy of Sciences of the United States of America* 115 (28): e6614–21. <https://doi.org/10.1073/pnas.1806107115>.
- Konovalova, A, DE Kahne, and TJ Silhavy. 2017. “Outer membrane biogenesis.” *Annual Review of Microbiology* 71: 539–56. <https://doi.org/10.1146/annurev-micro-090816-093754>.
- Kooyk, Y van, and GA Rabinovich. 2008. “Protein-Glycan interactions in the control of innate and adaptive immune responses.” *Nature Immunology* 9: 593–601. <https://doi.org/10.1038/ni.f.203>.
- Kosma, . 1999. “Chlamydial lipopolysaccharide.” *Biochimica et Biophysica Acta - Molecular Basis of Disease* 1455 (2–3): 387–402. [https://doi.org/10.1016/S0925-4439\(99\)00061-7](https://doi.org/10.1016/S0925-4439(99)00061-7).
- Kostic, AD, E Chun, L Robertson, JN Glickman, CA Gallini, M Michaud, TE Clancy, *et al.* 2013. “*Fusobacterium nucleatum* potentiates intestinal tumorigenesis and modulates the tumor-immune microenvironment.” *Cell Host and Microbe* 14 (2): 207–215. <https://doi.org/10.1016/j.chom.2013.07.007>.
- Krisanaprakornkit, S, JR Kimball, A Weinberg, RP Darveau, BW Bainbridge, and BA Dale. 2000. “Inducible expression of human β -defensin 2 by *Fusobacterium nucleatum* in oral epithelial cells: multiple signaling pathways and role of commensal bacteria in innate immunity and the epithelial barrier.” *Infection and Immunity* 68 (5): 2907–15. <https://doi.org/10.1128/IAI.68.5.2907-2915.2000>.
- Laguri, C, A Silipo, AM Martorana, P Schanda, R Marchetti, A Polissi, A Molinaro, and JP Simorre. 2018. “Solid state NMR studies of intact lipopolysaccharide endotoxin.” *ACS Chemical Biology*

- 13 (8): 2106–13. <https://doi.org/10.1021/acschembio.8b00271>.
- Laguri, C, P Sperandeo, K Pounot, I Ayala, A Silipo, CM Bougault, A Molinaro, A Polissi, and JP Simorre. 2017. “Interaction of lipopolysaccharides at intermolecular sites of the periplasmic Lpt transport assembly.” *Scientific Reports* 7 (1): 9715. <https://doi.org/10.1038/s41598-017-10136-0>.
- Lam, JS, EM Anderson, and Y Hao. 2014. “LPS quantitation procedures.” *Methods in Molecular Biology* 1149: 375–402. https://doi.org/10.1007/978-1-4939-0473-0_31.
- Lamarche, MG., SH Kim, S Crépin, M Mourez, N Bertrand, RE Bishop, JD Dubreuil, and J Harel. 2008. “Modulation of hexa-acyl pyrophosphate lipid A population under *Escherichia coli* phosphate (Pho) regulon activation.” *Journal of Bacteriology* 190 (15): 5256–5264. <https://doi.org/10.1128/JB.01536-07>.
- Lamers, RP, UT Nguyen, Y Nguyen, RNC Buensuceso, and LL Burrows. 2015. “Loss of membrane-bound lytic transglycosylases increases Outer Membrane permeability and β -lactam sensitivity in *Pseudomonas aeruginosa*.” *MicrobiologyOpen* 4 (6): 879–95. <https://doi.org/10.1002/mbo3.286>.
- Larrouy-Maumus, G, A Clements, A Filloux, RR McCarthy, and S Mostowy. 2016. “Direct detection of lipid A on intact Gram-Negative bacteria by MALDI-TOF Mass Spectrometry.” *Journal of Microbiological Methods* 120: 68–71. <https://doi.org/10.1016/j.mimet.2015.12.004>.
- Laugerette, F, C Vors, A Géloën, MA Chauvin, C Soulage, S Lambert-Porcheron, N Peretti, et al. 2011. “Emulsified lipids increase endotoxemia: possible role in early postprandial low-grade inflammation.” *Journal of Nutritional Biochemistry* 22 (1): 53–59. <https://doi.org/10.1016/j.jnutbio.2009.11.011>.
- Lee, DK, A Bhunia, SA Kotler, and A Ramamoorthy. 2015. “Detergent-type membrane fragmentation by MSI-78, MSI-367, MSI-594, and MSI-843 antimicrobial peptides and inhibition by cholesterol: a Solid-state Nuclear Magnetic Resonance study.” *Biochemistry* 54 (10): 1897–1907. <https://doi.org/10.1021/bi501418m>.
- Lee, KC, RI Webb, PH Janssen, P Sangwan, T Romeo, JT Staley, and JA Fuerst. 2009. “Phylum Verrucomicrobia representatives share a compartmentalized cell plan with members of bacterial phylum Planctomycetes.” *BMC Microbiology* 9: 5. <https://doi.org/10.1186/1471-2180-9-5>.
- Lehman, KM, and M Grabowicz. 2019. “Countering Gram-Negative antibiotic resistance: recent progress in disrupting the Outer Membrane with novel therapeutics.” *Antibiotics* 8(4):163. <https://doi.org/10.3390/antibiotics8040163>.
- Lehotzky, RE, CL Partchb, S Mukherjeea, HL Casha, WE Goldman, KH Gardner, and LV Hooper. 2010. “Molecular basis for peptidoglycan recognition by a bactericidal lectin.” *Proceedings of the National Academy of Sciences of the United States of America* 107: 7722–27. <https://doi.org/10.1073/pnas.0909449107>.
- Leipold, MD, E Vinogradov, and C Whitfield. 2007. “Glycosyltransferases involved in biosynthesis of the outer core region of *Escherichia coli* lipopolysaccharides exhibit broader substrate specificities than is predicted from lipopolysaccharide structures.” *Journal of Biological Chemistry* 282 (37): 26786–92. <https://doi.org/10.1074/jbc.M704131200>.
- Leo, JC, I Grin, and D Linke. 2012. “Type V secretion: mechanism(S) of autotransport through the bacterial outer membrane.” *Philosophical Transactions of the Royal Society B: Biological Sciences* 367(1592):1088-101. <https://doi.org/10.1098/rstb.2011.0208>.
- Leontein, K, B Lindberg, and J Lonngren. 1978. “Assignment of absolute configuration of sugars by g.l.c. of their acetylated glycosides formed from chiral alcohols.” *Carbohydrate Research* 62: 359–62. [https://doi.org/10.1016/S0008-6215\(00\)80882-4](https://doi.org/10.1016/S0008-6215(00)80882-4).
- Lerouge, Inge, and Jos Vanderleyden. 2002. “O-Antigen Structural Variation: Mechanisms and Possible Roles in Animal/Plant-Microbe Interactions.” *FEMS Microbiology Reviews*. [https://doi.org/10.1016/S0168-6445\(01\)00070-5](https://doi.org/10.1016/S0168-6445(01)00070-5).
- Li, Jun, Hui Chen Hsu, John D. Mountz, and John G. Allen. 2018. “Unmasking Fucosylation: From Cell Adhesion to Immune System Regulation and Diseases.” *Cell Chemical Biology* 25 (5): 499–512. <https://doi.org/10.1016/j.chembiol.2018.02.005>.
- Li, M, H Zhou, C Yang, Y Wu, X Zhou, H Liu, and Y Wang. 2020. “Bacterial Outer Membrane Vesicles as a platform for biomedical applications: an update.” *Journal of Controlled Release* 323: 253–68. <https://doi.org/10.1016/j.jconrel.2020.04.031>.
- Li, XZ, P Plésiat, and H Nikaido. 2015. “The challenge of efflux-mediated antibiotic resistance in

- Gram-negative bacteria.” *Clinical Microbiology Reviews* 28 (2): 337–418. <https://doi.org/10.1128/CMR.00117-14>.
- Li, Y, BJ Orlando, and M Liao. 2019. “Structural basis of lipopolysaccharide extraction by the LptB2 FGC complex.” *Nature* 567 (7749): 486–90. <https://doi.org/10.1038/s41586-019-1025-6>.
- Liang-Takasaki, CJ, PH Makela, and L Leive. 1982. “Phagocytosis of bacteria by macrophages: changing the carbohydrate of lipopolysaccharide alters interaction with complement and macrophages.” *Journal of Immunology* 128 (3): 1229–35.
- Ligon, BL. 2004. “Penicillin: its discovery and early development.” *Seminars in Pediatric Infectious Diseases* 15 (1): 52–57. <https://doi.org/10.1053/j.spid.2004.02.001>.
- Lima, S, MS Guo, R Chaba, CA Gross, and RT Sauer. 2013. “Dual molecular signals mediate the bacterial response to Outer Membrane stress.” *Science* 340 (6134): 837–41. <https://doi.org/10.1126/science.1235358>.
- Liu, C, J Ma, J Wang, H Wang, and L Zhang. 2020. “Cryo-EM structure of a bacterial lipid transporter YebT.” *Journal of Molecular Biology* 432 (4): 1008–19. <https://doi.org/10.1016/j.jmb.2019.12.008>.
- Liu, J, CL Hsieh, O Gelincik, B Devolder, S Sei, S Zhang, SM Lipkin, and YF Chang. 2019. “Proteomic characterization of Outer Membrane Vesicles from gut mucosa-derived *Fusobacterium nucleatum*.” *Journal of Proteomics* 195: 125–37. <https://doi.org/10.1016/j.jprot.2018.12.029>.
- Liu, L, W Dong, S Wang, Y Zhang, T Liu, R Xie, B Wang, and H Cao. 2018. “Deoxycholic acid disrupts the intestinal mucosal barrier and promotes intestinal tumorigenesis.” *Food and Function* 9 (11): 5588–5597. <https://doi.org/10.1039/c8fo01143e>.
- Liu, Y, and E Breukink. 2016. “The membrane steps of bacterial cell wall synthesis as antibiotic targets.” *Antibiotics* 5(3):28. <https://doi.org/10.3390/antibiotics5030028>.
- Lloyd-Price, J, A Mahurkar, G Rahnavard, J Crabtree, J Orvis, AB Hall, A Brady, *et al.* 2017. “Strains, functions and dynamics in the expanded Human Microbiome Project.” *Nature* 550 (7674): 61–66. <https://doi.org/10.1038/nature23889>.
- Loffredo, L, V Ivanov, N Ciobanu, E Deseatnicova, E Gutu, L Mudrea, M Ivanov, *et al.* 2020. “Is there an association between atherosclerotic burden, oxidative stress, and gut-derived lipopolysaccharides?” *Antioxid Redox Signal* 33 (11). <https://doi.org/10.1089/ars.2020.8109>.
- Lorenzo, F Di. 2017. “The lipopolysaccharide lipid A structure from the marine sponge-associated bacterium *Pseudoalteromonas* Sp. 2A.” *Antonie van Leeuwenhoek, International Journal of General and Molecular Microbiology* 110 (11): 1401–12. <https://doi.org/10.1007/s10482-017-0865-z>.
- Lorenzo, F Di, C De Castro, A Silipo, and A Molinaro. 2019. “Lipopolysaccharide structures of Gram-negative populations in the gut microbiota and effects on host interactions.” *FEMS Microbiology Reviews* 43(3):257-272. <https://doi.org/10.1093/femsre/fuz002>.
- Lorenzo, F Di, Ł Kubik, A Oblak, NI Lorè, C Cigana, R Lanzetta, M Parrilli, *et al.* 2015. “Activation of human Toll-like receptor 4 (TLR4)·myeloid differentiation factor 2 (MD-2) by hypoacylated lipopolysaccharide from a clinical isolate of *Burkholderia cenocepacia*.” *Journal of Biological Chemistry* 290 (35): 21305–19. <https://doi.org/10.1074/jbc.M115.649087>.
- Lorenzo, F Di, A Palmigiano, KA Duda, M Pallach, N Busset, L Sturiale, E Giraud, D Garozzo, A Molinaro, and A Silipo. 2017. “Structure of the lipopolysaccharide from the *Bradyrhizobium* Sp. ORS285 *rfaL* mutant strain.” *ChemistryOpen* 6 (4): 541–53. <https://doi.org/10.1002/open.201700074>.
- Lorenzo, F Di, A Palmigiano, A Silipo, Y Desaki, D Garozzo, R Lanzetta, N Shibuya, and A Molinaro. 2016. “The structure of the lipooligosaccharide from *Xanthomonas oryzae* Pv. *oryzae*: The causal agent of the bacterial leaf blight in rice.” *Carbohydrate Research* 427: 38–43. <https://doi.org/10.1016/j.carres.2016.03.026>.
- Lorenzo, F Di, MD Pither, M Martufi, I Scarinci, J Guzmán-Caldentey, E Łakomicz, W Jachymek, *et al.* 2020. “Pairing *Bacteroides vulgatus* LPS structure with its immunomodulatory effects on human cellular models.” *ACS Central Science* 6 (9): 1602–1616. <https://doi.org/10.1021/acscentsci.0c00791>.
- Luchetti, MM, F Ciccica, C Avellini, D Benfaremo, A Rizzo, T Spadoni, S Svegliati, *et al.* 2020. “Gut epithelial impairment, microbial translocation and immune system activation in inflammatory bowel disease-associated spondyloarthritis.” *Rheumatology* 60 (1): 92-102. <https://doi.org/10.1093/rheumatology/keaa164>.

- Lundstedt, EA, BW Simpson, and N Ruiz. 2020. "LptB-LptF coupling mediates the closure of the substrate-binding cavity in the LptB2FGC transporter through a rigid-body mechanism to extract LPS." *Molecular Microbiology* 114(2):200-213. <https://doi.org/10.1111/mmi.14506>.
- Luo, Q, X Yang, S Yu, H Shi, K Wang, L Xiao, G Zhu, *et al.* 2017. "Structural basis for lipopolysaccharide extraction by ABC transporter LptB2FG." *Nature Structural and Molecular Biology* 24 (7749): 469–474. <https://doi.org/10.1038/nsmb.3399>.
- Maalej, M, RE Forgione, R Marchetti, F Bulteau, M Thépaut, R Lanzetta, C Laguri, *et al.* 2019. "Human Macrophage Galactose-type Lectin (MGL) recognizes the outer core of *Escherichia coli* lipooligosaccharide." *ChemBioChem* 20 (14): 1778–82. <https://doi.org/10.1002/cbic.201900087>.
- MacAlister, TJ, WR Cook, R Weigand, and LI Rothfield. 1987. "Membrane-murein Attachment at the Leading Edge of the Division Septum: A Second Membrane-Murein Structure associated with morphogenesis of the Gram-negative bacterial division septum." *Journal of Bacteriology* 169 (9): 3945–51. <https://doi.org/10.1128/jb.169.9.3945-3951.1987>.
- Magnet, S, S Bellais, L Dubost, M Fourgeaud, JL Mainardi, S Petit-Frère, A Marie, D Mengin-Lecreulx, M Arthur, and L Gutmann. 2007. "Identification of the L,D-transpeptidases responsible for attachment of the Braun lipoprotein to *Escherichia coli* peptidoglycan." *Journal of Bacteriology* 189 (10): 3927–3931. <https://doi.org/10.1128/JB.00084-07>.
- Mainardi, JL, R Villet, TD Bugg, C Mayer, and M Arthur. 2008. "Evolution of peptidoglycan biosynthesis under the selective pressure of antibiotics in Gram-positive bacteria." *FEMS Microbiology Reviews* 32(2):386-408. <https://doi.org/10.1111/j.1574-6976.2007.00097.x>.
- Malojčić, G, D Andres, M Grabowicz, AH George, N Ruiz, TJ Silhavy, and D Kahne. 2014. "LptE binds to and alters the physical state of LPS to catalyze its assembly at the cell surface." *Proceedings of the National Academy of Sciences of the United States of America* 111 (26): 9467–72. <https://doi.org/10.1073/pnas.1402746111>.
- Man, WH, WAA De Steenhuisen Piters, and D Bogaert. 2017. "The microbiota of the respiratory tract: gatekeeper to respiratory health." *Nature Reviews Microbiology* 15(5):259-270. <https://doi.org/10.1038/nrmicro.2017.14>.
- Manat, G, S Roure, R Auger, A Bouhss, H Barreteau, D Mengin-Lecreulx, and T Touzé. 2014. "Deciphering the metabolism of undecaprenyl-phosphate: the bacterial cell-wall unit carrier at the membrane frontier." In *Microbial Drug Resistance*, 20(3):199–214. <https://doi.org/10.1089/mdr.2014.0035>.
- Mandler, MD, V Baidin, J Lee, KS Pahil, TW Owens, and D Kahne. 2018. "Novobiocin enhances polymyxin activity by stimulating lipopolysaccharide transport." *Journal of the American Chemical Society* 140 (22): 6749–53. <https://doi.org/10.1021/jacs.8b02283>.
- Marraffini, LA, AC DeDent, and O Schneewind. 2006. "Sortases and the art of anchoring proteins to the envelopes of Gram-positive bacteria." *Microbiology and Molecular Biology Reviews* 70 (1): 192–221. <https://doi.org/10.1128/mmr.70.1.192-221.2006>.
- Martin, DH. 2012. "The microbiota of the vagina and its influence on women's health and disease." In *American Journal of the Medical Sciences*, 343(1):2–9. <https://doi.org/10.1097/MAJ.0b013e31823ea228>.
- Matias, VRF, A Al-Amoudi, J Dubochet, and TJ Beveridge. 2003. "Cryo-Transmission Electron Microscopy of frozen-hydrated sections of *Escherichia coli* and *Pseudomonas aeruginosa*." *Journal of Bacteriology* 185 (20): 6112–6118. <https://doi.org/10.1128/JB.185.20.6112-6118.2003>.
- Matsumoto, M, T Tanaka, T Kaisho, H Sanjo, NG Copeland, DJ Gilbert, NA Jenkins, and S Akira. 1999. "A novel LPS-inducible C-type lectin is a transcriptional target of NF-IL6 in macrophages." *Journal of Immunology (Baltimore, Md. : 1950)* 163 (9): 5039–48.
- Mattsby-Baltzer, I, P Gemski, and CR Alving. 1984. "Heterogeneity of lipid A." *Reviews of Infectious Diseases* 159 (3): 900–904. <https://doi.org/10.1093/clinids/6.4.444>.
- May, KL, and TJ Silhavy. 2018. "The *Escherichia coli* phospholipase PldA regulates Outer Membrane homeostasis via lipid signaling." *MBio* 9 (2): e00379-18. <https://doi.org/10.1128/mBio.00379-18>.
- Mazgaen, L, and P Gurung. 2020. "Recent advances in lipopolysaccharide recognition systems." *International Journal of Molecular Sciences* 21 (2): 379. <https://doi.org/10.3390/ijms21020379>.
- McLaughlin, MI, and WA Van Der Donk. 2020. "The fellowship of the rings: macrocyclic antibiotic

- peptides reveal an anti-Gram-negative target.” *Biochemistry* 59(4):343-345. <https://doi.org/10.1021/acs.biochem.9b01086>.
- McLeod, SM, PR Fleming, K MacCormack, RE McLaughlin, JD Whiteaker, S Narita, M Mori, H Tokuda, and AA Miller. 2015. “Small-molecule inhibitors of Gram-negative lipoprotein trafficking discovered by phenotypic screening.” *Journal of Bacteriology* 197 (6): 1075–82. <https://doi.org/10.1128/JB.02352-14>.
- Mengin-Lecreulx, D, D Blanot, and J Van Heijenoort. 1994. “Replacement of diaminopimelic acid by cystathionine or lanthionine in the peptidoglycan of *Escherichia coli*.” *Journal of Bacteriology* 176 (14): 4321–4327. <https://doi.org/10.1128/jb.176.14.4321-4327.1994>.
- Mengin-Lecreulx, D, J van Heijenoort, and JT Park. 1996. “Identification of the *mpl* gene encoding UDP-N-acetylmuramate: L-alanyl- γ -D-glutamyl-meso-diaminopimelate ligase in *Escherichia coli* and its role in recycling of cell wall peptidoglycan.” *Journal of Bacteriology* 178 (18): 5347–5352. <https://doi.org/10.1128/jb.178.18.5347-5352.1996>.
- Meseguer, V, YA Alpizar, E Luis, S Tajada, B Denlinger, O Fajardo, JA Manenschijn, *et al.* 2014. “TRPA1 channels mediate acute neurogenic inflammation and pain produced by bacterial endotoxins.” *Nature Communications* 5: 3125. <https://doi.org/10.1038/ncomms4125>.
- Mi, W, Y Li, SH Yoon, RK Ernst, T Walz, and M Liao. 2017. “Structural basis of MsbA-mediated lipopolysaccharide transport.” *Nature* 549 (7671): 233–37. <https://doi.org/10.1038/nature23649>.
- Milani, C, S Duranti, F Bottacini, E Casey, F Turroni, J Mahony, C Belzer, *et al.* 2017. “The first microbial colonizers of the human gut: composition, activities, and health implications of the infant gut microbiota.” *Microbiology and Molecular Biology Reviews* 81 (4): e00036-17. <https://doi.org/10.1128/mmb.00036-17>.
- Miller, SI, and NR Salama. 2018. “The Gram-negative bacterial periplasm: size matters.” *PLoS Biology* 16(1):e2004935. <https://doi.org/10.1371/journal.pbio.2004935>.
- Mima, K, Y Sukawa, R Nishihara, ZR Qian, M Yamauchi, K Inamura, SA Kim, *et al.* 2015. “*Fusobacterium nucleatum* and T cells in colorectal carcinoma.” *JAMA Oncology* 1 (5): 653–61. <https://doi.org/10.1001/jamaoncol.2015.1377>.
- Miyamoto, T, M Katane, Y Saitoh, M Sekine, and H Homma. 2019. “Elucidation of the D-Lysine biosynthetic pathway in the hyperthermophile *Thermotoga maritima*.” *FEBS Journal* 286 (3): 601–14. <https://doi.org/10.1111/febs.14720>.
- . 2020. “Involvement of penicillin-binding proteins in the metabolism of a bacterial peptidoglycan containing a non-canonical D-amino acid.” *Amino Acids* 52: 487–497. <https://doi.org/10.1007/s00726-020-02830-7>.
- Miyazaki, K, K Sakuma, YI Kawamura, M Izawa, K Ohmori, M Mitsuki, T Yamaji, *et al.* 2012. “Colonic epithelial cells express specific ligands for mucosal macrophage immunosuppressive receptors Siglec-7 and -9.” *The Journal of Immunology* 188 (9): 4690–4700. <https://doi.org/10.4049/jimmunol.1100605>.
- Moffatt, JH, M Harper, and JD Boyce. 2019. “Mechanisms of polymyxin resistance.” In *Advances in Experimental Medicine and Biology*, 1145:55-71. https://doi.org/10.1007/978-3-030-16373-0_5.
- Mogensen, TH. 2009. “Pathogen recognition and inflammatory signaling in innate immune defenses.” *Clinical Microbiology Reviews* 22(2):240-73. <https://doi.org/10.1128/CMR.00046-08>.
- Mohammadi, T, A Karczarek, M Crouvoisier, A Bouhss, D Mengin-Lecreulx, and T Den Blaauwen. 2007. “The essential peptidoglycan glycosyltransferase MurG forms a complex with proteins involved in lateral envelope growth as well as with proteins involved in cell division in *Escherichia coli*.” *Molecular Microbiology* 65 (4): 1106–21. <https://doi.org/10.1111/j.1365-2958.2007.05851.x>.
- Molinaro, A, O Holst, F Di Lorenzo, M Callaghan, A Nurisso, G D’Errico, A Zamyatina, *et al.* 2015. “Chemistry of lipid A: at the heart of innate immunity.” *Chemistry* 21(2):500-19. <https://doi.org/10.1002/chem.201403923>.
- Moncla, BJ, P Braham, and SL Hillier. 1990. “Sialidase (neuraminidase) activity among Gram-negative anaerobic and capnophilic bacteria.” *Journal of Clinical Microbiology* 28 (3): 422–425. <https://doi.org/10.1128/jcm.28.3.422-425.1990>.
- Moran, AP, MM Prendergast, and BJ Appelmek. 1996. “Molecular mimicry of host structures by bacterial lipopolysaccharides and its contribution to disease.” *FEMS Immunology and Medical Microbiology* 16 (2): 105–15. [https://doi.org/10.1016/S0928-8244\(96\)00072-7](https://doi.org/10.1016/S0928-8244(96)00072-7).

- Morè, N, AM Martorana, J Biboy, C Otten, M Winkle, CK Gurnani Serrano, A Montón Silva, *et al.* 2019. "Peptidoglycan remodeling enables *Escherichia coli* to survive severe Outer Membrane assembly defect." *MBio* 10 (1): e02729-18. <https://doi.org/10.1128/mBio.02729-18>.
- Muldoon, J, AS Shashkov, SN Senchenkova, SV Tomshich, NA Komandrova, LA Romanenko, YA Knirel, and AV Savage. 2001. "Structure of an acidic polysaccharide from a marine bacterium *Pseudoalteromonas distincta* KMM 638 containing 5-acetamido-3,5,7,9-tetradeoxy-7-formamido-L-glycero-L-manno-nonulosonic acid." *Carbohydrate Research* 330 (2): 231–39. [https://doi.org/10.1016/S0008-6215\(00\)00280-9](https://doi.org/10.1016/S0008-6215(00)00280-9).
- Müller-Loennies, S, B Lindner, and H Brade. 2003. "Structural analysis of oligosaccharides from lipopolysaccharide (LPS) of *Escherichia coli* K12 strain W3100 reveals a link between inner and outer core LPS biosynthesis." *Journal of Biological Chemistry* 278 (36): 34090–101. <https://doi.org/10.1074/jbc.M303985200>.
- Nadesalingam, J, AW Dodds, KBM Reid, and N Palaniyar. 2005. "Mannose-binding lectin recognizes peptidoglycan via the N-acetyl glucosamine moiety, and inhibits ligand-induced proinflammatory effect and promotes chemokine production by macrophages." *The Journal of Immunology* 175 (3): 1785–94. <https://doi.org/10.4049/jimmunol.175.3.1785>.
- Nagaoka, K, K Takahara, K Tanaka, H Yoshida, RM Steinman, SI Saitoh, S Akashi-Takamura, *et al.* 2005. "Association of SIGNR1 with TLR4-MD-2 enhances signal transduction by recognition of LPS in Gram-negative bacteria." *International Immunology* 17 (7): 827–836. <https://doi.org/10.1093/intimm/dxh264>.
- Najdenski, H, E Golkocheva, A Vesselinova, JA Bengoechea, and M Skurnik. 2003. "Proper expression of the O-antigen of lipopolysaccharide is essential for the virulence of *Yersinia enterocolitica* O:8 in experimental oral infection of rabbits." *FEMS Immunology and Medical Microbiology* 38 (2): 97–106. [https://doi.org/10.1016/S0928-8244\(03\)00183-4](https://doi.org/10.1016/S0928-8244(03)00183-4).
- Natale, P, T Brüser, and AJM Driessen. 2008. "Sec- and Tat-mediated protein secretion across the bacterial Cytoplasmic Membrane-distinct translocases and mechanisms." *Biochimica et Biophysica Acta* 1778(9):1735-56. <https://doi.org/10.1016/j.bbamem.2007.07.015>.
- Nayar, AS, TJ Dougherty, KE Ferguson, BA Granger, L McWilliams, C Stacey, LJ Leach, *et al.* 2015. "Novel antibacterial targets and compounds revealed by a high-throughput cell wall reporter assay." *Journal of Bacteriology* 197 (10): 1726–34. <https://doi.org/10.1128/JB.02552-14>.
- Nickerson, NN, CC Jao, Y Xu, J Quinn, E Skippington, MK Alexander, A Miu, *et al.* 2018. "A novel inhibitor of the LolCDE ABC transporter essential for lipoprotein trafficking in Gram-negative bacteria." *Antimicrobial Agents and Chemotherapy* 62 (4): e02151-17. <https://doi.org/10.1128/AAC.02151-17>.
- Nicoloff, H, S Gopalkrishnan, and SE Ades. 2017. "Appropriate regulation of the Σ Ed-dependent envelope stress response is necessary to maintain cell envelope integrity and stationary-phase survival in *Escherichia coli*." *Journal of Bacteriology* 199 (12): e00089-17. <https://doi.org/10.1128/JB.00089-17>.
- Nikaido, H. 1976. "Outer Membrane of *Salmonella typhimurium*. Transmembrane diffusion of some hydrophobic substances." *BBA - Biomembranes* 433 (1): 118–32. [https://doi.org/10.1016/0005-2736\(76\)90182-6](https://doi.org/10.1016/0005-2736(76)90182-6).
- Noinaj, N, JC Gumbart, and SK Buchanan. 2017. "The β -Barrel Assembly Machinery in motion." *Nature Reviews Microbiology* 15(4):197-204. <https://doi.org/10.1038/nrmicro.2016.191>.
- Ohkusa, T, I Okayasu, T Ogihara, K Morita, M Ogawa, and N Sato. 2003. "Induction of experimental ulcerative colitis by *Fusobacterium varium* isolated from colonic mucosa of patients with ulcerative colitis." *Gut* 52 (1): 79–83. <https://doi.org/10.1136/gut.52.1.79>.
- Ohradanova-Repic, A, C Machacek, MB Fischer, and H Stockinger. 2016. "Differentiation of human monocytes and derived subsets of macrophages and dendritic cells by the HLDA10 monoclonal antibody panel." *Clinical and Translational Immunology* 5 (1): e55-9. <https://doi.org/10.1038/cti.2015.39>.
- Okahashi, N, T Koga, T Nishihara, T Fujiwara, and S Hamada. 1988. "Immunobiological properties of lipopolysaccharides isolated from *Fusobacterium nucleatum* and *F. necrophorum*." *Journal of General Microbiology* 134 (6): 1707–15. <https://doi.org/10.1099/00221287-134-6-1707>.
- Okuda, S, DJ Sherman, TJ Silhavy, N Ruiz, and D Kahne. 2016. "Lipopolysaccharide transport and assembly at the Outer Membrane: the PEZ model." *Nature Reviews Microbiology* 14(6):337-45. <https://doi.org/10.1038/nrmicro.2016.25>.

- Oliver, DB, and J Beckwith. 1982. "Regulation of a membrane component required for protein secretion in *Escherichia coli*." *Cell* 30 (1): 311–19. [https://doi.org/10.1016/0092-8674\(82\)90037-X](https://doi.org/10.1016/0092-8674(82)90037-X).
- Onoue, S, M Niwa, Y Isshiki, and K Kawahara. 1996. "Extraction and characterization of the smooth-type lipopolysaccharide from *Fusobacterium nucleatum* JCM 8532 and its biological activities." *Microbiology and Immunology* 40 (5): 323–31. <https://doi.org/10.1111/j.1348-0421.1996.tb01075.x>.
- Opal, SM, PF Laterre, B Francois, SP LaRosa, DC Angus, JP Mira, X Wittebole, *et al.* 2013. "Effect of Eritoran, an antagonist of MD2-TLR4, on mortality in patients with severe sepsis: the ACCESS randomized trial." *JAMA - Journal of the American Medical Association* 309 (11): 1154–1162. <https://doi.org/10.1001/jama.2013.2194>.
- Oviedo-Boyso, J, A Bravo-Patiño, and VM Baizabal-Aguirre. 2014. "Collaborative action of Toll-like and Nod-like receptors as modulators of the inflammatory response to pathogenic bacteria." *Mediators of Inflammation* 2014:432785. <https://doi.org/10.1155/2014/432785>.
- Owens, TW, RJ Taylor, KS Pahil, BR Bertani, N Ruiz, AC Kruse, and D Kahne. 2019. "Structural basis of unidirectional export of lipopolysaccharide to the cell surface." *Nature* 567 (7749): 550–53. <https://doi.org/10.1038/s41586-019-1039-0>.
- Panda, SK, S Saxena, and L Guruprasad. 2019. "Homology modeling, docking and structure-based virtual screening for new inhibitor identification of *Klebsiella pneumoniae* Heptosyltransferase-III." *Journal of Biomolecular Structure and Dynamics* 38 (7): 1887–1902. <https://doi.org/10.1080/07391102.2019.1624296>.
- Paradis-Bleau, C, M Markowski, T Uehara, TJ Lupoli, S Walker, DE Kahne, and TG Bernhardt. 2010. "Lipoprotein cofactors located in the Outer Membrane activate bacterial cell wall polymerases." *Cell* 143 (7): 1110–20. <https://doi.org/10.1016/j.cell.2010.11.037>.
- Park, BS, and JO Lee. 2013. "Recognition of lipopolysaccharide pattern by TLR4 complexes." *Experimental and Molecular Medicine* 45 (12): e66. <https://doi.org/10.1038/emm.2013.97>.
- Park, JT, and T Uehara. 2008. "How bacteria consume their own exoskeletons (turnover and recycling of cell wall peptidoglycan)." *Microbiology and Molecular Biology Reviews* 72 (2): 211–27. <https://doi.org/10.1128/mmr.00027-07>.
- Passel, MWJ van, R Kant, EG Zoetendal, CM Plugge, M Derrien, SA Malfatti, PSG Chain, *et al.* 2011. "The genome of *Akkermansia muciniphila*, a dedicated intestinal mucin degrader, and its use in exploring intestinal metagenomes." *PLoS ONE* 6 (3): e16876. <https://doi.org/10.1371/journal.pone.0016876>.
- Patin, EC, SJ Orr, and UE Schaible. 2017. "Macrophage inducible C-type lectin as a multifunctional player in immunity." *Frontiers in Immunology* 8: 861. <https://doi.org/10.3389/fimmu.2017.00861>.
- Pazos, M, and K Peters. 2019. "Peptidoglycan." *Subcellular Biochemistry*, 92:127-168. https://doi.org/10.1007/978-3-030-18768-2_5.
- Persat, A, CD Nadell, MK Kim, F Ingremeau, A Siryaporn, K Drescher, NS Wingreen, BL Bassler, Z Gitai, and HA Stone. 2015. "The mechanical world of bacteria." *Cell* 161(5):988-997. <https://doi.org/10.1016/j.cell.2015.05.005>.
- Peschel, A, and HG Sahl. 2006. "The co-evolution of host cationic antimicrobial peptides and microbial resistance." *Nature Reviews Microbiology* 4(7):529-36. <https://doi.org/10.1038/nrmicro1441>.
- Peters, K, S Kannan, VA Rao, J Biboy, D Vollmer, SW Erickson, RJ Lewis, KD Young, and W Vollmer. 2016. "The redundancy of peptidoglycan carboxypeptidases ensures robust cell shape maintenance in *Escherichia coli*." *MBio* 7 (3): e00819-16. <https://doi.org/10.1128/mBio.00819-16>.
- Peters, NT, T Dinh, and TG Bernhardt. 2011. "A fail-safe mechanism in the septal ring assembly pathway generated by the sequential recruitment of cell separation amidases and their activators." *Journal of Bacteriology* 193 (18): 4973–4983. <https://doi.org/10.1128/JB.00316-11>.
- Plötz, BM, B Lindner, KO Stetter, and O Holst. 2000. "Characterization of a novel lipid A containing D-Galacturonic acid that replaces Phosphate residues. The structure of the lipid A of the lipopolysaccharide from the hyperthermophilic bacterium *Aquifex pyrophilus*." *Journal of Biological Chemistry* 275 (15): 11222–28. <https://doi.org/10.1074/jbc.275.15.11222>.
- Plovier, H, Amandine E, C Druart, C Depommier, M van Hul, L Geurts, J Chilloux, *et al.* 2017. "A purified membrane protein from *Akkermansia muciniphila* or the pasteurized bacterium improves metabolism in obese and diabetic mice." *Nature Medicine* 23 (1): 107–13.

- <https://doi.org/10.1038/nm.4236>.
- Polissi, A, and P Sperandio. 2014. "The lipopolysaccharide export pathway in *Escherichia coli*: structure, organization and regulated assembly of the Lpt machinery." *Marine Drugs* 12 (2): 1023–1042. <https://doi.org/10.3390/md12021023>.
- Popham, DL, J Helin, CE Costello, and P Setlow. 1996. "Muramic lactam in peptidoglycan of *Bacillus subtilis* spores is required for spore outgrowth but not for spore dehydration or heat resistance." *Proceedings of the National Academy of Sciences of the United States of America* 93 (26): 15405–15410. <https://doi.org/10.1073/pnas.93.26.15405>.
- Price, AE, K Shamardani, KA Lugo, J Deguine, AW Roberts, BL Lee, and GM Barton. 2018. "A map of Toll-like receptor expression in the intestinal epithelium reveals distinct spatial, cell type-specific, and temporal patterns." *Immunity* 49 (3): 560–575.e6. <https://doi.org/10.1016/j.immuni.2018.07.016>.
- Priyadarshini, R, MA De Pedro, and KD Young. 2007. "Role of peptidoglycan amidases in the development and morphology of the division septum in *Escherichia coli*." *Journal of Bacteriology* 189 (14): 5334–47. <https://doi.org/10.1128/JB.00415-07>.
- Radkov, AD, YP Hsu, G Booher, and MS VanNieuwenhze. 2018. "Imaging bacterial cell wall biosynthesis." *Annual Review of Biochemistry* 87: 991–1014. <https://doi.org/10.1146/annurev-biochem-062917-012921>.
- Raetz, C. 1990. "Biochemistry of endotoxins." *Annual Review of Biochemistry* 59: 129–70. <https://doi.org/10.1146/annurev.biochem.59.1.129>.
- Raetz, CRH, CM Reynolds, MS Trent, and RE Bishop. 2007. "Lipid A modification systems in Gram-negative bacteria." *Annual Review of Biochemistry* 76: 295–329. <https://doi.org/10.1146/annurev.biochem.76.010307.145803>.
- Raetz, C, and C Whitfield. 2002. "Lipopolysaccharide endotoxins." *Annual Review of Biochemistry* 71: 635–700. <https://doi.org/10.1146/annurev.biochem.71.110601.135414>.
- Rajagopal, M, and S Walker. 2017. "Envelope structures of Gram-positive bacteria." In *Current Topics in Microbiology and Immunology*, 404:1-44. https://doi.org/10.1007/82_2015_5021.
- Rapin, JR, and N Wiernsperger. 2010. "Possible links between intestinal permeability and food processing: a potential therapeutic niche for glutamine." *Clinics* 65 (6): 635–43. <https://doi.org/10.1590/S1807-59322010000600012>.
- Ray, BL, G Painter, and CRH Raetz. 1984. "The biosynthesis of Gram-negative endotoxin. formation of lipid A disaccharides from monosaccharide precursors in extracts of *Escherichia coli*." *Journal of Biological Chemistry* 259 (8): 4852–4859.
- Rinninella, E, P Raouf, M Cintoni, F Franceschi, GA Donato Miggiano, A Gasbarrini, and MC Mele. 2019. "What is the healthy gut microbiota composition? a changing ecosystem across age, environment, diet, and diseases." *Microorganisms* 7 (1): 14. <https://doi.org/10.3390/microorganisms7010014>.
- Robinson, JA. 2019. "Folded synthetic peptides and other molecules targeting Outer Membrane protein complexes in Gram-negative bacteria." *Frontiers in Chemistry* 7:45. <https://doi.org/10.3389/fchem.2019.00045>.
- Rodríguez-Alonso, R, J Létoquart, VS Nguyen, G Louis, AN Calabrese, BI Iorga, SE Radford, SH Cho, H Remaut, and JF Collet. 2020. "Structural insight into the formation of lipoprotein- β -barrel complexes." *Nature Chemical Biology* 16(9):1019-1025. <https://doi.org/10.1038/s41589-020-0575-0>.
- Rodríguez, JM, K Murphy, C Stanton, RP Ross, OI Kober, N Juge, E Avershina, *et al.* 2015. "The composition of the gut microbiota throughout life, with an emphasis on early life." *Microbial Ecology in Health & Disease* 26: 26050. <https://doi.org/10.3402/mehd.v26.26050>.
- Ropy, A, G Cabot, I Sánchez-Diener, C Aguilera, B Moya, JA Ayala, and A Oliver. 2015. "Role of *Pseudomonas aeruginosa* low-molecular-mass penicillin-binding proteins in *ampC* expression, β -lactam resistance, and peptidoglycan structure." *Antimicrobial Agents and Chemotherapy* 59 (7): 3925–3934. <https://doi.org/10.1128/AAC.05150-14>.
- Rosenthal, RS, RM Wright, and RK Sinha. 1980. "Extent of peptide cross-linking in the peptidoglycan of *Neisseria gonorrhoeae*." *Infection and Immunity* 28 (3): 867–75.
- Round, JL, and SK Mazmanian. 2009. "The gut microbiota shapes intestinal immune responses during health and disease." *Nature Reviews Immunology* 9 (5): 313–323. <https://doi.org/10.1038/nri2515>.

- Round, JL, SM Lee, J Li, G Tran, B Jabri, TA Chatila, SK Mazmanian. 2012. The Toll-like receptor pathway establishes commensal gut colonization. *Science* 332 (6032): 974-977. <https://doi.org/10.1126/science.1206095>.
- Royet, J, D Gupta, and R Dziarski. 2011. "Peptidoglycan recognition proteins: modulators of the microbiome and inflammation." *Nature Reviews Immunology* 11(12):837-51. <https://doi.org/10.1038/nri3089>.
- Ruan, X, J Monjarás Feria, M Hamad, and MA Valvano. 2018. "Escherichia coli and Pseudomonas aeruginosa lipopolysaccharide O-antigen ligases share similar membrane topology and biochemical properties." *Molecular Microbiology* 110 (1): 95–113. <https://doi.org/10.1111/mmi.14085>.
- Sadek, F, DB Drucker, V Boote, KW Bennett, and A Eley. 1998. "Phospholipids of Fusobacterium Spp." *Journal of Applied Microbiology* 85 (2): 302–8. <https://doi.org/10.1046/j.1365-2672.1998.00506.x>.
- Saha, S, X Jing, SY Park, S Wang, X Li, D Gupta, and R Dziarski. 2010. "Peptidoglycan recognition proteins protect mice from experimental colitis by promoting normal gut flora and preventing induction of interferon- γ ." *Cell Host and Microbe* 8 (2): 147–62. <https://doi.org/10.1016/j.chom.2010.07.005>.
- Sansonetti, PJ, and R Medzhitov. 2009. "Learning tolerance while fighting ignorance." *Cell* 138(3):416-20. <https://doi.org/10.1016/j.cell.2009.07.024>.
- Sartor, RB, and GD Wu. 2017. "Roles for intestinal bacteria, viruses, and fungi in pathogenesis of inflammatory bowel diseases and therapeutic approaches." *Gastroenterology* 152 (2): 327–39. <https://doi.org/10.1053/j.gastro.2016.10.012>.
- Sauvage, E, F Kerff, M Terrak, JA Ayala, and P Charlier. 2008. "The penicillin-binding proteins: structure and role in peptidoglycan biosynthesis." *FEMS Microbiology Reviews* 32(2):234-58. <https://doi.org/10.1111/j.1574-6976.2008.00105.x>.
- Scheffers, DJ, and MG Pinho. 2005. "Bacterial cell wall synthesis: new insights from localization studies." *Microbiology and Molecular Biology Reviews* 69 (4): 585–607. <https://doi.org/10.1128/membr.69.4.585-607.2005>.
- Schenk, M, S Mahapatra, P Le, HJ Kim, AW Choi, PJ Brennan, JT Belisle, and RL Modlin. 2016. "Human NOD2 recognizes structurally unique muramyl dipeptides from Mycobacterium leprae." *Infection and Immunity* 84 (9): 2429–2438. <https://doi.org/10.1128/IAI.00334-16>.
- Schiffer, G, and JV Höltje. 1999. "Cloning and characterization of PBP 1C, a third member of the multimodular class a penicillin-binding proteins of Escherichia coli." *Journal of Biological Chemistry* 274(45):32031-9. <https://doi.org/10.1074/jbc.274.45.32031>.
- Schleifer, KH, and O Kandler. 1972. "Peptidoglycan types of bacterial cell walls and their taxonomic implications." *Bacteriological Reviews* 36(4):407-77. <https://doi.org/10.1128/membr.36.4.407-477.1972>.
- Schultz, KM, and CS Klug. 2017. "Characterization of and lipopolysaccharide binding to the E. coli LptC protein dimer." *Protein Science* 27 (2): 381–89. <https://doi.org/10.1002/pro.3322>.
- Schultz, KM, TJ Lundquist, and CS Klug. 2017. "Lipopolysaccharide binding to the periplasmic protein LptA." *Protein Science* 26 (8): 1517–1523. <https://doi.org/10.1002/pro.3177>.
- Schwandner, R, R Dziarski, H Wesche, M Rothe, and CJ Kirschning. 1999. "Peptidoglycan- and lipoteichoic acid-induced cell activation is mediated by Toll-like receptor 2." *Journal of Biological Chemistry* 274 (25): 17406–9. <https://doi.org/10.1074/jbc.274.25.17406>.
- Schwudke, D, M Linscheid, E Strauch, B Appel, U Zähringer, H Moll, M Müller, L Brecker, S Gronow, and B Lindner. 2003. "The obligate predatory Bdellovibrio bacteriovorus possesses a neutral lipid A containing α -D-Mannoses that replace phosphate residues. Similarities and differences between the lipid As and the lipopolysaccharides of the wild type strain B. bacteriovorus H." *Journal of Biological Chemistry* 278 (30): 27502–12. <https://doi.org/10.1074/jbc.M303012200>.
- Scott, JR, and TC Barnett. 2006. "Surface proteins of Gram-positive bacteria and how they get there." *Annual Review of Microbiology* 60: 397–423. <https://doi.org/10.1146/annurev.micro.60.080805.142256>.
- Sender, R, S Fuchs, and Ronilo. 2016. "Revised estimates for the number of human and bacteria cells in the body." *PLoS Biology* 14 (8): e1002533. <https://doi.org/10.1371/journal.pbio.1002533>.
- Seydel, U, M Oikawa, K Fukase, S Kusumoto, and K Brandenburg. 2000. "Intrinsic conformation of lipid A is responsible for agonistic and antagonistic activity." *European Journal of Biochemistry*

- 267 (10): 3032–39. <https://doi.org/10.1046/j.1432-1033.2000.01326.x>.
- Shang, FM, and HL Liu. 2018. “*Fusobacterium nucleatum* and colorectal cancer: a review.” *World Journal of Gastrointestinal Oncology* 10(3):71-81. <https://doi.org/10.4251/wjgo.v10.i3.71>.
- Sherman, DJ, MB Lazarus, L Murphy, C Liu, S Walker, N Ruiz, and D Kahne. 2014. “Decoupling catalytic activity from biological function of the ATPase that powers lipopolysaccharide transport.” *Proceedings of the National Academy of Sciences of the United States of America* 111 (13): 4982–4987. <https://doi.org/10.1073/pnas.1323516111>.
- Sherman, DJ, S Okuda, WA Denny, and D Kahne. 2013. “Validation of inhibitors of an ABC transporter required to transport lipopolysaccharide to the cell surface in *Escherichia coli*.” *Bioorganic and Medicinal Chemistry* 21 (16): 4846–51. <https://doi.org/10.1016/j.bmc.2013.04.020>.
- Shi, H, BP Bratton, Z Gitai, and KC Huang. 2018. “How to build a bacterial cell: MreB as the foreman of *E. coli* construction.” *Cell* 172(6):1294-1305. <https://doi.org/10.1016/j.cell.2018.02.050>.
- Shimomura, H, M Matsuura, S Saito, Y Hirai, Y Isshiki, and K Kawahara. 2001. “Lipopolysaccharide of *Burkholderia cepacia* and its unique character to stimulate murine macrophages with relative lack of interleukin-1 β -inducing ability.” *Infection and Immunity* 69 (6): 3663–69. <https://doi.org/10.1128/IAI.69.6.3663-3669.2001>.
- Shrivastava, R, X Jiang, and SS Chng. 2017. “Outer Membrane lipid homeostasis via retrograde phospholipid transport in *Escherichia coli*.” *Molecular Microbiology* 106 (3): 395–408. <https://doi.org/10.1111/mmi.13772>.
- Silhavy, TJ, D Kahne, and S Walker. 2010. “The bacterial cell envelope.” *Cold Spring Harbor Perspectives in Biology* 2 (5): a000414. <https://doi.org/10.1101/cshperspect.a000414>.
- Silipo, A, R Lanzetta, A Amoresano, M Parrilli, and A Molinaro. 2002. “Ammonium hydroxide hydrolysis: a valuable support in the MALDI-TOF Mass Spectrometry analysis of lipid a fatty acid distribution.” *Journal of Lipid Research* 43 (12): 2188–95. <https://doi.org/10.1194/jlr.D200021-JLR200>.
- Silipo, A, F Di Lorenzo, A De Felice, A Vanacore, C De Castro, D Gully, R Lanzetta, M Parrilli, E Giraud, and A Molinaro. 2014. “Structural and conformational study of the O-polysaccharide produced by the metabolically versatile photosynthetic bacterium *Rhodospseudomonas palustris* strain BisA53.” *Carbohydrate Polymers* 114: 384–91. <https://doi.org/10.1016/j.carbpol.2014.08.037>.
- Silipo, A, and A Molinaro. 2010. “The diversity of the core oligosaccharide in lipopolysaccharides.” *Sub-Cellular Biochemistry* 53: 69–99. https://doi.org/10.1007/978-90-481-9078-2_4.
- Simpson, BW, JM May, DJ Sherman, D Kahne, and N Ruiz. 2015. “Lipopolysaccharide transport to the cell surface: biosynthesis and extraction from the inner membrane.” *Philosophical Transactions of the Royal Society B: Biological Sciences*. 370(1679):20150029. <https://doi.org/10.1098/rstb.2015.0029>.
- Singh, SK, L Saisree, RN Amrutha, and M Reddy. 2012. “Three redundant murein endopeptidases catalyze an essential cleavage step in peptidoglycan synthesis of *Escherichia coli* K12.” *Molecular Microbiology* 86 (5): 1036–5. <https://doi.org/10.1111/mmi.12058>.
- Sjögren, P, E Nilsson, M Forsell, O Johansson, and J Hoogstraate. 2008. “A systematic review of the preventive effect of oral hygiene on pneumonia and respiratory tract infection in elderly people in hospitals and nursing homes: effect estimates and methodological quality of randomized controlled trials.” *Journal of the American Geriatrics Society* 56 (11): 2124–30. <https://doi.org/10.1111/j.1532-5415.2008.01926.x>.
- Sklar, JG, T Wu, D Kahne, and TJ Silhavy. 2007. “Defining the roles of the periplasmic chaperones SurA, Skp, and DegP in *Escherichia coli*.” *Genes and Development* 21 (19): 2473–84. <https://doi.org/10.1101/gad.1581007>.
- Smith, PA, MFT Koehler, HS Girgis, D Yan, Y Chen, Y Chen, JJ Crawford, *et al.* 2018. “Optimized arylomycins are a new class of Gram-negative antibiotics.” *Nature* 561 (7722): 189–94. <https://doi.org/10.1038/s41586-018-0483-6>.
- Sparks SP, MJ Steffen, C Smith, G Jicha, JL Ebersole, E Abner, and D Dawson. 2012. “Serum antibodies to periodontal pathogens are a risk factor for alzheimer’s disease.” *Alzheimer’s and Dementia* 8 (3): 196–203. <https://doi.org/10.1016/j.jalz.2011.04.006>.
- Sperandeo, P, R Cescutti, R Villa, C Di Benedetto, D Candia, G Dehò, and A Polissi. 2007. “Characterization of LptA and LptB, two essential genes implicated in lipopolysaccharide

- transport to the Outer Membrane of *Escherichia coli*.” *Journal of Bacteriology* 189 (1): 244–253. <https://doi.org/10.1128/JB.01126-06>.
- Srikannathasan, V, G English, NK Bui, K Trunk, PEF O’Rourke, VA Rao, W Vollmer, SJ Coulthurst, and WN Hunter. 2013. “Structural basis for type VI secreted peptidoglycan DL-Endopeptidase function, specificity and neutralization in *Serratia marcescens*.” *Acta Crystallographica Section D: Biological Crystallography* 69 (Pt12): 2468–2482. <https://doi.org/10.1107/S0907444913022725>.
- States, DJ, RA Haberkorn, and DJ Ruben. 1982. “A two-dimensional Nuclear Overhauser Experiment with pure absorption phase in four quadrants.” *Journal of Magnetic Resonance* 8 (2): 286–92. [https://doi.org/10.1016/0022-2364\(82\)90279-7](https://doi.org/10.1016/0022-2364(82)90279-7).
- Stefanetti, G, N Okan, A Fink, E Gardner, and DL Kasper. 2019. “Glycoconjugate vaccine using a genetically modified O-antigen induces protective antibodies to *Francisella tularensis*.” *Proceedings of the National Academy of Sciences of the United States of America* 116 (14): 7062–70. <https://doi.org/10.1073/pnas.1900144116>.
- Stephenson, HN, DC Mills, H Jones, E Milioris, A Copland, N Dorrell, BW Wren, PR Crocker, D Escors, and M Bajaj-Elliott. 2014. “Pseudamino acid on *Campylobacter jejuni* flagella modulates dendritic cell IL-10 expression via Siglec-10 receptor: a novel flagellin-host interaction.” *Journal of Infectious Diseases* 210 (9): 1487–98. <https://doi.org/10.1093/infdis/jiu287>.
- Stern, AS, KB Li, and JC Hoch. 2002. “Modern spectrum analysis in multidimensional NMR Spectroscopy: comparison of linear-prediction extrapolation and maximum-entropy reconstruction.” *Journal of the American Chemical Society* 124 (9): 1982–93. <https://doi.org/10.1021/ja011669o>.
- Storek, KM, MR Auerbach, H Shi, NK Garcia, D Sun, NN Nickerson, R Vij, *et al.* 2018. “Monoclonal antibody targeting the β -Barrel Assembly Machine of *Escherichia coli* is bactericidal.” *Proceedings of the National Academy of Sciences of the United States of America* 115 (14): 3692–97. <https://doi.org/10.1073/pnas.1800043115>.
- Storek, KM, R Vij, D Sun, PA Smith, JT Koerber, and ST Rutherford. 2019. “The *Escherichia coli* - Barrel Assembly Machinery is sensitized to perturbations under high membrane fluidity.” *Journal of Bacteriology* 201 (1): e00517-18. <https://doi.org/10.1128/JB.00517-18>.
- Straus, SK, and REW Hancock. 2006. “Mode of action of the new antibiotic for Gram-positive pathogens daptomycin: comparison with cationic antimicrobial peptides and lipopeptides.” *Biochimica et Biophysica Acta - Biomembranes* 1758(9):1215-23. <https://doi.org/10.1016/j.bbamem.2006.02.009>.
- Su, MY, N Som, CY Wu, SC Su, YT Kuo, LC Ke, MR Ho, *et al.* 2017. “Structural basis of adaptor-mediated protein degradation by the tail-specific PDZ-protease Prc.” *Nature Communications* 8 (1): 1516. <https://doi.org/10.1038/s41467-017-01697-9>.
- Sudhakara, P, I Sellamuthu, and AW Aruni. 2019. “Bacterial sialoglycosidases in virulence and pathogenesis.” *Pathogens* 8(1):39. <https://doi.org/10.3390/pathogens8010039>.
- Suits, MDL, P Sperandio, G Dehò, A Polissi, and Z Jia. 2008. “Novel structure of the conserved Gram-negative lipopolysaccharide transport protein A and mutagenesis analysis.” *Journal of Molecular Biology* 380 (3): 476–88. <https://doi.org/10.1016/j.jmb.2008.04.045>.
- Sukhithasri, V, N Nisha, L Biswas, V Anil Kumar, and R Biswas. 2013. “Innate immune recognition of microbial cell wall components and microbial strategies to evade such recognitions.” *Microbiological Research* 168(7):396-406. <https://doi.org/10.1016/j.micres.2013.02.005>.
- Szwedziak, P, and J Löwe. 2013. “Do the divisome and elongasome share a common evolutionary past?” *Current Opinion in Microbiology* 16 (6): 745-51. <https://doi.org/10.1016/j.mib.2013.09.003>.
- Také, A, T Nakashima, Y Inahashi, K Shiomi, Y Takahashi, S Ōmura, and A Matsumoto. 2016. “Analyses of the cell-wall peptidoglycan structures in three genera *Micromonospora*, *Catenuloplanes*, and *Couchioplanes* belonging to the family *Micromonosporaceae* by derivatization with FDLA and PMP using LC/MS.” *Journal of General and Applied Microbiology* 62 (4): 199–205. <https://doi.org/10.2323/jgam.2016.02.007>.
- Tan, K, R Li, X Huang, and Q Liu. 2018. “Outer Membrane Vesicles: current status and future Direction of these novel vaccine adjuvants.” *Frontiers in Microbiology* 9:783. <https://doi.org/10.3389/fmicb.2018.00783>.

- Tang, X, S Chang, Q Luo, Z Zhang, W Qiao, C Xu, C Zhang, *et al.* 2019. “Cryo-EM structures of lipopolysaccharide transporter LptB2FGC in lipopolysaccharide or AMP-PNP-bound states reveal its transport mechanism.” *Nature Communications* 10 (1): 4175. <https://doi.org/10.1038/s41467-019-11977-1>.
- Tao, H, NJ Brewin, and KD Noel. 1992. “*Rhizobium leguminosarum* CFN42 lipopolysaccharide antigenic changes induced by environmental conditions.” *Journal of Bacteriology* 174 (7): 2222–29. <https://doi.org/10.1128/jb.174.7.2222-2229.1992>.
- Teixeira, TFS, MC Collado, CLLF Ferreira, J Bressan, and M do Carmo, G Peluzio. 2012. “Potential mechanisms for the emerging link between obesity and increased intestinal permeability.” *Nutrition Research* 32 (9): 637–47. <https://doi.org/10.1016/j.nutres.2012.07.003>.
- Témoin, S, A Chakaki, A Askari, A El-Halaby, S Fitzgerald, RE Marcus, YW Han, and NF Bissada. 2012. “Identification of oral bacterial DNA in synovial fluid of patients with arthritis with native and failed prosthetic joints.” *Journal of Clinical Rheumatology* 18 (3): 117–121. <https://doi.org/10.1097/RHU.0b013e3182500c95>.
- Tesch, DM, and AA Nevzorov. 2014. “Sensitivity enhancement and contrasting information provided by free radicals in oriented-sample NMR of bicelle-reconstituted membrane proteins.” *Journal of Magnetic Resonance* 239: 9–15. <https://doi.org/10.1016/j.jmr.2013.11.010>.
- Thursby, E, and N Juge. 2017. “Introduction to the human gut microbiota.” *Biochemical Journal* 474(11):1823-1836. <https://doi.org/10.1042/BCJ20160510>.
- Tokuda, H, and SI Matsuyama. 2004. “Sorting of lipoproteins to the outer membrane in *E. coli*.” *Biochimica et Biophysica Acta - Molecular Cell Research*. 1693 (1): 5-13. <https://doi.org/10.1016/j.bbamcr.2004.02.005>.
- Tosoni, G, M Conti, and R Diaz Heijtz. 2019. “Bacterial peptidoglycans as novel signaling molecules from microbiota to brain.” *Current Opinion in Pharmacology* 48: 107–13. <https://doi.org/10.1016/j.coph.2019.08.003>.
- Toukach, PV. 2011. “Bacterial carbohydrate structure database 3: principles and realization.” *Journal of Chemical Information and Modeling* 51 (1): 159–70. <https://doi.org/10.1021/ci100150d>.
- Toukach, PV, and KS Egorova. 2016. “Carbohydrate structure database merged from bacterial, archaeal, plant and fungal parts.” *Nucleic Acids Research* 44 (D1): D1229–D1236. <https://doi.org/10.1093/nar/gkv840>.
- Tran, AX, C Dong, and C Whitfield. 2010. “Structure and functional analysis of LptC, a conserved membrane protein involved in the lipopolysaccharide export pathway in *Escherichia coli*.” *Journal of Biological Chemistry* 292(45):18731. <https://doi.org/10.1074/jbc.M110.144709>.
- Travassos, LH, SE Girardin, DJ Philpott, D Blanot, MA Nahori, C Werts, and IG Boneca. 2004. “Toll-like receptor 2-dependent bacterial sensing does not occur via peptidoglycan recognition.” *EMBO Reports* 5 (10): 1000–1006. <https://doi.org/10.1038/sj.embor.7400248>.
- Trimble, MJ, P Mlynářčik, M Kolář, and REW Hancock. 2016. “Polymyxin: alternative mechanisms of action and resistance.” *Cold Spring Harbor Perspectives in Medicine* 6 (10): a025288. <https://doi.org/10.1101/cshperspect.a025288>.
- Tsai, CM, and CE Frasch. 1982. “A sensitive silver stain for detecting lipopolysaccharides in polyacrylamide gels.” *Analytical Biochemistry* 119 (1): 115–19. [https://doi.org/10.1016/0003-2697\(82\)90673-X](https://doi.org/10.1016/0003-2697(82)90673-X).
- Tsang, MJ, AA Yakhnina, and TG Bernhardt. 2017. “NlpD links cell wall remodeling and outer membrane invagination during cytokinesis in *Escherichia coli*.” *PLoS Genetics* 13 (7): e1006888. <https://doi.org/10.1371/journal.pgen.1006888>.
- Tuffal, G, R Albigot, M Rivière, and G Puzo. 1998. “Newly found 2-N-acetyl-1,2,6-dideoxy- β -glucopyranose containing methyl Glucose polysaccharides in *M. bovis* BCG: revised structure of the mycobacterial methyl Glucose lipopolysaccharides.” *Glycobiology* 8 (7): 675–684. <https://doi.org/10.1093/glycob/8.7.675>.
- Typas, A, M Banzhaf, B van Den Berg Van Saparoea, J Verheul, J Biboy, RJ Nichols, M Zietek, *et al.* 2010. “Regulation of peptidoglycan synthesis by Outer-Membrane proteins.” *Cell* 143 (7): 1097–1109. <https://doi.org/10.1016/j.cell.2010.11.038>.
- Typas, A, M Banzhaf, CA Gross, and W Vollmer. 2012. “From the regulation of peptidoglycan synthesis to bacterial growth and morphology.” *Nature Reviews Microbiology* 10(2):123-36. <https://doi.org/10.1038/nrmicro2677>.
- Uehara, T, T Dinh, and TG Bernhardt. 2009. “LytM-domain factors are required for daughter cell

- separation and rapid ampicillin-induced lysis in *Escherichia coli*.” *Journal of Bacteriology* 191 (16): 5094–5107. <https://doi.org/10.1128/JB.00505-09>.
- Uehara, T, and JT Park. 2007. “An anhydro-N-acetylmuramyl-L-alanine amidase with broad specificity tethered to the outer membrane of *Escherichia coli*.” *Journal of Bacteriology* 189 (15): 5634–41. <https://doi.org/10.1128/JB.00446-07>.
- . 2008. “Growth of *Escherichia coli*: significance of peptidoglycan degradation during elongation and septation.” *Journal of Bacteriology* 190 (11): 3914–3922. <https://doi.org/10.1128/JB.00207-08>.
- Uehara, T, KR Parzych, T Dinh, and TG Bernhardt. 2010. “Daughter cell separation is controlled by cytokinetic ring-activated cell wall hydrolysis.” *EMBO Journal* 29 (8): 1412–1422. <https://doi.org/10.1038/emboj.2010.36>.
- Uehara, T, K Suefuji, N Valbuena, B Meehan, M Donegan, and JT Park. 2005. “Recycling of the anhydro-N-acetylmuramic acid derived from cell wall Murein involves a two-step conversion to N-acetylglucosamine-phosphate.” *Journal of Bacteriology* 187 (11): 3643–49. <https://doi.org/10.1128/JB.187.11.3643-3649.2005>.
- Vanaja, SK, AJ Russo, B Behl, I Banerjee, M Yankova, SD Deshmukh, and VAK Rathinam. 2016. “Bacterial outer membrane Vesicles mediate cytosolic localization of LPS and caspase-11 activation.” *Cell* 165 (5): 1106–1119. <https://doi.org/10.1016/j.cell.2016.04.015>.
- Varki, A, RD Cummings, M Aebi, NH Packer, PH Seeberger, JD Esko, P Stanley, *et al.* 2015. “Symbol nomenclature for graphical representations of glycans.” *Glycobiology* 25 (12): 1323–24. <https://doi.org/10.1093/glycob/cwv091>.
- Vasstrand, EN 1981. “Lysozyme digestion and chemical characterization of the peptidoglycan of *Fusobacterium nucleatum* Fev 1.” *Infection and Immunity* 33 (1): 75–82. <https://doi.org/10.1128/iai.33.1.75-82.1981>.
- Vasstrand, EN, . Hofstad, C Endresen, and HB Jensen. 1979. “Demonstration of lanthionine as a natural constituent of the peptidoglycan of *Fusobacterium nucleatum*.” *Infection and Immunity* 25 (3): 775–80. <https://doi.org/10.1128/iai.25.3.775-780.1979>.
- Vaure, C, and Y Liu. 2014. “A comparative review of Toll-like receptor 4 expression and functionality in different animal species.” *Frontiers in Immunology* 5: 316. <https://doi.org/10.3389/fimmu.2014.00316>.
- Velsko, IM, SS Chukkapalli, MF Rivera-Kweh, H Chen, D Zheng, I Bhattacharyya, PR Gangula, A Lucas, and L Kesavalu. 2015. “*Fusobacterium nucleatum* alters atherosclerosis risk factors and enhances inflammatory markers with an atheroprotective immune response in ApoE null mice.” *PLoS ONE* 10 (6): e0129795. <https://doi.org/10.1371/journal.pone.0129795>.
- Ventola, CL. 2015. “The antibiotic resistance crisis: causes and threats.” *P & T Journal* 40 (4): 277–83. <https://doi.org/Article>.
- Vermassen, A, S Leroy, R Talon, C Provot, M Popowska, and M Desvaux. 2019. “Cell wall hydrolases in bacteria: insight on the diversity of cell wall amidases, glycosidases and peptidases toward peptidoglycan.” *Frontiers in Microbiology* 10:331. <https://doi.org/10.3389/fmicb.2019.00331>.
- Vetterli, SU, K Zerbe, M Müller, M Urfer, M Mondal, SY Wang, K Moehle, *et al.* 2018. “Thanatin targets the intermembrane protein complex required for lipopolysaccharide transport in *Escherichia coli*.” *Science Advances* 4 (11): eaau2634. <https://doi.org/10.1126/sciadv.aau2634>.
- Viganò, E, CE Diamond, R Spreafico, A Balachander, RM Sobota, and A Mortellaro. 2015. “Human caspase-4 and caspase-5 regulate the one-step non-canonical inflammasome activation in monocytes.” *Nature Communications* 6: 8761. <https://doi.org/10.1038/ncomms9761>.
- Vinogradov, E, F St. Michael, and AD Cox. 2017a. “Structure of the LPS O-chain from *Fusobacterium nucleatum* strain 12230.” *Carbohydrate Research* 448: 115–17. <https://doi.org/10.1016/j.carres.2017.06.007>.
- . 2017b. “The structure of the LPS O-chain of *Fusobacterium nucleatum* strain 25586 containing two novel monosaccharides, 2-acetamido-2,6-dideoxy-L-Altrose and a 5-acetimido-3,5,9-trideoxy-gluco-non-2-Ulsonic acid.” *Carbohydrate Research* 440–441: 10–15. <https://doi.org/10.1016/j.carres.2017.01.002>.
- Vinogradov, E, F St. Michael, K Homma, A Sharma, and AD Cox. 2017. “Structure of the LPS O-chain from *Fusobacterium nucleatum* strain 10953, containing Sialic acid.” *Carbohydrate Research* 440–441: 38–42. <https://doi.org/10.1016/j.carres.2017.01.009>.
- Vinogradov, E, and Z Sidorchuk. 2001. “The structure of the carbohydrate backbone of the core-lipid

- A region of the lipopolysaccharide from *Proteus penneri* strain 40: new *Proteus* strains containing open-chain acetal-linked N-acetylgalactosamine in the core part of the LPS.” *Carbohydrate Research* 330 (4): 537–40. [https://doi.org/10.1016/S0008-6215\(00\)00312-8](https://doi.org/10.1016/S0008-6215(00)00312-8).
- Vinogradov, E, F St Michael, and AD Cox. 2018a. “Structure of the LPS O-chain from *Fusobacterium nucleatum* strain ATCC 23726 containing a novel 5,7-diamino-3,5,7,9-tetradeoxy-L-Gluco-non-2-ulosonic acid presumably having the D-glycero-L-Gluco configuration.” *Carbohydrate Research* 468: 69–72. <https://doi.org/10.1016/j.carres.2018.08.011>.
- . 2018b. “Structure of the LPS O-chain from *Fusobacterium nucleatum* strain MJR 7757 B.” *Carbohydrate Research* 463: 37–39. <https://doi.org/10.1016/j.carres.2018.04.010>.
- Vliet, SJ van, L Steeghs, SCM Bruijns, MM Vaezirad, C Snijders Blok, JA Arenas Busto, M Deken, JPM van Putten, and Y van Kooyk. 2009. “Variation of *Neisseria gonorrhoeae* lipooligosaccharide directs dendritic cell-induced T helper responses.” *PLoS Pathogens* 5 (10): e1000625. <https://doi.org/10.1371/journal.ppat.1000625>.
- Vollmer, W, and U Bertsche. 2008. “Murein (peptidoglycan) structure, architecture and biosynthesis in *Escherichia coli*.” *Biochimica et Biophysica Acta - Biomembranes* 1778(9):1714-34. <https://doi.org/10.1016/j.bbamem.2007.06.007>.
- Vollmer, W, D Blanot, and MA De Pedro. 2008. “Peptidoglycan structure and architecture.” *FEMS Microbiology Reviews* 32(2):149-67. <https://doi.org/10.1111/j.1574-6976.2007.00094.x>.
- Vollmer, W, and P Born. 2010. “Bacterial cell envelope peptidoglycan.” In *Microbial Glycobiology*. <https://doi.org/10.1016/B978-0-12-374546-0.00002-X>.
- Vollmer, W, B Joris, P Charlier, and S Foster. 2008. “Bacterial peptidoglycan (murein) hydrolases.” *FEMS Microbiology Reviews* 32 (2): 259-86. <https://doi.org/10.1111/j.1574-6976.2007.00099.x>.
- Vollmer, W, and SJ Seligman. 2010. “Architecture of peptidoglycan: more data and more models.” *Trends in Microbiology* 18 (2): 59–66. <https://doi.org/10.1016/j.tim.2009.12.004>.
- Vollmer, W, and A Tomasz. 2000. “The *pgdA* gene encodes for a peptidoglycan N-acetylglucosamine deacetylase in *Streptococcus pneumoniae*.” *Journal of Biological Chemistry* 275 (27): 20496–501. <https://doi.org/10.1074/jbc.M910189199>.
- Wall, E, N Majdalani, and S Gottesman. 2018. “The complex Rcs regulatory cascade.” *Annual Review of Microbiology* 72: 111–39. <https://doi.org/10.1146/annurev-micro-090817-062640>.
- Walter, A, and C Mayer. 2019. “Peptidoglycan structure, biosynthesis, and dynamics during bacterial growth.” *Extracellular Sugar-Based Biopolymers Matrices. Biologically-Inspired Systems, Vol 12*, edited by Merzendorfer H Cohen E. Springer, Cham. https://doi.org/10.1007/978-3-030-12919-4_6.
- Wang, G, A Olczak, LS Forsberg, and RJ Maier. 2009. “Oxidative stress-induced peptidoglycan deacetylase in *Helicobacter pylori*.” *Journal of Biological Chemistry* 284 (11): 6790–6800. <https://doi.org/10.1074/jbc.M808071200>.
- Wang, Y, and RB Cole. 1996. “Acid and base hydrolysis of lipid A from *Enterobacter agglomerans* as monitored by Electrospray Ionization Mass Spectrometry: pertinence to detoxification mechanisms.” *Journal of Mass Spectrometry* 31 (2): 138–49. [https://doi.org/10.1002/\(SICI\)1096-9888\(199602\)31:2<138::AID-JMS263>3.0.CO;2-Y](https://doi.org/10.1002/(SICI)1096-9888(199602)31:2<138::AID-JMS263>3.0.CO;2-Y).
- Wang, Z, E Vinogradov, J Li, V Lund, and E Altman. 2009. “Structural characterization of the lipopolysaccharide O-antigen from atypical isolate of *Vibrio anguillarum* strain 1282.” *Carbohydrate Research* 344 (11): 1371–75. <https://doi.org/10.1016/j.carres.2009.04.027>.
- Weadge, Joel T., John M. Pfeffer, and Anthony J. Clarke. 2005. “Identification of a New Family of Enzymes with Potential O-Acetylpeptidoglycan Esterase Activity in Both Gram-Positive and Gram-Negative Bacteria.” *BMC Microbiology* 5: 49. <https://doi.org/10.1186/1471-2180-5-49>.
- Westphal, O, and K Jann. 1965. “Bacterial Lipopolysaccharides. Extraction with Phenol-Water and Further Applications of the Procedures.” In *Methods Carbohydr. Chem.*, edited by RL Whistler and ML Wolfrom, 5:83–91. New York: Academic Press Inc.
- Whitfield, C, and MS Trent. 2014. “Biosynthesis and export of bacterial lipopolysaccharides.” *Annual Review of Biochemistry* 83: 99–128. <https://doi.org/10.1146/annurev-biochem-060713-035600>.
- Whitfield, C, DM Williams, and SD Kelly. 2020. “Lipopolysaccharide O-antigens - bacterial glycans made to measure.” *Journal of Biological Chemistry* 295(31):10593-10609. <https://doi.org/10.1074/jbc.rev120.009402>.
- Whitney, JC, and PL Howell. 2013. “Synthase-dependent exopolysaccharide secretion in Gram-negative bacteria.” *Trends in Microbiology* 21 (2): 63–72.

- <https://doi.org/10.1016/j.tim.2012.10.001>.
- WHO. 2015. "Global action plan on antimicrobial resistance." *Microbe Magazine*. <https://doi.org/10.1128/microbe.10.354.1>.
- . 2016. "WORLD HEALTH STATISTICS - MONITORING HEALTH FOR THE SDGs." *World Health Organization Licence: C*. <https://doi.org/10.1017/CBO9781107415324.004>.
- . 2017. "WHO Model List of Essential Medicines: 20th List." *WHO Medicines Web: Http://Www. Who. Int/Medicines/Publications/EML*. [https://doi.org/10.1016/S1473-3099\(14\)70780-7](https://doi.org/10.1016/S1473-3099(14)70780-7).
- . 2017b. "Global priority list of antibiotic-resistant bacteria to guide research, discovery, and development of new antibiotics." *WHO*.
- Wollenweber, HW, U Seydel L, B Lindner, O Lüderitz, and ET Rietschel. 1984. "Nature and location of amide-bound (R)-3-acyloxyacyl groups in lipid A of lipopolysaccharides from various Gram-negative bacteria." *European Journal of Biochemistry* 145 (2): 265–72. <https://doi.org/10.1111/j.1432-1033.1984.tb08547.x>.
- World Bank. 2019. *Pulling Together to Beat Superbugs Knowledge and Implementation Gaps in Addressing Antimicrobial Resistance*. Edited by Robert Livermash. *Pulling Together to Beat Superbugs Knowledge and Implementation Gaps in Addressing Antimicrobial Resistance*. The World Bank Group. <https://doi.org/10.1596/32552>.
- Wright, GD. 2011. "Molecular mechanisms of antibiotic resistance." *Chemical Communications* 47 (14): 4055–61. <https://doi.org/10.1039/c0cc05111j>.
- Xie, R, RJ Taylor, and D Kahne. 2018. "Outer Membrane translocon communicates with Inner Membrane ATPase to stop lipopolysaccharide transport." *Journal of the American Chemical Society* 140 (40): 12691–12694. <https://doi.org/10.1021/jacs.8b07656>.
- Yakhnina, AA, and TG Bernhardt. 2020. "The Tol-Pal system is required for peptidoglycan-cleaving enzymes to complete bacterial cell division." *Proceedings of the National Academy of Sciences of the United States of America* 117 (12): 6777–83. <https://doi.org/10.1073/pnas.1919267117>.
- Yan, Q, X Hu, and N Wang. 2012. "The novel virulence-related gene *nlxA* in the lipopolysaccharide cluster of *Xanthomonas citri* Ssp. *citri* is involved in the production of lipopolysaccharide and extracellular polysaccharide, motility, biofilm formation and stress resistance." *Molecular Plant Pathology* 13 (8): 923–34. <https://doi.org/10.1111/j.1364-3703.2012.00800.x>.
- Yang, DC, K Tan, A Joachimiak, and TG Bernhardt. 2012. "A conformational switch controls cell wall-remodelling enzymes required for bacterial cell division." *Molecular Microbiology* 85 (4): 768–781. <https://doi.org/10.1111/j.1365-2958.2012.08138.x>.
- Yang, NY, Q Zhang, JL Li, SH Yang, and Q Shi. 2014. "Progression of periodontal inflammation in adolescents is associated with increased number of *Porphyromonas gingivalis*, *Prevotella intermedia*, *Tannerella forsythensis*, and *Fusobacterium nucleatum*." *International Journal of Paediatric Dentistry* 24 (3): 226–33. <https://doi.org/10.1111/ipd.12065>.
- Ye, X, R Wang, R Bhattacharya, D Boulbes, F Fan, L Xia, H Adoni, *et al.* 2017. "*Fusobacterium nucleatum* Subspecies *Animalis* influences pro-inflammatory cytokine expression and monocyte activation in human colorectal tumors." *Cancer Prevention Research* 10 (July): canprevres.0178.2016. <https://doi.org/10.1158/1940-6207.CAPR-16-0178>.
- Yoneda, S, B Loeser, J Feng, J Dmytryk, F Qi, and J Merritt. 2014. "Ubiquitous sialometabolism present among oral *Fusobacteria*." *PLoS ONE* 9 (6): e99263. <https://doi.org/10.1371/journal.pone.0099263>.
- Zhang, T, Q Li, L Cheng, H Buch, and F Zhang. 2019. "*Akkermansia muciniphila* is a promising probiotic." *Microbial Biotechnology* 12(6):1109-1125. <https://doi.org/10.1111/1751-7915.13410>.
- Zhang, X, Y Li, W Wang, J Zhang, Y Lin, B Hong, X You, *et al.* 2019. "Identification of an anti-Gram-negative bacteria agent disrupting the interaction between lipopolysaccharide transporters LptA and LptC." *International Journal of Antimicrobial Agents* 53 (4): 442–48. <https://doi.org/10.1016/j.ijantimicag.2018.11.016>.
- Zhou, Z, AA Ribeiro, S Lin, RJ Cotter, SI Miller, and CRH Raetz. 2001. "Lipid A modifications in polymyxin-resistant *Salmonella typhimurium*: PmrA-dependent 4-amino-4-deoxy-L-Arabinose, and phosphoethanolamine incorporation." *Journal of Biological Chemistry* 276 (46): 43111–21. <https://doi.org/10.1074/jbc.M106960200>.
- Zipperle, GF, JW Ezzell, and RJ Doyle. 1984. "Glucosamine substitution and muramidase

- susceptibility in *Bacillus anthracis*.” *Canadian Journal of Microbiology* 30 (5): 553–559. <https://doi.org/10.1139/m84-083>.
- Zoeiby, AE, F Sanschagrin, and RC Levesque. 2003. “Structure and function of the Mur enzymes: development of novel inhibitors.” *Molecular Microbiology* 47(1):1-12. <https://doi.org/10.1046/j.1365-2958.2003.03289.x>.
- Zych, K, and Z Sidorczyk. 1989. “Lipopolysaccharides of *Proteus penneri* Species *novum*.” *Carbohydrate Research* 188: 105–11. [https://doi.org/10.1016/0008-6215\(89\)84063-7](https://doi.org/10.1016/0008-6215(89)84063-7).